Università degli Studi di Napoli Federico II
Facoltà di Ingegneria

Giulio Martire

THE DEVELOPMENT OF SUBMERGED FLOATING TUNNELS AS AN INNOVATIVE SOLUTION FOR WATERWAY CROSSINGS

Tesi di Dottorato
XXIII ciclo

Il Coordinatore
Prof. Ing. Federico M. MAZZOLANI

Dottorato di Ricerca in Ingegneria delle Costruzioni

To my Family, above all.

And to all my Special People.

OUTLINE OF THE THESIS

The present Thesis is organized in 10 chapters. In particular Chapter 1 gives a general overview of the modern solutions and technologies available in the field of waterway crossings, introducing briefly the revolutionary concept of Submerged Floating Tunnel.

Chapter 2 provides a deeper insight into the main characteristics of this innovative structural solution for waterway crossings: first its structural features are described and the relevant loading conditions discussed, subsequently the main advantages of the SFT with respect to the traditional crossing solutions, such as the Cable Supported Bridges and the Underground and Immersed Tunnel are described.

Chapter 3 traces the history of the SFT, starting from its first proposal made in 1969 for the Messina Strait crossing, describing all the feasibility studies and preliminary designs developed all over the world in the following years. This Chapter is concluded by a description of the Sino-Italian cooperation programmes, involving among the other partners the University of Naples "Federico II", which led to a feasibility study relative to the crossing of the Jintang Strait (P.R. of China) with a SFT and to the complete design of the first SFT full-scale prototype, planned to be realized in the forthcoming years in the Qiandao Lake (P.R. of China). A potential SFT crossing in the Pulau Seribu Archipelago (Indonesia), preliminary studied in the last years by the research team headed by Prof. Mazzolani, is also briefly illustrated.

Chapter 4 explains in the detail of the various aspects faced in the design of the Archimedes Bridge prototype. The features of the selected location and the structural scheme are illustrated. The structural analyses aimed at investigating the prototype behaviour under the environmental loads are discussed. The conception and the design of the constructional details are presented. Finally, the fabrication and erection procedures are briefly described.

Chapter 5 provides a description of the structural models which can be used to analyse the SFT structural behaviour: the beam on elastic foundation, which

can be used in the preliminary phase of the design, and a SFT Finite Element Model.

Chapters 6 and 7 are devoted to the study of the response of the SFT to the main environmental loads to which is subjected: the hydrodynamic actions due to the presence of waves and currents and the earthquakes. Numerical analyses are carried out with the Finite Element analyses aimed at the understanding of the SFT structural behaviour and at the definition of the optimal structural configurations.

In Chapter 8 potential SFT solutions developed for the Messina Strait and Gibraltar Strait crossings are illustrated and a technical-economical comparison with the Suspension Bridges designed for the same locations is made.

Chapter 8 describes a simple procedure for a quick comparison of the SFT and CSIB solutions with the Cable Supported Bridges one, providing useful curves highlighting the conditions under which the former ones are more competitive than the latter ones.

Finally, in Chapter 9 the future steps and challenges to be faced in the development of Submerged Floating Tunnel are presented. An alternative typology of floating tunnel is introduced too: the Cable Supported Immersed Inversed Bridge (CSIB), which is conceived as a combination of the submerged floating bridge concept with the cable system configurations and features several advantages also with respect to the “traditional” SFT solution.

Chapter 1

Waterway crossings: a never ending challenge

1.1 STRAIT CROSSINGS:THE STATE OF THE ART

1.1.1 Introduction

Connecting opposite shores of a lake, sea or river, has always been one of the major tasks to be faced by Civil Engineering, it being a fundamental need for the development of the areas surrounding a waterway. Nowadays, this issue is still topical and of great importance, as it is proved by the numerous large infrastructures which have been built or planned to be built in the last years all over the world, such as, for instance the Channel Tunnel, linking the shores of France with the ones of the United Kingdom, the Immersed Tunnel under construction in the Bosporus Strait (Turkey) or the Suspension Bridge designed to connect Calabria and Sicily in the Messina Strait (Italy). Numerous other important and noticeable cases could be mentioned, however the aforementioned ones probably represent the most advanced examples of the structural solutions which are traditionally most widely used to link areas divided by the presence of waterways: Cable Supported Bridges (i.e. Suspension or Cable stayed Bridges), Underground Tunnels and Immersed Tunnels (Figure 1.1).

The complexity of the design issues related to these classic technological

solutions, increases as the distance to be covered grows up, so that the crossing of long span waterways can be, in many cases, very difficult and sometimes impossible. Moreover, the traditional systems feature some disadvantages which in some cases are of great importance, leading to the necessity to find alternative technical solutions.

A revolutionary technical solution, which can get over the above mentioned disadvantages, is the Submerged Floating Tunnel (SFT), which is based on the idea of exploiting the load carrying capacity of water, due to the Archimedes buoyancy (Faggiano and Mazzolani, 2001; Faggiano et al. 2005). In fact, SFT is conceived as a tubular structure to be placed at a pre-fixed depth in the water (Figure 1.1), so that the dead and live loads are counterbalanced by the Archimedes buoyancy. The vertical and horizontal stability of SFT is guaranteed by the presence of adequate anchoring systems, conveniently placed along the longitudinal layout of the tunnel itself.

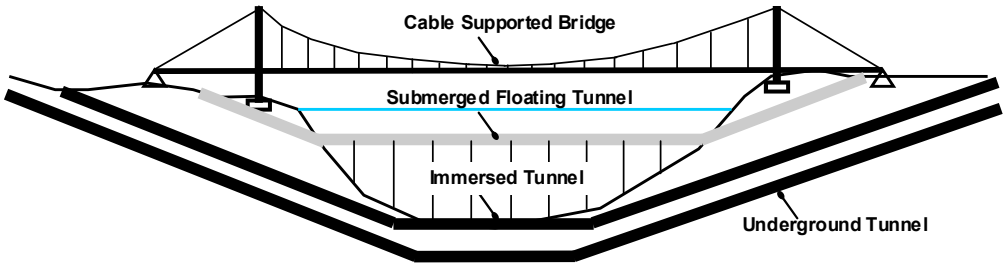

Figure 1.1. Possible waterway crossing solutions

1.1.2 Cable Supported Bridges

The family of Cable Supported Bridges (CSB) includes all the bridge solutions featuring a cable system supporting the deck and acting as the main bearing structural element. Among all the bridge typologies, the one of Cable Supported Bridges can be distinguished because of their ability to overcome large spans; as a matter of fact these bridges are competitive for spans in the range from 200 m to 2000 m and beyond, thus covering approximately 90% of the present span range (Gimsing, 1996).

The structural system of a Cable Supported Bridge is mainly composed of

four elements (Figure 1.2):

1) the bridge deck with the stiffening girder or truss;
2) the cable system, supporting the bridge deck;
3) the pylons, supporting the cable system;
4) the anchor blocks or piers, located at the ends of the cable system and transferring the cable force, or just its vertical component, to the ground.

Since the cable system is their main bearing element, Cable Supported Bridges are generally classified according to its configuration. The suspension system (Figure 1.2a) is composed of a main cable, assuming a parabolic shape, which supports vertical hangers which, in turn, support the bridge deck; the cable-stayed system comprises instead straight cables, named stays, connecting the bridge deck and the stiffening girder directly to the pylons; the stays can all be linked to the top of the pylon, giving rise to the Fan type cable-stayed system (Figure 1.2b), or can be parallel and connected uniformly along the pylon height in the Harp type Cable-stayed system (Figure 1.2c). Combined system (Figure 1.2d), where both the suspension system and the cable-stayed one are used, has also been realized (the most noticeable case is the Brooklyn Bridge) and, for large spans, can represents an optimal solution in terms of both material savings and structural efficiency (Gimsing, 1996).

The arrangement of the stiffening girder or truss represents another key element in the design of a Cable Supported Bridge, especially when large spans have to be surpassed. As a matter of fact, wind induced oscillations, such as the ones related to aeroelastic phenomena, constitute the major risk scenario for CSBs featuring a large main span length; besides of the wind velocity and direction, the most important factors influencing the dynamic response to wind excitation of a Cable Supported Bridge are the shape of the bridge girder/deck and the flexural and torsional stiffness of the whole structural system. Thus modern Cable Supported Bridges can be classified also on the basis of configuration of the girder, which can feature an aerodynamic shape and a large slenderness, thus avoiding the possibility of destructive oscillations by reducing the forces and the vortex shedding produced by the wind flow across the bridge deck, or it can consist of a massive truss, providing to the system a large flexural and torsional stiffness which increases the value of the critical wind velocity leading to the start of aeroelastic phenomena.

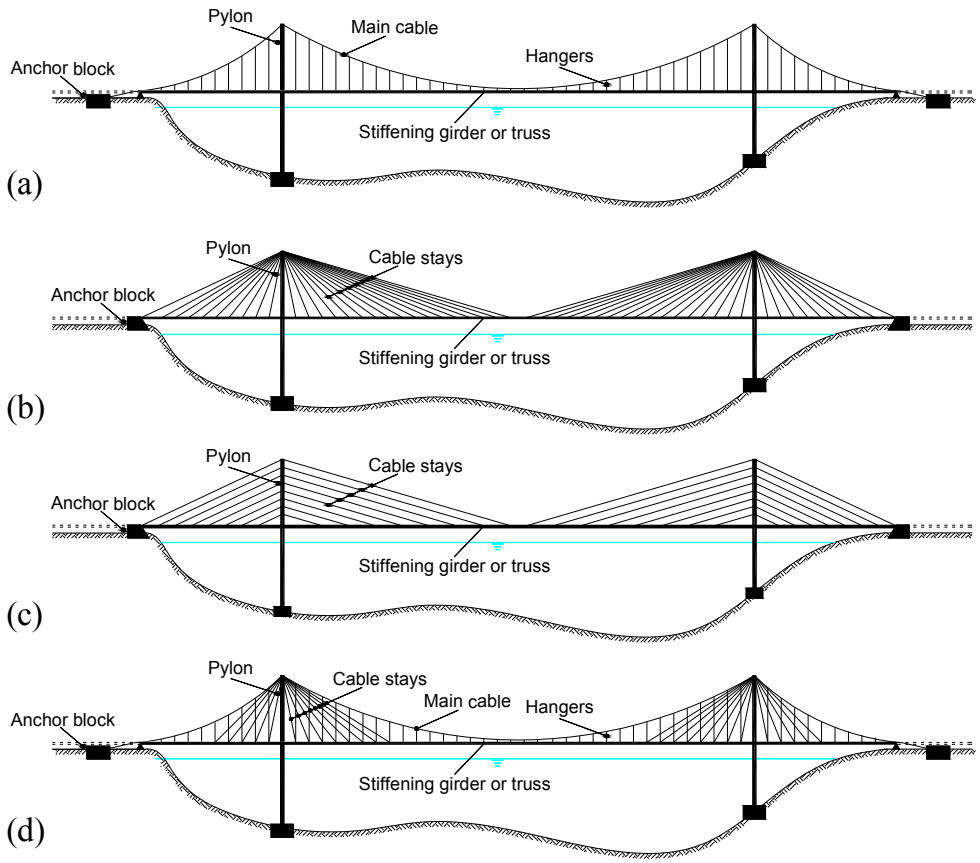

Figure 1.2. Cable Supported Bridges typologies: (a) Suspension Bridge; (b) Fan type Cable-stayed Bridge; (c) Harp type Cable-stayed Bridge; (d) Combined system.

The current trend in the design of long span Cable Supported Bridges is to have a stiffening girder of the first type, thus with a cross-section shaped to feature optimal aerodynamic performances. As a matter of fact, the most ambitious designs of CSBs (in particular, suspension bridges) developed in the recent years are characterized by an aerodynamic bridge deck.

Above all, it is worth to mention the final design of the Suspension Bridge in the Strait of Messina (Italy), having a main span long 3300 m, which would thus become the bridge featuring the larger main span length in the world. The Messina Strait Bridge (Figure 1.3a) is arranged as a single span suspension

bridge with two short side spans, due to local topography (Jensen, 2009) and its suspension cable system is made up of two twin main cables having a diameter of 1,20 m and a sag to span ratio equal to 1:11, leading to large quantities of cable steel but also stiffening the system with respect to the live loads presence (Gimsing, 1996). The Messina Bridge girder (Figure 1.3b) is composed of three shallow longitudinal boxes having a depth of about 2,5 m and characterized by a very high degree of streamlining through application of gently curved bottom plates. These three longitudinal boxes are connected between each other by means of box-shaped cross girders placed every 30 m and having a maximum depth in their central part equal to 4,68 m. Open grids are located in the areas located between the longitudinal and cross box girders, thus allowing for an almost undisturbed flow of air between top and bottom. The design of this girder constitutes the most advanced application of the principle of shaping the girder of a Cable Supported Bridge in order to obtain a critical wind velocity being adequately larger than the maximum expected in site and it was developed through an intensive full model testing in the wind tunnel. However, it is important to underline that the choice of considering a stiffening girder featuring an extremely large value of slenderness of 1/1320 (i.e. the ratio between the girder depth and the main span length) is still largely discussed and criticized in the scientific field (Mazzolani, 2005), in particular considering that the Messina Bridge is planned to carry both motorways and railways.

The same solution of stiffening girder has been considered for other designs of Suspension Bridges of large dimensions, such as the Yemen-Dijibouti Bridge, featuring four main spans of 2700 m (Jensen, 2009), and the Strait of Gibraltar Bridge proposal (COWI, 1995), a 27 km long bridge featuring three main spans having a record length of 3500 m.

When such large spans are considered, like in the cases of the Messina Strait and the Gibraltar Strait, traditional steel for cables is not anymore an effective material for the cable system of a Cable Supported Bridges, as a large part of the wire strength would be used to carry the own weight of the cables (Gimsing, 1996). In this perspective, it seems to be promising to use innovative materials, such as Kevlar fibers or Fiber Reinforced Polymers (FRP), to build the cable system of long span CSBs; in fact these materials are characterized by a strength-to-weight ratio being considerably higher than

steel. However, these innovative materials are currently too expensive and their performance in terms of durability is not adequately known, thus excluding their use in the next years.

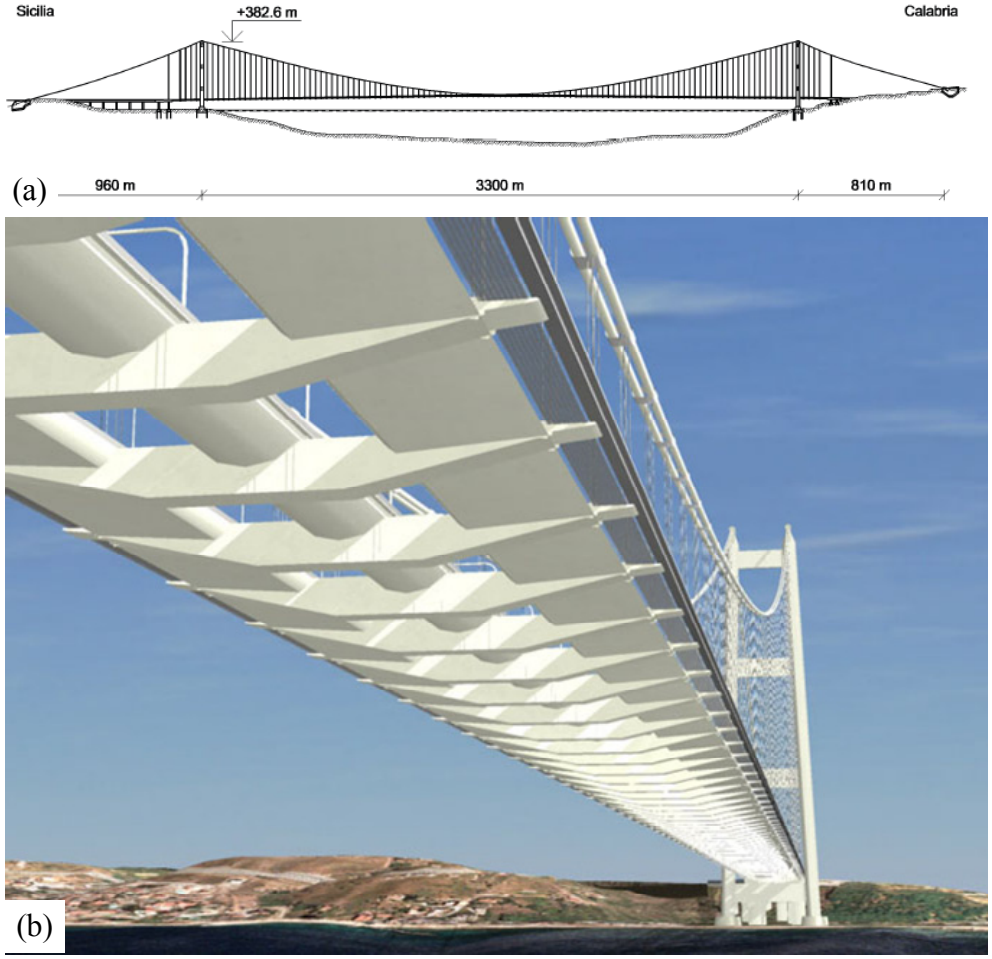

Figure 1.3. Messina Strait Suspension Bridge: (a) longitudinal lay-out; (b) perspective view from below.

Even though streamlined stiffening girders are more widely used in modern designs of CSBs, the Akashi Kaikyo Bridge (Figure 1.4), currently featuring the longer main span (1991 m), features a huge (and bluff-shaped)

stiffening truss, made up with 90000 tons of steel and able to withstand wind velocities up to 286 km/h and 8.5 Richter scale earthquakes. One of the most important reasons for choosing a heavy truss in order to achieve aerodynamic stability of the bridge is the large side-to-main span ratio, leading to a large deformability of the suspension cable system. It is important to underline that the Akashi Kaikyo Bridge is not designed to hold any railways.

Figure 1.4. View of the Akashi Kaikyo Bridge.

The problems related to the aerodynamic stability of Cable Supported Bridges featuring long spans could be solved by using a tri-dimensional configuration of the cable system, which would thus support the bridge also laterally. In this way the lateral and torsional stiffness of the structural system would be increased sufficiently, so that aeroelastic stability phenomena would be avoided. Spatial cable system have already been built in pipeline bridges, as the pipes feature a negligible lateral stiffness, and have only been proposed for normal bridges (Gimsing, 1996).

A particularly innovative and futuristic solution of Cable Supported Bridge featuring a tri-dimensional cable system was recently proposed by the Italian engineer Marco Peroni (2005) for the Gibraltar Strait (Figure 1.5) and Messina Strait Crossing. Peroni conceived an elaborated tri-dimensional

tensile structure made up of FRP cables supporting three independent box-shaped decks having a streamlined shape; the main cable net has the shape of an hyperboloid and is made up of cables whose diameter is equal to 2,5 m and is supported by extremely high towers (for the Gibraltar Strait the tower height is set to 1500 m). This structural system would be extremely stiff both flexurally and torsionally, despite of the extremely large values of the main span length (10 km for the Gibraltar Strait, 6 km for the Messina Strait).

These solutions, though innovative and fascinating, do not seem to be actually feasible as their cost seems to be considerably large at a first glance and, moreover, their environmental impact would be enormous, especially under the visual point of view.

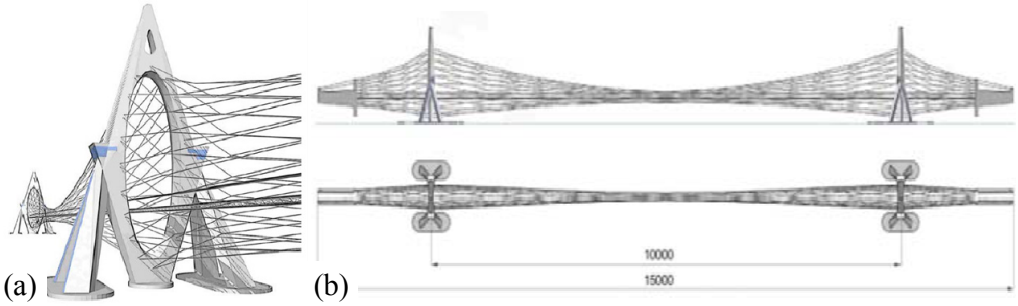

Figure 1.5. Gibraltar Strait Bridge as proposed by Peroni (2005): (a) perspective view; (b) bridge lay-out.

1.1.3 Underground Tunnels

Underground tunnels are galleries bored in the ground below the seabed and represent a crossing solution widely used in the past and still of great importance in waterway crossings practice. Underground tunnels are generally preferred to bridges when large distances have to be surpassed and intermediate piers could not be placed along the crossing path because they would interfere with the navigating vessels or when the urban zones adjacent to the crossings are densely built and populated, as the downward ramp leading to a tunnel leaves a smaller footprint compared to the upward ramps required by most bridges.

Probably the most famous example of Underground Tunnel is the "Channel Tunnel" (Figure 1.6), linking the United Kingdom France beneath the English Channel at the Strait of Dover. The Channel Tunnel, opened in 1998, has a total length of 50,5 km and an underwater length of 37,9 km, it being the longest underwater portion of a tunnel in the world; and it carries high-speed passenger trains and international freight trains. It is composed of two single track and single direction railway tunnels, 7.6m in diameter and 30m apart (Figure 1.6) and connected to a central service tunnel by cross-passages situated every 375m. The service tunnel has a diameter of 4,8 m and lies between the two rail tunnels 15m away from each of them, allowing the access to maintenance and emergency rescue teams and serving as a safe haven if passengers need to be evacuated in an incident.

Figure 1.6. View of the Channel Tunnel, connecting the UK and France.

Under a bilateral Cooperation Agreement (24th October 1980), the Governments of Spain and Morocco started to jointly carry out a process of studies on the feasibility of a fixed link between Europe and Africa across the Strait of Gibraltar (Pliego, 2005). Among various possible solutions, the Suspension Bridge (see section 1.1.2) and the Underground Tunnel (Figure 1.7) ones were preliminary selected; afterwards a comparison between the two solutions led to the selection of the latter for further development in the study process. The reasons for this selection were mainly related to technological experience, interference with maritime traffic in the Strait, security and environmental criteria, and, ultimately, cost effectiveness in foreseeable time horizons.

In 2006, Lombardi Engineering Ltd. won the contract to design the underwater tunnel, which will be similar to the Channel Tunnel solution, a bored, multi-tube rail tunnel (Pliego, 2006).

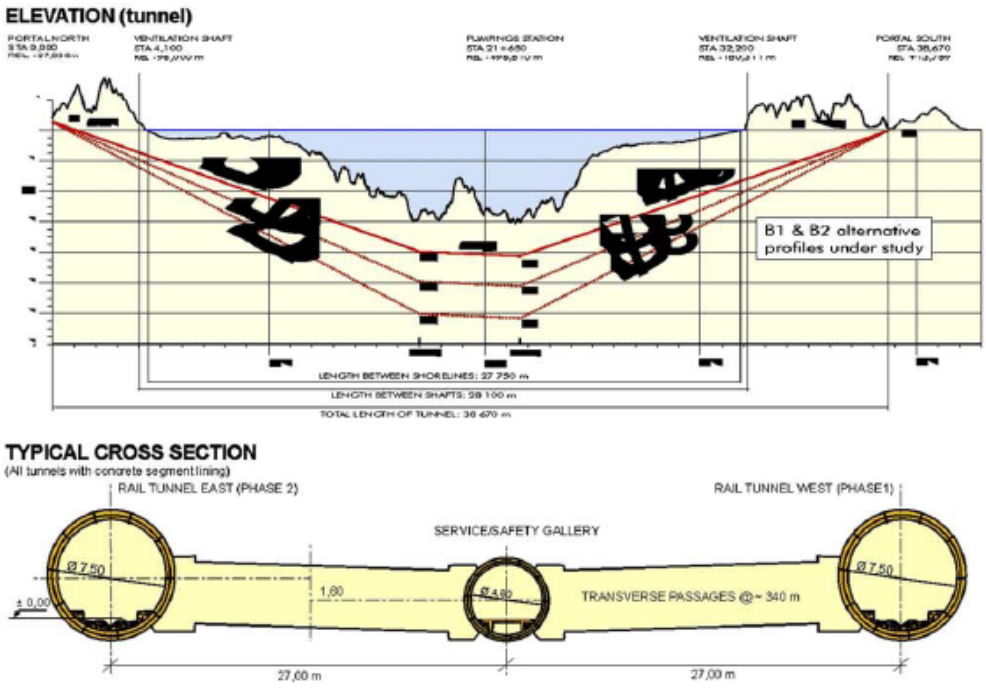

Figure 1.7. Longitudinal profile and cross-section of the preliminary design of The Gibraltar Strait Tunnel (Pliego, 2005).

1.1.4 Immersed Tunnels

Immersed Tunnels represent an additional way to cross a waterway by tunneling, whose main differences with Underground Tunnels are that they are modular structures assembled on site and that they are not bored below the seabed level, but they are placed directly on the seabed (Figure 1.8) . This type of structure, which might sound as an unusual structural solution, was actually proposed for the first time in 1810 by the British engineer CharlesWyatt and

then built in 1910 (Grantz, 1997). Since that date, over 150 Immersed Tunnels have been successfully built and are still functioning .

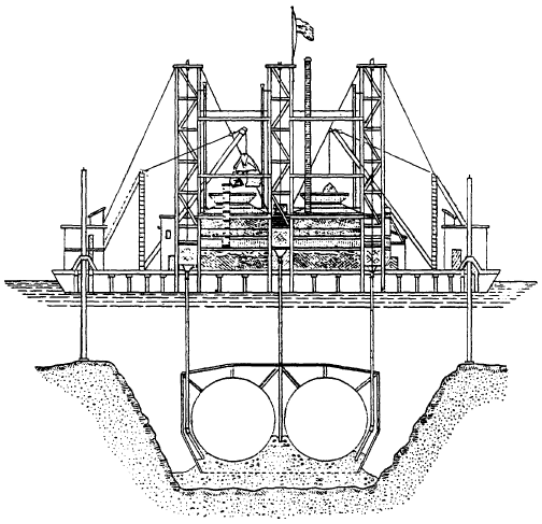

Figure 1.8. Placement procedure of a module of the Detroit River Tunnel (Grantz, 1997)

The construction procedure of an Immersed tunnel is the following:

1) a trench is dredged in the bed of the water channel;
2) tunnel elements are constructed in the dry, for example in a casting basin, a fabrication yard, on a ship-lift platform or in a factory unit. The tunnel modules can be made of concrete or with a composite concrete-steel shell structure (Saveur, Grantz, 1997).
3) the ends of the element are then temporarily sealed with bulkheads;
4) each tunnel element is transported to the tunnel site, usually floating, occasionally on a barge, or assisted by cranes;
5) the tunnel element is lowered to its final place on the bottom of the dredged trench;
6) the new element is placed against the previous element under water. Water is then pumped out of the space between the bulkheads;

7) water pressure on the free end of the new element compresses the rubber seal, already installed at the end of one of the two modules, between the two elements, closing the inter-modular joint;
8) backfill material is placed beside and over the tunnel to fill the trench and permanently bury the tunnel;
9) the end tunnel modules can be connected to the approach structures, usually bored tunnels, built on the shores.

Several important Immersed Tunnels, exploiting the most advanced technologies in this field, are currently under construction. Worth to be mentioned are the one being part of the Busan-Geoje Fixed Link (South Korea) and the Marmaray Tunnel, under construction in the Bosporus Strait (Turkey). The Busan – Geoje Fixed Link (Figure 1.9) will provide a road connection between the metropolis of Busan and Geoje Island. The Link comprises, besides of the Immersed Tunnel, two cable stayed bridges

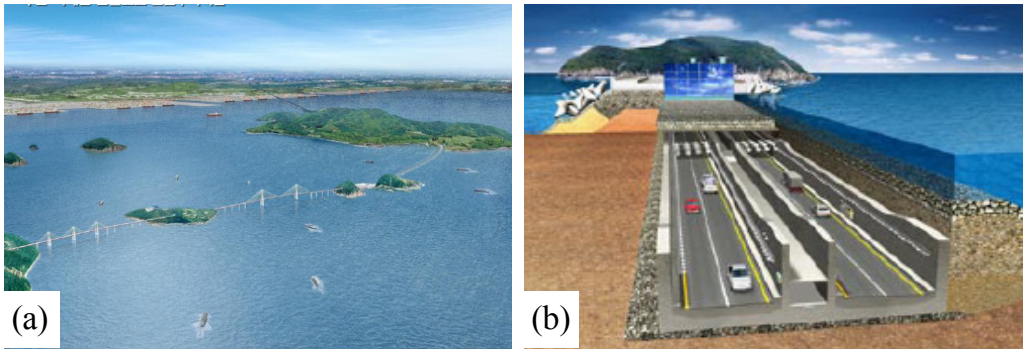

Figure 1.9. The Busan – Geoje Fixed Link: (a) overall view; section of the Immersed Tunnel (COWI, 2009).

The Busan-Geoje Immersed Tunnel, constructed as a concrete tunnel, has a number of special features: its length of 3,3 km, the large water depth, the severe marine conditions, the soft subsoil and alignment constraints, that, combined with the scale of the project, made the design and the construction of the tunnel a major challenge (Janssen et al., 2006). Several special methods have been applied to overcome the above mentioned difficulties, which will be of great importance in the future constructions of Immersed Tunnels (Kim et al., 2009). The tunnel, consisting of 18 precast tunnel elements placed

within a dredged trench at a maximum water depth of 50 m, is almost completed and constitutes the deepest Immersed Tunnel currently existing in the world.

However the maximum depth record of the Busan – Goeje Tunnel will be surpassed in few years by the Marmaray Immersed Tunnel, currently under construction (its completion is foreseen in 2013), which will be placed at 58 m below the water surface of the Bosporus Strait (Grantz, Iversen, 2009). The tunnel, which will feature a length of 1.4 km, will be assembled from 11 sections, each one being long 130 m and weighing up to 18,000 tons.

1.2 THE CONCEPT OF SUBMERGED FLOATING TUNNEL (SFT)

The Submerged Floating Tunnel (SFT), also known as Archimedes' Bridge, fundamentally consists in a tubular structure floating at an immersion depth, assuring a minimal water clearance in order to allow the free passage of the surface navigating vessels. It is fixed in position through anchorage systems made up of cables, rods or piles connected to the seabed, or buoys floating over the free water surface (Figure 1.10). The tunnel is permanently subjected to its own weight and to the buoyancy assured by the presence of the water; generally the tunnel cross section is designed so that the buoyancy overcomes the structural weight and the tunnel is then subjected to a volume force directed upward. In this case the anchorage system can be composed of tension legs or cables, to which the residual buoyancy confers a fundamental pretension state. The tether systems play also the role of constraining the tunnel, minimizing its displacements and stresses induced by the environmental loadings, such as the hydrodynamic and seismic actions, that can be particularly severe in case of sea strait crossings.

The SFT idea was born in the early decades of 1900 in Norway, but only the great improvements achieved in offshore and deep sea technologies in the last thirty years allowed to solve the numerous problems that hampered the realization of this kind of structure, so that several preliminary designs and feasibility studies have been proposed in the last years. Also the large experience gained in the field of Immersed Tunnels can be capitalised for the development of SFT, these two waterway crossing typologies being both

modular structures in which the joints have to be waterproofed, even if the dynamic behaviour of SFT is certainly more complex than the one of the Immersed Tunnel.

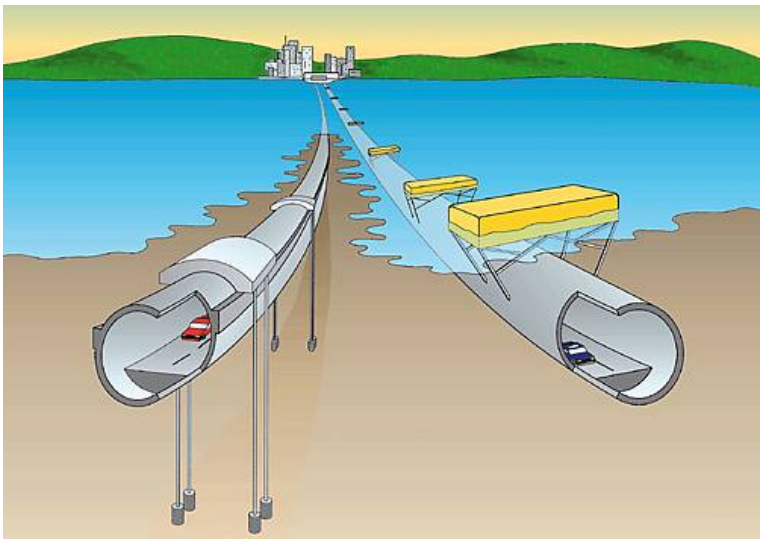

Figure 1.1 The SFT waterway crossing solution

With respect to traditional strait crossing solutions, the SFT undoubtedly features several advantages under the structural, economical and environmental impact point of view. However, the actual construction of a Submerged Floating Tunnel appears nowadays as a real challenge, since it deals with a completely innovative structural solution. A probably natural wariness is due to the fact that no SFT has been erected up to today. Consequently, no experimental data on its actual behaviour are available, which could fill the gap between the theoretical studies on SFT and its construction.

Based on the above considerations, it is apparent that the first necessary step for the actual development of Submerged Floating Tunnels, as a widespread technical solution for waterway crossings, is represented by the design and construction of a full-scale SFT prototype, useful for collecting the experimental data needed to support the numerical and theoretical studies, and for the complete comprehension of the actual behaviour of this kind of

structures. This important initial step is going to be undertaken in the near future, since a Sino-Italian joint venture (SIJLAB – Sino-Italian Joint Laboratory of Archimede's Bridge) has carried out the executive design of the first SFT prototype in the World (Mazzolani et al., 2007a, b) to be fabricated and erected in the Qiandao Lake (People's Republic of China) in the next years.

Chapter 2
A revolutionary solution: the Submerged Floating Tunnel

2.1 MAIN STRUCTURAL FEATURES

2.1.1 *Tunnel structure and cross-section*

2.1.1.1. *Design requisites*

The choice of the structural configuration of the tunnel and the definition of the geometrical and functional arrangement of its cross-section is one of the main aspects to be faced in the design of a Submerged Floating Tunnel.

The design of the of the tunnel structure and geometry of a SFT must be made according to some requisites:

1) The internal dimensions of the cross section should be large enough to accommodate the infrastructures, facilities and implants (ventilation, safety and fire systems, electrical implants) necessary to guarantee the normal development of the operations inside.
2) The structure of the tunnel cross-section must be designed in order to ensure enough stiffness, strength, ductility so that the desired structural performances are met, in terms of serviceability and safety. Moreover, waterproofing of the tunnel and its durability have to be assured.
3) The tunnel cross sections has to be designed so that the buoyancy ratio, which is the ratio between the buoyancy acting on the tunnel and the sum

of the permanent weights and live loads (for those design load combinations involving them), is larger than a minimum value.

This design condition is aimed at conveniently limiting inferiorly the residual buoyancy, which is the algebraic sum of the permanent loads, live loads and the buoyancy of the tunnel and is thus determined by the external dimensions and the internal arrangement of the cross sections, by the materials used and by the destination of use (determining the live loads acting on the tunnel). In fact it is necessary to ensure a minimum value of the residual buoyancy in operational condition so that so that no slackening of the anchorages can be induced by the environmental actions (i.e., hydrodynamic or seismic ones). Clearly this design criterion applies only when a positive (upward) residual buoyancy is assumed, whereas for SFTs conceived to be heavier than the water they displace, a different criterion has to be considered.

Moreover, in the design process it must be taken into account that the external dimensions of the cross section influence the amount of the hydrodynamic actions.

4) All the issues related to the fabrication and erection of the tunnel modules have to be considered in the design.

The third design requisite is of particular importance and deserves a more detailed discussion. In literature usually only a lower limit of the buoyancy ratio is usually considered and the eventuality of the slackening of any anchorage of the SFT is assumed as a condition to be absolutely avoided; as a matter of fact very large values of the lower limit of the buoyancy ratio were considered in the first studies and preliminary designs, up to 1,70. Numerical studies confirmed that larger values of the buoyancy ratio can improve noticeably the structural performance of the SFTs when they are subjected to severe environmental loading scenarios; in particular Brancaleoni et al. (1989) found that increasing the buoyancy ratio from 1,25 to 1,40 can lead to impressive improvements of the SFT response to extremely severe sea states.

Figure 2.1 provides a flow chart schematically describing the procedure to be followed in the geometrical design of the cross-section of a SFT, in particular to satisfy pre-requisites 1 and 3. Given the functional requirements for the crossing of interest (i.e. the infrastructures to be accommodated inside

the tunnel such as motorways, railways, escape ways, etc.) and once the materials to be used and the external shape of the tunnel are defined, a preliminary design can be carried out, determining relevant quantities like the tunnel buoyancy B_1 and own weight $g_{s,1}$. Established the limit α_1 for the minimum allowable value of the buoyancy ratio, it is thus possible to calculate the quantity of ballast $g_{b,1}$ needed (if needed) in order to impose the condition $R_{w,min}= \alpha_1$, which can be considered as a target value of the buoyancy ratio as it would ensure the required minimum pre-tensioning of the anchorages and at the same time it minimizes the permanent stress acting in the tunnel and, above all, in the anchorages and foundations.

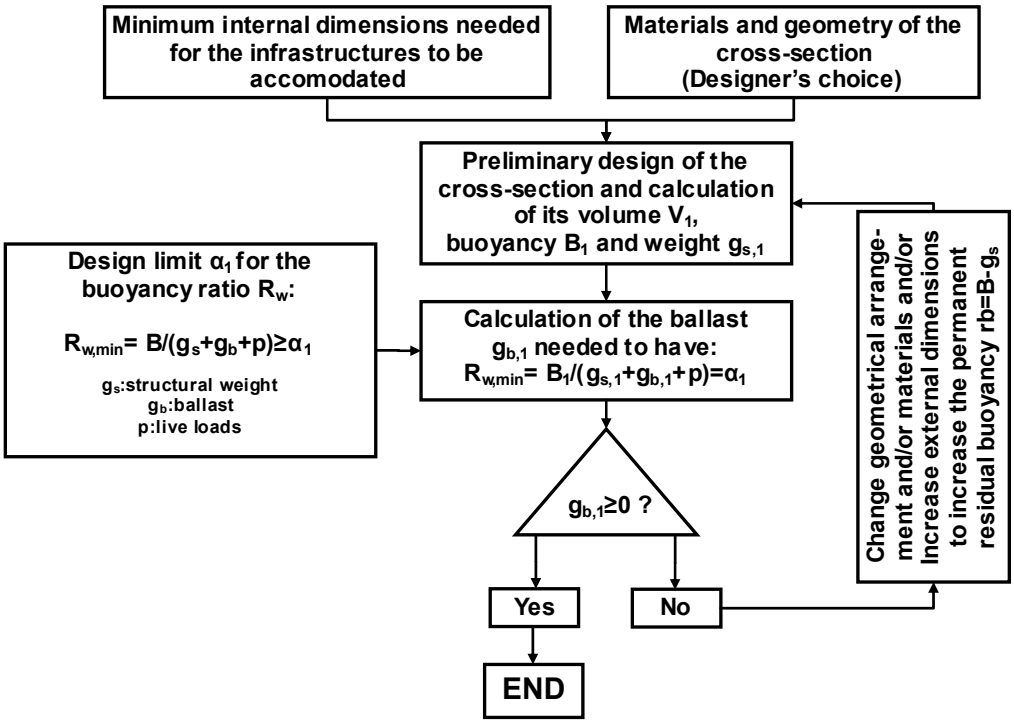

Figure 2.1. Flow chart for the conceptual design of the cross-section of a SFT.

If the outcome is $g_{b,1}<0$, it means that not enough buoyancy is provided, as it corresponds to the condition $B_1< \alpha_1 (g_{s,1}+p)$. Therefore it is necessary to increase the residual buoyancy of the tunnel, goal that can be achieved by one or a combination of the following changes:

- increase the external dimensions of the cross-section, thus increasing its buoyancy;
- reduce, if possible, the dimensions of the internal structural elements (i.e. inner walls or slabs, et cetera) in order to reduce the tunnel permanent weight;
- choose lighter materials, if possible, in order to reduce the tunnel permanent weight.

Once the condition on the minimum value of the buoyancy ratio is met and the needed ballast quantity is determined, the geometrical preliminary design of the SFT cross-section is concluded, provided that the internal spaces where the ballast is meant to be located are large enough to accommodate its necessary quantity.

In order to limit the permanent value of the residual buoyancy, and thus the permanent stress acting in the structure, it could seem rational at a first glance also a maximum value of the buoyancy ratio, as it was done for the design of the Archimedes' Bridge Prototype in Qiandao Lake, whose cross-section arrangement was made in order to have a buoyancy ratio larger than 1,20 and lower than 1,30, leading to a rational tunnel configuration and to an adequate performance of the anchorage cables under the action of waves, currents or earthquakes (Mazzolani et al., 2007, 2008).

However the AB prototype in Qiandao Lake constitutes a particular case, as it is a small pedestrian crossing. When a more complicated internal geometrical arrangement of the cross-section and larger inner spaces are needed, imposing a maximum design value for the buoyancy ratio may prove to be counterproductive, as it can lead to larger values of the residual buoyancy permanently acting on the tunnel. As a matter of fact at the end of the previously described design process it is also necessary to check if the condition $R_{w,max} \leq \alpha_2$ is met.

In case this condition is not satisfied, it is necessary to re-arrange the geometry of the cross-section, increasing its internal and external dimensions. Enlarging the tunnel-cross section in order to reduce the maximum value of the ratio of buoyancy might seem contradictory, but it has to be considered as the only way that can lead to the respect of both limiting the extreme values of this ratio, once the internal spaces needed for the internal infrastructures and the materials and cross-section shape are given. In order to have an indication

of the cross-section dimensions needed to fulfil the buoyancy ratio limits, it is possible to consider them as equal to the original ones multiplied by a scaling factor larger than one, named β, and to assume that the updated values of the buoyancy B_2 and permanent weight $g_{s,2}$ are equal to the previous ones multiplied by the same scaling factor. Therefore, imposing the two aforementioned conditions on the minimum and maximum value of the buoyancy ratio, it is possible to determine the value of the updated ballast quantity $g_{b,2}$ and of the scaling factor β.
If the initial configuration of the cross-section leads to a maximum buoyancy ratio $R_{w,max,1}>\alpha_2$, the ballast quantity $g_{b,1}$ and the permanent residual buoyancy rb_1 are equal to:

$$g_{b,1} = \frac{B_1 - \alpha_1 \cdot (g_{s,1} + p)}{\alpha_1} \tag{2.1}$$

$$rb_1 = B_1 - (g_{s,1} + g_{b,1}) = B_1 \cdot \left(1 - \frac{1}{\alpha_1}\right) + p \tag{2.2}$$

Enlarging the cross-section dimensions by scaling them by the factor β, the permanent residual buoyancy becomes:

$$rb_2 = \beta \cdot B_1 - (\beta \cdot g_{s,1} + g_{b,2}) = \beta \cdot B_1 \cdot \left(1 - \frac{1}{\alpha_1}\right) + p \tag{2.3}$$

Therefore the ratio between rb_2 and rb_1 is equal to:

$$\frac{rb_2}{rb_1} = \left. \beta \cdot B_1 \cdot \left(1 - \frac{1}{\alpha_1}\right) + p \right/ B_1 \cdot \left(1 - \frac{1}{\alpha_1}\right) + p > 1 \tag{2.4}$$

thus corresponding to an increment of the permanent residual buoyancy and stress regime of the tunnel.

2.1.1.2. *Materials*

The selection of the materials to be used to build a Submerged Floating Tunnel must be made accordingly to the structural and functional performances which are intended to be ensured, but it has also to be a

compromise among several factors such as the resistance to the marine environment, fabrication, assembly and maintenance issues, time needed for the supply, material and constructional cost, et cetera (FEHRL, 1996).

The structural solution can be optimized, considering the structural effectiveness, the constructability and the economical point of views: it is possible to conceive a SFT featuring a composite structure involving several materials, so that their defects are neutralized and their benefits exalted (Faggiano et al., 2005).

The materials that could be suitably used in the construction of the tunnel modules of a SFT are:

- Steel;
- (Reinforced) Concrete;
- Pre-compressed Reinforced Concrete;
- Aluminum alloys;
- Rubber foam.

Ordinary steel types and concrete are particularly suitable for SFT applications, as they are widely used in offshore structures and thus their performances are largely experienced, also concerning the long term behaviour.

Steel features several characteristics making it a very suitable material for offshore and SFT constructions, such as: good mechanical properties, good resistance to fatigue and abrasion, good workability and weldability and a large strength-to-weight ratio.

However, ordinary steel grades have also some defects, like the low resistance to corrosion, low performance of the welded connections with respect to fatigue due to the cyclic loads imposed by environmental actions. In order to improve its performances in maritime applications new types of steel have been introduced, featuring a lower content of carbon and resistant to corrosion, whose main problem seems to be only the difficulty to produce them in large scale (Ramasco et al., 1991). New production technologies led to the development of a new type of steel, named Fatigue Crack Arrester (FCA), whose microstructure ensures a better resistance to the propagation of fatigue cracks, especially in the welded joints, assuring also a strength slightly larger and a weldability equivalent to those of ordinary steel (Arimochi et al., 2003). Other new steel types, characterized by high strength and resilience,

have been lately developed and produced in large scale for the purpose of widely using them in the offshore field (Adachi et al., 2003).

Almost every structural component of a Submerged Floating Tunnel can be made up of steel, but its most suitable and reasonable application are in steel sheets to be combined with reinforced concrete, thus realizing a steel-concrete composite tunnel structure (Faggiano et al., 2005). Also, steel is certainly the most suitable material to be used for the connections between the anchorages and the tunnel structure, thanks to its high strength and good resistance to fatigue (Faggiano and Mazzolani, 2001). The combination of steel shells and concrete is widely and successfully used in the production of Immersed Tunnels modules (Saveur and Grantz, 1997).

Concrete is also widely used in maritime applications and its use is greatly recommended when a large structural weight is required in order to stabilize the structure. This is particularly true for SFTs, where concrete can be used to contribute to the structural strength and stiffness and, at the same time, to provide the weight needed to counteract the tunnel buoyancy. Other advantages offered by concrete are: good resistance to the corrosion in marine environment, to abrasion and to fire and high temperatures, low cost and possibility to be cast to realize complex shapes. Its main defect is its negligible resistance to tensile stresses. Pre-compression is largely applied to concrete offshore structures, as it leads to better mechanical performances and, above all, to a larger degree of waterproofing.

Another class of materials used in offshore engineering is the one of aluminium alloys, which offer a wide range of strength, comparable to the one of steel grades, feature a specific weight relatively low, it being equal to 1/3 of the one of steel, a good workability and, above all, a high resistance to marine corrosion, thus eliminating every need for protective coatings. Unfortunately, aluminium alloys feature also some disadvantages, such as the poor resistance to fire and a stiffness lower than steel. Their main application in offshore structures is in the emerged part of the offshore platforms, thus exploiting their resistance to corrosion and resilience. A similar use has been foreseen in the design of the Archimedes Bridge prototype in Qiandao Lake, which features an external layer made up of aluminium extruded elements, whose function is to protect the internal layers from corrosion and external impacts (Mazzolani et al., 2007, 2008, 2010).

Finally, the last material worth to be mentioned is the rubber foam, which is a porous rubber made up of expanded polyurethane used in the Naval Engineering to increase the buoyancy of vessels. This material has been considered for applications in SFTs by Grantz (2003) to create an external layer protecting the inner structure from corrosion and external impacts and increasing the tunnel buoyancy. In fact this material is extremely light and is also able to dissipate the energy transmitted by external impacts.

2.1.1.3. *Structural configurations*

The structural configurations of the tunnel can be categorized according to their geometrical arrangement and the materials involved.

In particular, concerning the geometrical arrangement, it is of great importance the external shape of the SFT cross-section. As a matter of fact its geometrical property significantly affects the interaction of the structure with the surrounding water, both considering the static and dynamic point of view, and also the module production procedures.

The geometrical configuration of an SFT cross section can be of the following types:

- circular (Figure 2.1);
- polygonal or elliptical, elongated in the horizontal direction (Figure 2.2);
- rectangular, with external keels providing a hydrodynamic shape (Figure 2.3);
- circular tubes connected by a frame substructure and enclosed inside an external shell having a streamlined shape (Figure 2.4).

Circular cross-sections have been often considered in SFT preliminary designs and feasibility studies, such as, for instance, the ones for the Messina Strait crossings (Figure 2.1a; Scolari et al, 1989), the Høgsfjord (Figure 2.1.b; Skorpa and Østlid, 2001) and Sulafjord (Figure 2.1c; Jakobsen et al., 2009) crossings. A circular cross-section features a very rational structural behaviour with respect to the hydrostatic pressure (Brancaleoni et al., 1989; Grantz, 1997), as this induces only compressive stresses and no bending in the cross-section plane. Since generally the outer ring shell of a circular SFT is at least partially made up of concrete, this is a great advantage, since no longitudinal cracks are produced by the hydrostatic pressure, thus not compromising the tunnel waterproofing. Moreover a circular cross-section features a good

response with respect to hydro-elastic stability issues, since, thanks to its polar symmetry, it should not be subjected to flutter or torsional divergence phenomena (Solari, 2010). On the other hand such a geometrical shape requires more complicated construction procedures than a rectangular cross-section (Saveur and Grantz, 1997).

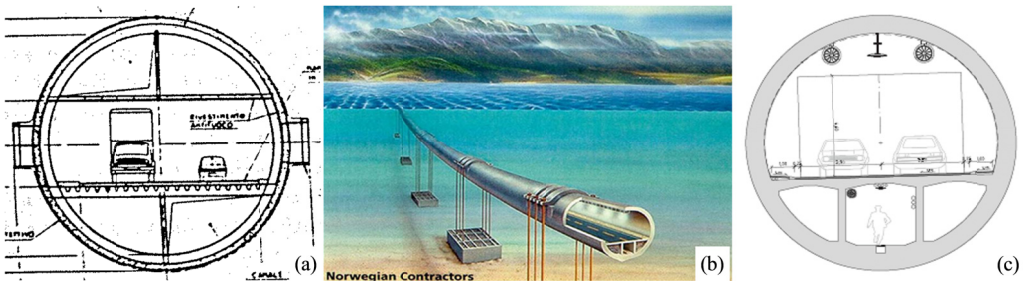

Figure 2.1. SFT preliminary designs featuring a circular cross-section: (a) Messina Strait crossing (Italy) as proposed by ATI-SSST (Scolari et al, 1989); (b) Høgsjord crossing (Norway), Norwegian Contractors proposal (Skorpa, Østlid, 2001); (c) Sulafjord crossing (Norway; Jakobsen et al., 2009).

Cross-section shapes elongated in the horizontal direction, such as polygonal or elliptical ones have been considered too, as they represent a suitable solution in those case where large water motion due to currents and waves is expected in the horizontal direction; in fact these shapes obviously implies larger values of stiffness and strength in the horizontal bending plan and should ensure a good hydrodynamic behavior. Clearly the construction procedures of the tunnel modules having an elliptical cross-section shape are more complicated than polygonal ones.

Figure 2.2. shows some examples of SFT crossing proposals featuring a polygonal or elliptical cross-section shape.

Rectangular cross-sections would represent the most rational solution, considering the easiness of the production procedures and the versatility in the organization of the internal spaces and facilities. As a matter of fact, nowadays this is the geometrical configuration most widely used for Immersed Tunnels, which, however, are not subjected to hydrodynamic actions. The water flow passing through a rectangular SFT would generate turbulences, thus increasing the regime of dynamic pressures induced on the

structure. In order to solve this problem, it is possible to provide the rectangular tunnel with lateral streamlined keels, which can be made up of steel sheets and trusses, as showed in the sketch given in Figure 2.3a. This solution would improved the fluid dynamic behavior of the tunnel, preserving the advantages of a rectangular cross-section. A similar idea is the one realized in the Tsing Ma Bridge, Hong Kong, whose stiffening truss has the peculiarity of being equipped with two side triangular brackets covered by non-participating stainless steel shells, which improve the aerodynamic properties of the girder (Figure 2.3b).

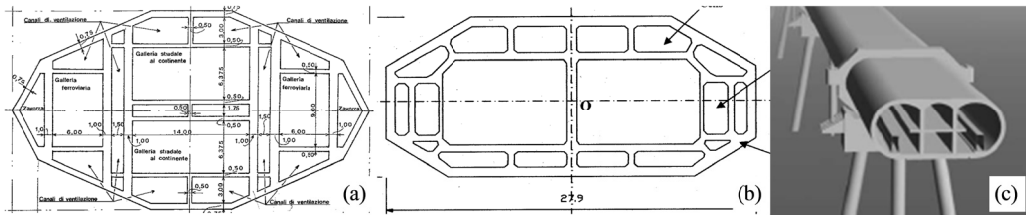

Figure 2.2. SFT preliminary designs featuring polygonal or elliptical cross-section: (a) Messina Strait crossing (Italy) as proposed by Ponte di Archimede S.p.A. (Ponte di Archimede S.p.A., 1984); (b) Jintang Strait crossing (P.R. of China; Faggiano et al., 2001a); (c) Washington Lake crossing (U.S.A.; Felch et al., 2001).

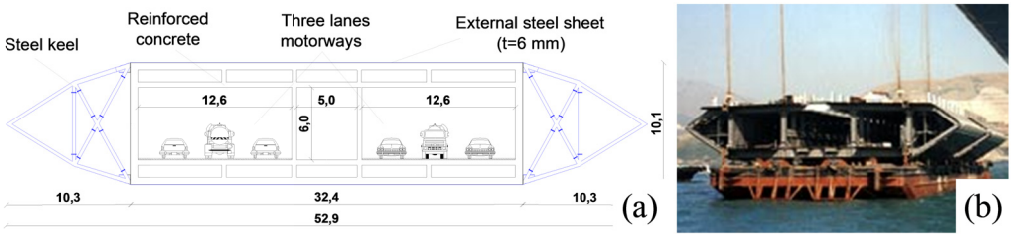

Figure 2.3. (a) SFT rectangular cross-section equipped with streamlined lateral steel keels; (b) segment of the Tsing Ma Bridge (Hong Kong) truss.

Another suitable option for the geometrical configuration of the SFT cross-section is to have one or more circular tubes holding the required traffic lanes and other related facilities connected to each other through a frame substructure and enclosed inside a streamlined shell. This solution was

envisaged in the first SFT proposal (Figure 2.4a), developed by Alan Grant in 1969 for the Messina Strait crossing and considered again later on, such as in the case of the Northern Japan Exchange Axis (Figure 2.4b).

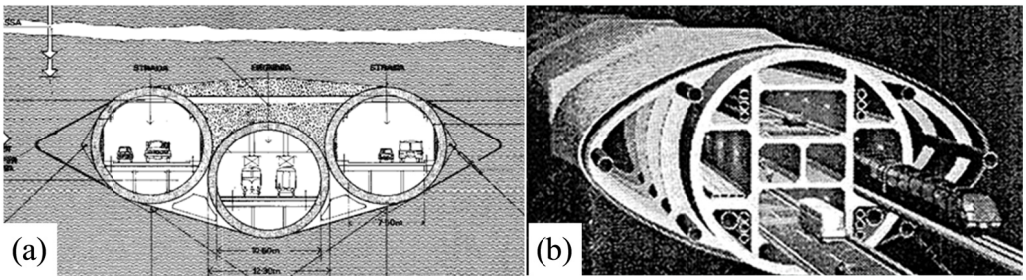

Figure 2.4. SFT proposals featuring a structure composed of circular tubes enclosed inside an external streamlined shell: (a) Messina Strait (Japan) crossing proposal by Grant; (b) Northern Japan Exchange Axis.

Concerning the materials to be used for the various elements of the tunnel structure, the most suitable and rational solutions are, in the author's opinion, the ones who involve more materials, leading to a multi-layer/multi-material composite structure. In this way each material is devoted at a particular function which exalts the material advantages and neutralizes its defects (Faggiano et al. 2001b), with the aim of optimizing the structural and functional behavior.

This kind of solution has been often proposed. One of the most noticeable examples is the Archimedes' Bridge Prototype in Qiandao Lake (Figure 2.5a; Mazzolani et al., 2007, 2008, 2010), which features an internal layer made of steel shells, so that its high mechanical performances are exploited, it being protected from the marine corrosion; an intermediate concrete layer, having the function of protecting steel from corrosion, assuring the ballast weight and cooperating with the steel shells for the axial, bending and shear resistance of the tunnel, the steel and concrete parts acting as a composite structure by means of shear connectors; finally, an external layer of aluminium, protecting the internal structure from corrosion, external impacts and water penetration.

The above described structural configuration, which can be named "sandwich" structure, presents good characteristics of flexural strength both in

elastic and post elastic fields; it is also able to face up without great damages exceptional events, such as internal impacts or explosions.

The most common composite structure solution is similar to the one of the Prototype, with the only difference that usually the also the external layer is made up of steel sheets. This solution is largely used also for Immersed Tunnels, namely double steel shell Immersed Tunnels, where the concrete is normally used only as a ballasting material (Grantz, 1997). The Baltimore Harbour Tunnel (U.S.A.; Grantz, 1997), showed in Figure 2.5b, is an example of double steel shell Immersed Tunnel. A similar solution is the one envisaged by Grant for its SFT proposal (Figure 2.4a): in fact each circular tube has a double steel shell-concrete structure and is enclosed inside an external steel shell having the function of protecting them from impacts and corrosion and of reducing the hydrodynamic actions due to incident wave flows.

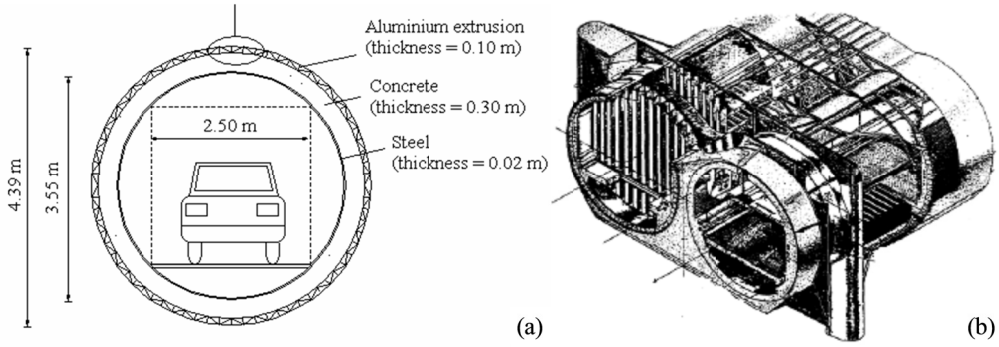

Figure 2.5. (a) Sandwich tunnel structure of the AB prototype in Qiandao Lake (P.R. of China; Mazzolani et al., 2007, 2008, 2010); the Baltimore Harbour Tunnel (U.S.A.; Grantz, 1997).

Another option is to realize the SFT structure entirely in steelwork, using some other material, characterized by large weight and low cost, as ballast. Such a kind of structure has been proposed in the study by Martire et al. (2009a,b): the outer shell is composed of two concentric steel tubes connected by means of stiffening ribs; internally, steel walls strengthen and stiffen the cross-section and the roadway decks are realized through orthotropic steel plates (Figure 2.6a). A similar proposal has been conceived by Grantz (2003): a double steel-shell hull reinforced with r.c. rings on correspondence of the

connections with the tethers and covered with an external layer of rubber foam, protecting and waterproofing the inner structure (Figure 2.6b).

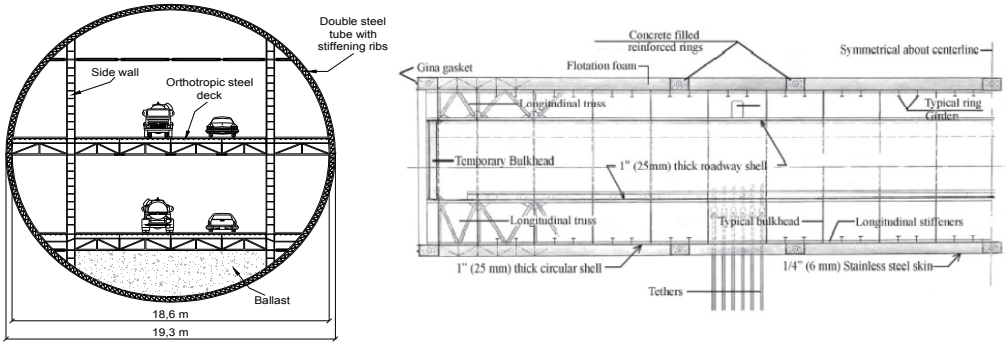

Figure 2.6. SFT entirely made up of steelworks as proposed by:(a) Martire et al. (2009a,b); Grantz (2003).

SFT made only of reinforced concrete, generally pre-compressed, have been proposed too, such as for instance the Messina Strait crossing proposal (Figure 2.2a; Ponte di Archimede S.p.A, 1984) or the Jintang Strait (P.R. of China) crossing (Figure 2.2b; Faggiano et al., 2001a). Clearly in these cases waterproofing becomes the most important issue; no cracks in the concrete can be allowed to take place as no external protection from the water penetration is guaranteed. In the practice of Immersed Tunnels, r.c. tunnels are also widely built, but in most of the cases waterproofing is assured by means a non-structural external layer which can be made of steel, bituminous or plastic membranes (Grantz et al., 1997).

2.1.2 *Anchoring system*

2.1.2.1. *Materials*

The material most suitable to be used for the anchoring system of a SFT is steel, which can be used to realize both rigid members, such as tension legs or tubular tethers, or cables made up of harmonic steel wires. The use of steel anchorages is common practice in Offshore Engineering, steel Tension Leg Platforms and Mobile Production Units moored with steel cables being some

of the most common offshore structures (CMPT, 1998).

In the last years the offshore industry gained experience also concerning innovative materials such as the synthetic fiber ropes, which have the advantage of being lighter than steel wire cables; this feature considerably facilitates their installation and improves their performance in deep waters. In the nineties the American Petroleum Institute (API, 1991), the American Bureau of Shipping (ABS, 1999) and several private companies published guidelines featuring indications about the mechanical properties of cables made up of synthetic fibers and their performance as mooring lines for offshore production unities.

The breaking strength of these materials ranges between 1000 and 4000 MPa. Their behaviour is non-linear as their axial stiffness varies with time; moreover their stiffness seem to be generally larger when subjected to dynamic loads (Banfield et al., 2004). For the aforementioned reasons it seems inappropriate to model their behaviour as elastic and it is recommended to consider different values for their axial stiffness, in particular with regard to its variation with the frequency of the applied dynamic loads (CMPT, 1998).

Synthetic fibers used in offshore applications are Aramid, Carbon and High Performance Polyester fibers. In particular, the latter ones are considered as the emerging material for deepwater mooring lines of offshore drilling platforms (Smith and Williams, 2003). Great attention has been focused on the use of HPP fibers by the United States Mineral Management Service, which promoted three workshop on this topic (Bugg et al., 2003), as mooring lines made up of this material are characterized by high strength, adequate stiffness and low weight, even though they are more prone to be damaged because of surface abrasions, especially during their installation.

Aramid and Carbon fibers feature a large strength – to-weight ratio and adequate stiffness, in particular the latter ones, whose Young's modulus ranges from 290 to 400 GPa, being larger than the one of steel and of the other synthetic fibers.

When it is possible to consider buoys as a suitable anchoring system, also concrete can be included in the list of materials to be considered for their construction.

2.1.2.2. *Typologies and configurations*

The main tasks of the anchoring system of a Submerged Floating Tunnel

are to bear its permanent residual buoyancy (or residual weight) and to hold the tunnel in its position when environmental actions, such as waves, currents and earthquakes, are loading the structure, in order to limit displacements and stresses within acceptable limits.

The direction of the resultant of buoyancy and permanent weight of the tunnel is the main factor determining the choice of the anchoring system typology. In fact, if the residual buoyancy is directed upwards (i.e. the buoyancy overcomes the permanent weights), the anchoring system can be made of tensioned members, such as cable or rigid members groups (Figure 2.7c). Otherwise, if the permanent weight of the structure overcomes its buoyancy (thus giving rise to a residual or net weight), the SFT can be restrained by single piers (Figure 2.7b), group of piles or buoys (Figure 2.7d). In any case the anchoring system is made up of groups of anchorages distributed along the length of the tunnel with a fixed inter-axis, which have to be chosen according to the intensity of the permanent, live and environmental loads. In case of crossings characterized by a limited length and placed in a favourable environment, it is possible to consider to build a self-bearing tunnel, restrained only at its ends (Figure 2.7a); in this configuration the permanent weight of the SFT should be equal to its buoyancy, in order to avoid any permanent stress in the structure.

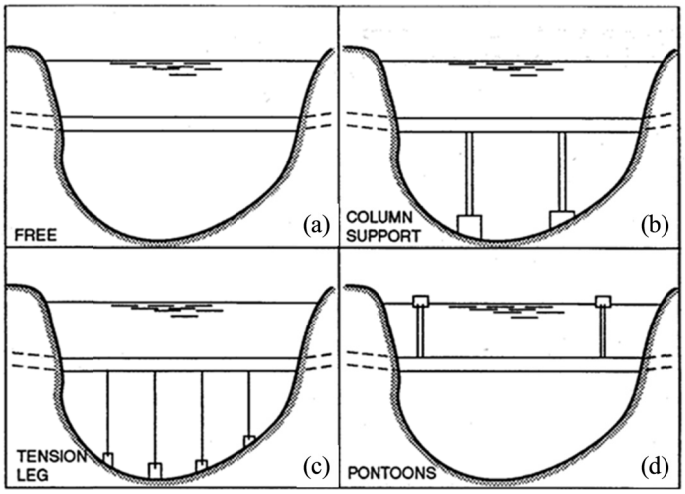

Figure 2.7. SFT Anchoring system typologies: (a) self-bearing tunnel; (b) piers; (c) tensioned members;(d) buoys. (Figure taken from: FEHRL, 1996).

Generally the most suitable design solution is to have a positive upward residual buoyancy and to restrain the SFT through tensioned members, opportunely inclined in the cross-section plane, in particular when it is necessary to provide an efficient lateral support due to severe environmental conditions or in deepwater crossings.

With respect to rigid tubular members, cables seem to be preferable as they feature a negligible bending stiffness and thus they are not subjected to the considerable stress increments induced by biaxial bending in the tubular members. Moreover, many technological drawbacks related to the use of tubular members, such as manufacturing problems due to the large thickness, imperfections, specific controls to test the quality of the welded joints, transport and installation difficulties, would be avoided (Faggiano and Mazzolani, 2001).

In the design of a SFT anchoring system made up of cables, the main choices to be made are related to the geometrical configuration of the cable system, the diameter to be assigned to the cables and the restraint condition to be provided at the ends of the cables.

The cable system of a SFT is usually conceived as a series of cables groups, disposed in the tunnel cross-section plane and repeated along the tunnel axis with a fixed inter-axis. Therefore the cable system restrains effectively the tunnel only in the transversal directions, and its stiffness is largely influenced by the geometrical arrangement of the cables groups. Several configurations have been proposed and tested, such as the ones depicted in Figure 2.8a (borrowed from Maeda et al., 1994), differing from each other by the number of cables involved and their inclination.

Physical predictions suggest that groups made up of two vertical cables configuration is effective only in the vertical direction, thus being suitable only in a calm environment; groups made up of four inclined cables are the most effective ones, as they support the tunnel vertically, horizontally and torsionally. Groups made up of only two sloped cables have been proposed too, but numerical analyses showed that this arrangement leads to high level of stresses in the cables and induces considerable torsional moments in the tunnel when it is subjected to horizontal actions (Martire, 2007). Experimental studies (Maeda et al., 1994) confirmed the physical intuitions, as they showed that wave actions induce limited oscillations of the axial force around its

initial value in vertical cables and that four inclined cables per group guarantee the best SFT performances, especially in terms of horizontal displacements.

A possible design solution is to have cable groups with a different configuration being alternated along the tunnel axis, such as in the case of the Archimedes Bridge Prototype in Qiandao Lake, whose cable system is made up of two groups with two vertical cables and a central one, "W-shaped", featuring four sloped cables.

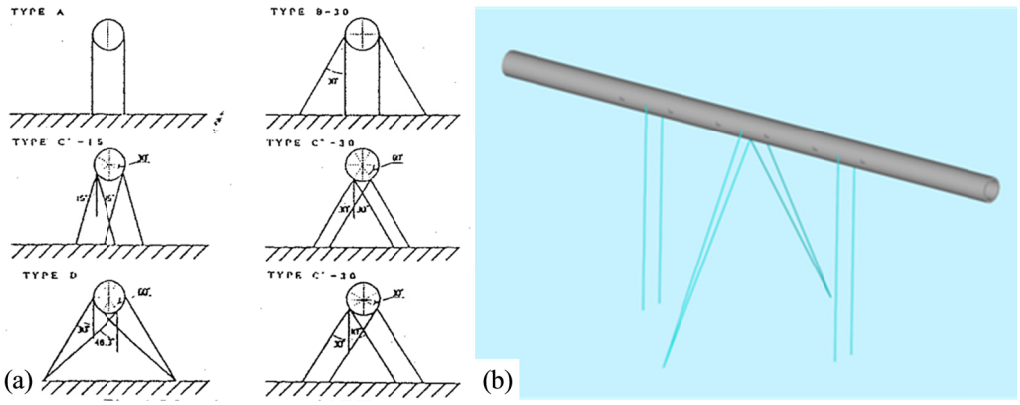

Figure 2.8. (a) Some possible configurations for the groups of cables (Maeda et al., 1994); (b) viewof the cable system of the AB Prototype in Qiandao Lake (P.R. of China; Mazzolani et al., 2007).

The cable system of a SFT could also feature cables inclined in the longitudinal direction of the tunnel, thus interacting also with the axial displacements of the tunnel. In this way it would be possible to reduce the permanent bending stresses induced in the tunnel by the residual buoyancy (RB) without increasing the number of foundation blocks This configuration would also induce a permanent axial force in the tunnel (Figure 2.9), which could also be exploited to improve the water tightness of the inter-modular joints (Mazzolani et al., 2009, Faggiano et al., 2010); moreover, eventual crossing cables could be tied together (see scheme named L2 in Figure 2.9), reducing their sag variation due to live and environmental loads and thus stiffening the system.

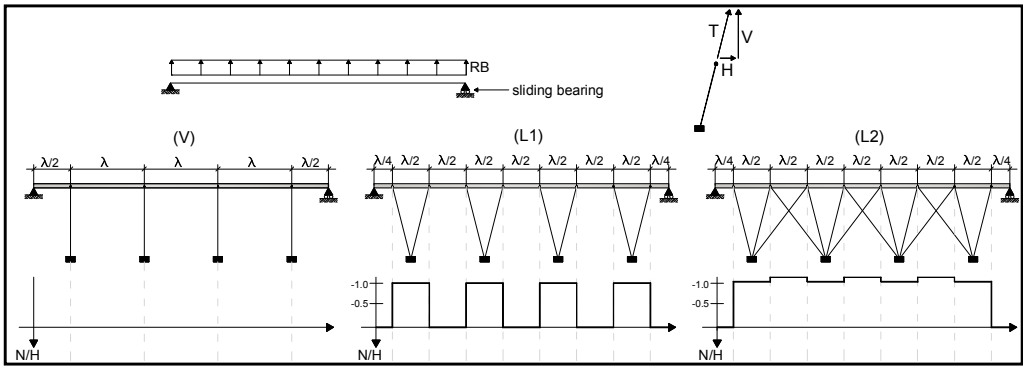

Figure 2.9. Examples of SFT cable system with longitudinally inclined cables and related tunnel a-dimensional axial force (N) diagram (Mazzolani et al., 2009; Faggiano et al., 2010).

It is worth to briefly discuss the main similarities and differences which exists between the SFT anchoring system made up with tensioned members and the cable system of cable supported bridges. The most natural classification of cable supported bridges is based upon the arrangement of their cable system, which can be of the suspension system or cable stayed type (see section 1.1.2). Another distinctive feature of the cable supported bridges is the way the cable system is anchored at its ends. The cable systems can be therefore classified as earth anchored, if both vertical and horizontal components of the cable force are absorbed by the anchor block, or as self-anchored, if only the vertical component is transferred to the anchor pier, while the horizontal one is taken by the stiffening girder. The earth anchored system, mainly used in suspension bridges, requires massive anchor blocks to withstand the large horizontal cable force, whereas self-anchored systems, mainly used in cable-stayed bridges, induce a compressive force in the girder.

In cable supported bridges designed to carry vehicular traffic the cable system is usually composed of vertical cable planes so that it is mainly able to transfer vertical loading. Generally two or more vertical cable planes are provided, thus assuring also torsional support to the stiffening girder. Clearly, with vertical cable planes the resultant of the cable forces is included in the vertical plane, providing no support against lateral loads, such as the wind ones, to the girder, if second order effects are not taken into account. Considering the second order effects, a restoring force due to out-of-plane

displacements arises in earth anchored systems, often referred as the pendulum effect, which is linearly proportional to the lateral displacement of the system (Figure 2.10).

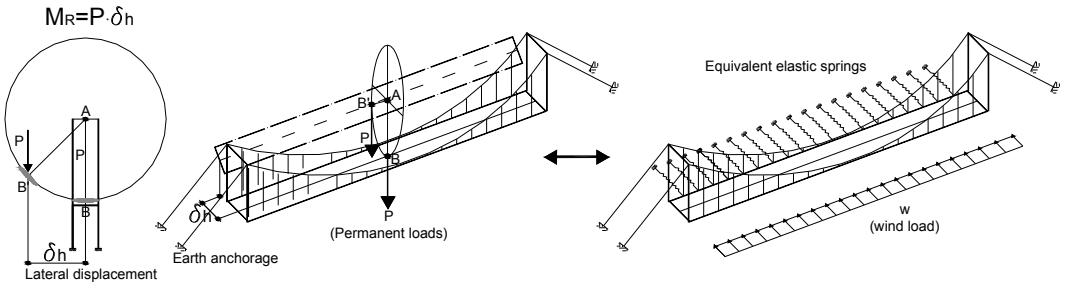

Figure 2.10. The pendulum effect for cable supported bridges: the lateral displacements of the cable system give rise to a restoring couple equal to $P \cdot \delta_h$; the cable system lateral support can be thought as a bed of elastic springs (Gimsing, 1996).

The pendulum effect gives rise to a significant reduction of bending moments induced in the girder, especially as the bridge main span increases but, to be effective, it requires pylons having considerable lateral stiffness and long side spans, the latter condition being unfavourable for the efficiency of the cable systems. Moreover, in the case of self-anchored system no lateral support to the stiffening girder is provided, which therefore has to carry the whole wind load. The problems induced by lateral wind loads in bridges featuring long spans and slender girders can be solved by using inclined cable systems. However, this solutions have been adopted only for some pipeline bridges.

Furthermore, the cable system of a cable supported bridge can offer different levels of stiffness, depending on its configuration. In fact, a cable system, here meaning the ensemble of cables and parts of the girder and the pylons necessary to transfer the axial forces induced by the cables forces, can be classified as (Gimsing, 1996): (a) stable of the 1° order, if the system is able to achieve equilibrium and no node displacements occur; (b) stable of the 2° order, if equilibrium can be attained only through displacements of the nodes of the system; (c) unstable, if the cable system is unable to achieve equilibrium. The fan type cable-stayed system featuring an anchor cable and

self anchoring is stable of the first order (Figure 2.11a), the suspension system is clearly stable of the 2° order (Figure 2.11b), whereas the harp type and the fan type without the anchor cable are usually unstable (Figure 2.11c). The level of stability of the cable system is very important for the rigidity offered by the cable systems under asymmetrical loading.

In the SFT tensioned anchorage system each anchorage of the system is subjected to the tension force due to residual buoyancy and traffic loads and to its own weight, lightened by the buoyancy, and it is anchored to the earth through the foundation block of its cable group.

The previous considerations lead to point out that the cable system of an SFT is stable of the first order (Figure 2.11d). In fact each cable group is able to transfer any load variation to the ground independently from the other cable groups, without requiring any displacement of the system nodes. Obviously, the live load intensity has to be conveniently lower than the residual buoyancy, in order to avoid the loosening of the cables.

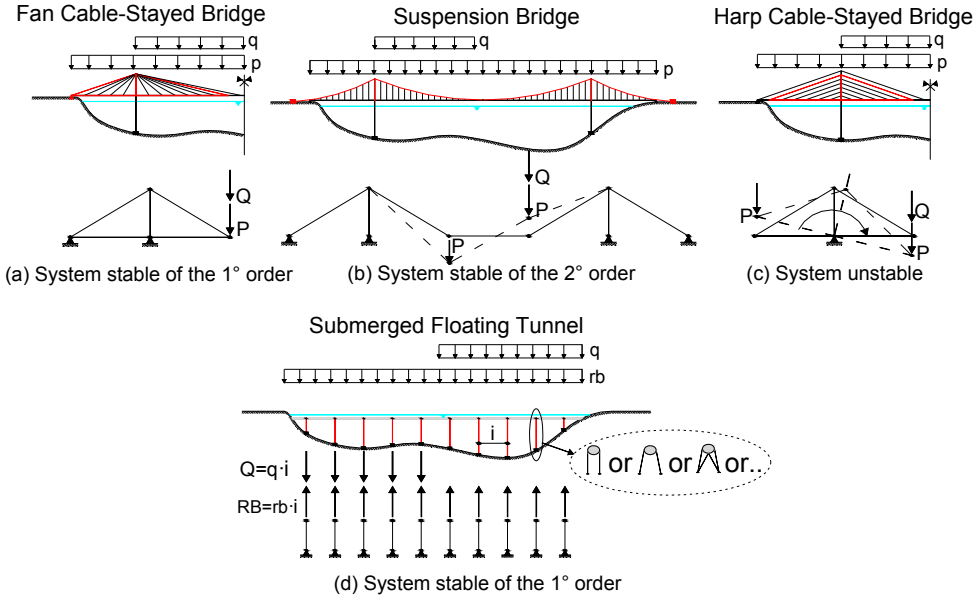

Figure. 2.11 Stability of the cable systems for cable supported bridges (a), (b), (c) and for SFTs (d).

Moreover the anchorages can be easily inclined laterally, as described

before (Figure 2.8a), thus supporting the tunnel in the horizontal plane way more effectively than the supporting system of cable supported bridges.

Given the permanent residual buoyancy and the cables length, choosing the diameter of the cables determines its axial tensile strength $T_{R,d}$, stiffness and also other relevant parameters, such as the ratios between the initial axial force T_0 and the cables strength and weight W, respectively. These two ratios are important for the performance of each cable, as they define the axial force increment due to live or environmental loads that can be carried by the cable and the importance of non-linear effects in the cable response. Concerning the initial axial force-to-weight ratio, experimental studies (Horiguchi et al, 2001) showed that, when this ratio assumes values larger than 5%, structural displacements and stresses considerably increase due to the non-linear behavior of the cables.

Moreover, it is of great importance to avoid the slackening of the cables due to environmental actions, as reaching this condition can lead to the "snapshot" phenomenon: the tensile force of the cable goes to zero and successively it reaches very large values; Kunisu et al. (1994) noticed this kind of behavior on SFT cable systems subjected to wave loading, when increasing the wave height during their experimental tests, as shown in the time plots of the axial force variation given in Figure 2.12.

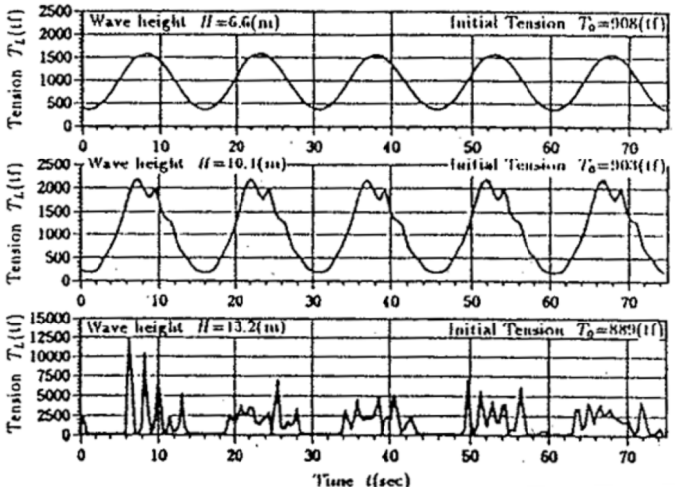

Figure 2.12. Time-histories of the cable axial force due to increasing wave height. Experimental results from Kunisu et al. (1994).

Concerning the restraining conditions at the ends of the cables, the pinned-pinned scheme seems to be the optimal solution as it avoids the local stress increments induced by bending of the cables at their clamped ends. As a matter of fact this stress increments can be very large; however, spherical hinges are more costly and difficult to build and maintain than rigid connections (Maeda et al., 1994), therefore the latter ones can still be considered for realization. Sometimes in offshore engineering practice mixed systems, made up of cables in the central part and chains at the ends, are used in order to facilitate their connections with the foundations and with the vessel/unit to be moored (CMPT, 1998).

An original solution for the anchoring system of SFT crossing wide and deep Norwegian fjords has been proposed by Odegard (1994): two tubular arches, linked to the sloped shores of the fjord, support vertical tensioned hangers which in turn support the tunnel (Figure 2.13).

The main advantage of using tubular members instead of cables is the possibility to design them in order to have no residual weight; in this way the deformability of the system is increased, especially in deep waters, where the sagging of the cables due to their own weight can largely reduce their axial stiffness.

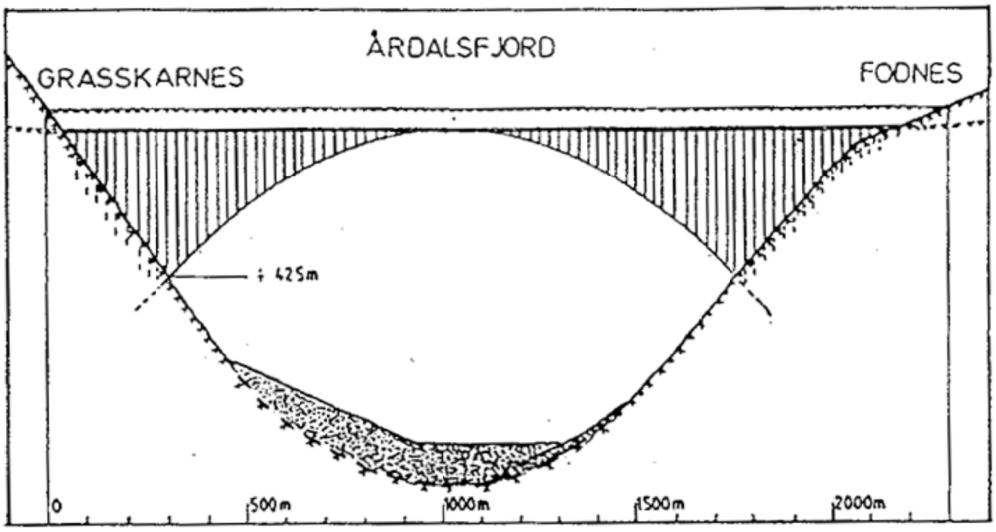

Figure 2.13. SFT supported by vertical cables linked to tubular arches (Odegard, 1994).

As already stated, the main disadvantage of tubular members is related to the increment of stresses due to biaxial bending induced by environmental loads, which can be particular onerous with respect to fatigue problems. Therefore particular care needs to be addressed to the quality controls of the welded joints. In order to reduce this problem it is possible to assemble more segments of the tubular tether through connectors allowing for relative rotations, thus distributing the curvature on limited length of the member (Ramasco et al., 1991). This solution, proposed in the ATI-SSST design of a SFT crossing the Messina Strait, would also facilitate the transport and installation procedures and in case of damages, allows for substituting only the interested parts (CMPT, 1998).

Tension Leg Platforms are offshore structure whose anchoring system is made of tensioned tubular members, namely the Tension Legs. The tethers of a TLP are vertical and very flexible, thus allowing for large lateral displacements of the platform, which would be probably not allowable for a SFT. Due to this large horizontal oscillations, specific flexible elements, called flexelements, are placed at their connections with the platform and the foundations in order to ensure free rotations. Figure 2.14 provides a sketch of a tether of a TLP and details of its end connectors.

In case of negative residual buoyancy (i.e. the weight overcomes the tunnel buoyancy) the supporting system of a SFT is made up of piers or columns. This solution is feasible and competitive only when the seabed depth does not exceed 100 m (FEHRL, 1996), as in deeper waters the dimensions needed to ensure the lateral stability of piers would be too large. Moreover, the inter-axis between successive piers is generally larger than the one it can be considered for groups of cables or tethers, thus leading to a larger permanent stress acting in the structure.

Piers with a hollow circular cross-section are the most reasonable choice, due to their ability to resist the external water pressure. The pier diameter has to be chosen considering several aspects, such as providing it enough strength and stability (it being a structural element mainly compressed), facilitating their connection with the tunnel and ensuring enough buoyancy to allow transport operations by towing.

Figure 2.15a shows a view of a pier of the Lugano Lake Crossing, as proposed by Haugerud et al. (2001). The connection between a pier and the

tunnel can be made in two ways. The first one is by means of an hollow bearing element, connected to the piers and allowing for the passage of the tunnel in its inside; a rubber ring is placed at the interface between the tunnel and the collar, thus reducing the effects of possible settlements. Otherwise it is possible to monolithically link the tunnel with the piers, it being an easier solution but more prone to induce stress increments due to ground settlements.

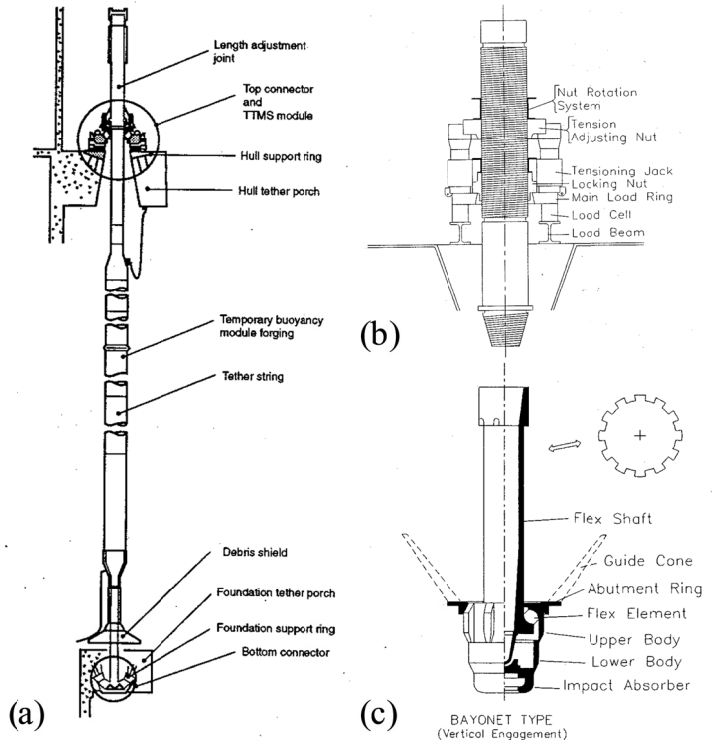

Figure 2.14. Tether of a Tension Leg Platform: (a) global view; (b) detail of the top connector; (c) detail of the bottom connector. (Figure borrowed from FEHRL, 1996).

Alternatively it is possible to integrate the supporting system with the foundation system, having a support system made up of group of piles, embedded in the ground at one end and connected to the tunnel at the other one; this solution has been considered in the design of the SFT crossing the Washington Lake (U.S.A), as showed in Figure 2.15b. The pile heads are

linked through a rigid cap, having the function to assure their cooperation and to accommodate slots for short tying cables, connecting it to the tunnel (Figure 2.16); a rubber bearing is placed above pile heads in order to ensure rotational flexibility.

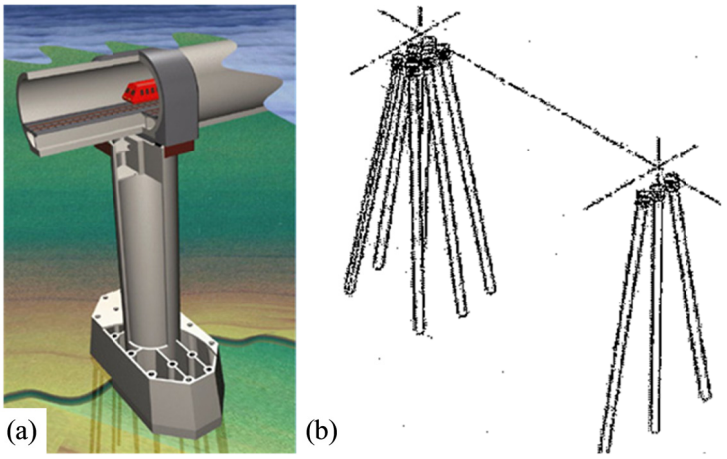

Figure 2.15. (a) Pier supporting the tunnel of the SFT crossing the Lugano Lake (Haugerud et al., 2001); (b) Groups of piles supporting the SFT crossing the Washington Lake (U.S.A.; Felch et al., 2003).

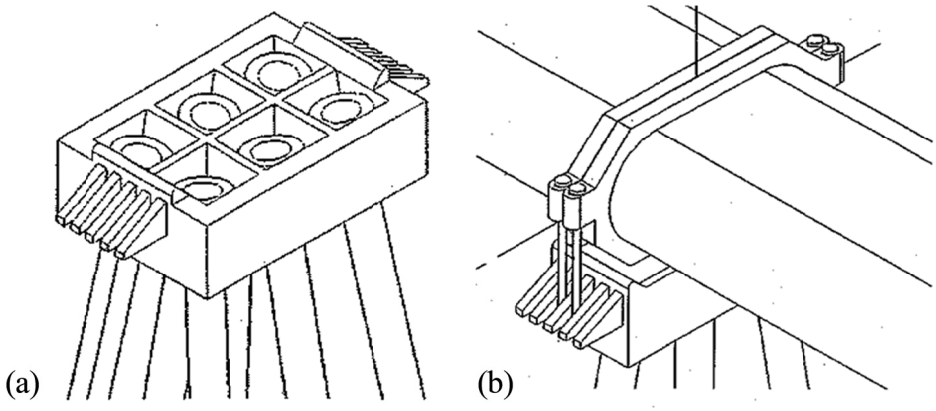

Figure 2.16. Details of the connection between the supporting groups of piles and the tunnel (Felch et al., 2001).

Buoys can be considered as a SFT supporting system, but only when the SFT has to be realized in a very calm environment. This solution has the advantage of being independent of the water depth; however buoys would represent an obstacle for navigating vessels, introducing a risk of collision which might lead to the collapse of a buoy and jeopardize the stability of the structure.

Buoys can be made of steel or r.c and have to be composed of watertight compartments, in order to reduce the risk of sinking in case of external impacts.

2.1.3 *Structural joints*

2.1.3.1. Inter-modular joints

A Submerged Floating Tunnel is a structure made up of pre-fabricated modules assembled in situ, as it would be rather complicated, if not impossible to build it as a single segment due to production and installation issues. Therefore the joints between adjacent modules constitute fundamental elements of this crossing typology, as they have to guarantee performances which do not invalidate the global behaviour of the structure, under the point of view of functionality and safety.

From this standpoint, the similitude between SFTs and Immersed Tunnels (ITs) (see section 1.1.4) is evident, since even the latter ones are modular structures assembled on site. Even though the structural scheme is quite different for the two crossing typologies, some of the requisites to be demanded from inter-modular joints are the same; above all, waterproofing is a fundamental property, it dealing with the safety of the people inside the tunnel.

The inter-modular joint nowadays in use for Immersed Tunnels are flexible and have to perform different tasks: to ensure the waterproofing of the tunnel, to allow for (limited) relative displacements in order to avoid excessive stress increments in the structure due to ground differential settlements or temperature variations and to guarantee the equilibrium of the structure. In the early applications of ITs monolithic joints were built, but their performance proved to be inadequate, leading to water penetration in concrete tunnels due

to formation of cracks and to damages of internal facilities in steel tunnels (Saveur and Grantz., 1997).

A typical inter-modular joint of an IT features a solid rubber gasket, generally named "Gina" gasket (Figure 2.17). It is used as a temporary seal at the installation stage and remains as a flexible compression seal for the permanent stage. The facing tunnel element ends are lined with steel plates that are matched as parallel planes. The gasket is clamped at its backside.

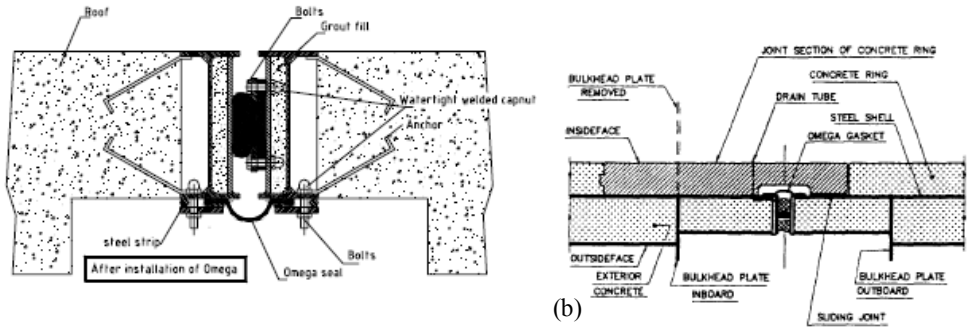

Figure 2.17. Flexible inter-modular joint with two rubber gaskets: (a) concrete IT (image from Trelleborg Bakker B.V., 2008); (b) steel IT (image from Saveur and Grantz, 1997).

The specifications for material characteristics and geometry are usually based on the permanent sealing requirement under expected long-term decompression and relaxation of the gasket. Nevertheless, a second flexible rubber water barrier is installed at the dewatered joint by bolting it to the inside faces of the two tunnel elements. This curved rubber gasket, often referred to as the "Omega" seal because of its shape (Figure 2.17), is sometimes considered to be the main seal. The space between the Gina gasket and the Omega seal is usually drained off to the inside of the tunnel, providing a direct indication of the performance of the outer gasket. The Gina-type gasket acts as a flexible joint under compression, and can practically be considered as a hinge in longitudinal moment transfer (Grantz et al. ,1997).

The flexible inter-modular joint is built in situ during the installation operations of the modules of the tunnel. Temporary bulkheads are placed at the ends of the module, in order to tow it to its final position and then immerse it. The Immersed Tunnel element is then pulled firmly up against the

preceding immersed element with hydraulic jacks (step a in Figure 2.18). The initial contact of the Gina should be accomplished using a low pulling force. When the Gina has full contact around the total circumference of the adjacent element (step b in Figure 2.18), the water between the bulkheads is pumped out (step c in Figure 2.18). Due to pressure differential between the bulkheads and the hydrostatic pressure on the outside of the tunnel, the Gina profile compresses and seals the joint. The secondary omega seal is then clamped across the joint on the inside of the tunnel (step d in Figure 2.18). In general the bulkheads are removed after approval of the pressure test between the Gina and Omega (Trelleborg Bakker B.V., 2008).

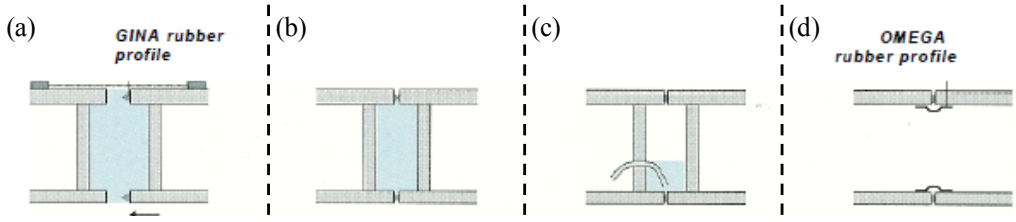

Figure 2.18. Steps of the construction of a IT flexible joint with Gina and Omega rubber seals (figure taken from Trelleborg Bakker B.V., 2008)

Shear resistance can be ignored, because Gina gasket has a tendency to slip along its base under shear deformation. For this reason, shear deformation across a joint is not limited by properties of the Gina gasket, but rather by the allowable shear strain of the Omega gasket, especially with regard to its corner sections. Therefore, additional bearing elements are placed in the joint, accomplishing the task of transferring shear forces. Transfer of large shear forces in intermediate joints is achieved by shear keys in the walls that are made in situ in front of the inner face of the permanent watertight gasket. They can also be installed prior to placement with provisions for in-situ adjustment. Shear transfer for small shear forces can be accomplished using shear keys or longitudinally movable dowels in the base slab area of the joint. In steel-concrete tunnels the shear continuity across the joint is ensured through an overlapping of the interior structural concrete ring (Figure 2.17b).

The flexible joint previously described has not been considered suitable in some applications where large displacements had to be absorbed by the joint, due to severe earthquakes or large ground settlements (Kiyomiya et al., 2004).

Therefore a new typology of flexible joint has been devised, able to withstand larger displacements without invalidating its dewatering performance, which relies on a main seal different from the Gina gasket, namely the Crown seal (Figure 2.20a). The main part of the joint is a rubber block installed at the outside of the module bulkhead. Flanges are connected to the rubber block and fixed to an attachment plate. The rubber block and flanges are subjected to water pressure. Water-tightness is achieved both by seal noses below the rubber block and at steel attachment part. A secondary Omega rubber seal is also attached at the joint to protect the leakage from the Crown Seal rubber block.

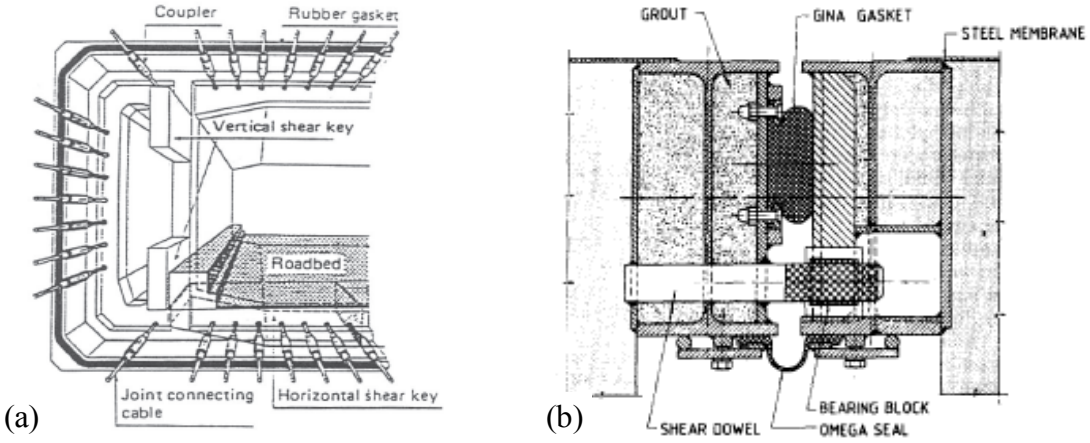

Figure 2.19. (a) Inter-modular joint featuring a vertical shear key in wall; (b) inter-modular joint featuring a vertical shear dowel.

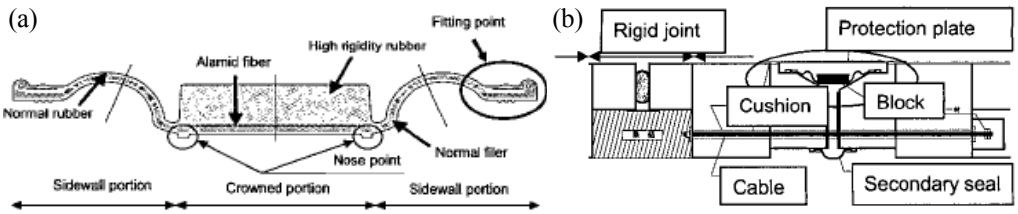

Figure 2.20. (a) Crown seal; (b) arrangement of a crown sealed flexible joint (Kiyomiya et al., 2004).

Cables are arranged to cope with unpredicted tensile displacements larger than the design value due to landslide by the earthquakes or unpredicted large settlement. These cables start to be stressed only for displacements larger than a fixed tolerance and thus have the role of preventing excessive tensile displacement at the joint parts, which might lead to opening of the joint and to water penetration inside the tunnel.

A similar solution is sometimes used also in flexible joints featuring Gina gaskets as the main seal: pre-stressed cables are provided in order to absorb tensile stresses induced by rotation or axial displacements of the joint. Couples of cables are embedded in the tunnel elements ends and connected by a coupler, which absorb dislocation of the cables (Figure 2.212). The couplers are sealed by rubber tapes to cope with corrosion of the coupler and of the cables (Kiyomiya, 2003).

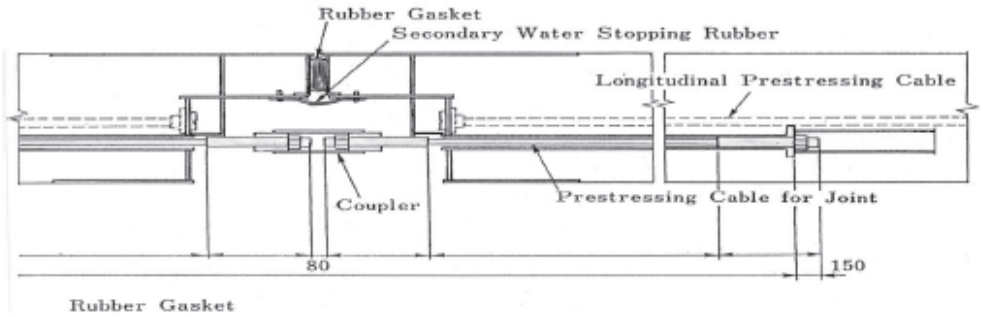

Figure 2.21. Flexible inter-modular joints featuring coupled pre-stressed cables (Kiyomiya, 2003).

Even though SFTs and Immersed Tunnels are very similar under the point of view of construction and installation, their structural behaviour is quite different: in fact the former ones are “suspended” in the water and can be subjected to significant displacements and rotations in the longitudinal bending planes, whereas the former ones are continuously supported by the seabed soil, thus being subjected to stresses and displacements in the longitudinal planes only because of ground settlements or earthquakes. Therefore the use of a flexible inter-modular joint does not seem to be a suitable solution for SFTs, for which the most rational solution is to have rigid

inter-modular joints and terminal joints allowing for axial displacements due to thermal variations and tri-axial rotations (see section 2.1.3.2).

As a matter of fact rigid joints between adjacent modules have been conceived in the design of the Archimedes Bridge Prototype in Qiandao Lake (P.R. of China). The inter-modular joints for the SFT prototype are essentially bolted connections, designed for being set up and assembled when the modules are already submerged. The joint consists in two steel ring end plates, each one belonging to one of the adjacent modules (Figure 2.22a). Flanges are mutually connected by means of high strength steel bolts. The bolted flanges are placed at the internal concrete and steel layers. At the external aluminium layer, a rubber ring crushed between the modules guarantees the water tightening of the connection. A sliding rubber ring is placed between steel and aluminium elements, in order to allow relative displacements due to thermal variations. The tensile forces are transmitted by the bolts in tension, whereas the compressive forces are transmitted by the contact between the adjacent steel end plates. The design shear forces are transmitted by friction, whereas the ultimate shear force is assumed to be transmitted by shear in the bolts.

The steel shell SFT proposed by Grantz (2003) also features rigid inter-modular-joints (Figure 2.22b): in fact the two main steel hulls of this structure are welded full-strength at the joints between the elements. These critical weld areas can be accessed after the Gina gasket, working as a temporary seal during installation of the modules, is compressed and the joint space is dewatered. The roadway space is provided with reusable temporary bulkheads during the placing operation. These temporary bulkheads, in conjunction with the permanent bulkheads of the surrounding compartments, make the ends of each element completely watertight and permit the conventional operation of the Gina connection. Reinforced concrete rings are placed at the module ends, in order to stiffen locally the structure, absorbing the rubber gasket compression force.

The alignment between the two shells of the element being placed and the tunnel already in place must be very accurate for good full-strength welds to be achieved connecting the main hulls. This alignment can be accomplished by providing large guide pins with receiving sockets at four quadrants of the joint face.

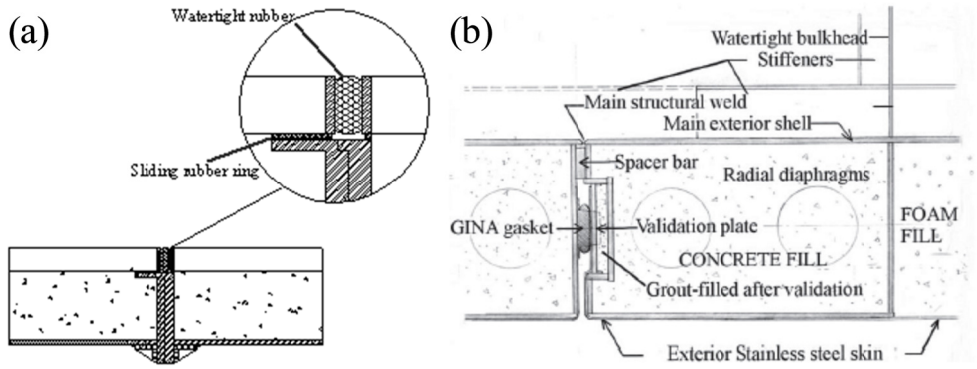

Figure 2.22. SFT inter-modular joints: (a) AB Prototype in Qiandao Lake (Mazzolani et al., 2007); (b) solution proposed by Grantz (2003).

In extreme cases, such as SFT crossings with very large lengths and seasonal temperature variations, quite large displacements might be required at the terminal joints of the tunnel. In this cases it would be possible to introduce one or more flexible/semi-rigid joints along the tunnel length, working as intermediate expansion joints. A reasonable solution could, in the writer's opinion, resemble the one of IT flexible joints featuring rubber gaskets and coupled pre-stressed cables; in fact, by a proper choice of the configuration of the rubber seals and of the cable system and of the amount of pre-compression, the designer could obtain a joint featuring the properties of stiffness and strength fulfilling both the functional and safety requirements.

2.1.3.2. Shore connections

The configuration of the connections of a Submerged Floating Tunnel with the shores is one of the most relevant issues in its design. In fact in these zones there is the transition between two different states of equilibrium (FEHRL, 1996):

- the floating tunnel, subjected to the actions due to the presence of water, to the retaining forces provided by the supporting system and eventually to seismic actions;
- the land bored tunnel, in equilibrium with the ground pressures and, eventually, with the seismic pressures induced by earthquakes.

A transition structure, coping with the interaction between these two different structural behaviours, is thus needed (Figure 2.23). This structural part of the tunnel, which could be referred as landfall tunnel, needs two structural joints at its ends (SJ1 and SJ2 in Figure 2.21), whose aim is to absorb, without inducing relevant stress increments, the relative movements expected at the interface between the two aforementioned systems due to thermal variations, earthquakes, settlements and so on (FEHRL, 1996). Clearly the shore connections design is strictly related to the hydro-geologic and geotechnical conditions of the submarine slopes and the shore area.

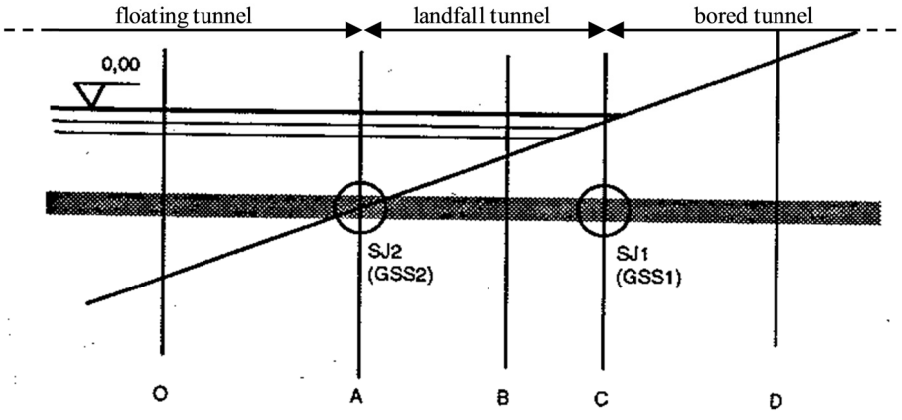

Figure 2.23. Shore connection between the SFT and the land bored tunnel (figure taken from FEHRL, 1996).

A detailed study of the configuration of the shore connections was made for the design of Messina Strait Crossing (Italy) made by the ENI Consortium (Nicolussi and Casola, 1994). In this solution the two structural joints behave differently:

- the joint between the land bored tunnel and the landfall tunnel (joint B in Figure 2.24a) releases all the six degrees of freedom between the two adjacent elements. In this way the structural response of the land bored tunnel and of the landfall tunnel are decoupled;
- the joint between the landfall tunnel and the floating tunnel (joint B in Figure 2.24a) releases all the rotational degrees of freedom and axial movements between the two adjacent elements. Therefore this joint

decouples the axial and bending behaviour of the floating tunnel and of the landfall tunnel, also reducing the stresses induced by wave, currents, thermal variations and seismic events.

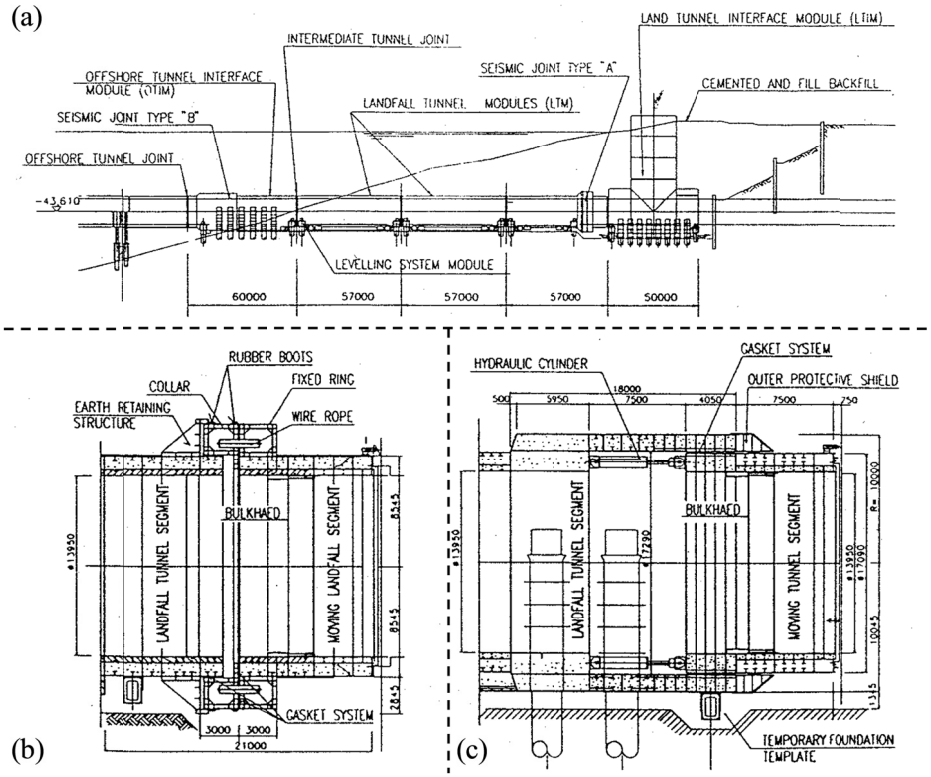

Figure 2.24. Shore connection of the SFT Messina Strait (Italy) crossing by ENI Consortium (Nicolussi and Casola, 1994): (a) global longitudinal view; longitudinal sections of Joint A (b) and Joint B (c).

Both joints include a gasket system, preventing water leakage inside the tunnel: natural rubber gaskets are squeezed between the surfaces of the joint elements in contact; teflon sheets are stuck on the steel surfaces in order to reduce the friction forces (Nicolussi and Casola, 1994). Joint A is provided with a pre-tensioned system of wire ropes, whose release allows free relative movements in all the six degrees of freedom (Figure 2.24b). Joint B includes an hydraulic system of 20 jacks distributed along the joint cross-section

(Figure 2.24c), which absorb axial loads induced by waves, currents and thermal variations in quasi-static conditions. During severe earthquakes, once the established threshold is exceeded, the hydraulic system opens allowing for free axial movements, while accumulators connected to the jacks develop a residual reaction able to maintain the maximum relative movement within allowable design limits. An active back-up system, based on acceleration sensors, controls the proper functionality of the hydraulic system (Nicolussi and Casola, 1994).

The design of the shore connections has been undertaken also in the design of the Archimedes Bridge prototype in Qiandao Lake (P.R. of China).The connections of the AB prototype to the shores are made by means of special end joints, which are connected to the modules of the prototype at the extremities. One of the two end joints must behave like a spherical hinge (Figure 2.25). With regard to the displacements, the tunnel is axially linked to the shore by means of a mechanical device, which behaves in elastic range (with high stiffness) in presence of axial forces smaller than a design limit value, but it can undergo large plastic deformations when axial forces exceed this limit value, giving rise to hysteretic dissipation of energy. The other end joint must allow both free rotations and axial displacements, in order to give the structure the possibility of free expansion in presence of thermal variations. Furthermore, both the end joints assure the water tightening. through an external waterproof and deformable element, avoiding water leakage in correspondence of axial movements within the design range.

The use of dissipating devices for seismic purposes could be foreseen also with respect to transversal (vertical and horizontal) movements at the terminal joints of a SFT. Such a kind of solution would significantly improve the structural response under severe earthquakes, in particular in case of short SFT crossings in shallow waters. In fact in these cases the SFT would be stiffer than usual SFT applications and its first natural vibration periods could fall within the frequency range of maximum intensity of the earthquake, leading to large dynamic excitation. Dissipative devices would allow to substantially reduce the amount of energy transferred from the ground to the structure at the shore approaches, thus reducing stresses and displacements induced by the seismic event.

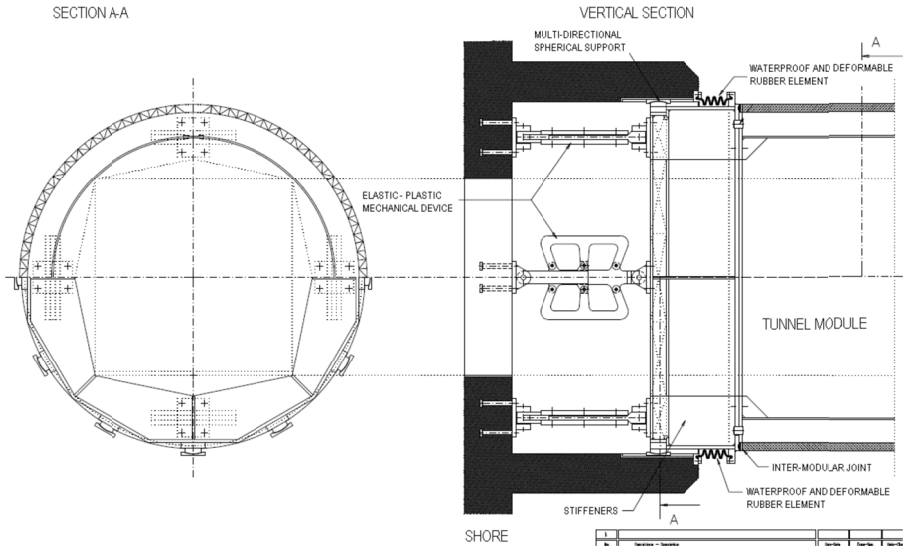

Figure 2.25. Detail of the terminal joint of the AB Prototype in Qiandao Lake, P.R. of China (Mazzolani et al., 2007).

Terminal joints represent a fundamental design issue also for Immersed Tunnels, for the same reasons previously described for SFTs, in particular with respect to the seismic aspect. In fact seismic motions may control the design of the joint and its waterproofing detailing, as the terminal structure to which the end tunnel module is connected (e.g., a ventilation building) will usually have a very different natural period of vibration than the tunnel, thus leading to large relative movements (Grantz et al., 1997). This condition may require a full seismic joint with tri-axial motion capability.

Such a joint was used for the BART Transbay Tunnel in San Francisco (Figure 2.26). The seismic joint was designed to permit tri-axial displacements of +8 cm in the longitudinal direction and +15 cm in any direction in a vertical plane, while maintaining watertight integrity (Grantz et al., 1994). The vertical and transverse horizontal motions are permitted by pre-compressed rubber gaskets sliding on radial Teflon bearing surfaces. The longitudinal motion is taken by similar gaskets sliding on a circumferential Teflon bearing surface. Both sets of bearings are compressed by tensioned cables that allow the motions by rotating on Teflon-coated spherical bearings. The assembly is protected from mud and the marine environment by exterior rubber boot

enclosures. The joints performed well during the 1989 earthquake in San Francisco.

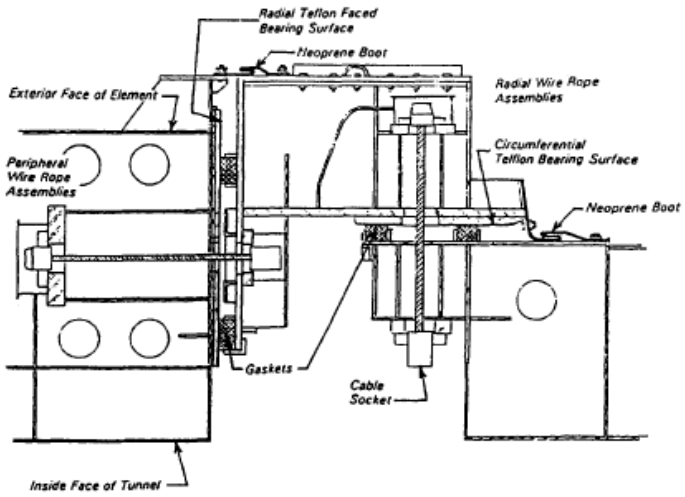

Figure 2.26. Seismic joint used for the Transbay Tunnel, San Francisco (Grantz et al., 1997).

More often terminal joints of Immersed Tunnels have been designed in order to allow free expansion and contraction, but no relative vertical movements.

2.1.4 *Foundations*

The foundations of a Submerged Floating Tunnel have the task to transfer to the ground the vertical and horizontal forces induced in the supporting system by permanent, live and environmental loads. Technologies developed and used in offshore structures can be exploited.

The SFT foundation system typologies which can be considered are:

- gravity foundations;
- piled foundations;
- rockbolts;
- Suction Caisson Anchors;
- deepwater anchors.

The choice of the solution to be adopted is based on the mechanical

properties of the soil and on the water depth, it influencing strongly the installation operations.

Gravity foundations are massive plinths, designed to have enough weight in order to counterbalance the upward residual buoyancy of the tunnel. Their main problems are related to the need of a superficial soil layer with good mechanical properties and to their low horizontal bearing capacity; moreover, in case of severe seismic events, the combination of the vertical upward and horizontal dynamic forces might lead to their permanent horizontal displacements, modifying the geometrical configuration of the anchoring system. Generally the plinths are made up of prefabricated elements to be filled with concrete casted on site, in order to facilitate their transport. This solution has been adopted for the Messina Strait Crossing preliminary design by Sirprogetti (1996) and for the Archimedes Bridge Prototype in Qiandao Lake (Mazzolani et al., 2007; Figure 2.27).

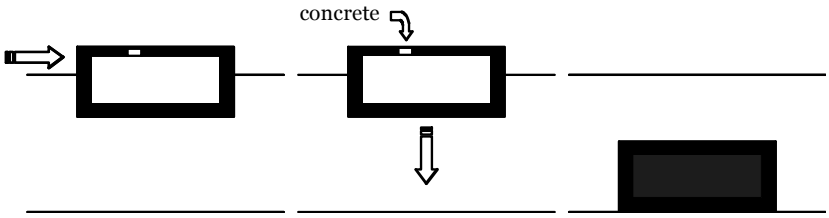

Figure 2.27. Set up procedure for prefabricated plinths of the Archimedes bridge Prototype in Qiandao Lake, P.R. of China (Mazzolani et al., 2007).

Piled foundations are composed of a group of piles linked on the top through a cap, making them collaborating and accommodating the connections with the tethers/piers of the SFT. This foundation system is reliable and widely used in marine applications, due to their very good attitude to bear vertical upward and horizontal forces but their installation/construction is more complicated than the one of gravity plinths, especially in presence of deep waters.

The pile cap can be made of a steel framed structure, featuring the slots and devices needed to accommodate the head of the piles and the tether ends (Figure 2.28). The prefabricated steel structure can be weighed down by filling it with concrete casted in situ, in order to lead to a vertical compression force in the piles or to reduce the tensile vertical force. The preliminary

designs for a SFT crossing the Messina Strait (Italy) made by ATI-SSST (Scolari et al., 1989) and by the ENI Consortium (Nicolussi and Casola, 1994) feature a solution of this type. Alternatively, the piles cap can be made of pre-stressed reinforced concrete, as proposed in the feasibility study for the crossing of the Lugano Lake (Switzerland; Haugerud et al., 2001).

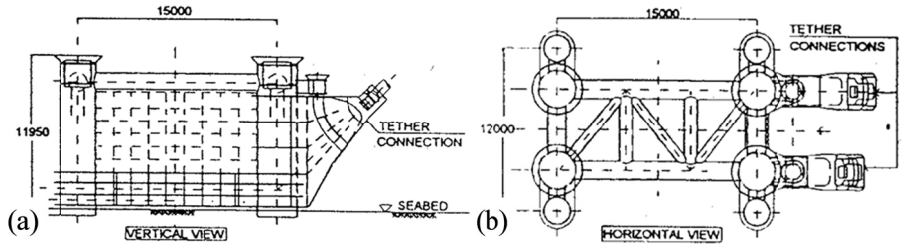

Figure 2.28. Steel framed cap of the piled foundation of an SFT anchoring group(Nicolussi and Casola, 1994).

Piles can also serve directly as supports for the tunnel, as in the proposal made by Felch et al. (2003) for the Washington Lake crossing (U.S.A.; see section 2.1.2.2).

Rockbolts, largely used in tunneling and underground mining, are mainly steel rods, featuring steel flanges along its surface, inserted in a hole drilled into the roof or walls of a rock formation to provide support to the roof or sides of the cavity. The hole is then filled with high pressure concrete grouting, which allows to transmit forces to the rock through their compression (Figure 2.29).

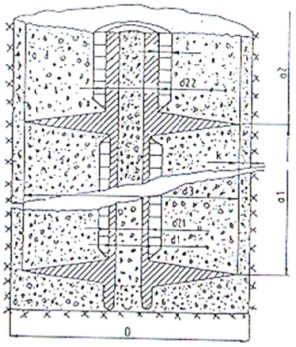

Figure 2.29. Detail of the terminal part of a rock bolt (Odegard, 1994).

Rock bolt reinforcement is simple and quick to apply, and is relatively inexpensive. Their installation can be fully mechanized. Rockbolts can be adapted for use as foundations of single cable or tether restraining a SFT; their use has been also proposed by Odegard (1994) as foundation system of the tubular arches composing the supporting system of its SFT proposal (see section 2.1.2.2).

In the latest years offshore platforms and production units moved into deeper waters, using taut moorings instead of catenary moorings; these developments lead to the need of innovative foundation systems, more easily installable and able to whit stand larger upward forces. Therefore innovative deepwater foundation solutions have been developed; the most used and experienced one is the Suction Caisson Anchor. They are pile/caisson foundations that consist of a stiffened cylindrical shell with a cover plate at the top and an open bottom and generally have large diameters of about 8 to 24 feet and length to diameter ratios in the range of 5 to 7 (Ehlers et al., 2004; Figure 2.30a).

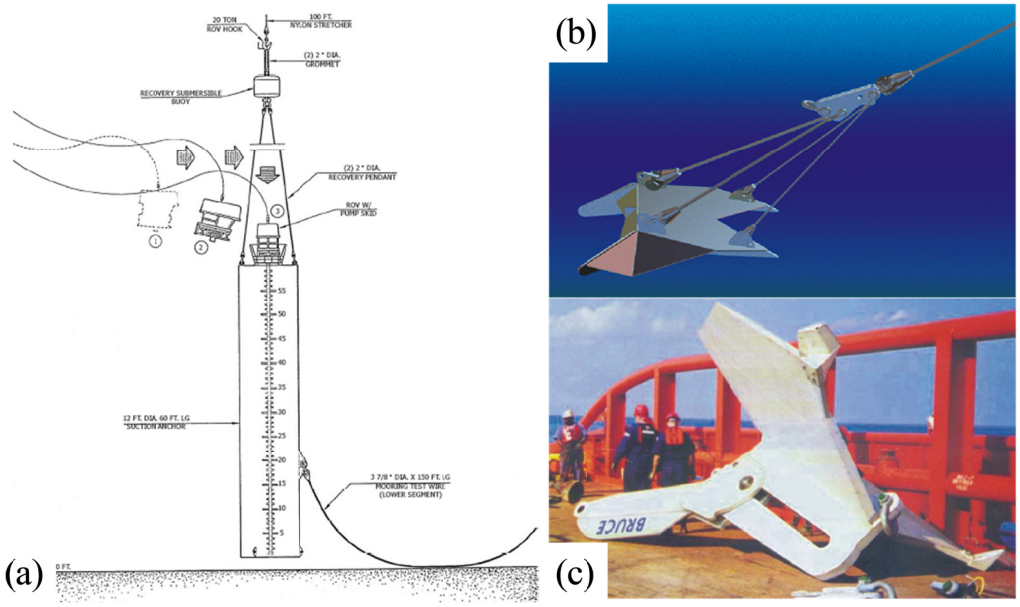

Figure 2.30. (a) Suction Caisson Anchor; (b), (c) deepwater anchor systems developed in offshore industry (images borrowed from Elhers et al., 2004).

The suction anchor penetrates under its weight to some depth and then is forced to the design penetration by pumping water out of the caisson to create an underpressure/suction within the caisson. The difference in pressure results in a downward force on the exposed end of the cylinder, which slowly pushes the anchors in the seafloor and provide the required bearing capacity.

Many other innovative anchor systems (Figures 2.30b and 2.30c), suitable for deepwater applications, have been developed in Offshore Engineering and are under study in order to have sufficient experimental data on their behavior (Elhers et al., 2004).

2.2 LOADING CONDITIONS

2.2.1 *Permanent loads*

The permanent loads acting on a SFT are the weight of the various structural and non-structural component, the water buoyancy and the hydrostatic pressure.

The algebraic sum of the first two defines the residual buoyancy of the tunnel, which is a fundamental factor for the stability of the structure. Thus particular attention has to be paid in evaluating its value, taking into account the following uncertainties (Ahrens, 1997):

- Tolerances in geometry and dimensions: the acceptable tolerances in the geometry and dimensions must be established during the design stage, depending on the choice of construction method, and controlled by the contactor during the construction. In case of significant variations from the weight design value, the ballast quantity can be modified at the end of construction.
- The specific weight of concrete: although the specific weight of concrete will vary during construction, it can easily be measured. Nevertheless, the acceptable range has to be established beforehand, during the design stage.
- The specific gravity of water: the specific gravity of the water can vary in a range which is characteristic of the site. These variations may be

significant, in particular in coastal areas, and the design has to consider these variations.

- The amount and stability of marine growth: marine growth is known to concentrate at the sea floor and at the surface. If the SFT is not located in the critical surface layer, the effects of marine growth will be minor.

The aforementioned uncertainties lead to time variations of the residual buoyancy; in order to keep these variations under control, avoiding negative effects on the structural stability, it is possible to use water as ballasting material (or part of it) and counteract the weight changes by varying the amount of ballast water. This operation can be easily made through hydraulic pumps.

Hydrostatic pressure has to be considered not only with reference to the buoyancy that generates on the tunnel and the other structural elements but also for the stress regime that induces in the tunnel cross-section plane. At large water depths this issue is particularly relevant, as it is proved by the fact that hydrostatic pressure is one of the main problems that has to be faced in the design of Immersed Tunnels. The definition of the hydrostatic pressure field is quite easy generally, but attention has to be focused on eventual stratification of water, whose changes in density influence the trend of the water pressure with its depth.

2.2.2 *Functional loads*

Functional loads are related to the development of the functions for which the SFT is designed for, therefore these loads are associated with the passage of cars, trucks, trains and/or pedestrians, according to the destination of use of the SFT.

The amount of traffic occurring in the tunnel is subjected to great variations also during a single day, so that the definition of the associated loading conditions is quite difficult. Usually codes (e.g., Eurocode 1, part 3, UNI ENV 1991-3, 1991) define conventional loading conditions determined on the basis of statistical data gathering and analysis; these loading schemes are intended to reproduce the most onerous stress conditions produced by traffic loads on the structure.

2.2.3 *Environmental loads*

2.2.3.1. Hydrodynamic loads

Hydrodynamic actions due to the water-structure interaction in presence of waves and currents often represent the most important and onerous environmental actions for a Submerged Floating Tunnel.

The motion of water due to currents and waves have been observed and studied extensively, as they are of great importance for the safety of offshore structures and navigating vessels. Therefore numerous observed data and theories are available to model the kinematics of water particles due to currents and waves.

Currents

Currents in waterways can be of the following types:

- wind generated currents: water motion is originated by the energy transferred to the water by the wind blowing over the water surface;
- tidal currents: horizontal water motion resulting from the rise and fall of the water level due to tides (a vertical motion);

Usually water motion due to currents take place in the horizontal plane and can be assumed to be constant, as small variations in its velocity occur in a sufficiently long time period. However short and long term fluctuations around the velocity mean value occur, therefore when the former ones are significant they should be considered.

Usually, for design purposes, water current is modelled as a horizontal velocity distribution along the water depth; this distribution can be roughly assumed to be constant or, more generally, can be represented by as a polyline, thus requiring observed data relative to the current velocity at the depths of the polyline vertices.

An analytical distribution often adopted for the current velocity is the following:

$$V_c(z) = V_T \cdot \left(\frac{z+d}{d}\right)^{1/7} + V_w \cdot \left(\frac{z+d}{d}\right) \tag{2.5}$$

where $V_c(z)$ is the current velocity at a depth equal to z (z axis with the origin on the free surface and directed upward), V_T and V_w are the surface current

velocity due to tides and wind, respectively. Thus the first addend represent the velocity contribution due to tidal currents and the second one the contribution due to wind generated currents, the latter being generally predominant.

Waves

Water waves differ from currents because they are characterized by an oscillating motion of the water particles and can be of two types:

- Wind generated waves: surface waves occurring on the free surface of waterways, due to the wind blowing over a vast enough stretch of fluid surface. When directly being generated and affected by the local winds, a wind wave system is called a wind sea. On the contrary, wind generated waves that are not affected by the local wind at that time and have been generated elsewhere, or some time ago, are called swells.
- Internal waves: water particles are kept in motion by the force of gravity acting on small differences in density. A density difference can exist between two fluids or between different parts of the same fluid because of a difference in temperature, salinity, or concentration of suspended sediment.

Although internal waves can be important and induce significant loads on marine structures, in most of the cases wave water motion is made of wind generated waves.

Several theories have been developed to describe the motion of water particles due to waves, which are generally based on the determination of the velocity potential satisfying the Laplace Equation, thus assuming an irrotational and incompressible fluid. A detailed overview of the wave theories available in literature is given in Sarpkaya and Isaacson (1981). The simplest wave theory is the Airy Linear (also called Sinusoidal) Wave Theory, which is based on the fundamental additional assumption that the wave height H_w is small, thus allowing to impose the free surface boundary condition at the still water surface height and to neglect higher order terms in the governing equations. Cleary this wave theory can be assumed to be valid as a first approximation only when the wave height H_w is considerably smaller than both the wave length L_w and the seabed depth d.

In order to represent more closely the complete solution of the equations governing the wave water motion higher order theories have been proposed, introducing a perturbation procedure with successive approximations. This method was developed by Stokes, assuming the velocity potential as a power series of the perturbation parameter, and converges towards the complete solution when the considered wave is not too steep and water depth is not too small (Sarpkaya and Isaacson, 1981); this approach is considered to be valid when the wave height-to-length ratio is largely lower than one ($H_w/L_w<<1$; Peregrine, 1972)) and when the wave length L_w is less than 8 times the water depth d (Laitone, 1962). The aforementioned procedure has been carried out considering power series form the second to the fifth order.

The low order Stokes finite amplitude theories are generally inadequate in shallow waters as many coefficients of the higher order terms become too large with respect to the lowest order terms. In shallow waters a different and more reliable non-linear procedure to describe the wave properties is the so-called Cnoidal Wave Theory, which expresses the wave characteristics in terms of the Jacobian elliptic function and leads to a wave profile featuring very steep and sharp crests and flat troughs. A limiting case of Cnoidal wave is the Solitary wave, characterized by an infinite wave length.

Other wave theories are available such as the Linearized Long Wave or the Trochoidal Theory. Thanks to modern computation capability, several iterative numerical methods providing an accurate description of steep waves over a complete range of depths have been proposed in the last forty years.

The choice of the adequate wave theory should be done in dependence of the wave parameters. In fact each wave theory can be considered reliable in different fields of application in terms of wave height, wave period and seabed depth. Abaci defining the fields of application of various wave theories are available in literature (Figure 2.31; Le Mehautè, 1976; CIRIA, 1978).

Swell waves can often be adequately described by one of the aforementioned theories. However, in most of the cases the water surface during wave motion appears to be strongly irregular, in particular when the waves are simultaneously generated by the storm in action (wind sea). Therefore the sea state is more often described on the basis of statistical criteria through superposition of infinite sinusoidal linear waves; thus the analytical expression determining the water surface elevation η_w at the point

of Cartesian coordinates (x,y) in the horizontal plane is the following:

$$\eta_w(x,y,t) = \int_0^{\infty} \int_{-\pi/2}^{\pi/2} \frac{dH_w}{2} \cdot \cos(k \cdot x \cdot \cos\varphi + k \cdot y \cdot \sin\varphi - \omega \cdot t + \varepsilon)\, d\varphi\, d\omega \quad (2.6)$$

where ω is the angular frequency (equal to $2 \cdot \pi / T_w$) of the elementary wave, k is the wave number, equal to $2 \cdot \pi / L_w$ and thus related to the wave period T_w through the dispersion relationship, φ is the angle between the direction of propagation of the elementary wave and the main direction of propagation of the sea state, dH_w is the height of the elementary wave and ε is the phase, which is generally assumed to be a random variable uniformly distributed between 0 and $2 \cdot \pi$ (thus, given the values of dH_w for each value of ω and φ, all the randomness of the sea state is concentrated in ε).

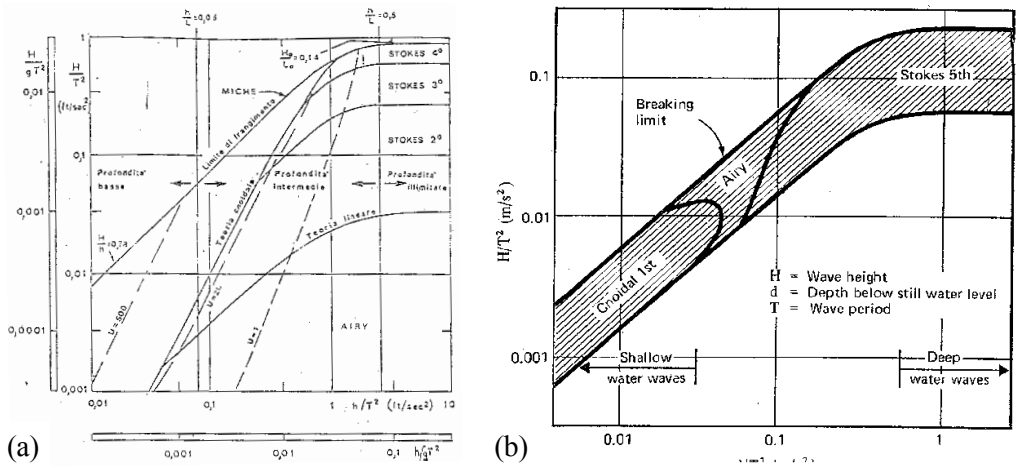

Figure 2.31. Abaci defining the fields of validity of the wave theories: (a) Le Mehautè (1976); (b) CIRIA (1978).

In case of unidirectional sea state, equation 2.6 turns into:

$$\eta_w(x,t) = \int_0^{\infty} \frac{dH_w(\omega)}{2} \cdot \cos(k \cdot x - \omega \cdot t + \varepsilon)\, d\omega \quad (2.7)$$

The water surface elevation is assumed to be an ergodic and Gaussian random process, which means that its statistical properties, such as mean value and variance, for instance, are constant with time and are the same for any realization of the process and that its probability distribution is the Gaussian

one. The ergodicity hypothesis allows to characterize the sea state through only one temporal recording, provided that is sufficiently long.

An irregular sea state is entirely described by its spectrum of energy density $S_\eta(\omega, \varphi)$, which represents the distribution in the frequency domain of the energy per surface unity of the wind sea and is related to the wave height $dH_w(\omega,\varphi)$ through the relationship:

$$S_\eta(\omega, \varphi) \cdot d\omega \cdot d\varphi = \frac{dH_w(\omega,\varphi)^2}{8} \tag{2.7}$$

In fact $S_\eta(\omega, \varphi)$ is equal to the energy of a single sinusoidal wave featuring a wave height dH_w, divided by the water specific weight γ_w, being constant with the frequency. It is clear that, given an analytical description of a sea wind of the type shown in equation 2.6, it is possible to calculate its energy spectrum through equation 2.8. Vice versa, given a certain spectrum it is possible to calculate the water surface elevation through the inverse procedure. Thus a spectrum energy completely describes the frequency decomposition of the wind sea profile and can lead to its infinite representations, due to the randomness of the phase of each harmonic component of the sea state.

An important feature of an energy spectrum is its band wideness index, which is a measure of how wide is the frequency range where the sea energy is concentrated. Longuet-Higgins (1952) defined this index as:

$$\varepsilon = \sqrt{1 - \left(\frac{T_c}{T_a}\right)^2} \tag{2.8}$$

where T_a is the mean apparent wave period (i.e., the mean value of the time occurring between two consecutive observation of water elevation equal to the mean water level and increasing) and T_p is the mean period occurring between two measured crests. Clearly, in case of a single harmonic wave, the energy would be all concentrated in a single value of frequency, T_a and T_p would be the same and the band wideness index ε would be equal to 0 (narrow band spectrum). On contrary, when the wind sea features a wide frequency content, T_a and T_p can be largely different and ε increases, tending to become one (wide band spectrum). Generally narrow band spectrum are used for design, as

their analytical representation is more simple and only few oceanographic observations on sea states with a wide frequency content are available.

Several models of energy spectrum, referred to unidirectional wind sea, have been developed and proposed in literature; the most widely used are the Pierson-Moskovitz Spectrum, the JONSWAP Spectrum, (outcome of the Joint North Sea Wave Project) or the Bretschneider Spectrum. A more detailed discussion of these analytical spectrum models is given in Sarpkaya and Isaacson (1981). These analytical spectrum have been obtained on the basis of many experimental observations and describe the sea state as a function of one or two parameters, which can be one of the following: characteristic wave height $H_{w,\,1/3}$ (i.e. the mean value of the wave heights being larger than the 67^{th} percentile), the mean apparent wave period T_a or the wind velocity at a specified height. These quantities are clearly related to each other and several relationships among them, based on empirical observations, are available in literature, sometimes introducing also other relevant parameters such as the wind duration and the fetch (i.e. the portion of the sea interested by the wind blowing).

Generally unidirectional wind seas turn out to be more onerous than multidirectional ones; nevertheless, in some cases it might be necessary to include the directional effect in the structural analyses. Multidirectional energy spectra $S_\eta(\omega,\varphi)$ are generally obtained from unidirectional ones $S_\eta(\omega)$ by means of the following equation:

$$S_\eta(\omega,\varphi) = G(\omega,\varphi)\cdot S_\eta(\omega) \tag{2.9}$$

where $G(\omega,\varphi)$ is the angular distribution function, providing the distribution in the direction domain of the energy density concentrated at each frequency. Clearly, for the conservation of the energy amount of the sea state at each frequency, $G(\omega,\varphi)$ has to meet the following condition:

$$\int_{-\pi/2}^{\pi/2} G(\omega,\varphi)\cdot d\varphi = 1 \tag{2.10}$$

Several angular distribution functions can be found in literature, such as the ones proposed by Pierson, by the SWOP (Stereo Wave Observation Project) or by Mitsuyasu (1975).

Computation of hydrodynamic loads

The computation of the hydrodynamic forces induced by the relative motion between water and a marine structure is a very complex issue, involving many variables, and it has been deeply and carefully studied in the past (Sarpkaya and Isacsson, 1981).

In offshore engineering practice, the most diffuse and simple way to predict the forces F_h per unit length arising from interaction between the water and a structural element of a marine structure, is the Morison's equation, conceived to calculate the hydrodynamic loads acting on slender cylindrical components of offshore structures. In case of flexible structures, the Morison's equation can be expressed as:

$$F_h = \rho_w \cdot \frac{\pi \cdot D^2}{4} \cdot [(C_I - C_M) \cdot (a_w - a_s) + C_M \cdot a_w]$$

$$+ \frac{1}{2} \cdot \rho_w \cdot C_D \cdot D \cdot (v_w - v_s) \cdot |v_w - v_s| \qquad (2.11)$$

where ρ_w is the water density, D is the external diameter of the structural element (i.e. tunnel or cable), C_I is the inertial coefficient, C_M is the added mass coefficient, C_D is the drag coefficient, a_w and a_s are the water particle and structure acceleration, respectively, v_w and v_s are the water and structure velocity, respectively.

The first addend of the Morison's equation is the inertial contribution, which, in turn, is the sum of two contributions. A first one is due to diffraction effects induced given by the presence of the structure is proportional to the relative acceleration between the water and the structure: the trajectories of the accelerating water particles are deviated due to the body presence and this requires a dynamic pressure field in the proximity of the body itself. This part of the inertial force is often referred as the added-mass contribution, as it can be interpreted as the additional inertia force needed to accelerate a body placed inside a fluid. The second contribution to the inertial force is the so-called Froude-Krilov force, related to the undisturbed water flow, and is the resultant of the dynamic pressure field which would have accelerated the amount of water displaced by the body. In case of an ideal fluid moving across a circular cylinder, it can be proved that the value of the inertial coefficient C_I and added mass coefficient C_M are equal to 2.0 and 1.0 respectively.

The second addend of the Morison's equation is the drag force or resistance, which is produced by the separation of the water flow from the body surface due to the viscosity of the fluid. The separation of the fluid leads to the generation of a turbulent wake, occurring mainly below the downstream portion of the body, thus entailing a difference between the pressures acting on the upstream and downstream part of the body, whose resultant is the form drag force. It is worth underlining that, even though the drag force is generated by the viscosity of the fluid (in a real fluid this force would be equal to zero, as it can be analytically proved), it is not a viscous force, as the contribution of tangential viscous stresses acting on the body surface is negligible.

The separation of the flow and the resulting turbulence is the key phenomenon influencing the dynamic pressure field occurring at the water-structure interface. Flow separation is strongly dependent on the flow regime, thus it has a strong dependence on the Reynolds number, which is defined as the ratio between the product of water velocity V and the cylinder diameter D (or the projection of the body cross-section in the direction orthogonal to the flow) and the kinematic viscosity of the water ν (equal to about 10^{-6} m^2/s). Many experiments on steady water flows passing over circular cylinders have been conducted in the past, which allowed to recognize four main flow/turbulence regimes in the proximity of the cylinder (Figure 2.32):

A. Subcritical flow regime: the flow is steady and laminar, up to Reynolds number equal to 50. In the Reynolds number range between 50 and 200 the flow is still laminar, but the near wake becomes unstable and oscillates periodically. At higher Reynolds number (up to about 1500) some turbulence starts to occur and spread downstream. When Re becomes larger than 1500, the turbulence move upstream and the far wake becomes increasing irregular. It can be noticed that, besides of the very large values due to viscosity tangential stresses in the Reynolds number range between 0 and 1000 (not relevant in actual flow cases), the drag coefficient C_D, defined as the ratio between the measured force and the product $\rho_w \cdot D \cdot V^2/2$, assumes an almost constant value approximately equal to 1.2.
B. Critical flow regime: when the Reynolds number is approximately equal to $5 \cdot 10^5$ the separation of the flow is laminar in its initial part, with the

formation of bubbles which end with the reattachment of the flow to the body and the successive turbulent separation, followed by a turbulent wake. Due to the formation of this bubbles the turbulent separation points move downstream and the resulting turbulent wake is narrower than the one occurring in the laminar flow regime; the reduction in the wake size leads to a sharp decrease of the drag force, usually named drag crisis. It is important to underline that the drag crisis does not always occur in correspondence of the same Reynolds number, depending on the flow characteristics; for instance an unsteady flow, such as the wave flow, could lead to the drag crisis at a different value of Re.

C. Supercritical flow regime: further increasing the Reynolds number leads to the start of turbulence in the reattached portion of the boundary layer, leading to an increase in the form drag.

D. Post-supercritical: the drag force is constant and equal to a value approximately equal to 0.6. No reliable experimental data are available at Reynolds number having a order of magnitude larger than 10^7, but it is expected that no relevant variations in the boundary layers and the consequent turbulent wake would occur (Sarpkaya and Isaacson, 1981).

(a)

	A Subcritical	B Critical	C Supercritical	D Post-supercritical
Boundary layer	laminar	transition	turbulent	turbulent
Separation	about 82 deg.	transition	120 - 130 deg.	about 120 deg.
Shear layer near separation	laminar		laminar separation, bubble turbulent reattachment	turbulent
Strouhal number	$S = 0.212 - \frac{2.7}{Re}$	transition	0.35 - 0.45	about 0.29
Wake	Re<60 laminar; 60<Re<5000 vortex street Re > 5000 turbulent	not periodic		
Approximate Re range	< $2x10^5$	$2x10^5$ to $5x10^5$	$5x10^5$ - $3x10^6$	> $3x10^6$

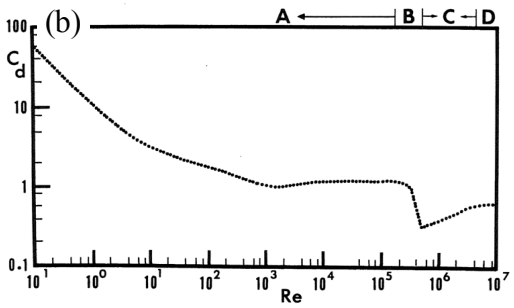

Figure 2.32. Flow regimes due to steady currents on circular cylinders. (a) regimes characteristics (Sarpkaya and Isaacson, 1981); (b) Drag coefficient as a function of the Reynolds number (Schlichting, 1968).

Due to the great dependence of the hydrodynamic forces and related force transfer coefficients C_D and C_I on the flow turbulence and on the past history

of the flow, it can be immediately recognized that differences occur in the water-structure interaction during the oscillatory motion due to waves.

Several experimental studies conducted in harmonically oscillating floes showed that the force transfer coefficients C_D and C_I are dependent on the Reynolds number (as already showed), on the Keulegan-Carpenter parameter K, which is equal to ratio between the product of the flow maximum velocity V_m and the wave period T_w, and the cylinder diameter D ($K=V_m \cdot T_w/D$), on the ratio between the superficial roughness factor k and the cylinder diameter D and on the time t.

With respect to time t it can be observed that, even though it is evident both intuitively that experimentally that instant values of C_D and C_I can be very different from the averaged values, it is an impossible to task to derive a suitable time-variation law, even for the most regular time-dependent flows (Sarpkaya and Isaacson, 1981), so that the time dependence has to be entirely assigned to the Morison's equation.

Concerning the dependence on Re and KC, some experimental plots are given in Figure 2.33 (Sarpkaya, 1976), showing the dependence on both parameters of the force transfer coefficients, which might lead to values significantly different from the ones usually considered for cylinders subjected to steady water motion, in particular in the range of KC between 8 and 25. It is worth underlining that in this particular range, which is also the range where the hydrodynamic forces are dominated by both drag and inertia terms, the Morison's equation is noticeably less accurate, so that several modified versions of the equation, including an additional corrective term, have been proposed in literature (Sarpkaya and Isaacson, 1981).

The choice of the appropriate values for the force transfer coefficients should therefore be made through an appropriate prior assessment of the water velocities and of the wave period. Since generally wave water motion is not monochromatic, but features several harmonic components, appropriate averaged values of the coefficients should be considered. However, since actual water motion is different for many reasons from the theoretically predicted one, it has to be kept in mind that some uncertainties in the hydrodynamic force evaluation cannot be removed and have to be covered with appropriate safety factors. Experimental test specifically conceived to fit a particular design case could be carried out in order to determine more

reliable values of the inertia and drag coefficients. In particular, Reynolds number relative to SFTs would generally be larger than 10^7, thus falling in the range where no extensive experimental data are available.

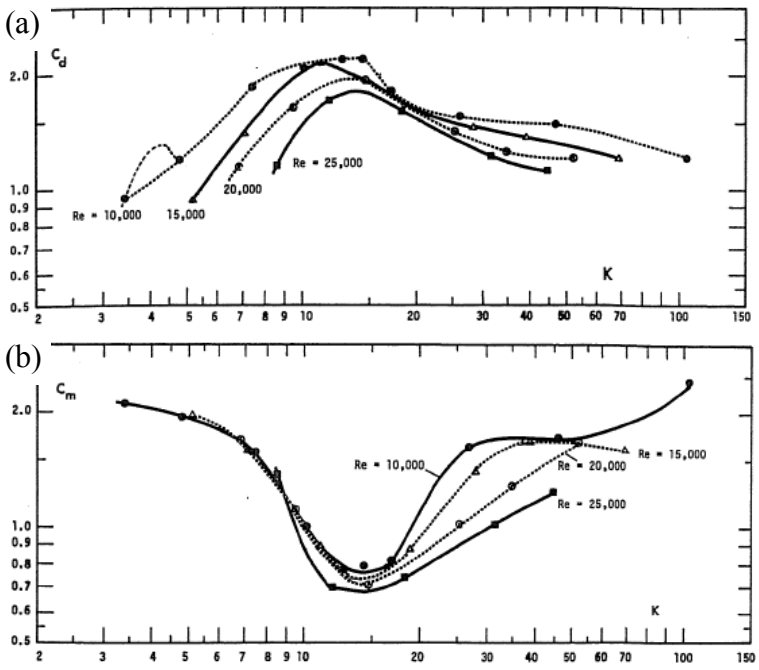

Figure 2.33. Replot of the Keulegan-Carpenter experimental data as a function of Re and K (Sarpkaya, 1976): (a) Drag coefficient; (b) Inertia Coefficient.

Concerning the influence of the surface roughness, this leads generally to an increase of the drag coefficient and also to a change in the value of the Reynolds number value corresponding to the drag crisis (Figure 2.34).

International codes or guidelines for the design of offshore structures recommend values of the drag and inertial coefficient ranging from 0.6 and 1.2, respectively, (smooth members) to 1.2 and 2.0 (rough members) for steady flows. In particular API-RP2A-WSD guidelines (2002) provide in the commentary useful diagrams allowing for modification of the steady flow values of the coefficients due to the effective surface roughness and to the wake effect due to the unsteady wave motion (Figure 2.35).

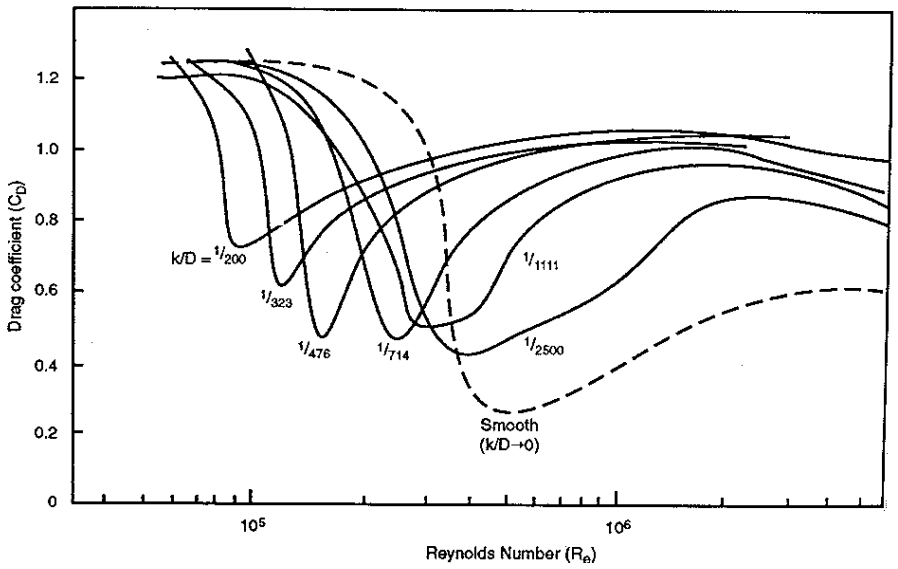

Figure 2.34. Drag coefficient of rough cylinders as a function of the Reynolds number (FEHRL, 1996).

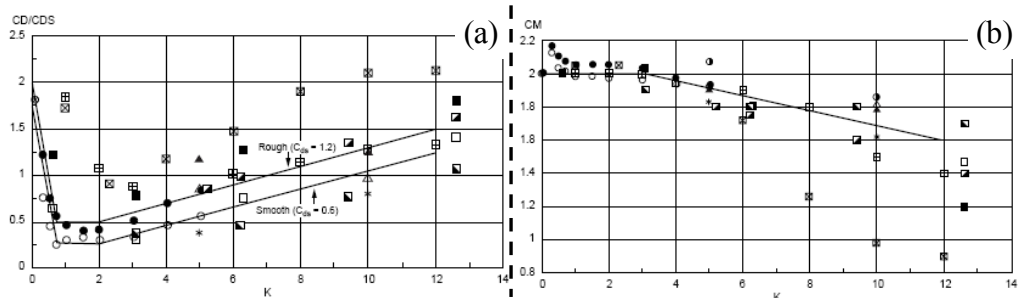

Figure 2.35. Modification factors for the wake effects as a function of K provided by API-RP2A-WSD guidelines (2002): (a) Drag coefficient; (b) Inertia coefficient.

The Keulegan-Carpenter parameter K is not only a measure of the unsteadiness of the water flow, but it is also directly related to the type of hydrodynamic force regime, which could be inertia-dominated, drag and inertia dominated or drag dominated. In fact, considering a harmonic water flow, it can be shown that the ratio between the maximum drag force $F_{d,max}$ and inertia force $F_{I,max}$ occurring is directly proportional to the ratio C_D/C_I and

to K. Moreover, since the drag and inertia force are out of phase, it can be proved that the maximum total hydrodynamic force is equal to maximum inertia force $F_{I,max}$ when the ratio $F_{d,max}/F_{I,max}$ is lower or equal to 0.5.

Thus, depending on the values of C_D and C_I, it can be determined a limiting value of K_{lim} which divides the range of values of K for which the drag force has to be taken into account ($K>K_{lim}$) or can be neglected ($K<K_{lim}$). Assuming C_D and C_I values commonly adopted in practice, it can be seen that the hydrodynamic force is inertia dominated when K<8-14, is drag and inertia dominated when K is enclosed between 8÷14 and 25÷30 and is drag dominated (inertia contributions are negligible as the flow tends to behave as a steady flow) when K>50. The difference between the different force regimes is particularly relevant from the computational point of view, considering the non-linearity of the drag force; therefore a linear modeling of the hydrodynamic load can be used in case of inertia dominated regime.

If the Airy wave theory is assumed to be valid, it is possible to determine a linear relationship between K and the wave height H_w and the structural diameter D. In particular, it can be seen that for values of the ratio H_w/D lower than 4÷6, the drag contribution to the hydrodynamic force can be neglected (Figure 2.36).

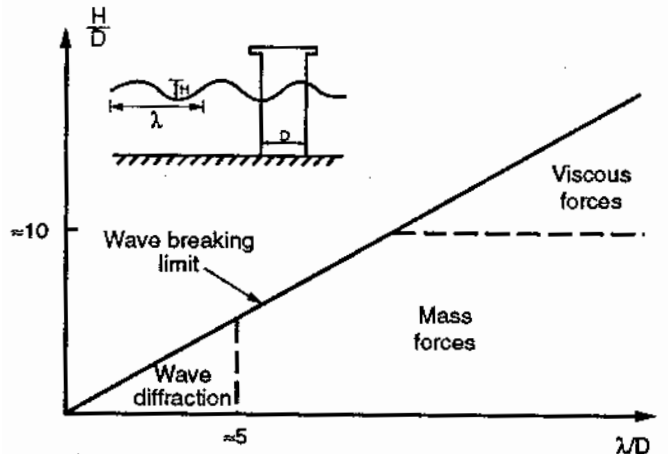

Figure 2.34. Wave loading regimes (FEHRL, 1996).

The Morison equation is derived on the basis of the assumption that the kinematics of the undisturbed flow in the region near the structure do not

change in the incident wave direction. Since flow velocities and accelerations actually vary in space with a gradient being proportional to the wavelength L_w, this equation can be assumed to be valid only for small values of the diameter-to-wave length ratio D/L_w. A comparison between the values of the inertia coefficient relative to a vertical cylinder given by the potential of a steady uniform current and by the application of the linear wave diffraction theory by Mac Camy and Fuchs (1954) indicates that the Morison equation can be assumed to be valid when D/L_w is approximately lower than 0.2 (Figure 2.34). SFT are generally slender structures, as the ratio between the tunnel diameter (or relevant cross-section dimension) and the tunnel length is usually small; nevertheless, when operational or fatigue design conditions have to be checked (so that the wavelength is smaller than 50-100 m), the ratio D/L_w is most likely to fall in the range of invalidity of the Morison equation

In those cases where the Morison equation should not be used the diffraction problem (linear or non-linear) has to be solved. Clearly diffraction problems are largely more complex than the application of the Morison equation; however the influence of wave diffraction is undoubtedly beneficial, as it leads to a reduction in the wave loads exerted on the structure. Physically, this result can be explained considering that when the particle accelerations of the undisturbed water flow are maximum over one portion of the structure they are not so over the rest of the structure (Sarpkaya and Isaacson, 1981).

Moreover, very often large values of D/L_w correspond to small values of H_w/D, so that the effects of flow separation can be disregarded and the hydrodynamic force is inertia dominated.

The solution of the diffraction problem consists in determining the potential of the flow occurring around the body as the sum of two or three components, depending on if the body is assumed to be fixed or to move rigidly. The three components of the total potential flow are the one relative to the undisturbed flow, the one relative to the scattered wave and, eventually, the one relative to rigid body motion of the structure, which in turn can be expressed as the sum of the unrestrained degrees of freedom. The solution has to meet the boundary conditions, which are the kinematic and dynamic boundary condition at the water free surface, the impermeability condition at the seabed (i.e., the flow normal to the seabed is equal to zero) and at the body surface (the flow normal to the body is null), the radiation condition, which

for a horizontal cylinder such as the SFT requires that the scattered waves travel outward.

Such a complicated problem has to be solved numerically; numerical solution procedures like the method developed by Garrison (1978) can be used. Alternatively more advanced numerical methods, exploiting the large computational capabilities of modern calculators, such as the Finite Element Method (F.E.M.) can be used. This method allows to model more realistically the water behaviour by solving the Navier-Stokes equations and to take into account the fluid-structure interaction resulting from the flexible motion of the structure. This kind of procedure has been used in Remseth et al. (1998), where a simple three-dimensional beam model of the SFT has been coupled with a two-dimensional shell model of the water in the SFT cross-section plane; however these procedures require large computational efforts and may lead to convergence problems or to potential errors hard to be noticed.

Vortex shedding

When a steady current is passing over a cylindrical body, separation of the flow occurs, due to the viscosity of the fluid. In certain ranges of values of the Reynolds number regular shedding of vortices can occur below the separation points, as described in the previous section. Generally the vortex shedding is asymmetric, i.e. vortex are generated alternately on both sides of the downstream portion of the cylinder, giving rise to dynamic pressure field exerted on the cylinder which varies with. The resultant of these time varying pressures is an oscillating force, which has a main component in the direction transversal to the flow propagation, named lift force, and a minor one in the direction of the flow, which is added to the steady value of the drag force and features a frequency being twice the one of the vortex shedding.

In 1878, Strouhal found a relationship between the frequency of the vortex shedding and the velocity of the incoming flow. In particular, he defined the following relationship:

$$St = \frac{f_v \cdot D}{V} \tag{2.12}$$

where f_c is the vortex shedding frequency and St is the Strouhal number. The Strouhal number is found to be nearly constant, equal to 0,2 for smooth circular cylinders and to 0, 25 for rough circular cylinders, in the Re range

from 10^3 to $5 \cdot 10^5$, and for Re belonging to the post-supercritical flow regime is nearly constant and equal to 0,5 for smooth circular cylinders (Figure 2.37). For very large values of Re ($\geq 10^8$), which are generally of interest for SFT cases, only experimental data in wind tunnel test are available. In the critical and supercritical flow regimes a broad band power spectral density of the vortex shedding is observed for rigidly held cylinders, whereas the lock-in phenomenon occurs for flexible cylinders, which will be discussed later on.

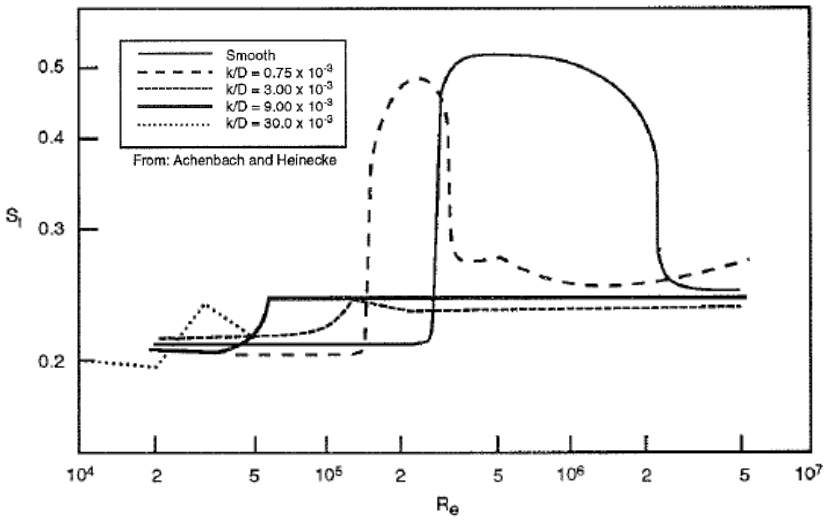

Figure 2.37.Variation of Strouhal number St with Reynolds number and surface roughness (Achenback, 1971).

Therefore, for most of the Reynolds number values, the lift force F_L can be assumed to be harmonic with a frequency corresponding to the one of the vortex shedding (in the critical and supercritical flow regimes a dominant frequency of the spectrum can be considered instead) and can be expressed similarly to the drag force:

$$F_L = \frac{1}{2} \cdot \rho_w \cdot C_L \cdot D \cdot {v_w}^2 \tag{2.13}$$

where C_L is the lift coefficient, assuming values varying from 0.2 to 0.25 for steady currents. More information on the values assumed by C_L in case of oscillating flow can be found in Sarpkaya and Isaacson (1981).

The previous discussion is valid only for fixed cylinders, whereas differences occur when the flow encounters a flexible body. In fact for flexible bodies there is a mutual interaction between the body oscillations and the vortex shedding which can be classified as an hydro-elastic phenomenon: when the vortex shedding frequency f_v becomes close to one of the natural frequency f_n of the structural element (in the transversal direction) vortices start to be shed with a frequency being equal to f_n instead of following the shedding frequency given by the Strouhal number (equation 2.12); this phenomenon is usually named lock-in and it is generally observed in a range of velocity corresponding to values of f_v being larger than approximately $\cdot f_n$ and lower than approximately $1.4 \cdot f_n$ (Figure 2.38). During the lock-in sustained oscillations of the cylinder occurs, which might lead to a severe increase in the structural stress regime. Large vibrations due to synchronization do not always occur in case of vortex shedding, but it is necessary that the oscillating lift force is sufficiently large, so that the structural vibrations can start and give rise to the hydro-elastic instability (Sarpkaya and Isaacson, 1981).

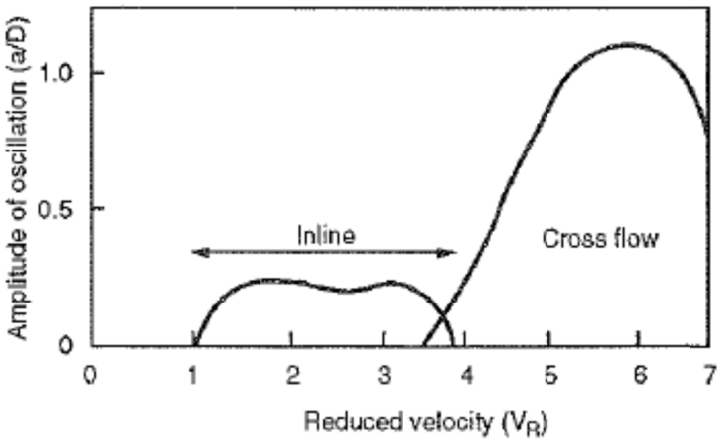

Figure 2.38. Typical amplitudes and regions of vortex shedding induced response for low damping systems (FEHRL, 1996).

It is worth underlining that the large amplifications of the oscillations induced by vortex shedding in the frequency range close to the natural frequency of the structural element are not due to resonance, as resonant

forced oscillations occurs at a frequency equal to the one of the driving force and feature a noticeable peak in correspondence of the resonant frequency, whereas the response spectrum relative to vortex induced oscillations features a slowly varying portion where values similar to the maximum amplitude of the response are attained (Figure 2.38).

It is evident from the foregoing considerations that the values of the velocity of the incoming flow V, the vortex shedding frequency f_v and the cylinder diameter D participate in determining the occurrence of vortex induced vibrations. It is also intuitive that the structural damping ratio ζ_s (i.e. the ratio between the structural damping and its critical value) plays a fundamental role, as the lock-in phenomenon requires that the body starts to oscillate significantly in order for it to start absorbing energy from the fluid and progressively increase its vibrations amplitude. As a matter of fact, it is well known from structural dynamics that the amplitude of forced oscillations are strongly influenced by the damping value when the oscillating force has a frequency close to natural vibration frequency of the system.

Two a-dimensional parameters can be defined as functions of the afore mentioned quantities, the reduced velocity V_r and the reduced damping K_r:

$$V_r = {V}/{(f_v \cdot D)} \tag{2.14}$$

$$K_r = {4 \cdot \pi \cdot m \cdot \zeta_s}/{(\rho \cdot D^2)} \tag{2.15}$$

Experimental tests carried out agree in indicating the excitation range of vortex induced vibrations is delimited by a lower bound of V_r approximately equal to 4÷4.5 and upper bound approximately equal to 10, with the maximum amplitudes falling within the range of $6.5<V_r<8$ (Figure 2.38).

In line oscillations occur too and too instability regions can be recognized (Figure 2.36). The first region is in the range $1.25<V_r<2.5$ and is accompanied by a symmetric vortex shedding (differently from the usual vortex shedding), as if the flow started impulsively from rest at each cycle (Sarpkaya and Isaacson, 1981); the second region is in the range $2.7<V_r<3.8$ and is accompanied by the “classic” alternate vortex shedding. The amplitude of in-line vortex induced vibrations is considerably lower than the one of

transversal vibrations. However, both numerical and experimental tests showed that there is an interaction between transversal and in-line oscillations: both the mean value and the amplitude of oscillations of the drag force increase due to growing amplitude of the transversal oscillations, so that the increase of the in-line force should be taken into account in the design of structural members which may undergo significant transversal vortex induced vibrations.

Several mathematical models have been developed with the aim of simulating the vortex induced vibrations experimentally observed. These models are generally based on a coupled system composed of a SDOF linear oscillator and a non-linear flow oscillator, whose differential equation features as unknown time function $C_L(t)$. The coupling is provided through the dependence of the lift force coefficient $C_L(t)$ on the structural velocity. Most of these models do not include the analysis of the flow field and the fluid-mechanical modelling does not seem sufficiently accurate (Sarpkaya and Isaacson, 1981), thus they can be assumed to be valid not as numerical tools to investigate the relationships occurring between the physical parameters influencing the phenomenon, but for their ability to be calibrated in order to reproduce the experimental results obtained in certain specific conditions. A number of flow-field models have been proposed too, which are generally based on discrete vortices. Moreover, thanks to the great improvements in computational capability of modern calculators, several numerical studies based on coupled F.E.M. of cylinders and Computational Fluid Dynamic model have been conducted.

A comprehensive review of the knowledge gained on the vortex induced vibrations phenomena and on their experimental test and numerical simulation is given in Sarpkaya (2004).

In common offshore practice the influence on vortex induced vibrations is taken into account in the design process by means of local analysis (API-RP2A-WSD guidelines, 2002), thus assuming that no interaction arises between the dynamic behaviour of each structural component and of the global structure due to vortex induced vibrations and to the other current and wave forces. Moreover, none of the previously described models, although some of them are extremely advanced, allow to simulate the vortex induced vibrations in a global structural model.

In the SFT case significant interaction can occur, in the low frequency range, between the local transverse oscillations of the cylindrical tethers of the anchoring system and the longitudinal and transversal oscillations of the tunnel, as outlined by Perotti and Di Pilato (2009). In the framework of their research studies aimed at developing suitable numerical tools specific for the SFT cases, they formulated a finite element able to represent the non-linear structural behaviour of SFT anchoring bars and to integrate in the global structural analysis their vortex induced vibrations. This finite element is formulated considering the integration of a non-linear bar element with a Distributed Vortex Layer model (DVL), which is connected on one side to the bar itself and on the other side to a fixed reference system. Both connections consist of non-linear spring dashpot systems, featuring a linear and cubic dependence on the relative velocity and displacement between the vortex layer and the body or fixed reference system (Figure 2.39). Clearly the spring dashpot parameters and the mass associated with the vortex layer have to be tuned on the basis of experimental results and to reproduce a vortex shedding frequency equal to the natural one provided by the Strouhal number.

This approach seems to be promising, but requires further studies, as pointed out by the authors themselves, because this model seems to be strongly dependent on the flow initial conditions and often produces results not consistent with experimental results available.

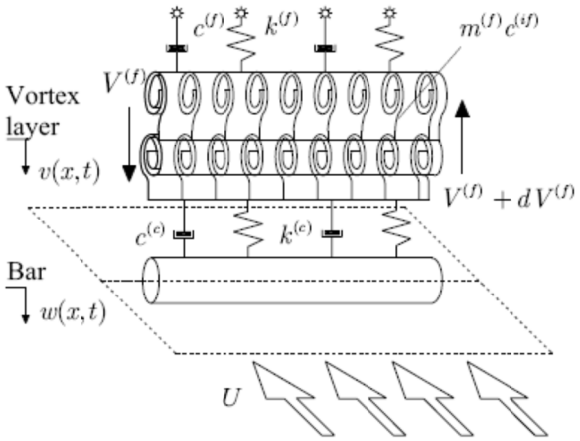

Figure 2.39. Sketch of the Distributed Vortex Layer model (Amoruso and Bettoni, 2009)

2.2.3.2. Earthquakes

Strong ground motion occurring to seismic events propagate in the structure by means of the tunnel shore connections and of the SFT anchoring system. Thanks to the overall deformability of the system and to the beneficial presence of the water, SFTs generally exhibit a very good response to seismic events. However some specific issues have to be considered in the design phase, such as, for instance, the configuration of the shore connections (see section 2.1.3.2) or the behaviour of shorter anchoring elements located close to the shores. More generally, it is necessary to assure that every structural component safely withstand extreme seismic events and that functional performances are met in case of more frequent earthquakes.

The seismic action must be characterized in the three dimensions on the basis of a careful seismological study of the crossing site, through analytical tools and available records from previous seismic events and can be modelled by means of design response spectra or ground motion acceleration. The former ones should be used only in case of moderately severe seismic events, as they are used in conjunction with a linear modal dynamic analysis which is thus unable to capture the non-linear structural behaviour. Moreover, there is no way to introduce in a modal analysis with response spectrum the spatial variability of the ground motion, which can be particularly relevant for a SFT, whose connections with the ground can be considerably distant. Therefore the most suitable option is to model the seismic event through sets of ground motion time histories, consistent with the seismic hazard of the site and adequately accounting for the spatial variability, to be introduced in a dynamic (linear or, preferentially, non-linear) three-dimensional dynamic analysis. Moreover, dynamic analysis allow to directly introduce structural elements designed to exhibit a dissipative post-elastic behaviour during severe seismic events, such as, for instance mechanical or fluid-mechanical dissipative devices located at the shore connections.

Recorded ground motion time-histories can be used in principle, but it is unlikely that the available records can adequately represent both the seismicity of the site and the spatial variability. Therefore artificial or synthetic accelerograms can be used. The former ones are generally obtained as Fourier series from Power Density and Cross Power Density Spectrum analytical models available in literature. This approach has been used by Fogazzi and

Perotti (2000) and Di Pilato et al. (2008) in the validation of the SFT F.E. model developed by them. However, this approach is often criticized as the produced accelerograms seem to be unrealistic. Synthetic accelerograms are instead derived through simulation of the fault mechanism rupture and thus represent a more reliable seismic scenario, provided that the simulation is carried out by an expert user and that all the data needed to properly model the seismic source and the wave propagation in the ground are reliable.

Horizontal ground motion cannot propagate into water, but vertical ground motion waves can travel in it and this water motion should therefore taken into account in SFT seismic analyses. Brancaleoni et al. (1989) studied the propagation of seismic synchronous vertical motion in the water through a two-dimensional Finite Element model, accounting also for the incompressibility of the water and showed that the water motion can be assumed to be equal to the ground motion, thanks to the reduced compressibility of the water itself. In Martire et al. (2010a, b) dynamic analyses are carried out considering both the spatial variability of the ground motion and the propagation of its vertical component in the water layer, calculating the sets of ground motion time histories and the water kinematic field through a three-dimensional simulation of the seismic fault rupture and propagation of the generated waves in the ground and water layers. The results of these analyses will be discussed in detail in Chapter 7.

2.2.3.3. Tsunamis

Tsunamis are waves generated by large mass movements at the seabed, such as the landslides, subsea earthquakes or volcano explosions. Tsunami waves are translational waves featuring very large wavelengths and small surface elevations in open water that can travel very long distances over entire oceans. Therefore SFTs may be exposed to Tsunamis even if the latter are generated very far from the SFT location. When Tsunamis reach shallow water near the shores, their height enormously increase. On the other hand Tsunamis periods are very long, so that their effects are significant also at large water depths, thus representing a potential serious hazard for SFTs.

To the Writer's knowledge, no studies on the SFT response to Tsunamis is available in literature. However such a kind of study should be similar to the ones devoted to the SFT response to wave actions, provided that a reliable estimate of the water flow is considered. The use of the solitary wave theory is

commonly suggested to calculate the water kinematics occurring during a Tsunami event.

2.2.4 *Accidental loads*

Accidental actions mainly include:

- Collisions due to dropping objects, sinking ships or impacts with submarines;
- Flooding.
- Rockslides
- Fire.

Few studies exist in literature, to the Author's knowledge, on these topics. Rambech et al. (1994) studied the elasto-plastic capacity of a submerged steel bridge in case of impacts with sinking ships. An extensive review of fire safety systems available for underground tunnels and applicable to SFTs is given by Fiorentino (2009).

2.3 THE MAIN ADVANTAGES OF THE SFT

2.3.1 *SFT vs Cable Supported Bridges*

Comparing the main features of Submerged Floating Tunnels with those of Cable Supported Bridges the following advantages of the former ones can be recognized:

- SFT is a modular structure, therefore it is theoretically feasible to surpass spans of any length, even though some specific issues have to be faced for very large lengths, whereas it is well known that Cable Supported Bridges do not represent an effective structural solution for long crossings.
- Thanks to its modularity, the cost per unit length of a SFT can be assumed to be constant, whereas it increases more than linearly with the main span length for Cable Supported Bridges.
- The crossing itinerary of a SFT can be chosen without being strongly influenced by the site characteristics, in particular by the crossing length, thus allowing for a selection of its location by taking into account with the

same importance the aspects related to urban development planning, economic and structural issues.

- SFT features a much lower environmental impact, both from the visual and gas pollution production standpoints, than a Cable Supported Bridge; in fact the SFT does not interfere at all with the landscape as it is invisible and, even though the gas pollution produced is approximately the same for SFTs and CSBs, the former ones can be provided by ventilation plants depurating the air that is released in the external environment.
- SFTs are not subjected to wind actions, which are the most onerous loading condition for a Cable Supported Bridge. Water waves and currents are similar to wind actions, but velocities and accelerations at the depth of interest for a SFT are largely lower than the wind velocities at the heights of interest for a CSB.
- SFTs do not interfere at all with the passage of navigating vessels on the water surface, whereas the pylons of a CSB represent relevant obstacles, thus leading to potential collisions.
- During the construction phases the anchoring system provides degree of stability larger than the one provided by the temporary structural schemes assumed by a CSB during its construction. Moreover, the construction of internal facilities can occur in parallel with the assembly of the tunnel modules, thus reducing the overall construction time, whereas on a CSB roadway and railway facilities can be built only when the construction of the structure is completed.
- The tunnel modules of a SFT can be towed from the production site to the crossing location. Therefore the construction yards for the tunnel modules can be located on any site on the adjacent coastal areas, avoiding the problems related to the arrangement of construction yards in urban areas

2.3.2 *SFT vs Subsea and Immersed Tunnels*

The principal advantages of SFTs with respect to Subsea and Immersed Tunnels are the following:

- Given a certain span to be surpassed, a SFT crossing would feature an overall length considerably lower than a Subsea or Immersed Tunnel

(Figure 1.1), as the encumbrance of the access ramps of the latter ones is necessarily larger.

- The access ramps of a SFT can be made with slope lower than the ones of Subsea and Immersed Tunnels, as this solution is not dependent on the seabed profile (only the anchorages length is influenced by it). This is a very important feature, as the steep access ramps imply a noticeably larger energy consumption, travel time, production of gas pollution and rate of car accidents (in particular with respect to the passage of heavy trucks).
  A study promoted by the Norwegian Public Road Administration for the Høgsfjord showed that the energy consumption and the production of gas pollution estimated for a Subsea Tunnel are 15 times larger than the ones estimated for a SFT (Skorpa, 1994).
- The presence of seismic faults along the tunnel path is not a big issue for a Submerged Floating Tunnel, whereas it is a critical issue for Subsea or Immersed Tunnels.
- SFT is much less dependent on the mechanical properties of the soil than Subsea or Immersed Tunnels.

Chapter 3
The history of the SFT

3.1 INTRODUCTION

The first idea of Submerged Floating Tunnels as a waterway strait crossing system dates back to the first decade of the Twentieth Century, in Norway (Hakkart, 1996), but it remained only as an idea for many years. The improvement and development of the offshore engineering technology has increased the interest for such technological solution. In fact the know-how developed in the field of offshore structures can be conveniently transferred to Submerged Floating Tunnels, they being, as a matter of fact, structures interacting with water. As a consequence, a large number of feasibility studies and preliminary designs was carried out, with the aim of developing the SFT concept and creating the necessary bases for its practical realization.

3.2 SFT PROPOSALS IN ITALY (MESSINA STRAIT)

A fundamental milestone in the history of the SFT development has been represented by the proposal for the Messina Strait Crossing (Italy) by Alan Grant, in 1969. The Grant SFT consists of three concrete tubes cast in two concentric steel shells (Figure 3.1a). The three composite tubes are connected together by a steel frame substructure and contained into a steel elliptical shaped shell, for guaranteeing good hydrodynamic performances to the whole structure; the cavities between the external box and the tubes are filled with ballast material. The central tube holds the railways, whereas the external ones

are devoted to the motor vehicles. The length of the SFT is equal to 3700 m, and the maximum depth equal to about 300 m. The anchorage system is realized by groups of four inclined steel cables, directly connected to the internal composite tubes, which counterbalance the upward residual buoyancy acting on the tunnel; they are placed at an inter-axis of 100-150 m along the length of the tunnel. Cables are fixed to the seabed by means of gravity foundations and rockbolts, depending on the seabed soil mechanical characteristics.

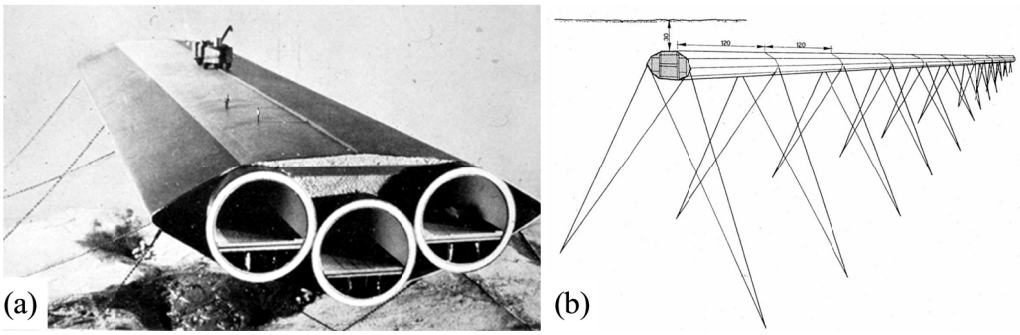

Figure 3.1. SFT proposals for the Messina Strait crossing by: (a) Alan Grant (1969); Ponte di Archimede International Company (1984).

The Grant original design was purchased in 1984 by the "Ponte di Archimede" Company (1984), which proposed and patented a new design solution under the name of "Archimedes Bridge". The cross-section of the "Archimedes Bridge" is made of pre-stressed reinforced concrete, with a polygonal external shape, whereas the anchoring system is similar to the one of the Grant's design, with a cable inclination ranging from 30° to 15°, depending on the distance from the coasts, and inter-axis of 120 m (Figure 3.1b). That solution was certified by the Italian Register for Navigation (RINA) and object of further investigations, in a subsequent refined study, by Faggiano et al. (2001b).

Further proposals, still referred to the Messina Strait Crossing, were made in later years. In particular, the ATI-SSST Italian temporary company association (joining Saipem, Snam Progetti, Spea, Tecnomare companies) conceived, in 1989, a solution consisting in three independent circular tunnels, placed at a distance of 500 m between each other, for both the railway and

motor vehicle traffic. The cross-section of the tunnels has a sandwich structure made of two concentric steel cylinders filled with concrete. The anchoring system is made of four steel or Kevlar cables, inclined of about 45°, which are connected to the tunnel by means of steel collars, placed at the upper side of the tunnel (Figure 3.2a).

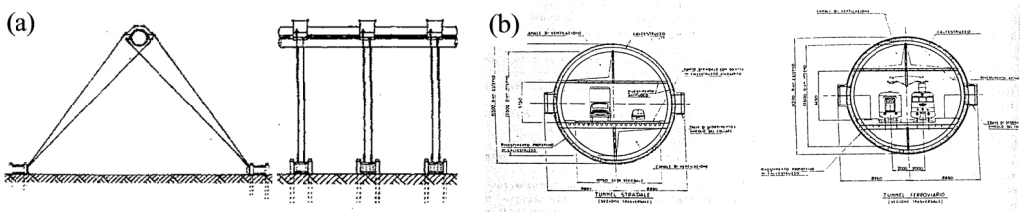

Figure 3.2. SFT proposal for the Messina Strait crossing by ATI-SSST (1989): (a)anchoring system set-up (b); tunnel cross-sections.

In 1993 the ENI Consortium completed another preliminary design of SFT crossing the Messina Strait (Nicolussi and Casola, 1994). Also in this case three independent tunnels, two accommodating roadways and one accommodating railways, are considered; the tunnels are positioned at 700 m and 1000 m one from the other and have the same structural configuration and lay-out. The tunnels feature a circular cross-section having a double steel shell-concrete composite structure with an internal diameter of 14 m and an external one of 17 m. Tunnel modules are 72 m long and feature in their central part special cast elements allowing for the connection of the anchorages (Figure 3.3a). The anchorage system is made up of groups of four inclined tubular tethers, whose slope is approximately equal to 45°.
The tension pipes have diameter and thickness ranging between 1850x62 mm and 2000x68 mm and have a small excess of weight with respect to their buoyancy, in order to facilitate their installation. The configuration of the shore connections is particularly interesting, featuring two special seismic joints, as described in detail in section 2.1.3.

In 1996, SirProgetti company designed a SFT with an original composite structure. This solution was conceived for providing both a suitable hydrodynamic behaviour, thanks to the elliptical external shape, and a safety system allowing the tunnel partial emersion and then the escaping of the people (Figure 3.4a). Moreover, the undulating internal steel tube shape has

been conceived to assure a large dissipation of energy in case of internal explosions (Figure 3.4b).
The anchorage system has a particular three-dimensional arrangement, featuring vertical and inclined cables connecting the seabed with truss cantilevers attached to the external surface of the inner steel tube (Figure 3.4b). The length of the SirProgetti SFT is equal to about 4000 m, and the inter-axis between anchoring groups is 50 m.

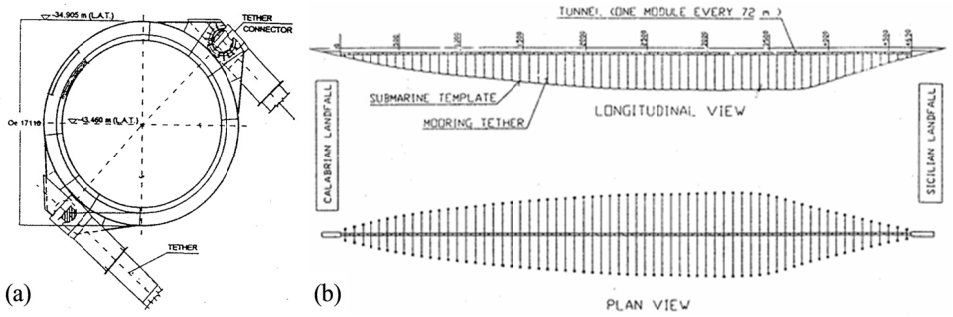

Figure 3.3. SFT proposal for the Messina Strait crossing by ENI Consortium (Nicolussi and Casola, 1994): (a) tunnel cross section and detail of the tether connections; (b) tunnel lay-out.

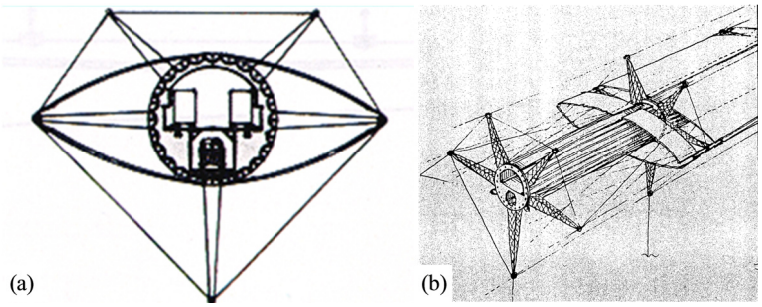

Figure 3.4. SFT proposal for the Messina Strait crossing by SirProgetti Company (1996): (a) tunnel cross section (b) perspective view.

3.3 SFT PROPOSALS IN THE WORLD

In parallel with the above mentioned studies carried out in Italy for the Messina Strait Crossing, further studies were contemporeanously carried out

also with reference to other strait crossings all over the World.

In Norway, in 1987, the Norwegian Public Road Administration (NPRA) promoted the preliminary design of SFTs in the Høgsfjord (Skorpa, 1989; Ostlid, 2010). The fjord is about 2000 m wide, with a depth ranging from 150 to 250 m. Four of the most important Norwegian civil engineering companies participated to such invitation. In all cases, the proposals are characterized by a tunnel with a circular cross-section, which can be made of steel, concrete or a combination of the two materials. The main differences between the designs lie in the conception of the anchorage system, made of different buoy typologies or of vertical tether groups (Figure 3.5).

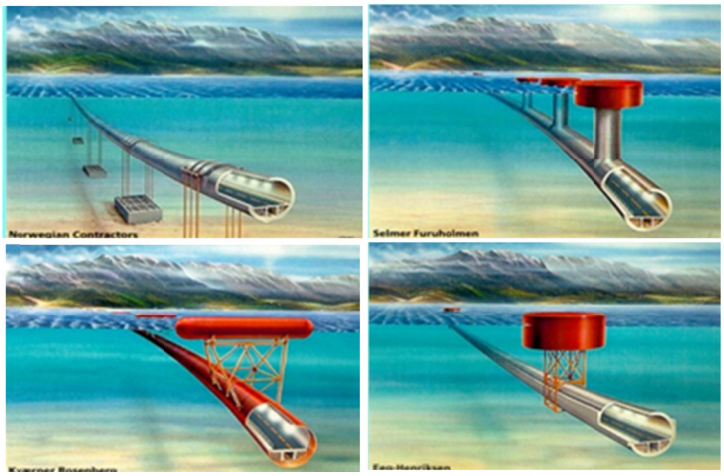

Figure 3.5. SFT proposal for the Høgsfjord crossing by four major Norwegian civil engineering companies.

In 1998 the Norwegian Submerged Floating Tunnel Company AS (NSFT) was established to develop and market the concept of submerged floating tunnels; the owners of NSFT are the consulting engineering companies Dr. Techn. Olav Olsen a.s and Aadnesen as. These companies and the senior staff of NSFT have remarkable experience in general bridge design (including the Høgsfjord project) and the delivery of large concrete structures for the offshore production of oil and gas in the North Sea. NSFT has a cooperation agreement with the Norwegian Public Roads Administration and therefore has access to their SFT experience and relevant software, receiving financial

support from the Norwegian Industrial and Regional Development Fund (SND) and from the Norwegian Research Council (NFR).

In 1999 the NSFT company carried out a preliminary design of an SFT crossing the Storfjorden in Norway. The proposed crossing is 2500 m long, encountering 400 m deep waters (Figure 3.6a). The tunnel structure is made up of pre-compressed r.c. and has a circular shape. The anchorage system is made up of groups of sloped tubular tethers, arranged in the W-shape configuration (Figure 3.6b). Each anchorage group involves 24 tethers (6 sub-groups of 4 sloped cables, with a small longitudinal distance between them); the inter-axis between the anchorage groups is 250 m. Local increase of the tunnel dimensions in the zones around the stays is provided, in order to assure enough buoyancy for tethers pre-tensioning without giving rise to large permanent bending stresses in the tunnel.

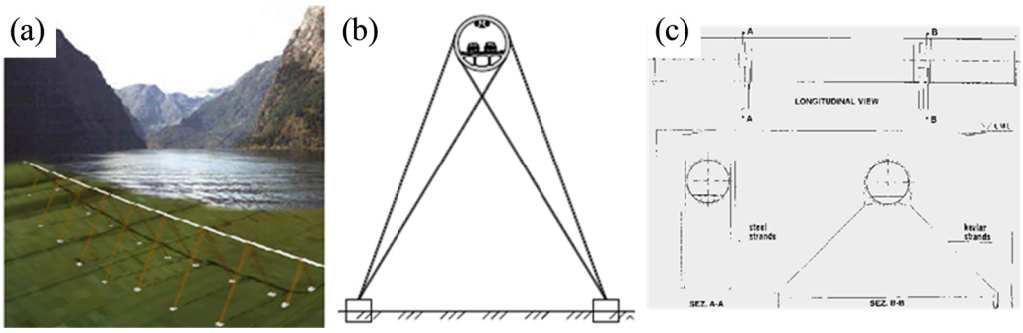

Figure 3.6. SFT proposals for the: (a), (b) Storfjord crossing (Jakobsen, 2009);(c) Lugano Lake crossing (Haugerud et al., 2001).

Further general feasibility studies have been carried out in Switzerland, for the Lugano Lake (Figure 3.6c; Haugerud et al., 2001), in Greece for the Rion-Antirion strait, in Italy for the Como Lake and in Turkey for the Bosforo Strait and in the United States for the Lake Washington (Felch, 2001).

In 1990, the "Society of Submerged Floating Tunnel Research in Hokkaido" was founded in Japan, which was involved in a campaign of studies concerning several aspects of the SFT design and construction. In that framework, several feasibility studies were conducted, which are listed in the table depicted in Figure 3.7. The most important feasibility studies carried out in Japan is related to one of the connections of the "Northern Japan Exchange

axis", namely the Funka Bay's crossing, connecting Hokkaido and Honshu islands (Fujii, 1996).

Name of project	Location	Purpose	Length (m)	Max. Water depth (m)
Funka Bay Crossing	Bay threshold	Motor vehicle Railroad	30,000	120
Toya Lake crossing	Lake crossing	Pedestrian Mono-rail	3,000	100
Rishiri Rebun Crossing	Strait Crossing	Lifeline Transportation system	22,000	200
Ishikariwan Shinko In-port Crossing	In-port Crossing	Motor vehicle	972	15
Daikokujima Crossing	In-port Crossing	Pedestrian	120	10
Soya Strait Crossing	Strait Crossing	Motor Vehicle Railroad	43,000	180
Otaru In-port Crossing	In-port Crossing	Pedestrian	300	10
Okinawa-Ie island Strait Crossing	Strait Crossing	Motor Vehicle	3,000	150

Figure 3.7. Major feasibility studies done by the society of SFT research in Hokkaido (Kanie, 2010).

In particular, with regard to the Funka Bay's crossing, the SFT is characterized by a steel-concrete composite cross-section. The whole length of the crossing is equal to 30 km, and the water depth reaches a maximum value of 120 m. Four different anchoring systems are proposed, consisting in vertical or sloped tendons (Types A to D in Figure 3.8b): the solution which has been considered as the optimal one for economic and structural reasons is Type D one. In order to ensure the same initial tension in the left side and right side tendons, guides having an internal low friction surface is built on the external surface of the circular tunnel cross-section: in this way a single cable passing through one of this guide can serves as left and right side tendon, thus clearly featuring the same value of the initial tension (Kanie, 2010).

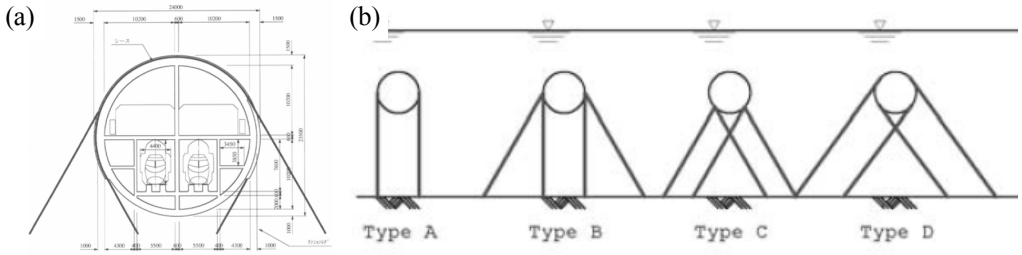

Figure 3.8. SFT crossing Funka Bay (Japan; Kanie, 2010): (a) tunnel cross-section; (b) proposed cable groups arrangement.

Another proposal is the one relative to the Daikokujima crossing (Figure 3.9a), conceived as a small SFT to be built for experimental purposes: the pedestrian crossing features a120 m length and a maximum water depth of 12 m. The tunnel structure is extremely light and features an unusual buoyancy to weight ratio equal to 5.0. The SFT is firmly supported by tension legs supported by piled foundations (Figure 3.9b) located along the tunnel length with an inter-axis of 12 m.

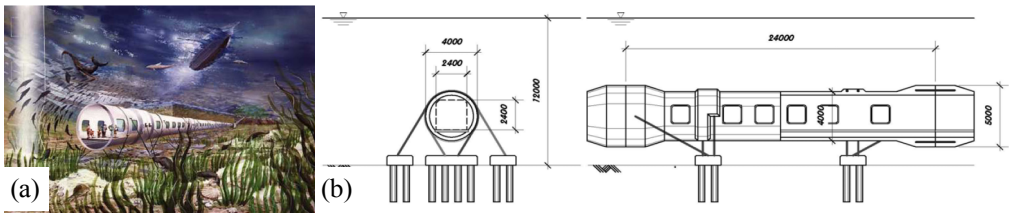

Figure 3.9. Daikokujima SFT crossing (Japan; Kanie, 2010): (a) tunnel cross-section; (b) proposed cable groups arrangement.

In 2010 also Korea showed interest for using SFT as a strait crossing solution. As a matter of fact in 2010 a preliminary design of a SFT crossing the Jeju Strait has been conceived (Kim et al., 2010): the proposed solution features a tunnel with an elliptical cross-section rigidly supported by steel jacket structures. The crossing has a length of 68 km and maximum water depth of 120 m.

An important step in the development process of SFTs is the analysis report published in 1996 by the Danish Road Institute, the Italian company "Ponte di Archimede S.p.A." and the Norwegian road research Laboratory on the behalf of Forum of European National Highway Research Laboratories (FEHRL, 1996).

3.4 SFT PROPOSALS DEVELOPED BY THE UNIVERSITY OF NAPLES FEDERICO II (WITH OTHER PARTNERS)

3.4.1. The Sino-Italian cooperation programmes

A milestone in the SFT history is represented by the international cooperation programmes between scientific institutions coming from Italy and

People's Republic of China, activated since 2001. In 2001 a contract between the Italian Ministry of Foreign Affairs and the University of Naples "Federico II" was signed, whose aim was the development of the Italian-Chinese cooperation project entitled "*Development of a scientific analysis, with technology transfer of a submerged stable crossing in the Jintang Strait in the People's Republic of China*". The principal partners of that cooperation were, further to the Italian Ministry of Foreign Affairs and the University of Naples "Federico II" (Italy) with A. Fiorentino as project manager, also the Zhejiang Provincial Science Technology Commission (PR of China) and the "Ponte di Archimede" Company, with the participation of the "Bocconi" University and the Technical University of Milan (Italy). Within the frame of the mentioned cooperation, the feasibility study and the preliminary design of a Submerged Floating Tunnel for the Jintang crossing in the Zhejiang Province (People's Republic of China; Figure 3.10) were carried out (Faggiano et al., 2001a).

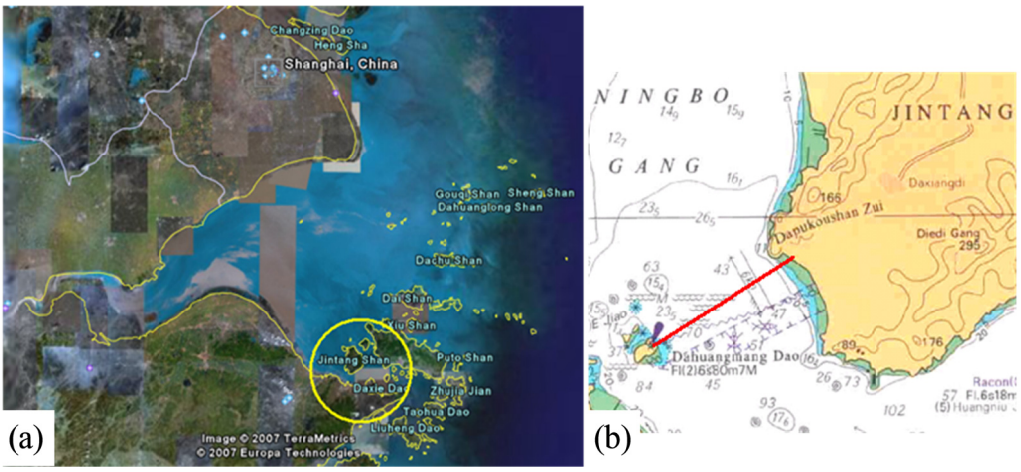

Figure 3.10. The Zhejiang Province (PR of China), location of the Jintang AB:(a) global view; (b) focus on the AB position.

The total length of the crossing was equal to 3200 m and so the Jintang AB was divided into three main longitudinal parts (Figure 3.11): the ones near the costs, each 1100 m long, had a 3% slope, in order to provide the central part of the tunnel with the necessary depth for the free passage of ships, which was equal to 25 m; the central one, 1000 m long, was horizontal.

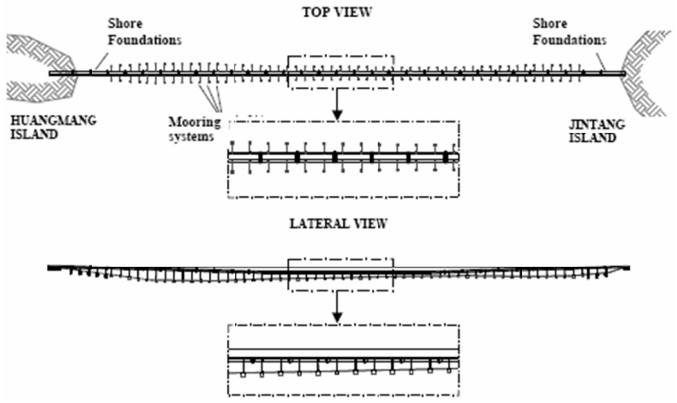

Figure 3.11. Main longitudinal views of the Submerged Floating Tunnel in the Jintang Strait (PR of China).

The tunnel was made of 32 modules, each of them 100 m long, which were planned to be pre-fabricated as single units in the yard and then assembled together in situ. The cross-section was made of pre-stressed precast reinforced concrete and it measured 12.1 m along the vertical direction and 27.9 m along the horizontal transverse direction (Figure 3.12a). The Jintang AB was conceived to hold two road traffic tunnels in the main cavities. Additional lateral cells were provided, they being useful for assuring sufficient residual buoyancy, for lodging the equipments (electric, fire, air conditioned plants) and for safety against the water access inside the tunnel due to accidental events. The anchoring system was made of couples of inclined steel tubular members (Figure 3.12b), located at a 50 m inter-axis along the longitudinal layout of the tunnel.

The global response of the structure to the environmental loads was investigated by means of a simplified tri-dimensional model of the SFT, in which both the tunnel and the anchoring tubes were modelled using beam elements. Full strength connections were considered between adjacent tunnel modules and cylindrical hinges were modelled at the end of each anchoring member. Different load conditions were considered, say the residual buoyancy, the hydrodynamic actions due to currents and waves, and the seismic action. The behaviour under the residual buoyancy action was

evaluated by means of a static analysis. The response to the hydrodynamic loads was evaluated by means of both static and dynamic analyses, the first one being useful for obtaining a first estimation of the structural response in terms of internal forces and displacements, and the second one for achieving more accurate results. Finally, the seismic behaviour of the tunnel was studied by means of multi-modal response spectrum analyses, considering three different Peak Ground Acceleration magnitudes, each of them corresponding to a pre-determined probability of occurrence.

The results of the analyses proved the SFT to be a suitable solution for the Jintang strait crossing, both from the structural and economical points of view.

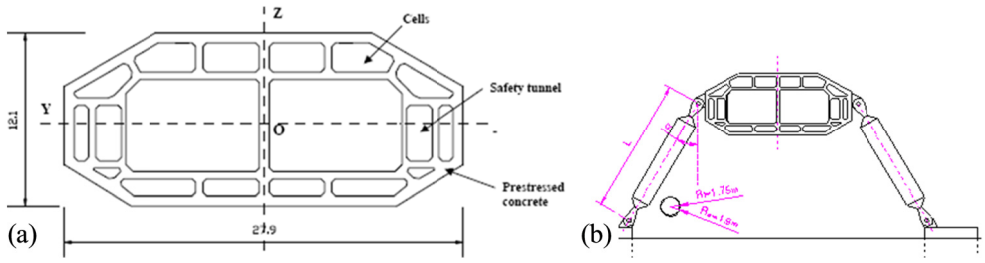

Figure 3.12. The AB for the Jintang strait crossing: (a) pre-stressed reinforced concrete cross-section; (b) anchoring systems

In 2004 an Executive Protocol of Scientific and Technological Cooperation between the People's Republic of China and the Italian Republic (Minister of Foreign Affairs) was signed to start the "Sino-Italian Joint Laboratory of Archimedes Bridge" project. The partner of this cooperation from the Chinese side is the Chinese Academy of Sciences – Institute of Mechanics (People's Republic of China). The main aim of SIJLAB is to produce and erect the first Archimedes Bridge prototype in the World, to be built in the Qiandao Lake (People's Republic of China). The activity of SIJLAB has been carried out following two main directions. The first one has a general research character, therefore theoretical studies and numerical investigations were carried out focusing on the improvement of the knowledge about Submerged Floating Tunnels. The second direction is completely focused on the executive design of the prototype, with a twofold function: on one hand, a full-scale laboratory allowing measurements and tests necessary

for its dynamic identification; on the other hand, a tourist attraction, it being left to the Qiandao Lake City municipality.

The general description of the main aspects of the design of the Archimedes Bridge Prototype (ABP) in Qiandao Lake are presented and discussed in detail in Chapter 4.

In 2008 the possibility to cross the Huang Pu river in Shangai (PR of China) by means of an Archimedes Bridge was also investigated. The AB would have served as a pedestrian passage allowing the visitors of the Expo 2010 to quickly cross the river. The area of the Huang Pu River selected for the SFT is characterized by an average width (corresponding to the span to be covered) of 400 m and an average depth of 12 m. Based on the weight of the largest ships which could be present in the river, a minimum depth equal to 8 m was estimated for the free surface navigation.

Two solutions were proposed for the Huang Pu River AB, characterized by the same cross-section features and anchoring systems, the difference among them being the vertical layout. Solution 1 (Figure 3.13a) was characterized by the presence of two straight parts, the first one going down from one river bank to the centre of the river cross-section, and the second one going up towards the other bank. At both banks the AB was at the water surface level, whereas in the central part it was underground. The constant slope of the two AB parts is equal to 6%. In this way, three configuration types of AB could be identified: an underground part (total horizontal length of 30 m), a partially underground part (total horizontal length of 100 m) and a sloped floating part (total horizontal length of 270 m). A free navigation width of 135 m in the central part of the river was guaranteed with this solution.

Solution 2 (Figure 3.13b) was characterized by the presence of five straight parts, arranged as follows: starting from one river bank, the first part was horizontal; the second one was sloped and allowed to reach the third one, which was horizontal and underground; the fourth part was sloped, allowing to go up towards the fifth one, which was in turn horizontal, reaching the opposite bank. The slope of the non-horizontal parts was about 13.3%. In this way, four configuration types of AB could be identified: an underground part (total horizontal length of 100 m), a partially underground part (total horizontal length of 60 m), a sloped floating part (total horizontal length of 90 m) and a horizontal floating part (total horizontal length of 150 m). A free

navigation width of 160 m in the central part of the river was guaranteed with this solution.

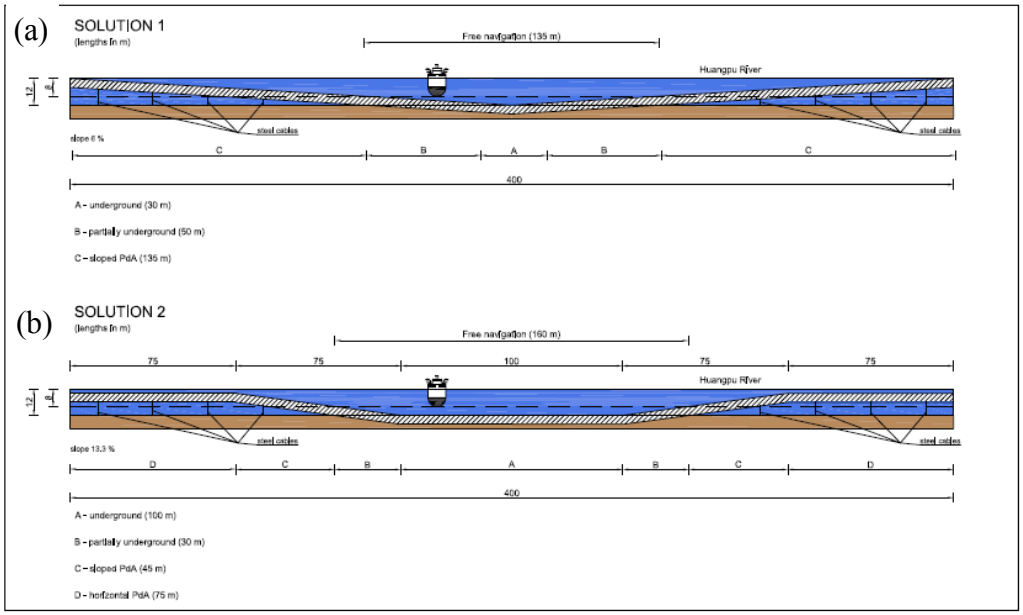

Figure 3.13. Longitudinal lay-out solutions proposed for the Archimedes Bridge crossing the Huang Pu river in Shangai (PR of China).

In both the solutions, the AB was composed of assembled modules, whose length was equal to 25.00 m. The cross-section of AB had the same features for the two proposed solutions. It is composed by two parallel tubes included into a hydro-dynamically shaped shell (Fig. 3.14). Aluminium, concrete and steel were used, obtaining a sandwich composite cross-section, which allowed to exploit the advantageous features of the used materials. Additional concrete, between the tubes and the aluminium shell, was provided for counterbalancing the Archimedes buoyancy.

The anchoring system was made of steel cables, which were arranged in groups of four, forming a sort of W in the vertical plane.

The pedestrian traffic was foreseen to take place into the two tubes, in opposite directions. Into each concrete-steel tube, one-way tapis-roulant was used for facilitating the pedestrians crossing into the AB. Parallel to the tapis-roulant, a free path is present, which could be covered by walking.

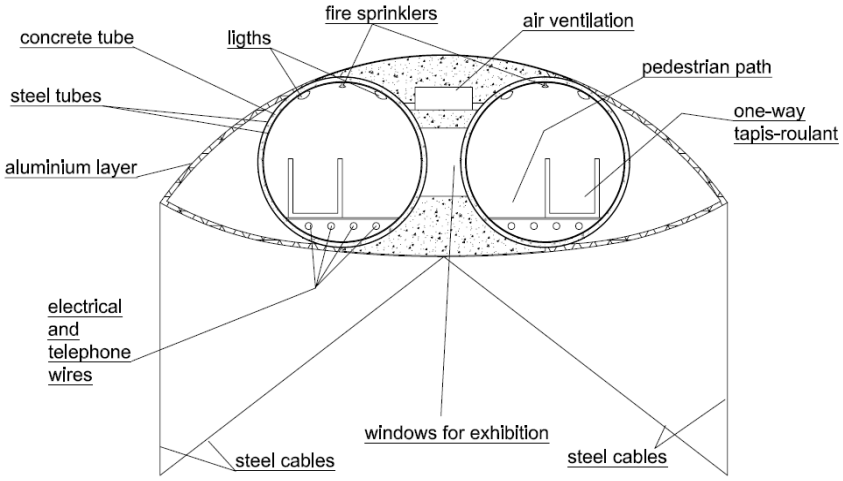

Figure 3.14. Cross-section of the Archimedes Bridge crossing the Huang Pu river in Shangai (PR of China).

3.4.2. SFT proposals in the Pulau Seribu Archipelago (Indonesia)

In the latest Indonesian institutions and technicians showed interest in the SFT solution for waterway crossings. This is testified by the dedicated meeting which was held in 2007 in Lecco (Italy), where Indonesian experts, led by Ir. Iskendar, Director for the Center of Assessment and Application of Technology for Transportation System and Industries, participated with SIJLAB engineers, from the Sino-Italian Archimedes Bridge project. In fact, as an archipelagic country, consisting of more than 13 thousand islands, Indonesia could benefit of SFTs, which represent a more environment respectful and economic way than ferries to connect adjacent islands. Moreover, for the infrastructure, that would connect Bali to Thailand, two options were considered, a conventional bridge or a SFT. The construction was planned to start in 2005 and be ready to use by 2018. However, the bridge option was later favoured.

In this context, preliminary studies for connecting islands belonging to the Pulau Seribu archipelago (Figure 3.15a) were carried out in 2008, under the request of local institutions. Their first intention was to create a link between Pangangg and Karya islands (Figure 3.15b); however it did not seem to be a

suitable application because of the modest seabed depths available (0-10 m). An Archimedes Bridge connecting Panggang and Pramuka islands (Figure 3.15b)was therefore proposed, which turned out to be also more suitable for the enhancement of the transport net of the local community; the crossing length was estimated to be equal to 1200 m, with water depths ranging from 0 to 29 m.

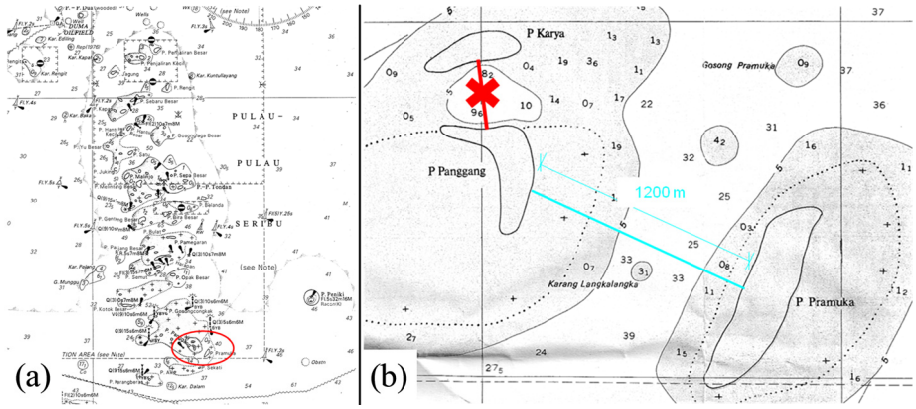

Figure 3.15. (a) General map of the Pulau Seribu Archipelago; (b) paths of the proposed AB crossings between Karya and Pangangg islands and Panganng and Pramuka islands.

Several solutions for the tunnel structure were considered, made of steel-r.c. or steel only tubes framed into an external steel shell or steel-concrete-aluminium tunnels. All solutions featured a hydrodynamic shape elongated in the horizontal direction, allowing also to reduce the overall height of the tunnel due to the limited water depths available. Moreover, solutions allowing for bikeway-pedestrian or motorway traffic were envisaged. Figure 3.16 shows two of the proposed tunnel cross-sections. In the end, the solution involving steel tubes placed inside an external steel shell was selected (Figure 3.16a).

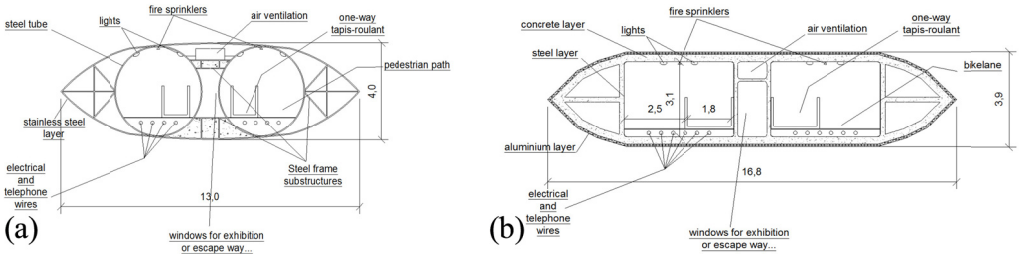

Figure 3.16. Tunnel cross-sections proposed for the AB connecting Pangangg and Pramuka islands of the Pulau Seribu archipelago (Indonesia): (a) steel tubes framed into an external steel sheel;(b) steel-concrete-aluminum layered structure.

The proposed solution is a "hybrid" tunnel solution: in the external parts, where the seabed depth is minor than 5 m, the tunnel is assumed to be tied by means of short tendons to large concrete foundations (Figure 3.17a), whose weight counterbalance the tunnel buoyancy whereas in the central part of the crossing (estimated length of 1200 m) the tunnel is restrained by cable groups made up of our cables (Figure 3.17b). The longitudinal lay-out of the crossing is sketched in Figure 3.17c.

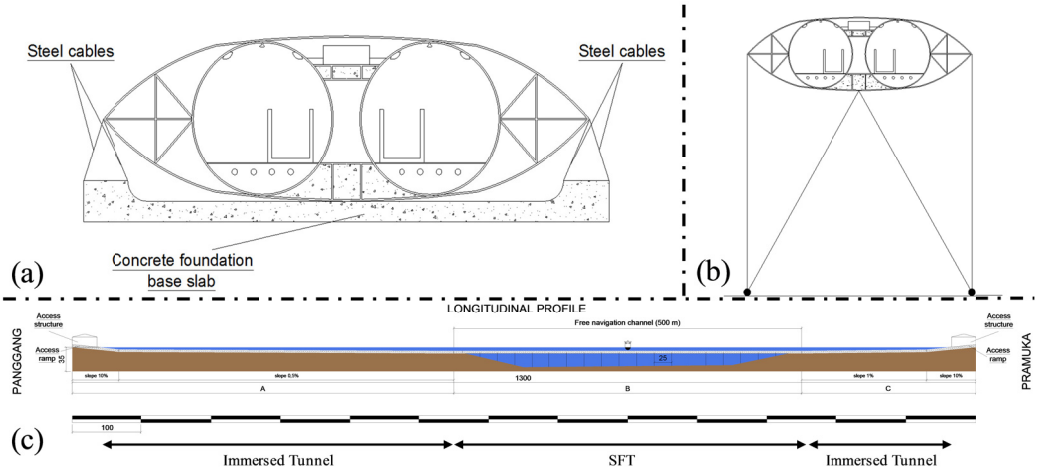

Figure 3.17. Pangangg-Pramuka Crossing (Indonesia): (a) Immersed Tunnel part; (b) SFT part; (c) crossing longitudinal view.

Chapter 4

The design of the AB Prototype in Qiandao Lake (PR of China)

4.1 THE CONCEPTUAL DESIGN OF THE PROTOTYPE

The design of the Archimede's Bridge prototype, carried out by the Italian Team of the SIJLAB (Mazzolani et al., 2007), in Qiandao Lake is based on some pre-requisites, which are summarized hereafter:

- The size of the prototype should be large enough to represent a full-scale specimen, but at the same time not too large, for allowing its suitable excitation and stress during the experimental simulations of the dynamic behaviour; moreover, the final destination of use of the prototype being a pedestrian tourist crossing, the prototype size is fixed accordingly.
- The ratio between the characteristic height of the cross-section and the whole length of the tunnel is small enough, so that experimental results can have a general validity and can be extrapolated to other SFT structural cases.
- The materials are selected in order to work together in a composite action so to exploit and optimize their behavioural peculiarities, at the same time neutralizing their disadvantages; as a result, the cross-section is conceived to fulfill all the strength, stiffness, ductility, durability and waterproof requisites.
- All the issues related to the fabrication and erection of the prototype are considered in the design.

The total length of the prototype is equal to 100 m. It is obtained by assembling five 20 m long modules, which are pre-fabricated in the yard and then assembled together in situ. The tubular structure has a multi-layer cross-section (Figure 4.1a), composed by three different materials, thus achieving a "sandwich" configuration of the cross-section: an internal layer made of steel, an intermediate layer made of concrete and an external layer made of aluminium. Therefore a synergetic cooperation between used materials is attained. Steel is characterized by low weight, due to the small size of the structural elements, high mechanical performances (tensile strength, resistance to fatigue and against impacts, ductility), but it is vulnerable to corrosion. Consequently, it is placed in the internal part of the structure, to be protected from the contact with water. Concrete is characterized by low cost, stabilizing weight against the Archimedes buoyancy, good mechanical behaviour in compression and good response to the water environment, but it shows a very poor behaviour in tension. As a consequence, it is the intermediate layer of the cross-section, holding different tasks, such as: protecting steel from corrosion, assuring the ballast weight and cooperating with the steel pipe for the axial, bending and shear resistance of the tunnel, the steel and concrete pipes being conceived as a composite structure. Finally, the aluminium is characterized by high resistance to corrosion, good mechanical resistance and workability, but by poor fire resistance and low stiffness. According to this, an alveolate aluminium extrusion is placed as external tube of the sandwich structure, so to create a corrosion resistant layer. Furthermore, the aluminium alveolate shape works as an energy absorber in case of external impact. Beside the above motivations, the relative position of the metal layers at the internal and external sides of the cross-section proves to be advantageous also from the constructional point of view, they serving as a formwork for the concrete casting.

The materials used for the prototype are S235 steel grade, C20/25 concrete and 6061-T6 aluminium alloy.

The size of the prototype cross section has been fixed in order to assure the possibility of introducing an automotive for carrying inside and install all the necessary test apparatus. The carriage way being 2.50 m in net width (Fig. 4.1a), the internal diameter should be equal to 3.55 m. The thicknesses of the steel and concrete pipes have been assigned in order that the related self-

weight of the tunnel could balance the Archimedes buoyancy, for the optimization of the residual buoyancy, which is the resultant between self weight and Archimedes buoyancy. In fact, the larger the steel and concrete thicknesses are, the larger the self weight of the tunnel is, but also the Archimedes buoyancy increases, because the overall volume grows up. As a consequence, the residual buoyancy decreases. After all, the thicknesses have been fixed considering the Archimedes buoyancy over the self-weight ratio (including live loads) equal to approximately 1.20. The minimum residual buoyancy is calculated accordingly. Based on the previous consideration, the steel pipe is 20 mm thick, whereas the concrete pipe is 300 mm thick. For what concerns the alveolate aluminium layer, it is obtained through assembling 30 extruded elements (Figure 4.1a), 450 mm width each, which is the largest size for a 20 m long extruded element, this being the length of a prototype module. A preliminary design, by ALCAN, for such extruded elements is shown in Figure 4.1b. This solution is based on a classical groove-and-tongue mutual constraint on the internal side (i.e. at the concrete interface) and a continuous friction stir welding (Figure 4.2b) (TWI Ltd, 2006) on the external side in contact with the water.

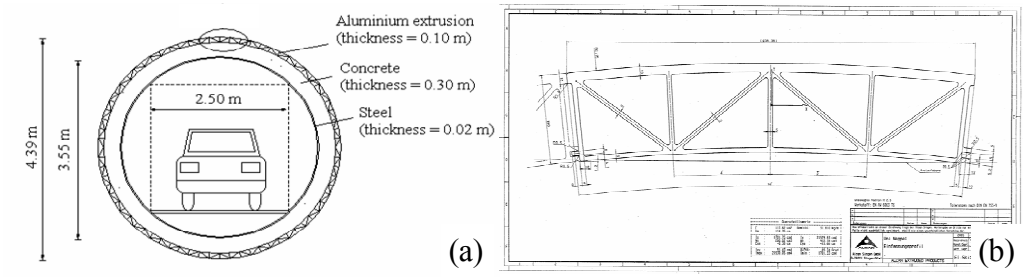

Figure 4.1.(a) The multi-layered cross-section of the AB prototype in Qiandao Lake; (b) ALCAN preliminary design for the extruded cross-section constituting the aluminium layer of the prototype.

The steel and concrete tubes are designed in order to work together as a composite steel-concrete section. At this aim, 24 steel shear connectors per cross-section, 0.40 m spaced along the longitudinal axis of the tunnel, are provided (Figure 4.2b). Connectors are designed as ductile devices, according

the Eurocode 4 (CEN, 2004a). They have a 360 MPa strength, a 18 mm diameter and a 120 mm height.

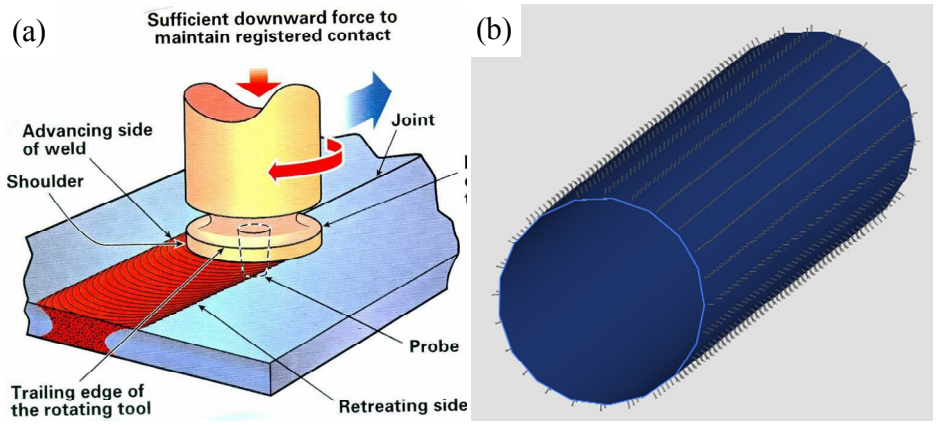

Figure 4.2.(a) The Friction Stir Welding process (TWI Ltd, 2006); (b) Shear connectors for the composite steel-concrete AB tube.

4.2 FEATURES OF THE SELECTED LOCATION

The first Archimede's Bridge prototype in the World is planned to be built in Qiandao Lake, which is an artificial lake located in Chun'an County (Zhejiang Province, PR of China). The name of the lake can be translated into "Lake of thousand islands", since there are 1078 large islands in the lake with a few thousand more smaller ones (Figure 4.3a). It covers an area of 573 square kilometres and it has a capacity of 17.8 cubic kilometres. The lake is an important tourist area of the Zhejiang Province. This is the reason why it has been selected as prototype location, in fact the prototype itself would represent a tourist attraction.

The exact location of the prototype has been identified after a careful inspection in Qiandao Lake by a joint Sino-Italian committee (Figure 4.3b). This area has some advantages for the prototype installation: it is near to a main road, which can be conveniently used for reaching the site, also by heavy trucks; moreover, there is the possibility of creating a construction yard, with none or reduced need for excavations, close to both the main road and the bay, so that the launching operations can be easily carried out.

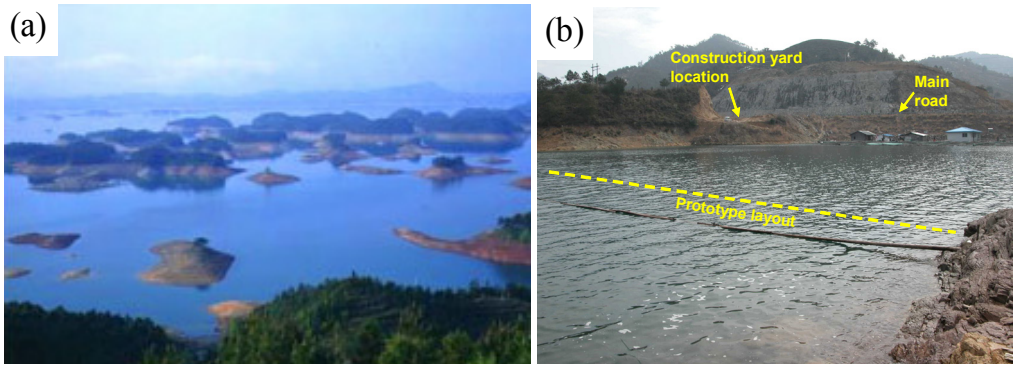

Figure 4.3. (a) A view of Qiandao Lake (Zhejiang Province, PR of China); (b) Location of the AB prototype at Qiandao Lake (PR of China).

The location of the two accesses to the prototype has been selected in order to achieve a tunnel total length equal to 100 m (Figure 4.4). The ad-hoc access structures are linked to the existing main road through two approach roads, planned to be for pedestrian and vehicular uses, respectively.

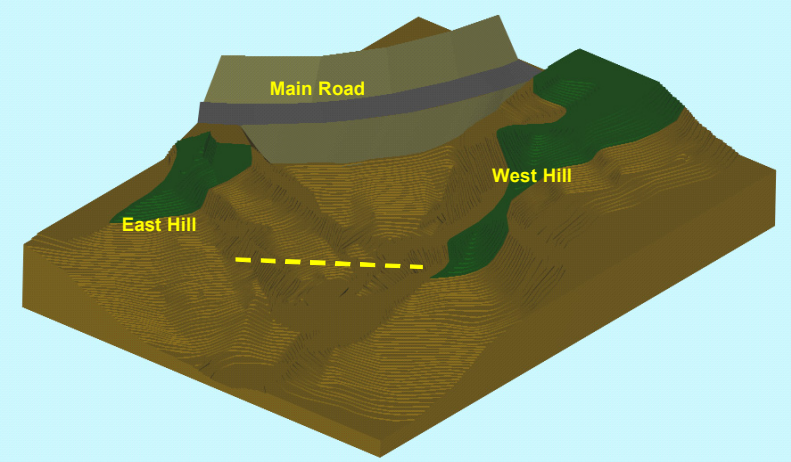

Figure 4.4. Virtual sketch of the AB prototype location

Useful data for the characterization of the environmental actions were collected by the Chinese team. They are:

- the water surface level is not constant during the year, it varying between 103 m and 95 m above the sea level;

- the maximum wave height (H_w) is equal to 1.0 m;
- three values of the wave period (T_w) have been estimated, namely 1.3 s, 1.8 s and 2.3 s;
- the maximum surface current velocity is equal to 0.1 m/s;
- the water temperature at the surface has a yearly average value equal to 21.4 °C, with an yearly variation equal to 20 °C;
- the peak ground acceleration is equal to 0.1g (g being the gravity acceleration);
- the minimum clearance of the water above the tunnel should be equal to 2.0 m, based on the surface traffic data in the site.

4.3 THE STRUCTURAL SCHEME

The prototype is a straight tubular structure located at a water depth corresponding to a net water clearance ranging from 2.0 m to 10.0 m, due to the variation of the water surface level through the seasons. The tunnel axis is horizontal. It is located at 90.8 m above the sea level.

Two different restraint conditions are considered for the two ends of the tunnel, which allow the free elongation of the structure, due to thermal variations or seismic actions: at one end, all the translational degrees of freedom are restrained; at the opposite end, only the translational degrees of freedom transversal to the tunnel axis are restrained, whereas the longitudinal displacements and the rotations are allowed.

The tunnel stability is assured by an adequate anchoring system, made of steel cables fixed at the lakebed and connected to the tunnel by means of spherical hinges. During a preliminary design of the prototype, five different cable configurations (Figure 4.5) have been analyzed and their behaviour under both vertical and horizontal loads has been evaluated and compared by means of an equivalent static analysis. The analysis results have confirmed the physical predictions: vertical cables are very effective in presence of vertical actions only, whereas their restraint effect in the horizontal direction is negligible; inclined cables are effective, both in vertical and horizontal direction, only if they are four cables in a W-shaped configuration, whereas

the restraint effect of two inclined cables only in the vertical direction is not very effective and in the horizontal direction is negligible.

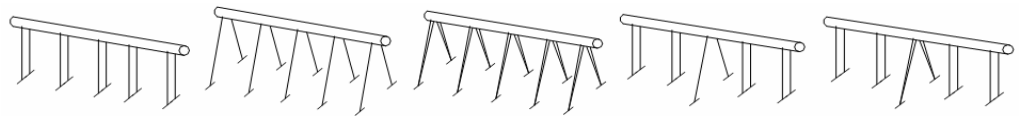

Figure 4.5. The five cable configurations considered during the preliminary phase of the prototype design.

It is worth noticing that the preliminary studies for the efficiency evaluation of the anchoring configurations were based on the hypothesis of a horizontal lakebed profile. Based on the actual lakebed geometry, which is characterized by gradual depth increment from the shore to the centre of the inlet, two groups of cables have been eliminated, due to their short length. As a consequence, the prototype structural schemes are endowed with three groups of cables only (Figure 4.6).

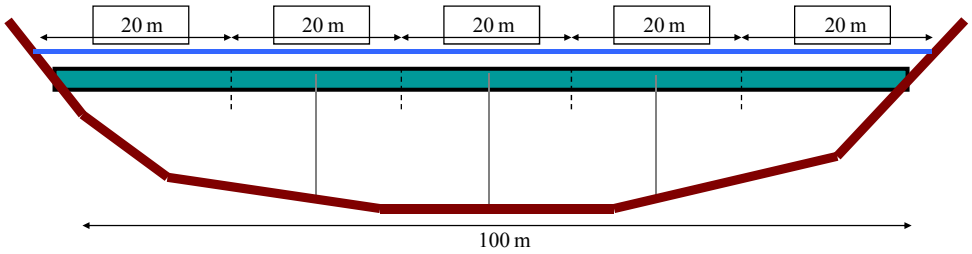

Fig. 4.6. Longitudinal view of the prototype.

The three cable configurations shown in Figure 4.7 have been selected. The first and second ones are considered only for the sake of comparison, the most effective configuration for the prototype being evidently the third one. In any case, numerical analyses have been carried out considering all the cable configurations. In addition, the prototype is arranged to set up all the cables systems for testing.

The joints between adjacent modules of the tunnel are fully restrained, so that no relative displacement or rotation is allowed between them; they are designed as full strength connections.

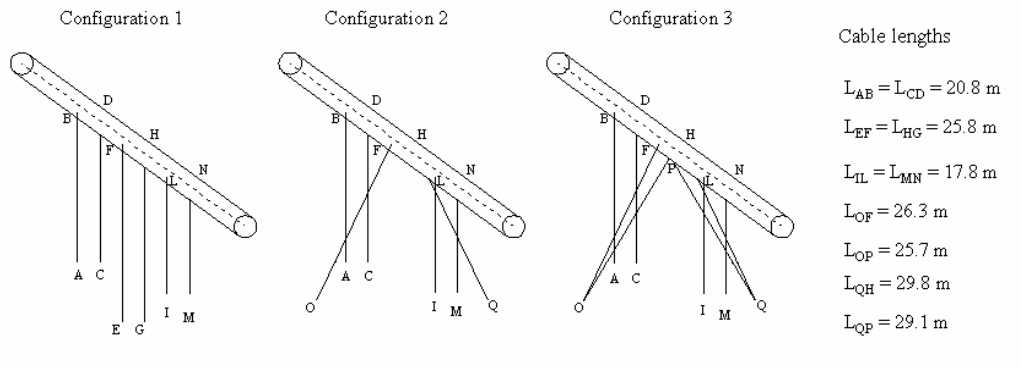

Figure 4.7. The cable configurations considered for the AB prototype.

4.4 STRUCTURAL ANALYSES

4.4.1. Structural model

The behaviour of the SFT prototype under the environmental actions has been analyzed by means of both static and dynamic analyses. The software Abaqus (2004) has been used, which allows to examine the hydrodynamic behaviour of structures immersed in a fluid by means of a specific analysis routine, namely the Abaqus/Aqua package. The static analyses are obviously affected by some approximations, they serving as a first rough evaluation of the order of magnitude of displacements and internal forces rising in the tunnel due to the hydrodynamic loads.

The tunnel is modeled through twenty tri-dimensional quadratic beam elements. The steel-concrete-aluminium composite cross-section is modeled by an equivalent concrete section, with a total area equal to 5.1 m^2 and a moment of inertia equal to 12.33 m^4. The cross section area is calculated through an equivalence in terms of weight, considering all the permanent loads acting in the tunnel, i.e. the weight of structural and non structural elements. The moment of inertia of the tunnel, for the sake of simplicity, is calculated considering the steel and concrete tubes only, they acting as a composite structure, through an equivalence in terms of stiffness.

Also the cables are modeled through beam elements, with a circular cross-section (nominal diameter equal to 60 mm) characterized by an area equal to 0.00249 m^2 and a moment of inertia equal to $6 \cdot 10^{-7}$ m^4.

Internal rigid constraints are imposed between the end nodes of the cables and the centre of mass of the tunnel cross-section, where the anchoring system is located (Figure 4.8). According to the assumed structural scheme, one end of the tunnel is pinned and the other one is free to have axial displacements. Geometric non-linearity is considered in the model, in order to adequately reproduce the cables non-linear behaviour and the effects of large displacements.

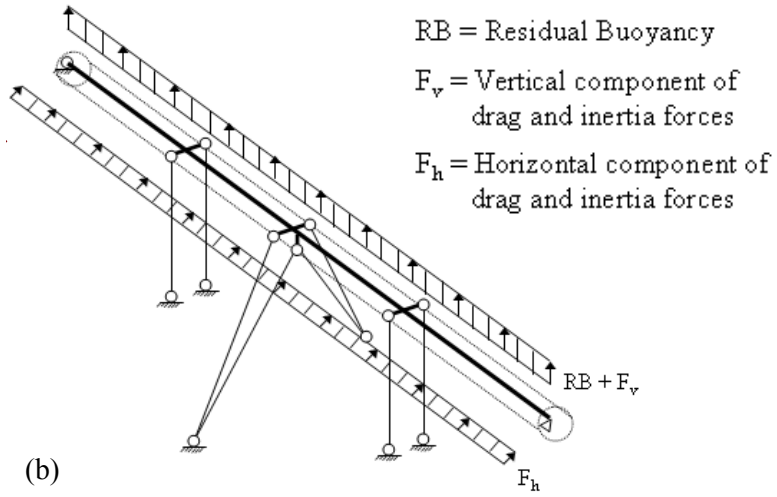

Fig. 4.8. Structural model for the simplified static analyses (third cable configuration).

4.4.2. Loading conditions

In the simplified structural model for static analyses (Figure 4.7b) both the vertical loads, corresponding to the residual buoyancy as the resultant of the self-weight and the Archimedes buoyancy, and the horizontal loads, due to waves and currents, are modelled as static distributed loads acting on the tunnel only and they are calculated a priori, therefore neglecting the effect of their direct application on the cables. The characteristic value of the self weight (G_k), the Archimedes buoyancy (B_k) and the residual buoyancy (RB_k), together with the characteristic load corresponding to dense crowd (C_k) are indicated in Table 4.1.

Table 4.1. Characteristic values of prototype dead and live loads

G_k [kN/m]	B_k [kN/m]	RB_k [kN/m]	C_k [kN/m]
125.0	160.0	35.0	10.0

The hydrodynamic action F due to waves and currents is modelled through the Morison equation (see section 2.2.3):

$$F(t)= F_D(t)+ F_I(t)=0.5\rho_w C_D D\cdot|u(t)| u(t)+ \rho_w C_I\cdot\pi D^2/4\cdot a(t) \quad (4.1)$$

The inertia coefficient C_I is assumed equal to 2.0 and the drag coefficient C_D is assumed equal to 1.0, these values being commonly adopted in offshore engineering practice for circular structural elements.

As far as the dynamic analyses are concerned, the special purpose ABAQUS/Aqua package allows to automatically calculate, in each instant of time, the buoyancy, the drag and the inertia loads. The drag and inertia forces are calculated by means of the Morison equation, in which, differently from the "static" case, the u(t) and a(t) vectors are the water-structure relative velocity and acceleration vectors, respectively.

The water velocity vector is due to the steady current and to the waves, whereas the water acceleration vector is due to the waves only. The steady current is modelled by a velocity vector parallel to the still water surface, linearly decreasing with the depth, becoming zero at the lakebed. The waves action is evaluated by the Airy wave theory, which allows to determine both the horizontal and vertical components of the velocity and acceleration at each point of the water and at each instant of time.

The field data necessary to evaluate the hydrodynamic actions were given by the Chinese team :

- wave height (H_w) equal to 1.0 m;
- wave length (λw) equal to 8.25 m;
- surface current velocity equal to 0.1 m/s.

with the assumption that the lakebed profile is at a constant depth equal to 30.0 m.

The consequent "static" values of the drag and inertia horizontal (F_h) and vertical (F_v) components, due to both current and waves, are, respectively, 4.875 kN/m and 4.860 kN/m.

Five load combinations are defined, according to the Eurocode 0 provisions (CEN, 2002a). Combinations 1, 2 and 3 are relative to service conditions under: vertical dead loads only, vertical dead loads and hydrodynamic action, vertical dead and live loads, together with hydrodynamic action, respectively. Combinations 4 and 5 are relative to ultimate conditions under: vertical dead loads and hydrodynamic action, vertical dead and live loads, together with hydrodynamic action, respectively. It is worth noticing that combinations 2 and 4 are the worst ones for the behaviour of the tunnel and the cables in tension, whereas combinations 3 and 5 are considered because they could lead to the loosening of the cables.

4.4.3. Analysis of results

The results of both the static and dynamic analyses are summarized in Tables 4.2 to 4.4, where the maximum displacements and internal forces are indicated for all the study cases. With regard to the tunnel behaviour, it can be noticed that generally the static analyses underestimate both the internal forces and displacements, as it was expected.

Therefore, the effect of the cable configurations on the structural behaviour is evaluated on the basis of the dynamic analyses results. It is evident that the cable configuration 3 assures the best structural performance, leading to the smallest stress and displacements demands, whereas the configuration 1 is the worst performing one. In fact, as respect to the configuration 1, configurations 2 and 3 have a 48% and 64% reduction of displacements, respectively and 62% and 80% reduction of bending moments. With reference to the cable behaviour, the worst condition is related to the configuration 2, in fact the axial forces in configurations 1 and 3 have a 26% and 36% reduction as respect to configuration 2, respectively.

The limit value for the tunnel displacements in service conditions (d_{lim}) is assumed to be equal to 0.20 m, corresponding to 1/500 of the whole length (L) of the tunnel; the deign value of ultimate bending moment of the tunnel (M_{Rd}) is equal to 70000 kNm and the design axial force strength for the cables (N_{Rd}) is equal to 1045 kN.

Table 4.2. Maximum tunnel displacements, from static and dynamic analyses (d_h: horizontal displacement, d_v: vertical displacement; d: total displacement).

Cable Configuration	Type of Analysis	Displacements [m]			
		d_h	d_v	d	d/L
1	Static	0.018	0.027	0.033	1/3030
	Dynamic	*0.092*	*0.019*	*0.094*	*1/1064*
2	Static	0.012	0.030	0.032	1/3125
	Dynamic	*0.040*	*0.029*	*0.049*	*1/2040*
3	Static	0.008	0.025	0.026	1/3846
	Dynamic	*0.025*	*0.022*	*0.034*	*1/2940*

Table 4.3. Maximum tunnel bending moments from static and dynamic analyses ($M_{sd,h}$: horizontal moment demand; $M_{sd,v}$: vertical moment demand; M_{sd}: resultant moment demand; M_{rd}: bending strength of the tunnel)

Cable Configuration	Type of Analysis	Bending Moments [kNm]			
		$M_{Sd,h}$	M_{Sd}	M_{Sd}	M_{Sd}/M_{Rd}
1	Static	12408	8701	15155	0.216
	Dynamic	*86270*	*7235*	*86573*	*1.237*
2	Static	13943	5857	15123	0.216
	Dynamic	*30242*	*12117*	*32580*	*0.465*
3	Static	11817	3394	12295	0.176
	Dynamic	*13650*	*10127*	*16996*	*0.243*

Table 4.4. Maximum cable axial forces, from static and dynamic analyses

Cable Configuration	Type of Analysis	Axial forces [kN]	
		N_{Sd}	N_{Sd}/N_{Rd}
1	Static	618	0.591
	Dynamic	*761*	*0.728*
2	Static	677	0.648
	Dynamic	*1030*	*0.986*
3	Static	574	0.549
	Dynamic	*663*	*0.634*

Based on the dynamic analyses results, the following considerations can be made:

- In service conditions, the displacement limit value is not achieved in the tunnel for any cable configuration;
- In ultimate conditions, for the tunnel the safety checks in terms of bending moment are not satisfied in configuration 1; whereas the shear force checks are always satisfied;
- In ultimate conditions, the axial force in the cables is approximately equal to the design one (1045 kN) for configuration 2, whereas it is smaller for configurations 1 and 3.

Concerning the cables behaviour under the hydrodynamic actions, it must be noticed that they could undergo get loose, without any negative consequences on the tunnel behaviour.

The methodology for the seismic analysis of SFTs, developed in general and applied to the case study of the Messina Strait Crossing (Di Pilato et al., 2008) by the team of prof. Federico Perotti at the Technical University of Milan, has been used for the analysis of the seismic behaviour of the prototype (Mazzolani et al. 2007, 2008). The obtained results show that the assumed design configuration of the prototype is able to safely withstand the worst conditions expected in the area.

4.5 CONSTRUCTIONAL DETAILS

4.5.1. Anchoring connections

The anchoring system is made of three series of steel cables, which link the tunnel to the foundation. The end connections of the cables are conceived and modelled as spherical hinges. They are essentially based on a “hook” concept, as schematically shown in Figure 4.9a.

The tunnel sections at the cables location are equipped with three anchoring connection devices (Figure 4.9b), in order to allow to set up all the cables configurations. The detail of the anchoring connection is shown in Figure 4.10. The conception derives from the necessity of satisfying both the strength and waterproof requirements and, at the same time, of allowing an easy installation procedure, compatible with the fabrication of the whole AB

module. It is a stainless steel hook connected to the internal steel tunnel tube through a bolted system contained inside a "pyramidal" steel box, filled of cement mortar, which is placed between the steel and aluminium layers, within the concrete cast, and welded to the steel tube.

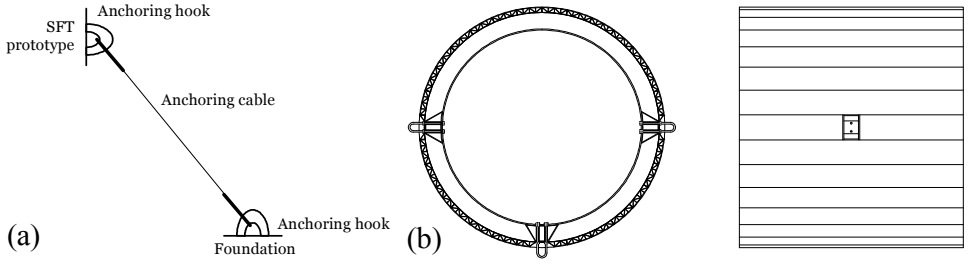

Figure 4.9.(a) Scheme of the anchoring system; (b) Cross-section where the anchoring connection devices are located

This system assures the appropriate strength and stiffness of the system connection and facilitates its installation. The latter consists in the following procedure:

- the holes for the bolted connection of the hooks are drilled in the steel tube;
- the "pyramidal" steel boxes are placed and welded to the steel tube;
- the aluminium layer is installed at the external side of the tunnel;
- the hooks are placed inside the boxes and bolted to the steel tube;
- the pyramidal boxes are filled with mortar;
- the casting of the concrete layer is carried out.

Near the anchoring device, the aluminium layer is adapted with a special configuration (Fig. 4.11), obtained by cutting a small portion of the aluminium extrusion and by placing additional aluminium plates.

The anchoring connections to the foundations also use hook elements, which are integrated into the cast of the foundation.

With regards to the cable ends, two different special devices are used, in order to link the cables to the tunnel and to the foundations hooks. In particular, the device at the tunnel side guarantees a pin joint behaviour, it allows an easy substitution of the cable and it gives the possibility of stretching the cable after its positioning, if necessary, whereas the device at

the foundation side has a fixed length. The "stretching" device is located at the tunnel side since it is easier to reach from the water surface.

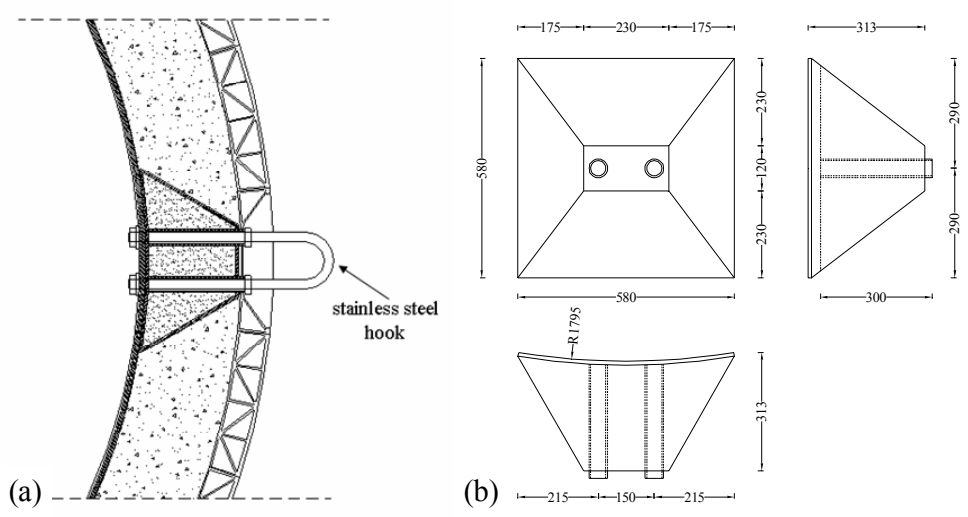

Figure 4.10. Anchoring connection detail: (a) section; (b) details of the "pyramidal" reinforcing box (dimensions in mm).

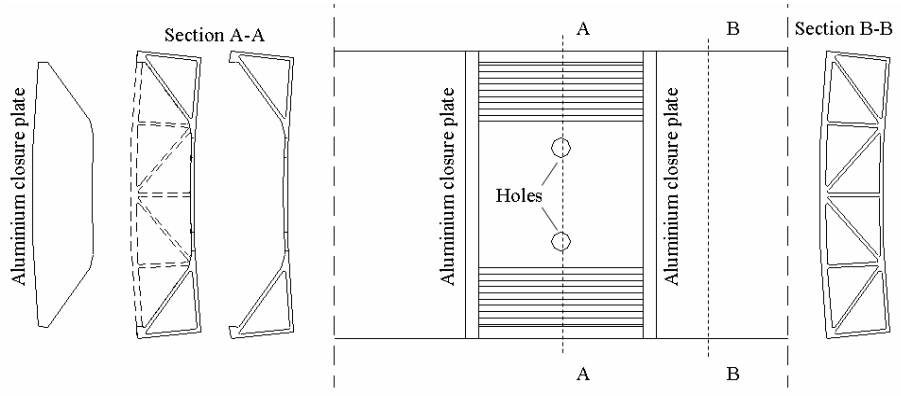

Figure 4.11. Detail of the aluminium layer next to the anchoring device.

4.5.2. Windows

Two couples of windows per module are provided (Figure 4.12), in view of the tourist attraction destination of the tunnel.

The design of the window detail is based on the necessity of passing from the internal steel layer to the external aluminium layer, allowing the concrete casting and guaranteeing the waterproof behaviour. The window glass is located inside a pre-assembled box made of four aluminium plates (Figure 4.13), which is inserted in the AB module before the concrete casting is made. The window is completed by four cold-formed stainless steel edge elements at the internal side.

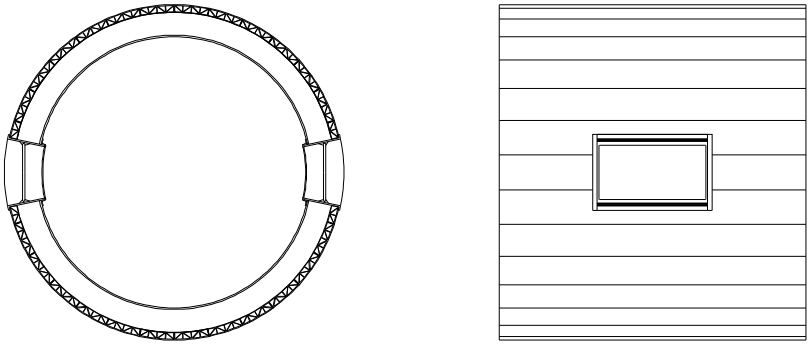

Figure 4.12. Tunnel cross-section where the windows are located

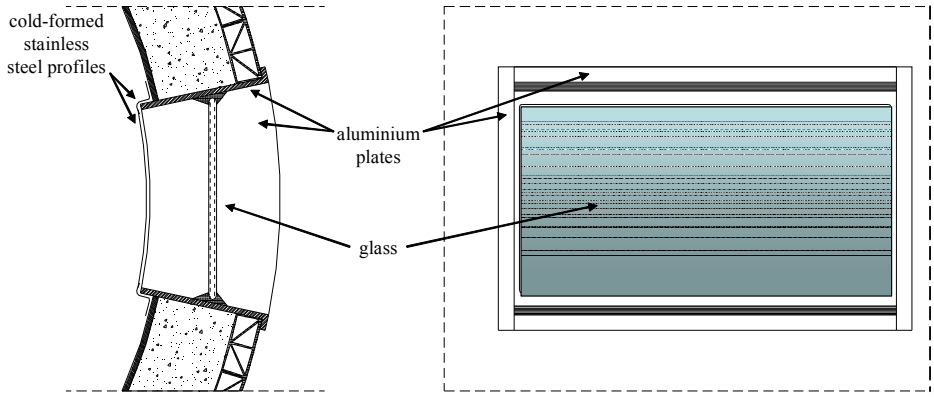

Figure 4.13. Detail of the window

4.4.4. Internal joints

The joints between adjacent modules are designed as full strength connections, i.e. to be able of transmitting the ultimate forces and moments of

the current section of the tunnel. They are designed according to the Eurocode 3 provisions (CEN, 2005a).

The inter-modular joints for the AB prototype are essentially bolted connections, designed for being set up and assembled when the modules are already submerged. The joint consists in two steel ring flanges, each one belonging to one of the adjacent modules. Flanges are mutually connected by means of high strength steel bolts. The bolted flanges are placed at the internal concrete and steel layers. At the external aluminium layer, a rubber ring crushed between the modules guarantees the water tightening of the connection. A sliding rubber ring is placed between steel and aluminium elements, in order to allow relative displacements due to thermal variations. Details of the joint and of its water proofing system are shown in Figure 4.14.

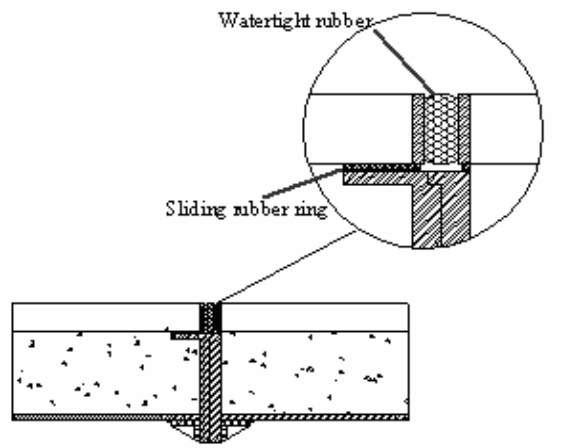

Figure 4.14. Detail of the inter-modular joints

The tensile forces are transmitted by the bolts in tension, whereas the compressive forces are transmitted by the contact between the adjacent steel flanges. The design shear forces are transmitted by friction, whereas the ultimate shear force is assumed to be transmitted by shear in the bolts.

The steel flange plates are 40 mm thick. Their external diameter is equal to the external one of the concrete layer, the width of the steel ring is larger than the total thickness of the concrete and steel tubes, in order to allow the bolts to be accommodated inside the tunnel (Figure 4.15a). The diameter of the bolts is equal to 30 mm and their class is 10.9. Stiffening ribs are provided between

two consecutive bolt holes (Figure 4.15b). For each connection, 144 bolts are required.

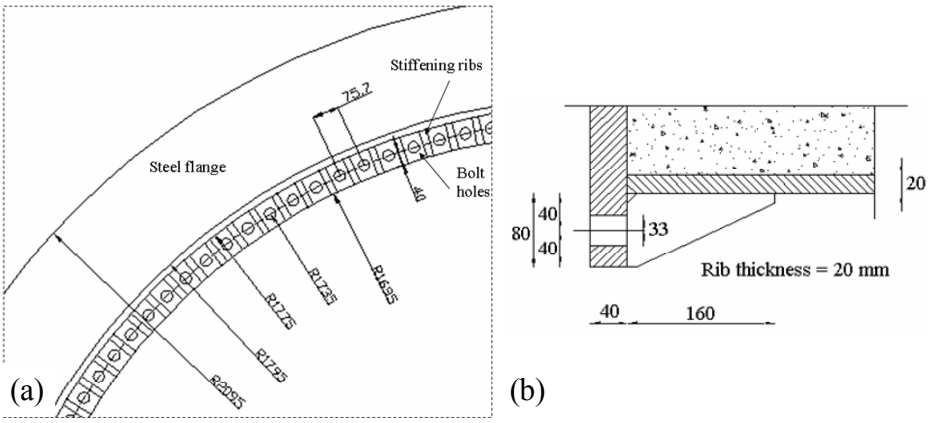

Figure 4.15. Geometry of the inter-modular joints: (a) bolt holes; (b) stiffening ribs (dimensions in mm)

4.5.3. End joints

The connections of the AB prototype to the shores are made by means of special end joints, which are connected to the modules of the prototype at the extremities. One of the two end joints must behave like a spherical hinge. With regard to the displacements, the tunnel is axially linked to the shore by means of a mechanical device, which behaves in elastic range (with high stiffness) in presence of axial forces smaller than a design limit value, but it can undergo large plastic deformations when axial forces exceed this limit value, giving rise to hysteretic dissipation of energy. The other end joint must allow both free rotations and axial displacements, in order to give the structure the possibility of free expansion in presence of thermal variations. Furthermore, both the end joints must assure the water tightening. The design of the end connections fulfils all the mentioned requirements. It is based on the concept of separating the waterproof and mechanical functions of the device, as schematically shown in Figure 4.16. The constructional solution of this system has been developed in cooperation with ALGA, leading to the output shown in Figure 4.17.

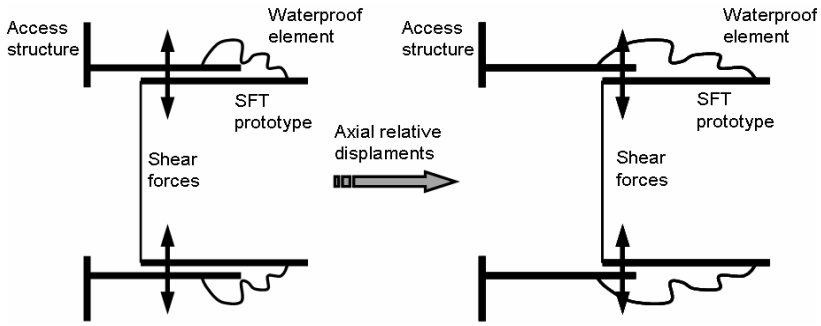

Figure 4.16. Conceptual design of the tunnel end joints: mechanical and waterproof devices.

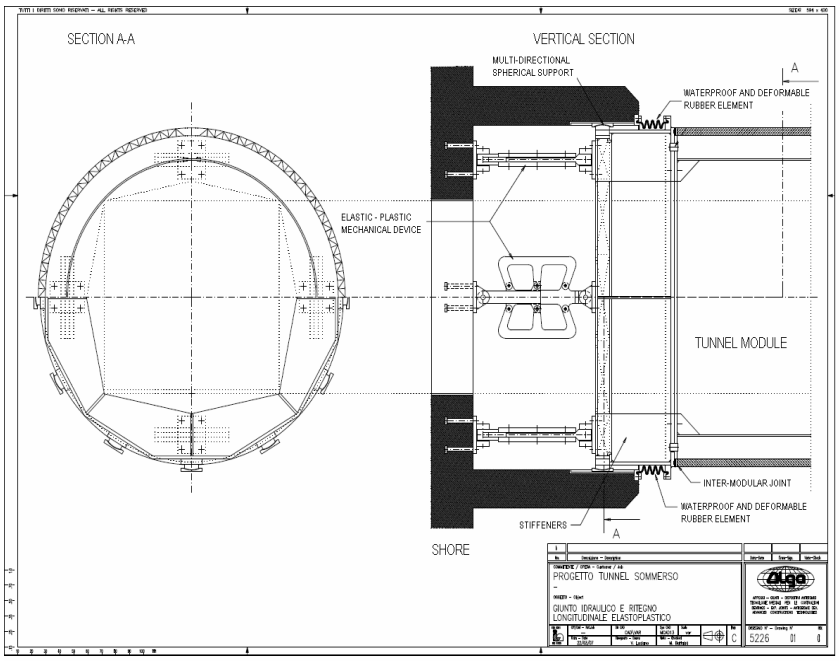

Figure 4.17. ALGA solution for the end connections of the AB prototype.

4.6 ACCESS STRUCTURES

The AB prototype is located under the lake water level and its axis is at 90.8 m above the sea level, in order to guarantee at least the 2.0 m minimum

clearance as respect to the water surface during the dry season. The tunnel level is reached through two ad-hoc access structures, located at the extremities of the tunnel. The access structures are linked to the existing main road by means of two approach roads (Figure 4.18).

Figure 4.18. View of the Archimede's Bridge (in absence of water).

One of the two access structures is conceived for allowing both the vehicular and pedestrian access, since the use of an automotive is necessary during the initial experimental phase. The other one is only pedestrian, although it has a circular layout at the tunnel level, which allows the automotive U-turn (Figure 4.19a). The access structures are completed by roofs, whose structural features are inspired to the Chinese traditional architecture (Figure 4.19b). The access structures are made of reinforced concrete.

The vehicular access structure has the shape of a "tube in tube" structure, made of two concentric vertical cylinders, 16 m high, and an helicoidal ramp in-between (Figure 4.20). The top of the cylindrical structure is covered by a "Chinese pagoda" shaped roofing structure, supported by 8 circular columns. The cable stayed metal antenna at the top of the roof has the statical function of counterbalancing the Archimedes buoyancy on the access structure, which

is partially immersed in the water: four steel cables from the top of the antenna are anchored to the ground for stabilizing the structure.

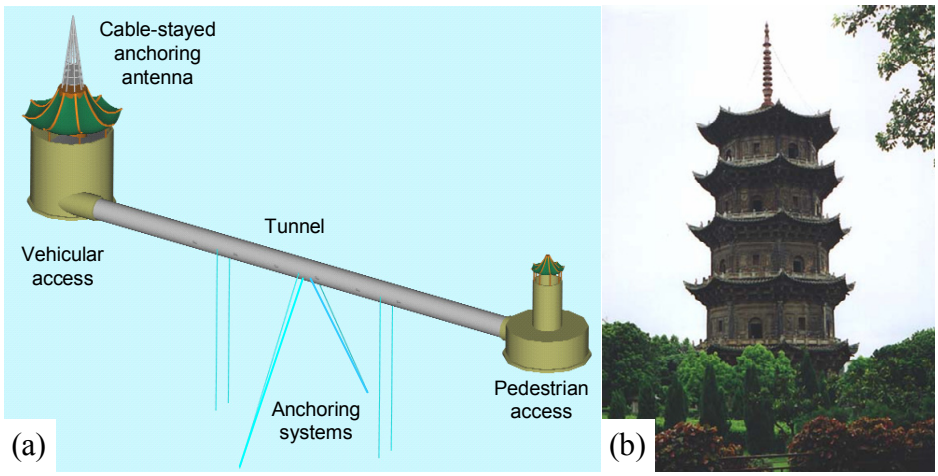

Figure 4.19. The AB prototype access structures: (a) global view; (b) "cultural background" for the roof architecture.

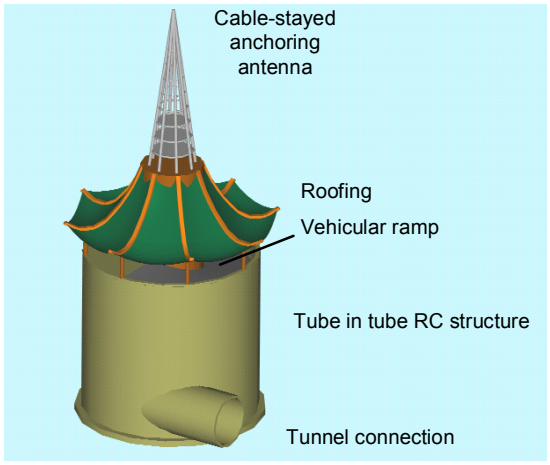

Figure 4.20. Global view of the vehicular access structure.

Alternative solutions for this problem can be based on the use of ballast material or by founding the structure on piles, able to withstand both the lifting and horizontal actions. Although the helicoidal ramp can be exploited

also for pedestrian use, the presence of a lift located into the internal vertical cylinder is envisaged (Figure 4.21a). The geometrical details of the structural section are shown in Figure 4.21b.

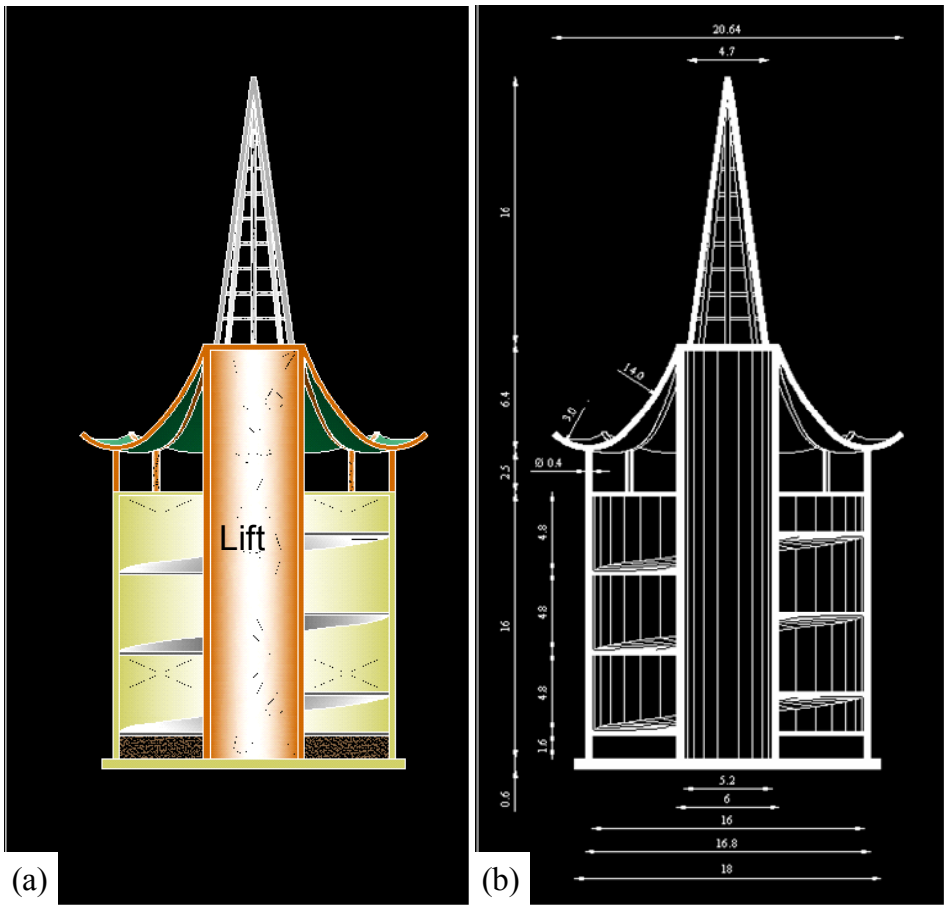

Figure 4.21. Vertical sections of the vehicular access structure: (a) location of the lift; (b) geometrical details of the ramp and the roof (m)

The pedestrian access structure differs from the vehicular one because a smaller size is necessary and the helicoidal ramp is not required. In addition, as already specified, at the tunnel level, a larger circular shape should allow the U-turn of the automotive crossing the tunnel for testing. Consequently, the pedestrian access structure is composed of two cylinders, the largest one being 6 m high and the smallest one being 16 m high (Figure 4.22).

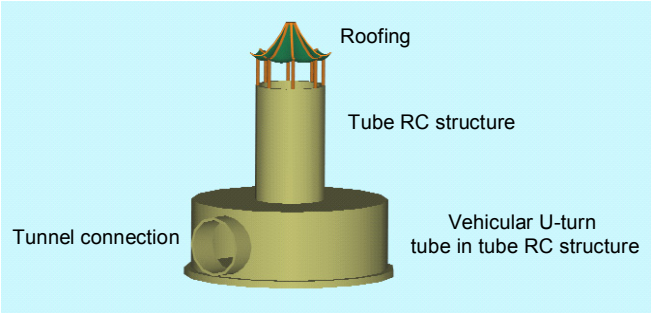

Figure 4.22. Global view of the pedestrian access structure.

Also in this case, the structure is completed by a roofing structure characterized by a Chinese pagoda shape and supported by 8 circular columns. The space into the internal cylinder is used for locating both a lift (Figure 4.23a) and a staircase. The geometrical details of the structural section are shown in Figure 4.23b.

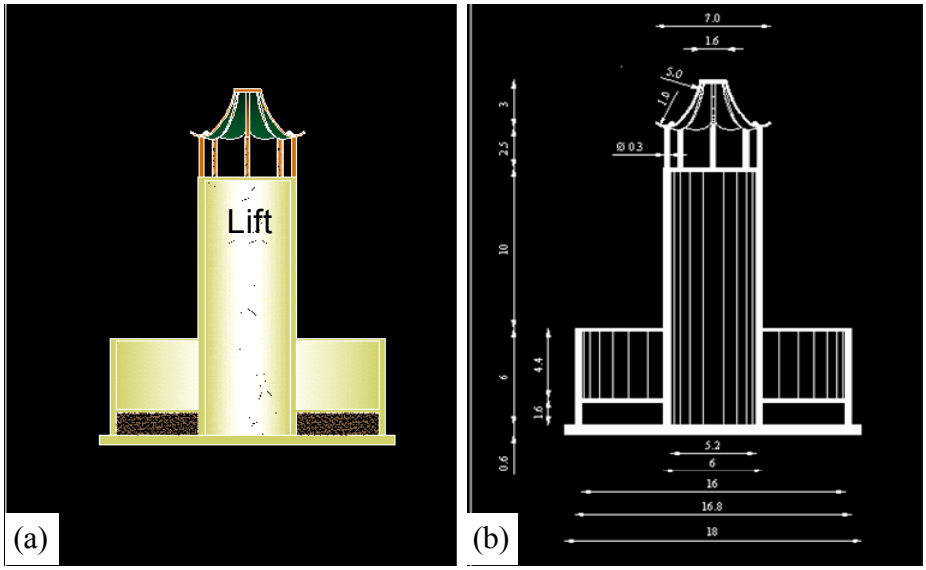

Figure 4.23. Vertical sections of the pedestrian access structure: (a) location of the lift; (b) geometrical details.

In order to reach the access structures from the existing main road, both a vehicular and a pedestrian approach roads are designed, as shown in Figure

4.24. The vehicular road is approximately 90 m long and it fills a vertical gap of 3 m, with an average slope equal to 3.3%. The pedestrian road is approximately 255 m long and it fills a vertical gap of 7 m, with an average slope equal to 2.7%.

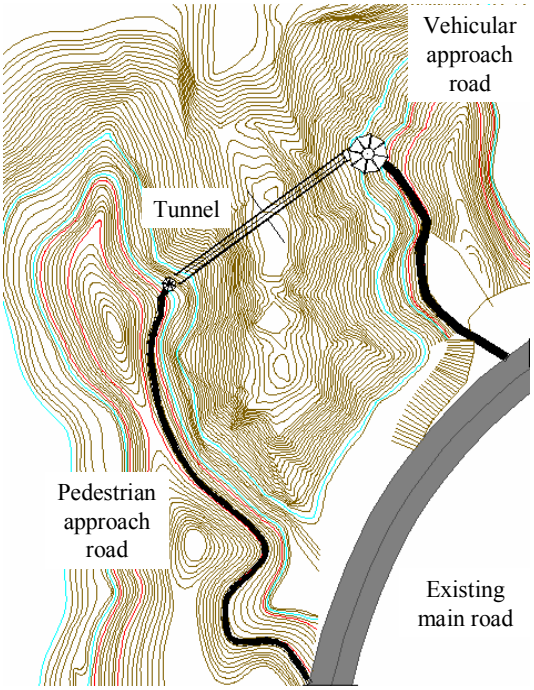

Figure 4.24. Approach roads to the AB prototype.

4.7 FOUNDATIONS

The anchoring system is fixed to gravity foundations at the lakebed, which are designed to withstand the upward forces transferred by the anchoring cables by means of the self-weight, taking account of the buoyancy. A single foundation block is designed per couple of cables, namely “coupled block”, whereas separate foundation blocks are used for the inclined cables, namely “single block”.

The gravity foundation typology has the advantage that the blocks can be partially pre-fabricated in the construction yard in the initial configuration,

which should guarantee the necessary buoyancy to be towed on site by a towboat. The technical solution consists of foundation blocks composed of a pre-cast and a in-situ cast part. The pre-cast part of the foundation is essentially an empty open box made of reinforced concrete walls. Once towed to its final destination, it is then filled with concrete, in order to get increasingly heavier up to reach the lakebed (Figure 4.25) and then achieve the design weight for foundation stability.

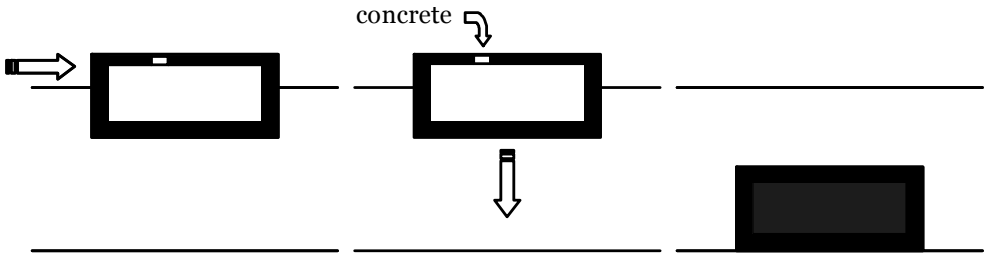

Figure 4.25. Scheme of the set up of the foundation blocks

The pre-cast structure is endowed with stiffening reinforced concrete ribs. At the intersections between perpendicular ribs, a special reinforcement is located, for anchoring the cable connection device to the concrete block. The plan views and the structural sections of both the coupled and single blocks are shown in Figures 4.26 and 4.26.

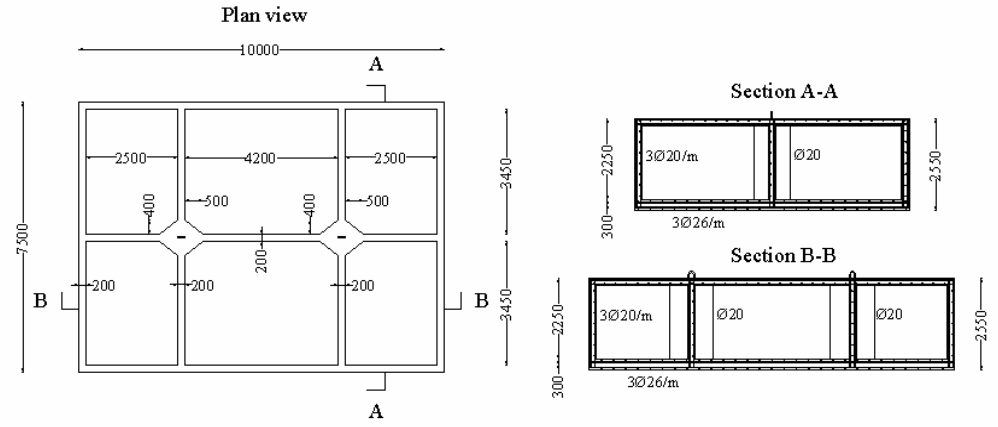

Figure 4.26. Plan view and sections of the pre-cast foundation: coupled block.

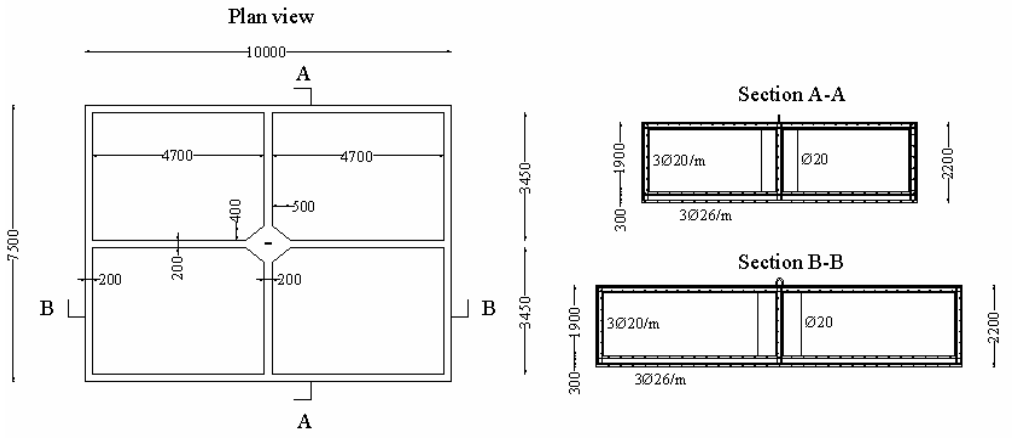

Figure 4.27. Plan view and sections of the pre-cast foundation: single block.

As an alternative, pile foundations could be used, with the consequent advantage of reducing the material volume, counterbalanced by the disadvantage of a more difficult installation.

4.8 FABRICATION AND ERECTION

One of the most interesting and challenging aspects of the design of the AB prototype in Qiandao Lake is undoubtedly the selection and, in some cases, the complete conception of appropriate fabrication and erection procedures. All the construction phases, from the fabrication of the modules to the installation in the Lake, have been studied in detail and fitting practical solutions have been developed. A short description of such procedures is given hereafter.

The 100 m long tunnel is made of five 20 m long pre-fabricated modules, which are pre-assembled in the construction yard. The construction of each module is carried out according to the following steps:

1) The internal steel tube is obtained by using five 4 m long tubular sub-elements. Each of these sub-elements is obtained starting from steel sheets (20 mm thick) whose extreme edges are butt-welded after bending (Fig. 4.28a). After the set up of the sub-elements, they are mutually welded in the transversal direction (Figure 4.26b). Steel shear

connectors are then welded to the external surface of the steel tube, as shown in Figure 4.2b.

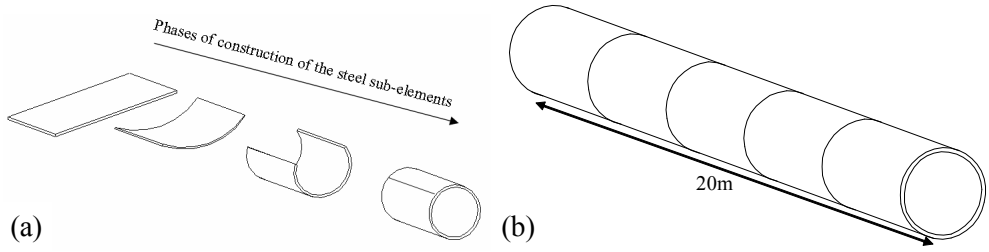

Figure 4.28. The construction of the steel tube: (a) sub-element; (b) the complete module.

2) Once the steel tube is ready, a steel closure plate is welded at its base, then it is put in vertical. The aluminium layer, composed of 30 extruded elements, is placed around the steel tube, so creating a couple of vertical concentric cylinders (Figure 4.29). The aluminium elements are adequately coated on the internal side, in order to avoid any danger of electro-corrosion due to the contact with the concrete. The connection between adjacent aluminium modules is carried out thanks to a groove-and-tongue system at the internal side and to a longitudinal friction stir welding at the external side.

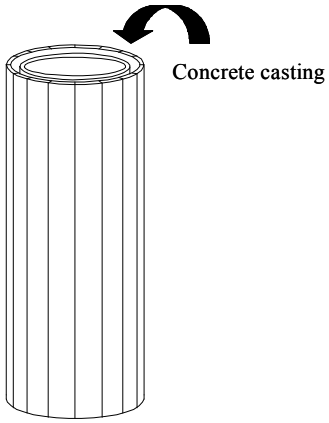

Figure 4.29. Steel and aluminium layers during the construction

3) The steel and aluminium cylinders are used as a formwork for the concrete casting. After this operation, a steel plate, prepared for setting up the inter-modular joint, is located on the top. The complete module is put in horizontal and then it can be launched.

The erection procedure for the AB prototype is carried out according to the following steps:

1) Set up of the construction yard.
2) Construction of the vehicular and pedestrian approach roads.
3) Set up of adequate systems of bulkheads made of steel piling in the areas where the access structures are erected, in order to allow the construction in dry conditions.
4) Water suction from the areas delimitated by the bulkheads.
5) Contemporary cable block foundations construction.
6) Construction of the reinforced concrete access structures.
7) Transportation and positioning of the foundation blocks.
8) Contemporary construction of the AB prototype modules in the construction yard.
9) Set-up of the special end joints at the access structures.
10) Launching of the AB prototype modules and connection between them.
11) Set up of the anchoring system.

As already pointed out, although the target configuration is the one with two couples of vertical cables and a W-shaped cables system (cable configuration 3), all the cable configurations will be sequentially set up, in order to compare by testing the behavioural differences.

4.9 THE FULL-SCALE LABORATORY

The Archimedes Bridge prototype in Qiandao Lake (PR of China) is designed for carrying out a full-scale experimental tests campaign, for acquiring comprehensive knowledge about the SFT actual dynamic behaviour in presence of the environmental actions. This is an essential task for the development of such a kind of innovative technology for the waterway crossing. In particular, the collected data will be useful for catching many

aspects which are difficult to foresee from the theoretical point of view and, at the same time, for calibrating and then improving and refining the analytical and numerical models, which have been used for this prototype and, more in general, for the Submerged Floating Tunnel typology.

The AB prototype would represent a full-scale laboratory, in all the phases of its life. Starting from the fabrication and erection phases, useful information for further designs of new SFTs will be available. Moreover, during the initial experimental phase, dynamic excitations will be provided by an automotive running into the tunnel, or by using vibrodines. The extreme hydrodynamic actions would be produced by generating waves, for instance by large ships navigating at the water surface level above the tunnel, whereas the steady currents will be provided by using external hydraulic turbines. Finally, during the service life, a monitoring system will be provided for collecting additional information on the long-term behaviour of the AB prototype.

Based on the described design, the first Archimedes Bridge prototype in the World could be a reality in few years: a permanent full-scale laboratory for investigating the behaviour of such type of constructions. The importance of this construction is enormous, since Submerged Floating Tunnels represent an innovative and technological revolution in the field of waterway crossings. The main result of this activity would probably succeed in a more confident and effective approach to such a kind of technical solution, leading to a widespread use of Submerged Floating Tunnels all over the World.

Chapter 5
SFT structural analyses

5.1 SFT PRELIMINARY DESIGN MODEL: BEAM ON ELASTIC FOUNDATION

5.1.1. Introduction

Simple models for preliminary evaluation of the global behaviour of structures are very useful in engineering practice, as they enable the designer to estimate quickly the structural dimensions in the first phase of the design. In particular, SFTs are structures whose response to environmental actions, such as hydrodynamic and seismic ones, requires cumbersome dynamic analyses to be performed. Therefore simplified models allowing for a preliminary assessment of the structural dimensions would be very effective in simplifying the SFT design process, which would thus require more sophisticated analyses only for the purposes of checking and refining the structural design.

In this perspective, the model of beam on equivalent elastic foundation (which will be here abbreviated as BOEF) could be used as a preliminary design model for Submerged Floating Tunnels (Figure 5.1c), provided that the tunnel dimensions are small enough with respect to the crossing length, so that the tunnel can be suitably modelled as a beam, and that the ratio between the the stiffness of the elastic supports represented by the SFT anchorage groups (Figure 5.1b) and the inter-axis between the anchorage groups are low enough with respect to the flexural stiffness of the tunnel, so that the retaining effect

provided by the anchorages can be suitably considered to be distributed along the tunnel length.

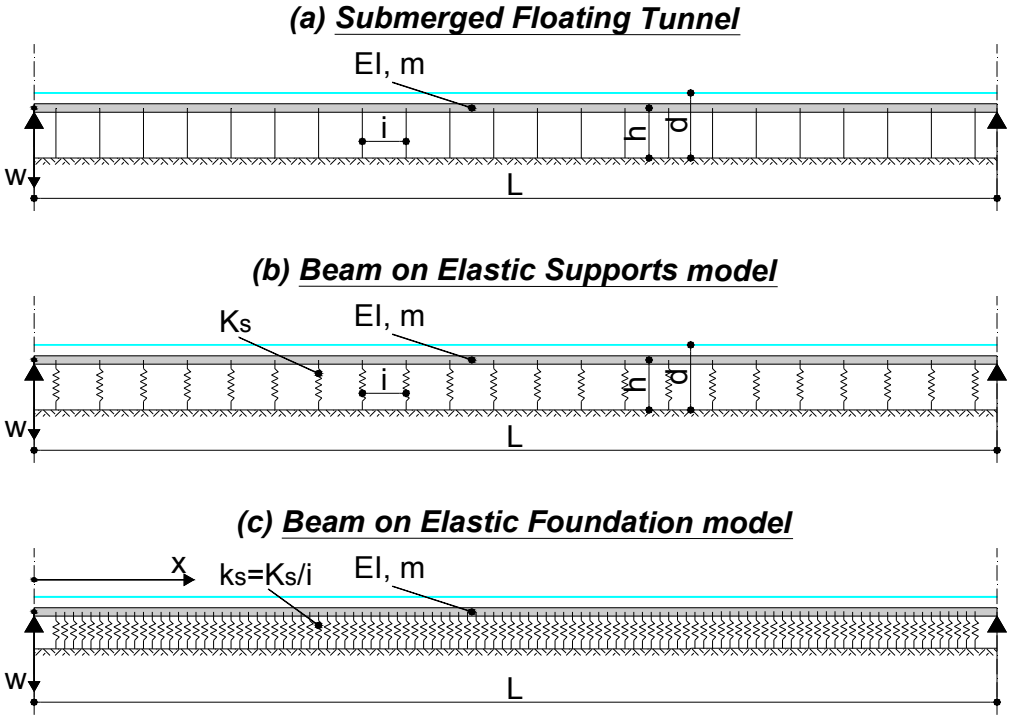

Figure 5.1. Idealization of a SFT as a Beam on Elastic Foundation: (a) real structure; (b) Beam on Elastic Supports (BOES) structural model; (c) Beam on Elastic Foundations (BOEF) structural model.

5.1.2. Mathematical formulation

5.2.2.1. *Free vibrations*

The structural scheme of a SFT can be idealized as a Beam on Elastic Supports (Figure 5.1b), uniformly spaced (i: inter-axis between the supports) along the tunnel axis. The transversal stiffness K_s of the elastic supports, in both the horizontal or vertical plane, can be easily determined on the basis of the mechanical properties and dimensions of the anchorages (i.e. the Young's modulus E and the anchorage cross-section area A) and on the geometrical

arrangement chosen for the anchorages groups. If the anchorage system is made up of cables, an equivalent Young's modulus can be considered to take into account the catenary effects.

The passage from the model of BOES to the one of BOEF can be made by replacing the discrete elastic supports by a continuous elastic foundation whose stiffness modulus k_s is obtained as the ratio between the stiffness of the supports Ks and the inter-axis i between the supports (Figure 5.1c).

Imposing the dynamic equilibrium between the inertia forces and the elastic reactions acting on the beam/tunnel elementary segment, the equation of motions of the BOEF relative to free vibrations can be obtained:

$$EI \cdot w^{IV}(x,t) + m \cdot \ddot{w}(x,t) + k_s \cdot w(x,t) = 0 \tag{5.1}$$

where EI and m are the bending stiffness and distributed mass (including the water added mass contribution) of the beam/tunnel, respectively, w (x,t) is the beam/tunnel deflection at the abscissa x and at the time instant t, $w^{IV}(x,t)$ and $\ddot{w}(x,t)$ are its fourth derivative (with respect to tunnel abscissa x) and second derivative (with respect to time t), respectively.

Assuming a solution having the following form:

$$w(x,t) = \Psi_n(x) \cdot \Phi_n(t) \tag{5.2}$$

and substituting it into equation 5.1 we obtain:

$$\left(EI \cdot \Psi_n^{IV}(x) + k_s \cdot \Psi_n(x)\right) \cdot \Phi_n(t) = -m \cdot \Psi_n(x) \cdot \ddot{\Phi}_n(t) \tag{5.3}$$

which leads to:

$$\frac{EI \cdot \Psi_n^{IV}(x)}{m \cdot \Psi_n(x)} + \frac{k_s}{m} = -\frac{\ddot{\Phi}_n(t)}{\Phi_n(t)} = \omega^2 \tag{5.4}$$

where ω has to be a constant, in order to satisfy the equality between the first and second member of equation 5.4.

Therefore we have from (5.4) the following two equations:

$$\ddot{\Phi}_n(t) + \omega^2 \cdot \Phi_n(t) = 0 \tag{5.5a}$$

$$EI \cdot \Psi_n^{IV}(x) = \left(\omega^2 - \frac{k_s}{m}\right) \cdot m \cdot \Psi_n(x) \quad (5.5b)$$

The solution of (5.5a) and (5.5b) are:

$$\Phi_n(t) = A \cdot \sin(\omega_n \cdot t - \varphi) \quad (5.6a)$$

$$\Psi_n(x) = C_1 \cdot \sin(\beta_n \cdot x) + C_2 \cdot \cos(\beta_n \cdot x) + C_3 \cdot \sinh(\beta_n \cdot x) + C_4 \cdot \cos h(\beta_n \cdot x) \quad (5.6b)$$

where A, φ and C_1, C_2, C_3, C_4 are constants which depend on the initial and boundary conditions respectively and β is a constant defined by the following relationship:

$$\beta_n^4 = \left(\omega_n^2 - \frac{k_s}{m}\right) \cdot m / EI \quad (5.7)$$

Assuming that the tunnel is simply supported at its ends, i.e. displacements and bending moments are equal to zero at the tunnel ends, it can be shown that the shape of the vibration modes of the BOEF is exactly the same of a simply supported beam (with distributed mass and elasticity) not supported by an elastic foundation (Chopra, 2006):

$$\sin(\beta_n \cdot L) = 0 \quad \rightarrow \quad \beta_n = n \cdot \pi / L \quad (5.8a)$$

$$\Psi(x) = C_1 \cdot \sin(n \cdot \pi / L \cdot x) \quad (5.8b)$$

Combining equations 5.7 and 5.8a it is possible to derive the relationship providing the angular frequencies of free vibration of the simply supported BOEF:

$$\omega_n = \sqrt{(n \cdot \pi / L)^4 \cdot \frac{EI}{m} + \frac{k_s}{m}} \quad (5.9)$$

Equation 5.9 shows an intuitive result: the effect of the presence of the elastic foundation is to increase the natural frequencies of the system. In fact, comparing (5.9) with the correspondent equation providing the angular frequencies of a simply supported beam, it can be noticed that only difference

is related to the presence of the second addend under the root square (i.e. k_s/m) in equation 5.9, which can be considered as the squared angular frequency of free vibration of a BOEF featuring EI=0, i.e. of the system composed by the beam distributed mass and the foundation distributed springs.

The mathematical analogy between a beam on elastic supports (BOES) and a beam on elastic foundation (BOEF) has been studied by Sato et al. (2008). The results of their study show that the natural vibration modes and frequencies of a BOEF and a BOES are the same for K_v being lower than 0.05 and are still close for K_v lower than 0.5 (Figure 5.2), where K_v is a constant that is inversely proportional to the degree of concentration of the stiffness of the anchorage system and is defined by the following relationship:

$$K_v = {k_s \cdot i^3}/{24 \cdot EI} \tag{5.9}$$

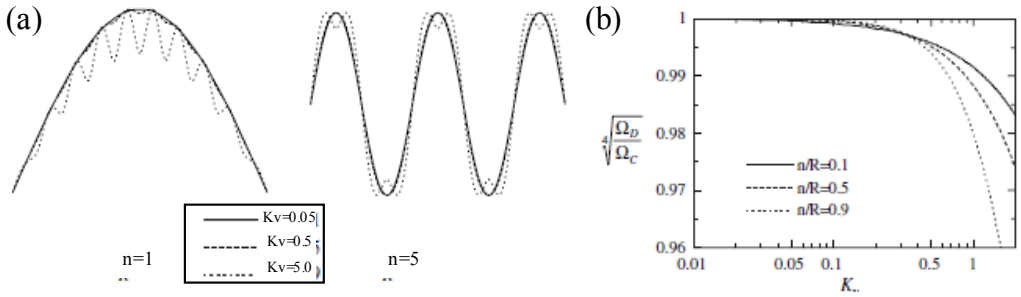

Figure 5.2. Comparison of modal shapes (a) and natural frequencies (b) of a BOES and a BOEF (Figures borrowed from Sato et al., 2008).

As for every other system with distributed mass and elasticity, the property of orthogonality of the natural vibration modes is still valid. In fact, if we rewrite equation 5.5b considering the beam vibrating at its n^{th} and r^{th} natural vibration mode we get:

$$EI \cdot \Psi_n^{IV}(x) + k_s \cdot \Psi_n(x) = \omega_n{}^2 \cdot m \cdot \Psi_n(x) \tag{5.10a}$$

$$EI \cdot \Psi_r^{IV}(x) + k_s \cdot \Psi_r(x) = \omega_r{}^2 \cdot m \cdot \Psi_r(x) \tag{5.10b}$$

Multiplying both sides of (5.10a) by $\Psi_r(x)$, both sides of (5.10b) by $\Psi_n(x)$ and integrating both equations over the beam/tunnel length we have:

$$\int_0^L EI \cdot \Psi_n^{IV}(x) \cdot \Psi_r(x) \cdot dx + \int_0^L k_s \cdot \Psi_n(x) \cdot \Psi_r(x) \cdot dx =$$

$$= \omega_n{}^2 \cdot \int_0^L m \cdot \Psi_n(x) \cdot \Psi_r(x) \cdot dx \qquad (5.11a)$$

$$\int_0^L EI \cdot \Psi_r^{IV}(x) \cdot \Psi_n(x) \cdot dx + \int_0^L k_s \cdot \Psi_r(x) \cdot \Psi_n(x) \cdot dx =$$

$$= \omega_r{}^2 \cdot \int_0^L m \cdot \Psi_r(x) \cdot \Psi_n(x) \cdot dx \qquad (5.11b)$$

Integrating by parts the first addend at the first member of (5.11a) and (5.11b), and imposing the boundary conditions (whatever they are) we obtain:

$$\int_0^L EI \cdot \Psi_n^{II}(x) \cdot \Psi_r^{II}(x) \cdot dx + \int_0^L k_s \cdot \Psi_n(x) \cdot \Psi_r(x) \cdot dx =$$

$$= \omega_n{}^2 \cdot \int_0^L m \cdot \Psi_n(x) \cdot \Psi_r(x) \cdot dx \qquad (5.12a)$$

$$\int_0^L EI \cdot \Psi_r^{II}(x) \cdot \Psi_n^{II}(x) \cdot dx + \int_0^L k_s \cdot \Psi_r(x) \cdot \Psi_n(x) \cdot dx =$$

$$= \omega_r{}^2 \cdot \int_0^L m \cdot \Psi_r(x) \cdot \Psi_n(x) \cdot dx \qquad (5.12b)$$

Subtracting (5.12b) from (5.12a) we finally have:

$$0 = (\omega_n{}^2 - \omega_r{}^2) \cdot \int_0^L m \cdot \Psi_r(x) \cdot \Psi_n(x) \cdot dx \rightarrow 0 = \int_0^L m \cdot \Psi_r(x) \cdot \Psi_n(x) \cdot dx \qquad (5.13)$$

since ω and are different, as proved by (5.9). Substituting (5.13) into (5.12) we finally have:

$$\int_0^L EI \cdot \Psi_r^{II}(x) \cdot \Psi_n^{II}(x) \cdot dx + \int_0^L k_s \cdot \Psi_r(x) \cdot \Psi_n(x) \cdot dx = 0 \qquad (5.14)$$

so that the orthogonality of the vibration modes of a BOEF is proved.

5.2.2.2. *Forced vibrations*

In case of forced vibrations equation 5.1 becomes:

$$EI \cdot w^{IV}(x,t) + m \cdot \ddot{w}(x,t) + k_s \cdot w(x,t) = p(x,t) \qquad (5.15)$$

where p(x,t) is the function defining the external distributed load acting on the beam/tunnel at abscissa x at the time instant t.

Expressing in (5.15) w(x,t) as the superposition of the infinite number of vibration modes of the BOEF we get:

$$EI \cdot \sum_1^\infty \Psi_n^{IV}(x) \cdot \Phi_n(t) + k_s \cdot \sum_1^\infty \Psi_n(x) \cdot \Phi_n(t) + m \cdot \sum_1^\infty \Psi_n(x) \cdot \ddot{\Phi}_n(t) = p(x,t) \quad (5.16)$$

Multiplying both sides of (5.16) by $\Psi_r(x)$ and integrating both equations over the beam/tunnel length we have, thanks to the modal orthogonality (see equations 5.13 and 5.14):

$$K_r \cdot \Phi_r(t) + M_r \cdot \ddot{\Phi}_r(t) = P_r(t) \quad (5.17)$$

where:

$$K_r = \int_0^L EI \cdot \left(\Psi_r^{II}(x)\right)^2 \cdot dx + \int_0^L k_s \cdot \left(\Psi_r(x)\right)^2 \cdot dx \quad (5.18a)$$

$$M_r = \int_0^L m \cdot \left(\Psi_r(x)\right)^2 \cdot dx = {K_r}/{\omega_r{}^2} \quad (5.18b)$$

$$P_r(t) = \int_0^L p(x,t) \cdot \Psi_r(x) \cdot dx \quad (5.18c)$$

Therefore K_r, M_r, and $P_r(t)$ are, respectively, the generalized stiffness, mass and force relative to the r^{th} natural vibration mode. Thus we have an infinite number of differential equations like (5.17), one for each mode; the partial differential equation 5.15 in the unknown w(x,t) is transformed to a set of infinite differential equation in unknows $\Phi_r(t)$. Each of the infinite equations (5.17), equivalent to the equation of motion of a SDOF system, can be solved independently and the total displacement w(x,t), bending moment M(x,t) or any other response parameter can be obtained as the superposition of the respective modal contributions:

$$w(x,t) = \sum_1^\infty \Psi_r(x) \cdot \Phi_r(t) \quad (5.19a)$$

$$M(x,t) = -EI \cdot \sum_1^\infty \Psi_r^{II}(x) \cdot \Phi_r(t) \quad (5.19b)$$

Equation (5.17) makes reference to an undamped system. Dividing both sides by M_r it is possible to introduce the modal damping ν_r (whose values

should take into account also the hydrodynamic damping provided by the water presence) obtaining the usual form of equation of motion of a damped SDOF system:

$$\omega_r{}^2 \cdot \Phi_r(t) + 2 \cdot \nu_r \cdot \omega_r \cdot \dot{\Phi}_r(t) + \ddot{\Phi}_r(t) = {}^{P_r(t)}/_{M_r} \tag{5.20}$$

5.2 SFT FINITE ELEMENT MODELS

5.2.1. Introduction

The Finite Element Method (F.E.M.) nowadays represents the most powerful and widely used analysis tool available in engineering practice to solve problems whose complexity is such that traditional analytical models are not suitable for their solution. The class of problems which can be solved only by means of such numerical methods is quite large, involving, for instance, structures featuring complex geometries, mechanical and geometrical non-linearities and so on.

F.E.M basically consists in the discretization of a continuous problem, governed by differential equations whose analytical solution can be rarely found. The continuous domain is thus subdivided in smaller elements, i.e. finite elements, whose behaviour is entirely defined by a finite number of parameters. This discretization of the problem allows to turn the differential equations governing the original continuous problem into a set of algebraic equations, whose unknowns are the set of parameters defining the behaviour of the ensemble of finite elements of the model.

It is evident that the previous definition of the Finite Element Method is extremely superficial. The reader interested can make reference to one of the many books devoted to this topic, such as the one from Zienkiewicz et al. (2004).

Submerged Floating Tunnels are structures whose geometry and structural scheme is not really complex. Nevertheless, their response to dynamic excitation, such as the ones occurring during a seismic or storm event, could be rather complex, due to many aspects, the most important of them being the non-linear behaviour of the anchorages. Therefore it is appropriate to perform F.E. analyses to carefully investigate the dynamic behaviour of SFTs, in

particular considering the novelty of this structural typology and the importance of such a kind of structures. Moreover, due to the peculiarities of the structural configuration and environmental conditions of SFTs, the development of ad hoc numerical tools to investigate their dynamic behaviour seems to be worthwhile, in order to improve the ease and efficiency of the dynamic analysis and allow for an easier development of special loading models and analysis methods. In this context, it has to be mentioned the work performed by the research group of Prof. Perotti at the Politechnic of Milan; this work is mainly devoted at developing finite element models able to reproduce the behaviour of the anchorages of SFTs, taking into account the complex interaction with the fluid environment, at the same time ensuring sustainable computational costs (Di Pilato et al., 2008; Perotti, Di Pilato, 2009; Fogazzi and Perotti, 2000; Perotti et al., 2010; Martinelli et al., 2010).

In this work, Finite Element analyses are carried out by means of the F.E. software Abaqus (Abaqus Inc., 2007), which features a block, namely Aqua, allowing for the modeling of the hydrodynamic loads and of the water-structure dynamic interaction. A brief description of the Abaqus environment can be found in Esposto (2007).

In the following sections the main aspects of the F.E.M. developed in this study for the analysis of the dynamic response of SFTs to environmental actions is given.

5.2.2. Description of the SFT Finite Element Model

5.2.2.1. *Structural model*

A three-dimensional model of the SFT structure, made up of mono-dimensional elements, is set up (Fig. 5.3a).

The tunnel is modelled by means of quadratic beam elements (elements B32 in the Abaqus nomenclature; Abaqus Inc., 2007). Each tunnel module, whose length has been set equal to 100 m, is subdivided into 20 beam elements, thus each tunnel beam element features a length of 5 m. The mechanical, geometric and inertia properties of the beam cross-section are set equal to those of the tunnel cross-section. Since the SFTs feature a steel-concrete composite structure, the cross-section characteristics are determined considering a concrete section equivalent to the actual steel-concrete

composite structure, in terms of stiffness. Non structural mass is also assigned to the beam elements, so that the actual values of the total (structural and non-structural) mass of the structure is considered in the model. Inter-modular joints between adjacent tunnel modules are assumed to behave rigidly, therefore rigid connections are introduced in the model.

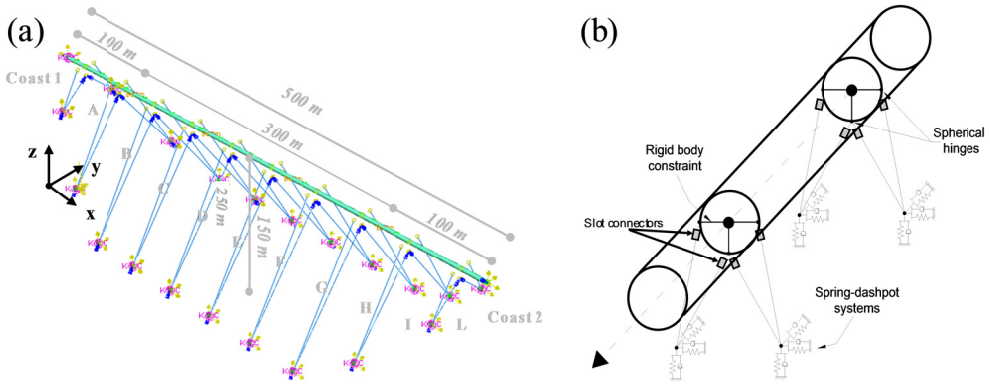

Figure 5.3. (a) perspective view of the F.E model; (b) Detail of the modelling of connections between the anchorages and the tunnel and of the ground-foundation systems.

Anchorages (both cables or tubular tethers) are modelled through quadratic beam hybrid elements (elements B32H in the Abaqus nomenclature; Abaqus Inc., 2007). Hybrid beam element types are provided in Abaqus/Standard for use in cases where it is numerically difficult to compute the axial forces in the beam by the usual finite element displacement method. This problem arises most commonly in geometrically nonlinear analysis when the beam undergoes large rotations and is very rigid in axial deformation, such as in a flexing long pipe or cable. The problem in such cases is that slight differences in nodal positions can cause very large forces, which, in turn, cause large motions in other directions. The hybrid elements overcome this difficulty by using a more general formulation in which the axial and transverse shear forces in the elements are included, along with the nodal displacements and rotations, as primary variables. Although this formulation makes these elements more expensive, they generally converge much faster when the beam's rotations are large and, therefore, are more efficient overall in such cases (Abaqus Inc.,

2007). Negligible values of inertia moments of the cross-section are assigned to the hybrid beam elements; in this way, since geometrical non-linear effects are taken into account, cables buckle when subjected to axial compressive load, well approximating the actual behaviour of the anchorages. It is worth to underline that also the tubular tethers considered here are unable to withstand compressive axial force, since they are assumed to be made as an assembly of several segments connected through joints which allow free rotations, in order to enormously reduce the stresses induced by hydrodynamic transversal loading (see section 2.1.2.2).

The connection between the anchorage groups and the corresponding tunnel sections is modelled through a rigid body constraint, so that the actual dimensions of the SFT cross-section are taken into account. Spherical hinge constraints are considered at both ends of each anchorages connected to the tunnel and the foundations (Figure 5.3b). Slot connector elements, allowing free cable-tunnel relative displacements in the anchorage axial direction are used to model the connection between the anchorage ends and the points representing the tunnel external surface at the tunnel cross-sections in correspondence of the location of the anchorage groups (Figure 5.3b). Connectors are specific elements provided in Abaqus to model complicated kinematic constraints (Abaqus Inc., 2007). In this way the pre-tensioning of the cables can be properly introduced in the model in a first step of the analysis, in which the connectors are unlocked (see section 5.2.2.2). In the subsequent analysis steps the connectors are locked, so that the described spherical hinge constraint is obtained. Moreover, non-linear mechanical axial behaviour can be assigned to the slot connectors, in order to reproduce post-elastic behaviour of the anchorages, when necessary.

The foundation system is considered to be made up of groups of piles. The dynamic behaviour of the ground-foundation system is also taken into account in the model, as the assumption of rigid restrain seems to be unrealistic in such a kind of problem. The most rigorous way to consider the soil-foundations behaviour in a F.E. structural model would be to introduce the soil (by means of solid elements) and the piles (beam elements) into the model itself; in this way the F.E. model would take into account the kinematic interaction between the piles and the soil and the dynamic interaction between the superstructure and the foundation structures but, at the same time, it would be too

computationally burdensome (a resume of the methods currently available for the design and analysis of piles foundations can be found in Aversa et al., 2005). Therefore it is widely used a less rigorous, but still quite well approximated, method which is based on sub-modelling: the soil-foundation interaction and the superstructure interaction are analysed independently and then the results obtained are combined in order to obtain displacements and stresses distribution in the piles foundations. A simple and widely used way to introduce in the global model the dynamic behaviour of piles foundations is to model them through a Lumped Parameters Model (LPM): in each of the 3 translational degrees of freedom the pile foundations are represented by a spring and a dashpot in parallel. In a steady-state dynamic analysis (then a frequency-domain analysis) the pile foundations dynamic properties can be directly introduced through their dynamic impedance, but this is not possible for a time-domain dynamic analysis, where frequency-constant values of stiffness, mass and damping have to be introduced.

In the present work the dynamic impedance of a single pile is evaluated through the freeware version of the ad-hoc FEM software Versat-P3D (Wu et al, 1997). In this software a quasi-3D motion of the soil is considered; the soil is modelled through 4-nodes solid elements with an elastic behaviour and hysteretic damping (introduced by means of a complex valued shear modulus G*), whereas piles are modelled through beam elements (Figure 5.4).

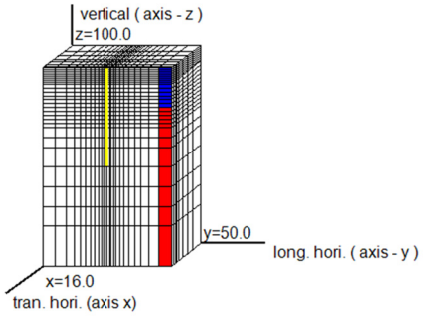

Figure 5.4. FE model of the pile-ground system in Versat-P3D.

The interaction between the piles composing the single foundation block in this case are computed through the simplified method proposed by Dobry e Gazetas (1988) which introduces dynamic interaction coefficients, thus

adopting a procedure similar to the one commonly adopted in the static design of pile foundations. The dynamic impedances of the piles group can be easily computed through few matricial operations, based on the assumption that the foundation cap is a rigid element, thus imposing a rigid body constraint to the head of the piles. This procedure is illustrated in more detail in Dobry and Gazetas (1988) and Chellini and Salvatore (2008). The dynamic impedances values obtained are referred to 10 frequency values ranging from 0.628 Hz to 10 Hz, thus covering the frequency range of interest; furthermore, for higher frequency the soil behaviour is influenced by other phenomena which are not represented in the adopted model (Dezi et al., 2007).

In the LPM, the dynamic impedance of the pile foundation is described by the complex valued frequency function:

$$Z(\omega) = (K_f - \omega^2 \cdot M_f) + \omega \cdot C_f \tag{5.21}$$

where K_f is the stiffness constant, M_f the mass constant and C_f the damping constant. The values adopted for the three constants in the horizontal and vertical direction are determined in order to minimize the difference between the real and imaginary parts of the dynamic impedance computed through (5.21) and through the Dobry-Gazetas procedure.

5.2.2.3. *Multi-step structural analysis*

Abaqus allows to carry out multi-step analysis; each step can be a static, dynamic or linear perturbation step and considers at its beginning the final configuration of the structure at the end of the previous step. The structural analyses performed in this study consist of five successive steps, allowing for the modelling of the SFT configuration under permanent and live loads, the evaluation of its dynamic characteristics and, finally, of its response to a multi-support seismic excitation:

1) Permanent condition step-a: the pre-tensioning provided to the anchorages by the permanent residual buoyancy is introduced. Concentrated forces T_0 equal to the initial anchorage design forces are applied to the cable top vertices. The slot connectors are unlocked in this step, so that anchorages-tunnel relative displacements along the anchorage axis direction are left free and no stress is induced in the

tunnel (Figure 5.5). Each anchorage group carries a resultant vertical force equal to RB·i (RB=permanent residual buoyancy; i=inter-axis between the anchorage systems).

2) Permanent condition step-b: the local bending due to the transmission of the residual buoyancy distributed along the tunnel to the cable systems is modelled. The anchorages-tunnel connection is now fixed and the distributed tunnel residual buoyancy RB applied, together with the residual weight (i.e. the weight of the cables reduced by the water buoyancy) of the anchorages (Figure 5.5). The connectors are now locked and the and the pre-tension anchorage forces are released.
By means of these two steps the SFT initial configuration under permanent loads is modelled in a simple way and with good approximation.

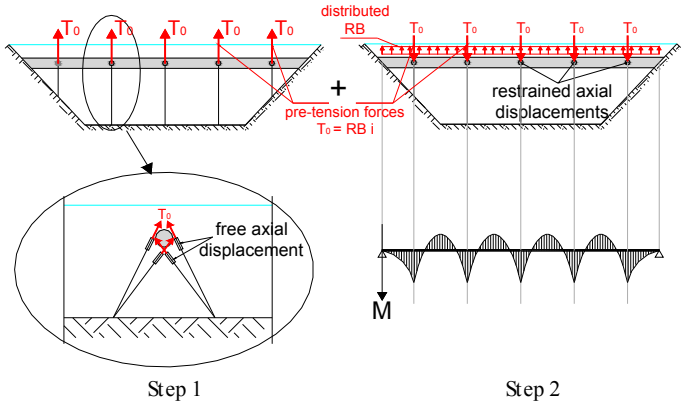

Figure 5.5. SFT permanent stress condition modelling through multi-step analysis.

3) Traffic loading step: the traffic loads (20% of the nominal value) are applied to the structure.

4) Frequency extraction step: the vibration modes are extracted through a linear perturbation step (ABAQUS, 2007) carried out on the SFT model, subjected to its permanent stress condition, thus taking into account the anchorages pre-tensioning effect. The added mass

contribution due to the presence of water (see section 2.2.3.1) is taken into account.

5) Dynamic analysis step: dynamic non-linear time-history analysis is performed, adding the hydrodynamic (forces induced by water and currents calculated by means of the Morison's equation) or seismic actions (ground motion time histories imposed at each anchorage group foundation and tunnel shore connection) to the loads acting in the previous step. An implicit time integration is used to calculate the transient dynamic response of a system; implicit integration schemes determine dynamic quantities at time $t+\Delta t$ based not only on values at time t , but also on these same quantities at $t+\Delta t$. In the implicit time integration scheme the integration operator matrix must be inverted at each time increment, and a set of simultaneous nonlinear dynamic equilibrium equations must be solved at each time increment. This solution is done iteratively using Newton's method. (Abaqus Inc., 2007).

The implicit time integration procedure is computationally more expensive than the explicit one, but it has the advantage that it is that it is unconditionally stable for linear systems: there is no mathematical limit on the size of the time increment that can be used to integrate a linear system. Moreover, the Aqua block, which allows to introduce the water-structure interaction in the analysis can be used only in implicit dynamic analysis.

An automatic incrementation scheme is provided for implicit dynamic analysis, which evaluates the values of time increments that should be considered of the time increments during the analysis, in order to ensure an accurate dynamic solution. The scheme uses a half-step residual control, which consists in the check of the equilibrium residual error (out-of-balance forces) halfway through a time increment. If the half-step residual is small, it indicates that the accuracy of the solution is high and that the time step can be increased safely; on the contrary, if the half-step residual is large, the time step used in the solution should be reduced.

The acceptable half-step residual tolerance has to be indicated in the definition of the dynamic step and it should be chosen by comparison with typical force values F, such as applied forces or expected reaction forces. Half-step residual tolerance approximately belonging to the range $0.1 \cdot F \div 0.5 \cdot F$ is used, in order to obtain an highly accurate solution (Abaqus Inc., 2007).

Chapter 6

The response of SFTs to hydrodynamic actions

6.1 AIMS OF THE STUDY

The study of the response of Submerged Floating Tunnels to environmental actions is probably the most important research topic to be investigated in this field. As a matter of fact the poor level of knowledge on the performances of this innovative waterway crossing solution, when subjected to environmental loads, can be considered to be one of the main reasons why nowadays no SFT has been built yet in the world.

Among the environmental actions, hydrodynamic ones, induced by the presence of water waves and currents, are the most relevant ones, together with seismic actions. Therefore it is of great importance to study the behaviour of SFTs during severe storm events, with the aim of characterizing their structural response and determine the structural configurations which exhibit the better performances.

In this work the response of SFTs to hydrodynamic actions is studied by means of numerical analyses, carried out through the Finite Element Analysis software Abaqus (version 6.7, 2007), in order to:

- characterize the structural behaviour of SFTs during severe storm events;
- estimate the performance of several structural configurations, mainly differing on the arrangement of the anchoring system, with the aim of determining the optimal ones;

- investigate the influence of the crossing length on the structural behaviour and performances of SFTs;
- investigate the influence of the model adopted to represent the water flow during a storm event (extreme wave versus multi-chromatic sea state based on sea energy spectrum, see section 2.2.3.1) on the structural response;
- investigate the influence of the values adopted for the hydrodynamic force coefficients (i.e. drag and inertia coefficients, see section 2.2.3.1) on the structural response.

The work is articulated in two phases: a first one, where a large number of structural configurations are considered, in order to estimate their performance and select the ones proving to withstand better hydrodynamic actions; a second one, where a restricted number of structural configurations are considered, on the basis of the results obtained in the first phase, studying their behaviour and focusing the attention also on the model adopted to represent the water kinematic field and the hydrodynamic loads arising from the water-structure interaction.

The case studies considered, the analyses performed and the results obtained in phase 1 and 2 of the work are described in following sections 6.2 and 6.3, respectively.

6.2 PRELIMINARY EVALUATION OF HYDRODYNAMIC PERFORMANCES OF SFT STRUCTURAL CONFIGURATIONS

6.2.1. Case studies

6.2.1.1. *Design scenarios: location features and destinations of use*

Different design conditions are considered, in order to obtain a wide range of significant case studies. The assumed design conditions differ for the length and for the destination of use of the crossing.

In particular, the following situations are considered:

- three destinations of use: pedestrian (P), motorway (M) and rail-motorway (RM) crossings, thus including the whole range of transport demand;

- five crossing lengths, ranging from 200 m to 1000 m for pedestrian crossings and from 600 m to 3000 m for railway and motorway crossings;
- seabed profile is assumed as flat, having a depth of 100 m.

6.2.1.2. *Structural features*

The principal aim of this phase of the work is to compare the hydrodynamic performances offered by different structural configurations of SFTs. Thus a quite large number of structural solutions are considered, obtained through the combination of the following features:

- two external shapes of tunnel cross-section: elliptic (E), featuring good fluid dynamic performances and larger strength and stiffness properties in the horizontal bending plane, and circular (C), more rational from the construction point of view and more suitable with respect to the hydrostatic behaviour (see section 2.1.1.3).
- three cable system configurations in the transversal plane (Figure 6.1a), namely composed of: two vertical steel cables (type A); two inclined cables (type B) and four inclined W-shaped cables (type C);
- different values of inter-axis between anchorage systems; in particular, for motorway and rail-motorway crossings SFTs, each tunnel module, (100 and 125 m long, respectively), are restrained by one, two or three cable systems (Figure 6.1b), whereas each pedestrian tunnel module, 25 m long, is restrained only by one or two cable systems, due to its significantly minor length.

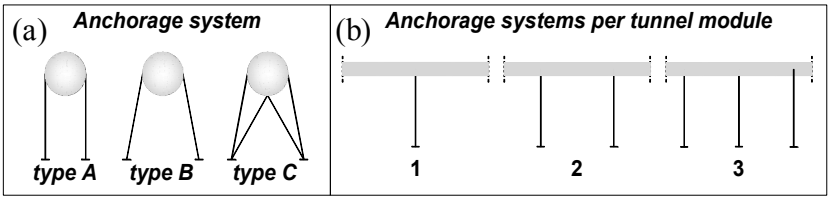

Figure 6.1. Anchorage system configurations: (a) anchorage group arrangements; (b) number of anchorage groups per tunnel module.

The tunnels structure is the same multilayer sandwich structure conceived for the design of the Archimedes Bridge Prototype in Qiandao Lake (PR of China; see section 4.1), characterized by an internal layer of steel sheets, an intermediate layer of concrete and an external layer of aluminium.

Table 6.1 illustrates the main mechanical properties, namely the density ρ, the Young modulus E and the design strength f_d, of the adopted materials: steel S235, concrete C20/25 and aluminium alloy 6061-T6.

Table 6.1. Material properties

Material	ρ [kg/m^3]	E [MPa]	f_d [MPa]
Steel S235	7850	210000	213.6
Concrete C20/25	2400	28850	11.0
Aluminium 6061-T6	2700	70000	218.0

The design of the tunnel cross-sections is carried out considering the requisites listed in section 2.1.1.1. The minimum value of the residual buoyancy is always larger than 1.20. Table 6.2 provides the value of the area, horizontal and vertical moments of inertia and bending moment strengths for all the designed tunnel structures. The aforementioned properties of the tunnel cross-sections are calculated considering the steel and concrete tubes only, they acting as a composite structure.

Table 6.2. Tunnel cross-section inertia and strength properties

	A [m^2]	I_h [m^4]	I_v [m^4]	$M_{Rd,h}$ [kNm]	$M_{Rd,v}$ [kNm]
P-E	7.5	23.2	17.4	123989.7	110205.4
M-E	127.3	9553.8	3327.1	9324518.7	5942226.3
RM-E	149.2	11420.8	5824.3	10550209.9	8431691.9
P-C	7.3	20.1	20.1	114955.0	114955.0
M-C	135.8	6536.3	6329.4	7737019.4	7628294.1
RM-C	165.6	9417.1	102465.5	9400921.8	8809491.4

Figure 6.2 shows the elliptical tunnel cross-sections designed for the considered destinations of use.

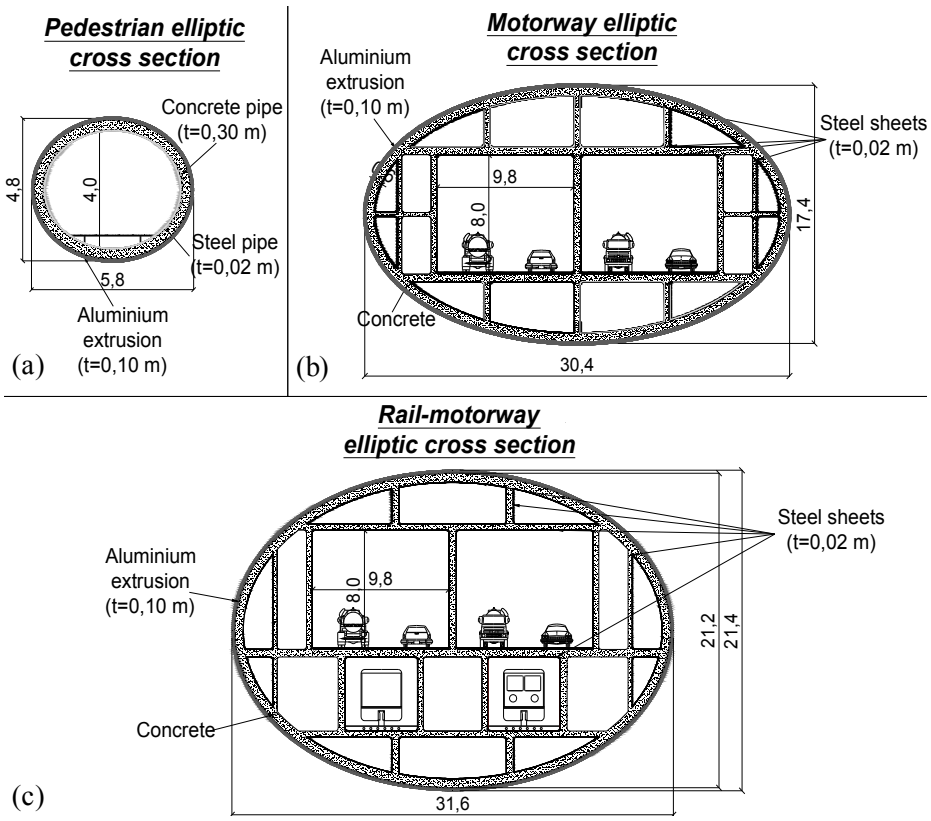

Figure 6.2. Tunnel cross-sections featuring elliptical external shape: (a) pedestrian (P), (b) motorway (M) and (c) rail-motorway (RM) crossing.

In the present work, a very simple method for the preliminary design of cables diameter is used. The procedure is carried out only for type B cable systems, since it is the most onerous for the cables integrity; therefore, the same diameter is assigned to cables belonging to type A and type C configuration. A bi-dimensional scheme, referred to the tunnel cross-section plane involving one cable system, is considered. Spherical hinges are assumed as restraint conditions at the cables ends, thus the structural scheme in the cross-section plane can be thought as a four hinges arch, which is an hypostatic scheme, as far as the rotational degree of freedom of the tunnel around its axis is unrestrained. However, considering the global tri-dimensional structural scheme, the torsional rotation of the tunnel is governed by the tunnel torsional stiffness, together with the end restraints. As a

simplifying hypothesis, it is assumed that no torsional rotation of the tunnel occurs; therefore, the structural scheme in the cross-section plane can be thought as a three hinges arch. It is assumed that each cable system has to withstand the resultant of vertical and horizontal loads acting on a tunnel part, whose length corresponds to the anchorage system inter-axis.

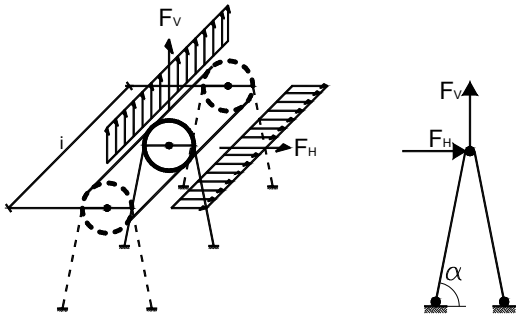

Figure 6.3 Simplified static scheme for the cables design

The uniformly distributed load is given by the combination of residual buoyancy and hydrodynamic actions, due to waves and currents. The hydrodynamic actions are computed through the Morison's equation in its static version (see section 2.2.3.1). The axial force values obtained are then amplified by a dynamic coefficient C_{dyn} set equal to 1.5 on the basis of the results obtained from some preliminary dynamic analyses carried out.

The cables are made of steel having a density of 8500 kg/m^3, a tensile strength equal to 1260 MPa and a Young's modulus of 140 GPa. Table 6.3 shows the diameters adopted for each configuration as a function of the ratio i/ℓ, where i is the cable systems inter-axis and ℓ is the tunnel module length.

Table 6.3. Material properties

i/ℓ [-]	P-E	P-C	M-E	M-C	RM-E	RM-C
1	0.09	0.09	0.52	0.55	0.67	0.55
1/2	0.06	0.06	0.37	0.39	0.47	0.39
1/3	-	-	0.30	0.32	0.41	0.32

6.2.1.3. *Hydrodynamic actions*

In this study, the storm scenario assumed consists of a single sinusoidal wave, featuring a wave height H_w of 5.8 m and period T_w of 7.0 s, and a steady current having a surface velocity equal to 4.1 m/s. These values are related to severe environmental conditions of the Jintang Strait in China, which were considered for a SFT crossing feasibility study in a previous international cooperation project (Mazzolani et al. 2001). Water wave motion is computed by means of the Airy wave theory. The water velocity due to currents is assumed to vary linearly in the vertical direction, reaching the zero value at the seabed depth.

Hydrodynamic actions are calculated by means of the Morison's equation. For most of the case studies the ratio between the dimension D of the structure and the wave length λ_w exceeds 0.2, which is the limit of validity of Morison's equation. However, computing the hydrodynamic loads by means of the equations provided by Jamieson and Mogridge (Dawson, 1983), which takes into account diffraction effects, it was found that the Morison's equation provides larger forces, so that the calculation of hydrodynamic actions through Morison's equation, directly implemented in Abaqus/AQUA, can be used, being the calculated results on the safe side.

Commonly, the drag force coefficient C_D ranges within 0.5÷1.2, whereas the inertia force coefficient C_I oscillates from 1.5 to 2.0. Here values close to the upper bounds of their range of variation are assumed: in particular C_I=2.0, C_D=0.8 (elliptical cross-sections) and C_D=1.0 (circular cross-sections) are assumed. The added mass coefficient C_M is set equal to 1.0.

6.2.2. Structural analyses

The dynamic behaviour of the SFTs is analysed through dynamic non-linear time-history analysis carried out on a Finite Element Model of the structure using the software ABAQUS 6.7 (2007).

Details on the structural Finite Element Model and on the performed structural analyses are given in section 5.2. The only difference is related to the foundations, which are here modelled as rigid constraints.

6.2.3. Results of the analyses

6.2.3.1. *Structural dynamic properties*

The first 200 vibration modes are extracted for all case studies considered. This ensemble of vibration modes features a total participant mass always larger than 85% of the total structural mass.

A large number of vibration modes regards only transverse oscillations of the cables (Figure 6.4). The vibration modes involving transversal oscillations of the tunnel are similar to those of a beam on elastic foundation (BOEF) with distributed mass and elasticity, featuring a number of sinusoidal waves progressively increasing.

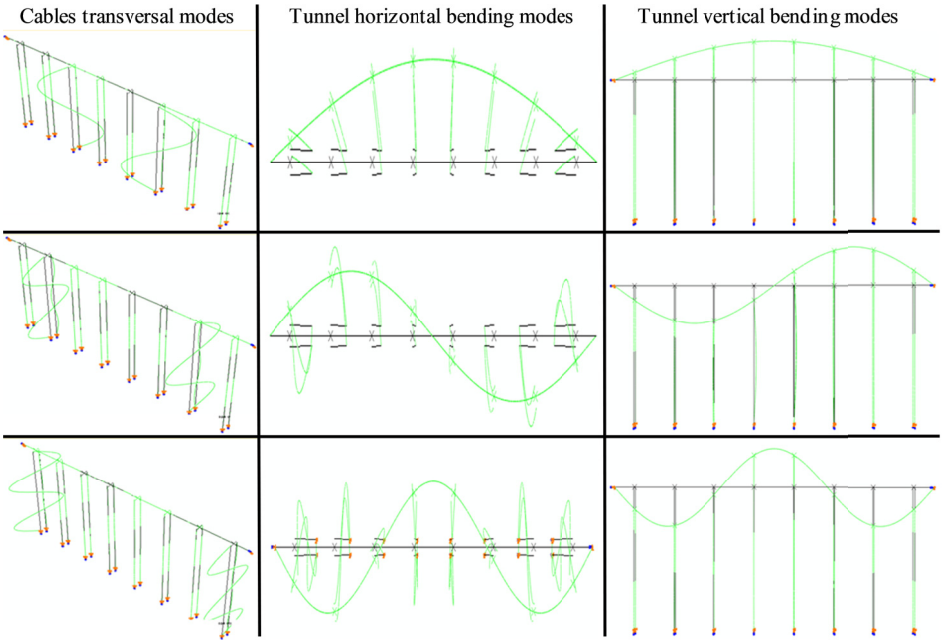

Figure 6.4. First vibration modes of one of the considered case studies: transversal vibrations of cables, horizontal and vertical bending vibrations of the tunnel.

The first vibration mode always involves horizontal oscillations of the tunnel whereas the second one regards its vertical oscillations, exception made when vertical cables are provided: in the latter cases the structure is extremely

more deformable in the horizontal direction (the first vibration period of longer tunnels holding railways and motorways is approximately 34.0 s), so that in most of the cases also the second horizontal flexural vibration mode features a period larger than the one of the first vibration mode in the vertical bending plane.

Clearly structural configurations involving type C anchoring groups are considerably stiffer in both bending directions with respect to other case studies featuring different cable groups arrangement and the same crossing length; type B cable groups give rise to structures being stiffer in the horizontal direction and more deformable in the vertical direction than type A cable groups. Increasing the number of anchoring groups retaining each tunnel module, which basically means distributing more uniformly the same stiffness of the anchoring system, does not provide relevant variations of the vibration periods.

6.2.3.2. *SFT dynamic response and performances*

The performed analyses provide results which confirm many of the physical intuitions on the structural behaviour of SFTs, even though they sometimes evidences the complexity of the SFT dynamic response, which can be strongly affected by geometrical non-linearities. SFT structural configurations being more prone to exhibit non-linear behaviour are those featuring type A and type B anchoring groups; moreover tunnel designed to hold walkways, featuring smaller cross-section dimensions and thus stiffness, show a response characterized by more pronounced non-linear effects than motorway and rail-motorway SFTs.

In the pedestrian crossings, tunnel displacements continuously increase during analysis, attaining in the horizontal plane such high values that induce large rotations of the cables which, in turn, pull down the tunnel, leading to increasing vertical downward displacements in the central part of the tunnel. This down-pulling mechanism, which resembles the pendulum effect of earth anchored cable supported bridges (see section 2.1.2.2), can be noticed for all cable system arrangements, it being more pronounced for type A cable systems and longer tunnels.

Figure 6.5 illustrates the horizontal (u_h) and vertical (u_v) oscillations of tunnel mid-span section of a pedestrian crossing featuring type A cable systems.

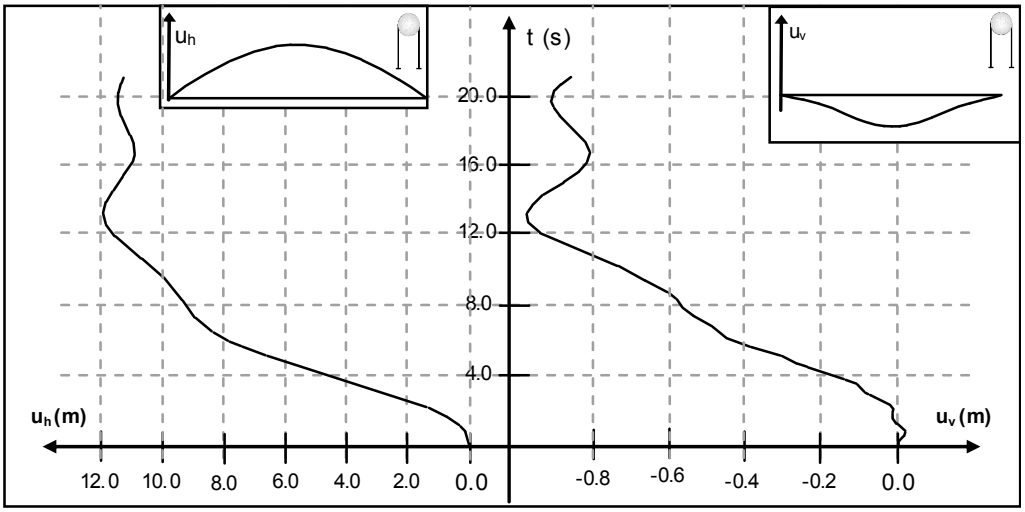

Figure 6.5. Horizontal and vertical oscillations of pedestrian tunnel middle span section (Type A cables, i/l=1; L=400 m)

In pedestrian crossings maximum values of tunnel transversal displacements are always attained nearby the tunnel mid-span section. In case of type B and C cables systems, or smaller tunnel lengths (200 – 600 m); the maximum displacements increase with length, whereas for larger lengths they attain almost constant values. The maximum horizontal displacements attain values which may be incompatible with tunnel functionality in almost all the cases, they being of the order of 1/100 of the tunnel length or larger, exception made for longer crossings featuring two type C cable systems per tunnel module. Figure 6.6 illustrates the trend of maximum horizontal and vertical displacement as the crossing length varies.

It can be noticed that the maximum displacements occurring for type A systems are extremely larger than those attained when type B and type C anchoring systems are provided.

Moreover, the increase in the value of the maximum horizontal displacement becomes lower as the crossing length increases, as vertical cables are subjected to such large rotations that can effectively prevent further horizontal displacements, the pendulum effect becoming more and more pronounced.

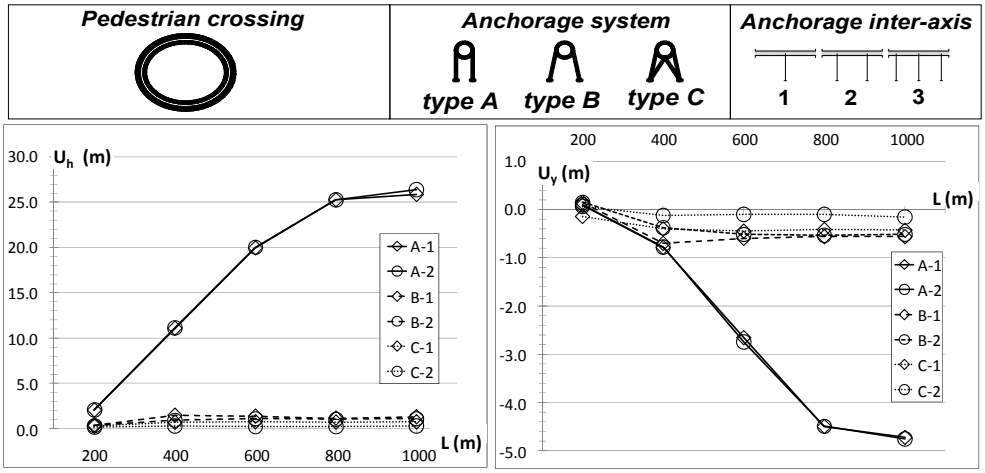

Figure 6.6. Maximum horizontal and vertical displacements of pedestrian SFTs as function of length

Motorway and rail-motorway crossings show more regular behaviours. The down-pulling mechanism previously described is of evidence only in the central part of SFTs restrained by type A cables, while SFTs featuring type B or type C cable systems undergo limited horizontal displacement that do not induce vertical downward ones.

The anchorage system configuration also influences the position of the tunnel section where the maximum displacements are attained. Figure 6.7 shows a qualitative comparison between deformed shapes of STF featuring different cable system arrangements and crossing lengths. In particular, for type A configuration, the maximum horizontal displacement is reached in the mid-span section, whereas the maximum vertical displacement occurs in a section closer to the tunnel ends. When type B configuration is provided, the maximum horizontal displacement is attained nearby the tunnel mid-span, but, as the crossing length increases, similar values are reached in sections closer to the shore connections. The maximum vertical displacement of the tunnel occurs at a distance, from the tunnel ends, which progressively reduces, as the tunnel length increases, while in the mid-span section a slightly lower value is attained. For type C configuration, the maximum displacement in both bending planes takes place in a tunnel section becoming closer to tunnel ends as the tunnel length increases.

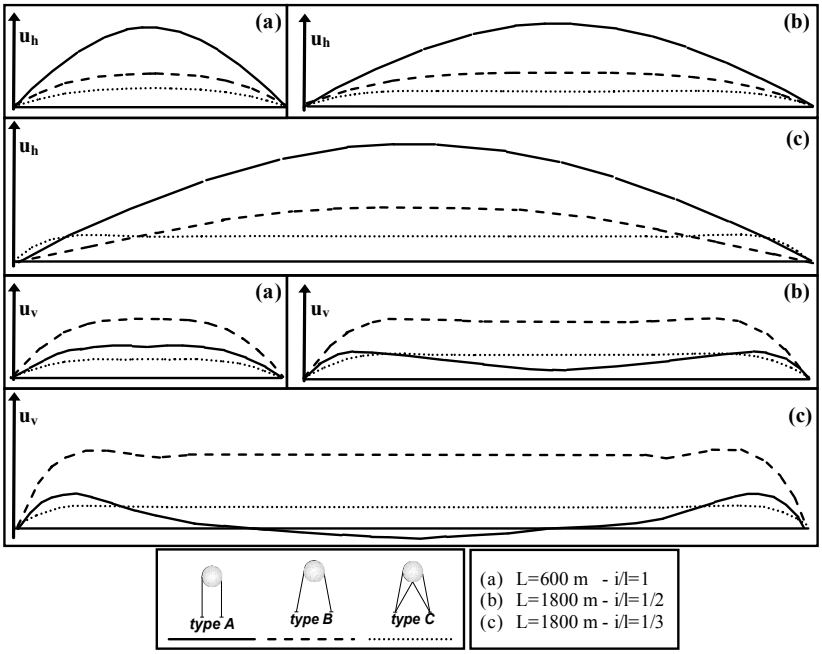

Figure 6.7. Comparison between dynamic displacement distributions of various case studies differing for cable system configurations and tunnel length.

Figure 6.9 illustrates the trends with the crossing length of SFT maximum displacements and bending moments for motorway crossings. When type A or B cable systems are provided, the maximum SFT horizontal displacement, u_h, initially increases as crossing length increases and then slightly decreases, whereas in the case of type C configuration, it is almost constant. The vertical displacements, u_v, attain a maximum value which is nearly constant with length, whatever the considered cable system configuration is. In few cases, featuring intermediate tunnel length and type B cable systems, resonance phenomena occur, leading to slackening of some cables in the tunnel central zone and to higher values of the maximum displacements. Therefore this configuration of the anchoring groups seems to be unsuitable, as it is more prone to show an unstable response: in fact sloped cables are clearly subjected to larger dynamic variations of the axial force which can thus lead to slackening and unacceptable structural behaviour if only two cables per group

are used. Moreover, relevant torsional effects induced by horizontal actions arise when this configuration is used.

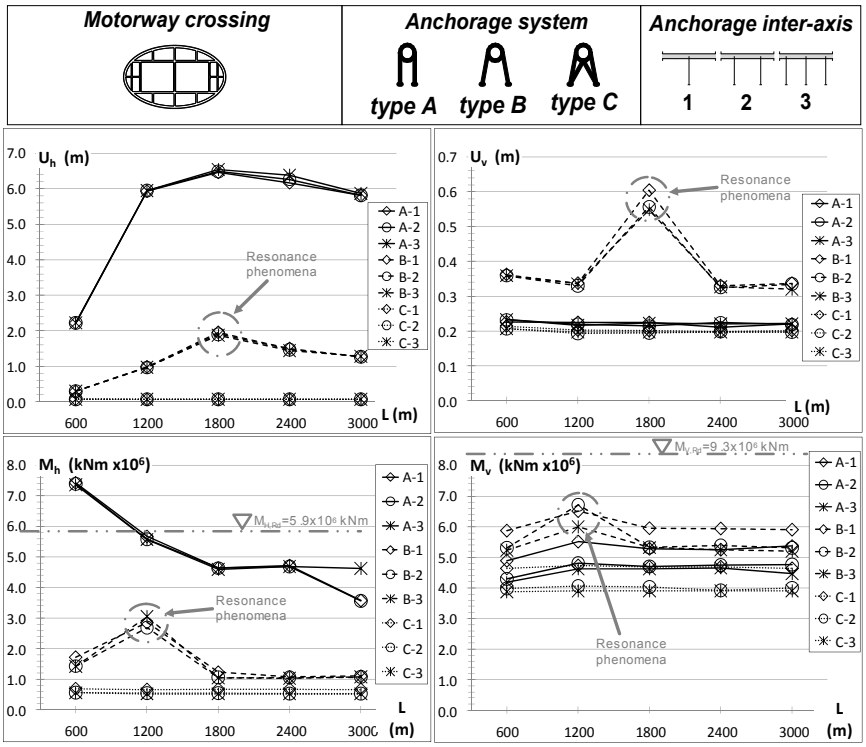

Figure 6.9. Maximum bending moments and displacements in the horizontal and vertical planes for motorway SFTs.

The maximum bending moments occurring in the tunnel are almost constant with the crossing length, exception made for SFTs featuring type A systems, where the horizontal bending moment decreases as crossing length increases. Type A systems prove to be unsuitable, as the composite bending moment overcomes the tunnel resistance, whereas in most of the cases SFTs restrained by inclined cables satisfy the strength safety checks; these results confirms that SFT represents a suitable solution for long waterway crossings, provided that an effective anchorage system is conceived.

Concerning the maximum axial force stressing the cables, once again no noticeable variations occur increasing the crossing length. Type B

configuration proved to be the most onerous one, leading to tension forces quite larger with respect to other configurations (Figure 6.10).

Increasing the number of cable systems per tunnel module produces no relevant advantages in terms of maximum displacements, whereas it can significantly reduce maximum bending moments if two cable systems per module are provided instead of one (reductions ranging from 5% to 20%); minor reductions can be observed as the number of cable systems per module increases from two to three.

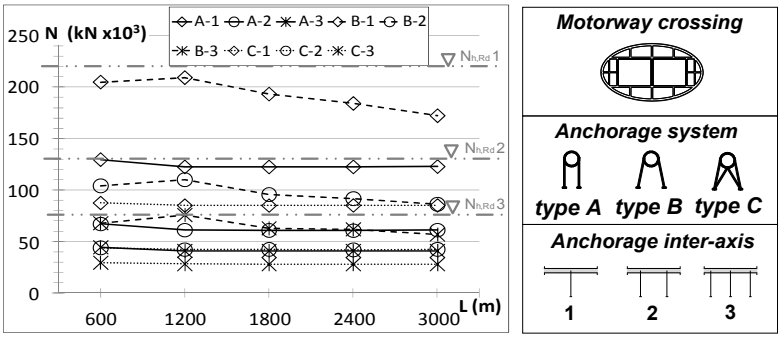

Figure 6.10. Maximum cable axial force as a function of length

Concerning the comparison between elliptical and circular cross-section, no relevant differences between the structural response are noticed. Due to the simplicity of construction and its better hydrostatic behaviour, circular cross-section seems to be preferable.

The results of all the performed analyses are summarized in performance charts, where the maximum values of tunnel displacements u_x and u_y, bending moments M_x and M_y, shear forces T, and cables axial force N attained for each structural configuration considered are reported for comparison. Each of these charts features six x-y diagrams, where x is the length of the tunnel and y represents the maximum value attained by the previous response parameters.

These performance charts are shown on Figures 6.11, 6.12 and 6.13 for pedestrian, motorway and rail-motorway SFTs with circular cross-section. The remaining performance charts can be found in Martire (2007), where more details on the obtained results are given too.

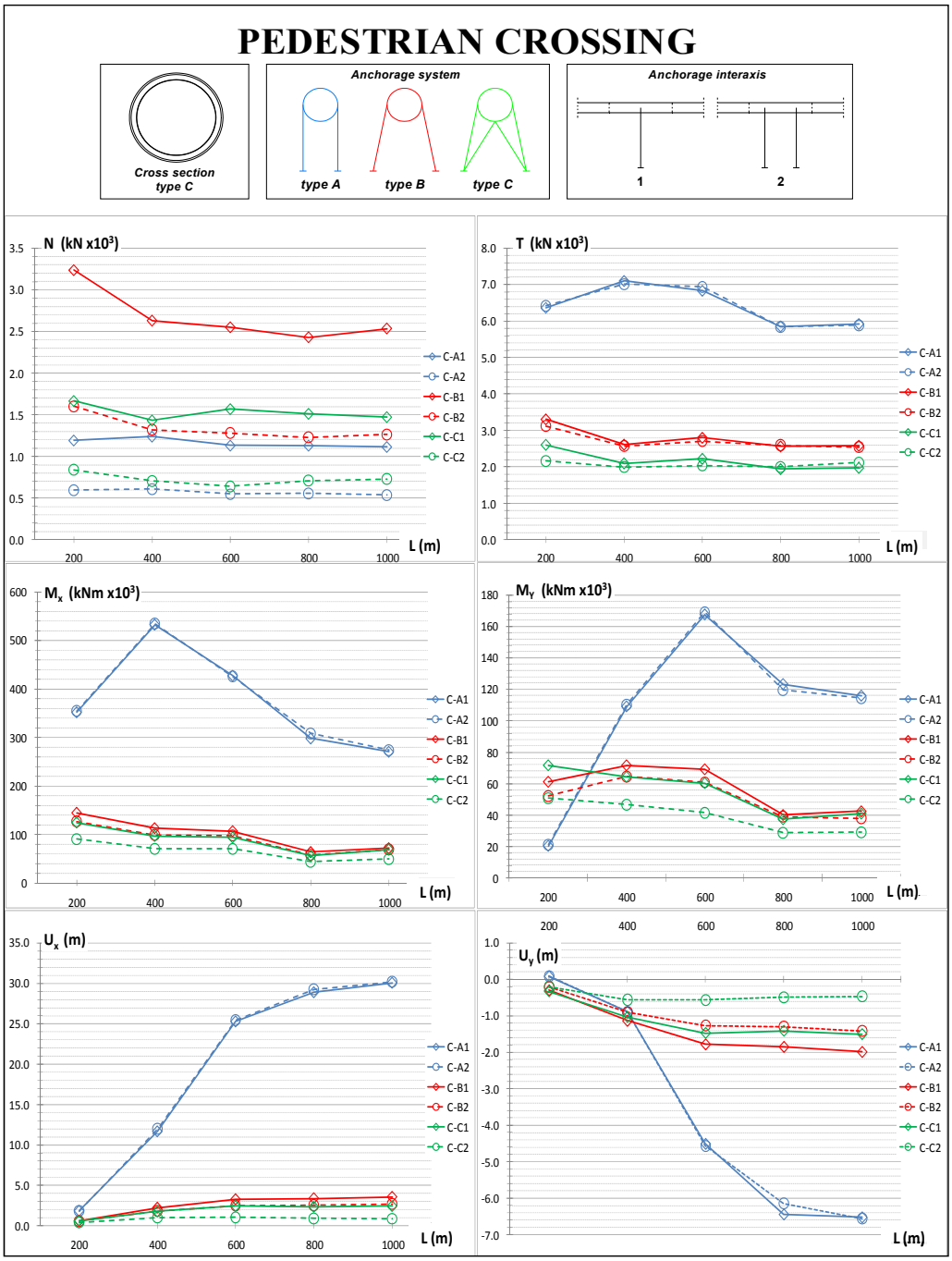

Figure 6.11. Performance chart for pedestrian SFTs (circular cross-section).

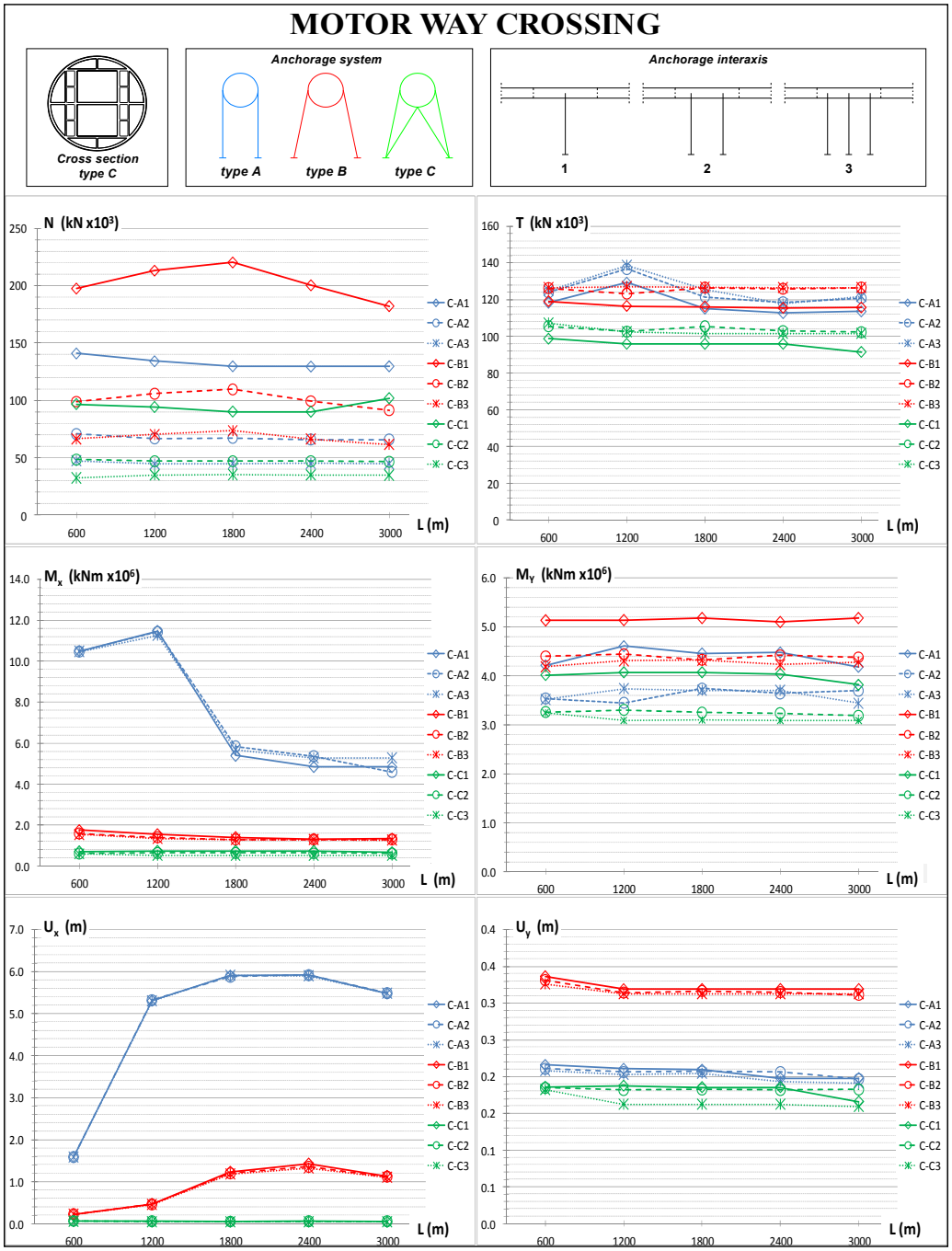

Figure 6.12. Performance chart for motorway SFTs (circular cross-section).

Figure 6.13. Performance chart for rail-motorway SFTs (circular c.-s.).

6.3 ANALYSIS OF THE SFT RESPONSE DURING SEVERE STORM EVENTS

6.3.1. Case studies

6.3.1.1. *Geometrical features of the location site*

The Messina Strait (Italy) is the location considered here as a crossing case study, it being one of the most challenging cases of waterway crossings still to be realized in the world. However, since the aim of the study is to investigate the seismic behaviour of SFTs in a general way, 3 values of the crossing length are assumed to define the crossing scenarios, namely 500 m, 3000 m and 4600 m. The first value is considered to study the hydrodynamic behaviour of not very long SFT crossings; the second value is chosen since it is close to the actual length (about 3300 m) of the suspension bridge designed to be built in the Messina Strait (Jensen, 2009) and the third value is assumed as it is the approximate length of an alternative crossing path of the Messina Strait (Figure 6.14); this alternative location of the crossing has been conceived in the context of a proposal of integrated urban development of the cities of Messina and Reggio Calabria.

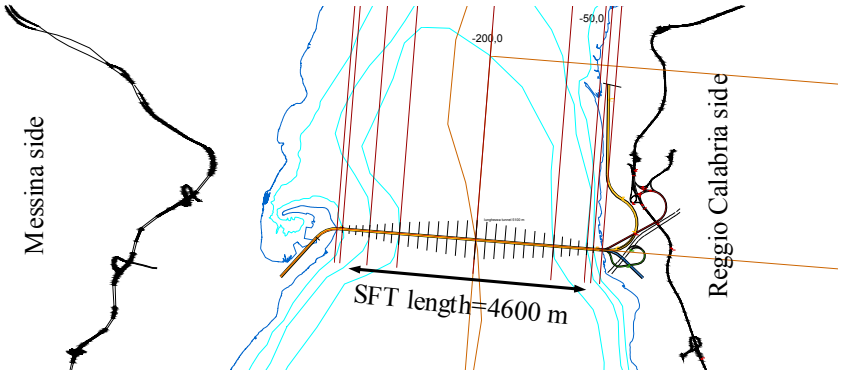

Figure 6.14. Alternative location of the Messina Strait Crossing, proposed in the context of an integrated urban development plan for the cities of Messina and Reggio Calabria.

The seabed profile is a relevant geometric characteristic of the crossing, as it defines the length of the anchorage groups. An idealized profile is assumed

here, being flat in the central part of the crossing, whereas sloped segments are considered at the shore connections; the ratio between the sloped segments and the overall crossing length is always set equal to 0.2. The seabed depth is set equal to 250 m, corresponding to the average water depth of the Messina Strait.

Longitudinal view of the SFTs relative to the three crossing lengths considered are given in Figure 6.15.

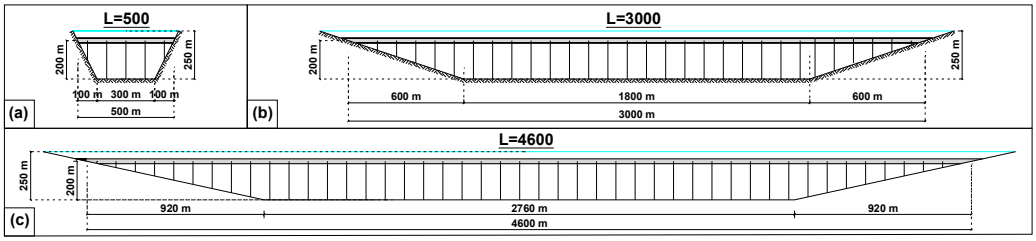

Figure 6.15. Longitudinal view of SFTs for: (a) L=500 m, (b) L=3000 m and (c) L=4600 m.

6.3.1.2. *Storm scenarios: models for water flow and hydrodynamic loads*

The storm scenarios considered in the performed structural analyses are based on hydrographical data (i.e. significant wave height $H_{w,s}$, peak period T_p and free surface current velocity V_c) relative to the area of the Messina Strait. Indications on the values to be assumed for the aforementioned hydrographical data are taken from Franco et al. (2004) and Nicolussi and Casola (1994). Values of wave and current parameters relative to two levels of probability of occurrence of the storm event are assumed, corresponding to return periods T_R equal to 100 years and 2475 years. Similarly to current seismic design practice, these events can be considered as design events to check the structural performances at the Serviceability Limit State (S.L.S.) and Collapse Limit State (C.L.S.), respectively.

In the design of offshore structures it is common practice to adopt one of two methods to calculate the water kinematic flow and to check the safety of the structure on the basis of the aforementioned wave and currents data: the Maximum Design Wave method and the Wave Energy Spectrum method (Sarpkaya, 1978; Campanile, 2005; see also section 2.2.3.1), the first method

being clearly quicker and more widely used in old design practice. In this work both methods are used, with the aim of comparing them.

According to a widely diffused convention, the value of the maximum wave height $H_{w,max}$ is assumed as the maximum wave height recorded in a run of 1000 waves; with this assumption, it is possible to estimate the maximum wave height as 1.86 times the significant wave height (Campanile, 2005).

The Jonswap energy spectrum (see section 2.2.3.1) is used to define the multi-chromatic sea state, assuming a value of the peak parameter γ equal to 2.2, it being the mean value of its probability distribution, according to the indications given in Franco et al. (2004). The peak parameter constitutes the ratio between the peak of the Jonswap spectrum and the peak of the Pierson-Moskowitz spectrum, calculated with the same values of significant wave height and peak period.

A number of 21 harmonic components, whose frequency ranges from 0.6 to 2.6 Hz, are generated from the energy spectrum.

The current velocity profile is assumed to vary linearly from the free surface value to a value of 2.0 m/s at a water depth of 30 m, according to indications given in (Faggiano et al., 2001b). Below 30 m, the current velocity is assumed to be constant; this conservative assumption is made because it has been observed that often in the Messina Strait the current velocity do not reduces consistently as the water depth increases.

The values considered for the significant wave height $H_{w,s}$, peak period T_p, wave length $\lambda_{w,p}$ (associated to the peak period), free surface current velocity V_c and the maximum wave height are given in Table 6.4.

Table 6.4. Wave and current parameters

T_R [years]	$H_{w,s}$ [m]	$H_{w,max}$ [m]	T_p [s]	$\lambda_{w,p}$ [m]	v_c [m/s]
100	3.8	6.9	7.8	94.9	3.6
2475	7.7	14.3	9.4	137.4	4.0

Hydrodynamic actions are computed by means of the Morison's equation. The values of the drag coefficient CD, inertia coefficient CI and added mass coefficient CM depend on several factors, such as the value of the Reynolds

number Re and of the Keulegan-Carpenter number, the surface roughness and others, as discussed more extensively in section 2.2.3.1. Moreover, when diffraction effects are not negligible (i.e. when the ratio between the tunnel diameter D and the wave length λ_w is lower than 0.2) inertia and added mass coefficient, defined in terms of equivalence of the force resultants of the dynamic water pressure field, can be significantly lower than the values commonly adopted when these effects are not considered (Sarpkaya, 1978; MacCamy and Fuchs, 1954). It is worth to underline that, considering the wave length associated with the peak periods, the value of D/λ_w is larger than 0.2 only for the peak wave associated to T_R=100 years. However, when a multi-chromatic sea state is considered, some wave would feature lower periods and wave lengths, so that the corresponding values of the ratio D/λ_w would be larger than the limit value of 0.2.

In this work, different values of the hydrodynamic force coefficients are considered, in order to study their influence on the structural response. Therefore, a lower bound (indicated with subscript 1 in Table 6.5) and upper bound value (indicated with subscript 2 in Table 6.5) are considered for each coefficient. These values are defined on the basis of indications given in literature (Sarpkaya, 1978; Campanile, 2005; API, 2002). Analyses are carried out considering four sets of values, associating each value (C_{D1} and C_{D2}) of the drag coefficient with the two associated values of the inertia and added mass coefficient (C_{I1}-C_{M1} and C_{I2}-C_{M2}).

Table 6.5. Hydrodynamic force coefficients

	C_D	C_I	C_M
C_1	0.4	1.4	0.6
C_2	1.0	2.0	1.0

The aforementioned values are considered only for the tunnel, whereas for the anchorages of the SFT only the upper bound values are assumed.

6.3.1.3. *Structural features*

The tunnel features a composite r.c-steel multi-cellular structure: an external steel sheet (t=30 mm) encloses the main r.c tube, having inner walls

and slabs which give the multi-cellular arrangement (Figure 6.16). The r.c. structure provides good strength capacity, large stiffness and stabilizing weight, whereas the external steel sheet guarantees waterproofing, protection against external impacts and ductility. Moreover, this solution is widely used in the field of Immersed Tunnels (see section 2.1.1.2).

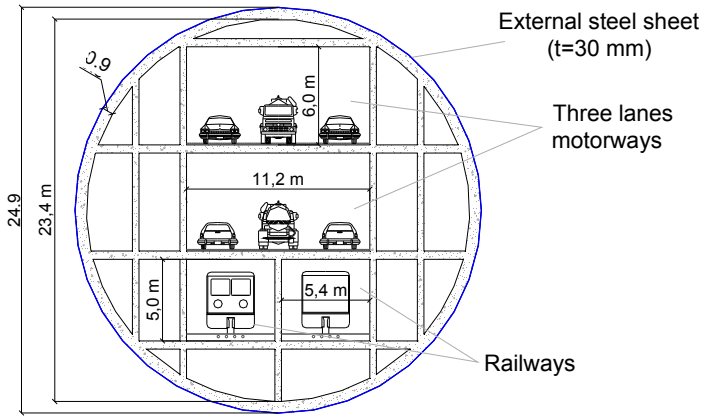

Figure 6.16. SFT cross-section.

Table 6.6 shows the main mechanical properties of the adopted materials: steel S355 and concrete C30/35. Table 6.7 reports the geometrical and mechanical properties of the tunnel cross-section.

Table 6.6. Material properties (tunnel structure)

Material	ρ [kg/m^3]	E [MPa]	f_d [MPa]
Steel S355	7850	210000	322.7
(Reinforced) Concrete C30/35	2500	33282	19.8

Table 6.7. Tunnel cross-section inertia and strength properties

A [m^2]	I_h [m^4]	I_v [m^4]	$M_{Rd,h}$ [kNm]	$M_{Rd,v}$ [kNm]
137.0	7886.9	7650.8	20454325.1	20278762.7

The internal multi-cellular arrangement allows for accommodating motorways, railways and escape ways; moreover the external cells can hold additional ballast and constitute a further barrier against water penetration inside the traffic cells.

Two values of the buoyancy ratio R_W are considered, namely 1.25 ($R_{w,1}$) and 1.40 ($R_{w,2}$), as this parameter is very important for the design of the anchorage system and for the response of the structure to severe environmental loads (Brancaleoni et al., 2009). Different ballast quantities are defined according to the considered value of R_w. Permanent residual buoyancy RB_K (characteristic value) is approximately equal to 1200.0 kNm (RB_1) and 1700.0 kNm (RB_2). The characteristic value of traffic loads, due to trains and motor-vehicles passage, is 245.0 kNm.

On the basis of the results illustrated in section 6.2, two configurations of the anchoring groups are considered: type C (figure 6.1a), featuring four inclined anchorages in a W-shaped arrangement, and type A, featuring two vertical cables and providing only vertical stability to the tunnel (Figure 6.1a). Two kinds of longitudinal arrangement for the cable systems are also considered: the first one, named CW, features only type A cables systems, whereas the second one, named CH, is an hybrid solution featuring the alternation of type A and type C systems. The latter solution could represent a good compromise solution, considering both the restrain effectiveness and the cost of the cable system. One or two anchoring groups restrain each tunnel module, 100 m long, thus corresponding to an inter-axis of 100 m and 50 m, respectively.

Two solutions of anchorages are considered: cables and tubular tethers. The latter ones are considered as an alternative to former ones, because they guarantee larger stiffness, for the following reasons (see also section 2.1.2.2):

- the additional deformability due to catenary behaviour is very low, as tubular tethers can be designed in order to have a buoyancy being very close to their own weight.
- Steel cables feature a Young's modulus E which is lowered to take into account of slipping occurring between the wires composing them (Gimsing, 1996); the amount of reduction depends on the way the cable is manufactured.

Moreover, the dimensions of the tethers are here defined in order to have the same design axial resistance of the cables. Since the steel wires feature a larger design strength than the steel used for tethers, cross-section area of the tethers is larger than the one of the corresponding cables. In order to minimize the diameter and thickness of the tubular tethers, high strength steel is adopted for them.

Cables are made of steel having a density of 8500 kg/m^3, a tensile strength (characteristic value) equal to 1860 MPa and a Young's modulus of 140 GPa. Tubular tethers are made of high strength steel TN890, featuring a density of 8500 kg/m^3, a tensile strength (characteristic value) equal to 850 MPa and a Young's modulus of 210 GPa.

Anchorages dimensions are defined by means of a procedure similar to the one described in section 6.2.1.2, with the difference that here different dimensions are assigned to anchorages belonging to type A and B groups, taking into account the number of anchorages per group and their inclination. Table 6.8 shows the diameter D (and thickness t for tethers) adopted for each configuration as a function of the ratio i/ℓ (i: anchorage systems inter-axis, ℓ: tunnel module length) and of the residual buoyancy level (RB_1 – RB_2).

Table 6.8. Anchorages cross-section dimensions

		Cables		Tethers	
	i/ℓ [-]	Type A D [m]	Type B D [m]	Type A D x t [m]	Type B D x t [m] [m]
RB_1	1	0.41	0.50	0.85x0.06	1.24 x0.06
	1/2	0.32	0.35	0.55x0.06	0.65 x0.06
RB_2	1	0.54	0.68	1.44x0.06	2.22 x0.06
	1/2	0.41	0.50	0.85x0.06	1.24 x0.06

Each cables supporting system is fixed to the seabed through pile foundations consisting of six piles linked together at the top by means of a rigid cap. The piles are realized in reinforced concrete (R_{ck}=35.0 MPa), have a diameter of 2,0 m and a length of 50 m.

The shore connection design represents a critical issue of the SFT design, as discussed in section 2.1.3.2. In this study it is assumed, for the sake of simplicity, that free rotations in the vertical and horizontal plane are allowed at both tunnel ends; axial displacement is set free at one of the shore connections, whereas at the other SFT end is rigidly restrained.

6.3.2. Structural analyses

The dynamic behaviour of the SFTs is analysed through dynamic non-linear time-history analyses carried out on a Finite Element Model of the structure using the software ABAQUS 6.7 (2007). General details on the structural Finite Element Model and on the performed structural analyses are given in section 5.2.

The foundation systems of the anchorage groups are here introduced in the model through the Lumped parameter model, whose properties are calculated with the procedure described in section 5.2. The soil is assumed to be composed of two deformable layers: a first one, having intermediate properties of stiffness and a thickness of 80,0 m, and a second upper one, more deformable (the shear waves transmission velocity $V_{S,30}$ belongs to the range of values related to class D soils, according to the Italian seismic code classification), whose thickness is 20,0 m. The main mechanical characteristics of the two layers (G: shear modulus, ν: Poisson's ratio, ρ: soil density, β: damping ratio) of soil mentioned are summarized in Table 6.9; the soil mechanical behaviour is assumed to be elastic with non-zero hysteretic damping, according to indications given in Wu and Finn (1997).

Table 6.9. Soil layer properties

	G [MPa]	ν [-]	ρ [kg/m^3]	β [-]
Layer 1	120	0.25	2000	0.05
Layer 2	50	0.3	1800	0.05

The obtained values of mass M_f, stiffness K_f and damping coefficient C_f for horizontal and vertical motion are illustrated in Table 6.10. The same values calculated for the horizontal transversal direction are considered for the

longitudinal one, for the sake of simplicity and considering that the involvement of cables in longitudinal motion of the tunnel is negligible. Moreover the same values of mass are adopted in vertical and horizontal directions, as Abaqus does not allow to specify different values for the different translational degrees of freedom.

Table 6.10. Soil layer properties

	M_f [Ton]	K_f [kN/m]	C_f [Ton/s]
Horizontal	7500.0	1700000.0	352831.3
Vertical	7500.0	4800000.0	1300000.0

The dynamic analysis step has a duration of 5 times the wave peak period, when the water flow is calculated considering the maximum design wave method; thus 5 wave runs are considered in the analysis. However, it is important to stress that this one represents probably a quite onerous and improbable scenario, as it is unlikely that the maximum wave height will occur for five times consecutively.

When a multi-chromatic sea state is considered, the dynamic step duration is of 300 seconds. Such a large duration is needed in order to have a sufficient number of cycles of oscillations of the structure, allowing for a statistic evaluation of the maximum values of the structural response parameter. In fact, the maximum values of the structural response can be estimated as 1.86 times the significant value of the structural response parameter of interest (Campanile 2005, Sarpkaya, 1978), which is defined as the average of the values being larger than the 67% percentile.

6.3.3. Results of the analyses

6.3.3.1. *Structural dynamic properties*

For each case study the vibration modes of the SFT are calculated through a linear perturbation step based on the deformed configuration of the structure after the application of residual buoyancy and part of the traffic loads (see section 5.2.2). In most of the case studies the first 300 modes are extracted, as

this group of vibration modes features a total participant mass being at least larger than 85% of the total structural mass. A larger number of vibration modes is needed to obtain the above mentioned value of the total participant mass in case studies featuring larger length and stiffer anchorage system, as the contribution of higher modes becomes more relevant.

In shorter SFTs, the vibration modes involving transversal oscillations of the tunnel are characterized by a number of sinusoidal waves increasing with the vibration frequency (Figure 6.16), similarly to those of a simply supported beam on elastic foundation (see section 5.1.2) and to the ones shown in section 6.2.3.1, where a flat seabed profile is considered.

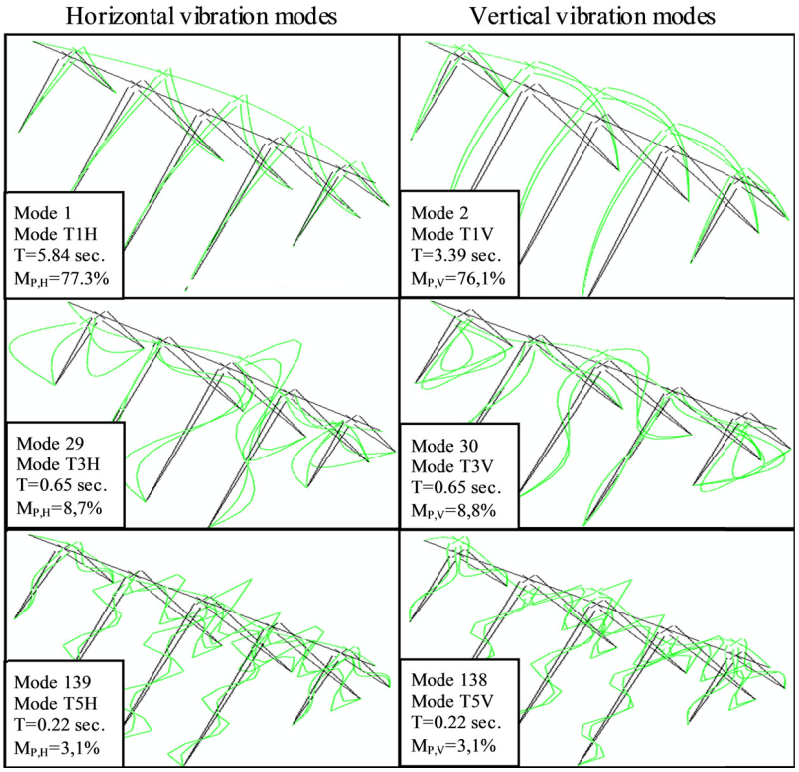

Figure 6.16. First tunnel vibration modes in the horizontal and vertical bending planes (CW1 L500, RB=RB1, C_M=C_{M1}).

In most of the cases the first vibration mode concerns horizontal oscillations of the tunnel, whereas the second one regards its vertical

oscillations. The first periods of vibration ranges from 6.67 to 3.10 seconds in the horizontal plane and from 4.05 to 2.10 second in the vertical plane, depending on the assumed coefficient of added mass, anchorage groups inter-axis, anchorages type (cables or tethers) and arrangement (type CH or CW).

The first horizontal and vertical vibration mode features a large participant mass, it being generally larger than 75% of the total mass of the structure. Subsequent modes whose shape features an odd number of waves have a participant mass progressively reducing.

Figure 6.17 shows the distribution of bending moments associated with the vibration modes of the tunnel. These distributions closely resemble the modal shapes, exception made for the first vibration modes (modes 1H and 1V): in these cases the effect of the concentrated forces is more noticeable and slightly modifies the shape of the moments distribution.

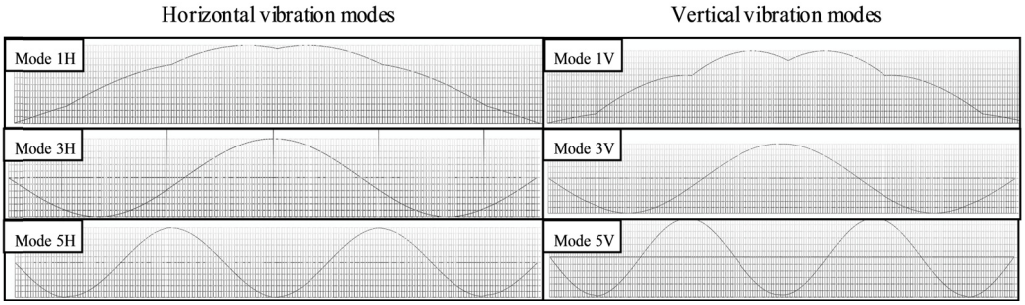

Figure 6.17. Bending moment distributions relative to first tunnel vibration modes in the horizontal and vertical planes (CW1 L500, RB=RB$_1$, C_M=C_{M1}).

This very regular progression of the tunnel bending modes is not followed by SFTs which feature larger length (3000 m and 4600 m); tunnel flexural modes still feature a progressively increasing number of waves, but they cannot be described anymore as sinusoidal. In fact the first modes do not involve the end parts of the tunnel, where the shortest, and thus stiffer, cable anchorage systems are located (Figure 6.18); in the higher modes the extension of the end parts not participating to the vibrations progressively reduce (Figure 6.18). This result can be explained considering that in longer crossings the increased length of the sloped part of the seabed profile implies a larger number of shorter cable systems, whose axial frequencies of vibration

are considerably higher than the ones of longer central cable systems; therefore in the first vibration modes, featuring lower frequencies, the shortest cable systems are not involved in the vibrations and, consequently, the end parts of the tunnel do not vibrate too. The higher modes are characterized by increasing frequencies, thus a larger number of cables and part of the tunnel participate to the vibrations.

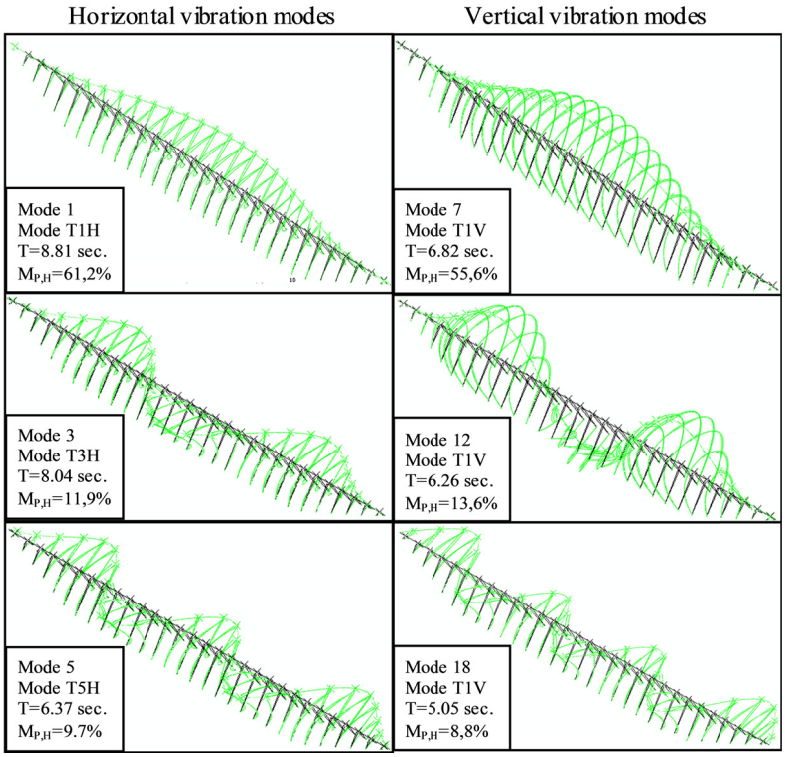

Figure 6.18. First tunnel vibration modes in the horizontal and vertical bending planes (CW1 L3000, RB=RB1, C_M=C_{M1}).

Furthermore, higher vibration modes becomes more and more relevant as the stiffness of the anchoring system increases. In few cases, generally featuring RB=RB1 and two anchoring groups per tunnel module, higher modes feature a participant mass larger than the first mode.

The first periods of vibration ranges from 10.1 to 3.90 seconds in the horizontal plane and from 4.8 to 2.80 seconds in the vertical plane for L=3000 m, from 10.6 to 4.13 seconds in the horizontal plane and from 4.5 to 2.36

seconds in the vertical plane for L=3000 m. It can be thus noticed that the vibration periods do not change largely when the crossing length increases. This result could be expected and it is true also for the ideal case of beam on elastic foundations, as proved by equation 5.9. Furthermore, in the considered case studies the aforementioned effect of the shorter and stiffer anchorages groups becomes more relevant as the tunnel length increases.

SFTs with larger crossing length feature a considerable lower difference between vibration frequency related to successive vibration modes with respect to shorter crossing cases, as in the former cases the scatter between the frequencies of two subsequent tunnel vibration modes is very low.

Figure 6.19 illustrates the bending moment distributions of the first vibration modes shown in Figure 6.18. The effects of the presence of shorter anchorage groups close to the shore connections are again clearly visible, being progressively less noticeable for higher modes.

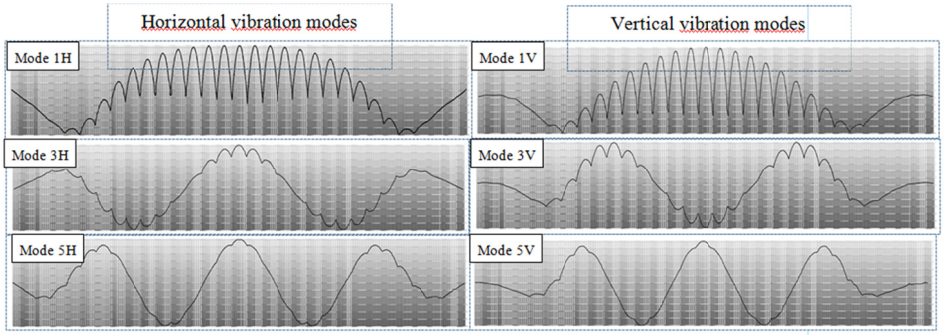

Figure 6.19. Bending moment distributions relative to first tunnel vibration modes in the horizontal and vertical planes (CW1 L3000, RB=RB$_1$, C_M=C_{M1}).

Peculiarities arises in the modal shapes of longer SFTs featuring CH type arrangement of the anchorage systems: in fact in these cases the first horizontal modes with an odd number of waves clearly show the effect of the presence of two consecutive W-shaped cable groups, placed in correspondence of the mid-span cross section to provide an efficient concentrated lateral support (Figure 6.20). This effect leads also to a further reduction of the participant mass of the first vibration modes. Moreover, in few cases, it leads to a switch between the first and second horizontal modes (Figure 6.20), whose corresponding vibration frequencies are almost the same in these cases.

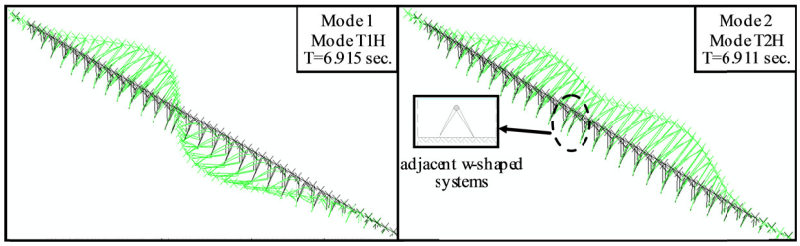

Figure 6.20. First two tunnel horizontal vibration modes for SFTs featuring CH arrangement of the cable system (CH1 L3000, RB=RB_2, C_M=C_{M1}).

Figure 6.21 and 6.22 show the comparison of the first vibration period in the horizontal and vertical plane for all case studies featuring cable anchoring system.

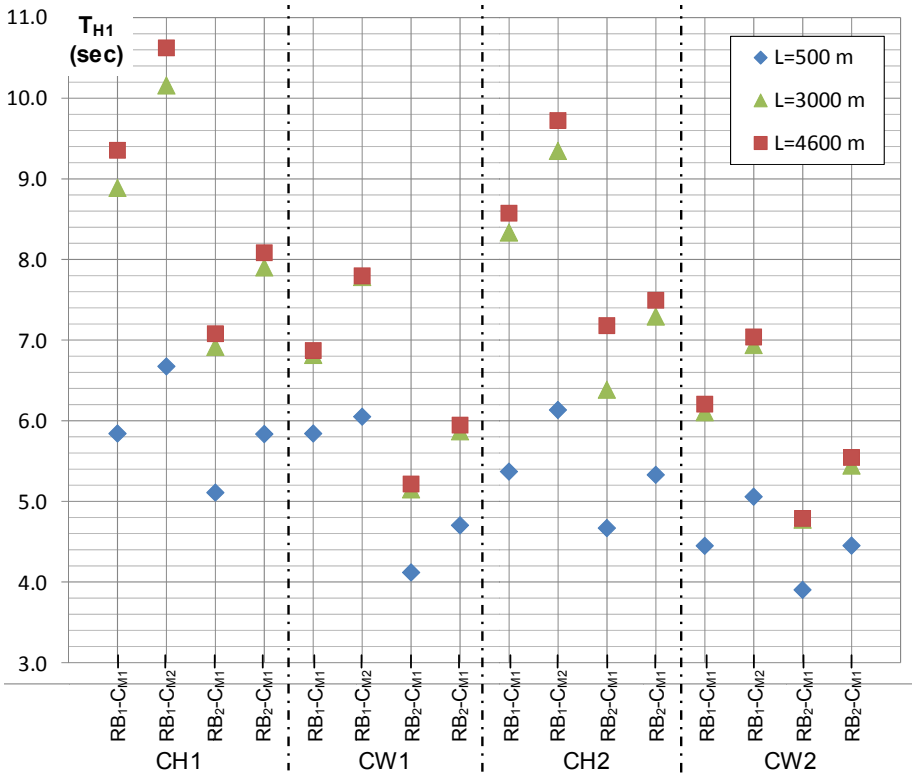

Figure 6.21. First period of vibration of the tunnel in the horizontal bending plane (cable anchoring system).

Evidently, SFT configurations featuring CW arrangement of the anchoring system turn out to be substantially stiffer in the horizontal plane, whereas CH type arrangement is quite stiffer in the vertical bending plane. Increasing the number of anchoring groups per tunnel module generally leads to a low reduction of the first vibration periods.

Concerning the influence of the value of the coefficient mass, increasing it from 0.6 (C_{M1}) to 1.0 (C_{M2}) leads to variations of the first vibration periods ranging from 5 to 15 %, generally closer to the former upper value.

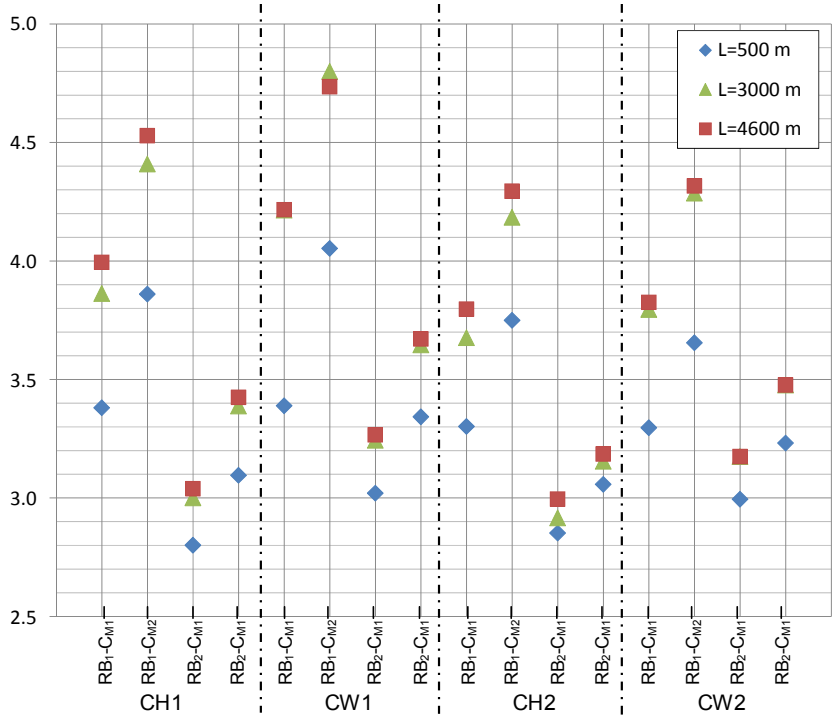

Figure 6.22. First period of vibration of the tunnel in the vertical bending plane (cable anchoring system).

Anchoring systems made up of tethers considerably stiffen the structure in both bending planes, as the first vibration periods of the tunnel reduce of 20 to 35% with respect to the corresponding cable anchoring systems.

The longitudinal vibration modes of the tunnel are poorly affected by the anchoring system configuration, as it could be easily expected. The first

vibration mode features a participating mass being enclosed between 75 to 85% of the total mass of the structure. The first longitudinal vibration period is approximately equal to 0.55 seconds (L=500 m), 3.33 seconds (L=3000 m) and 5.31 seconds (L=4600 m).

6.3.3.2. *Structural behavior*

The structural behaviour of SFTs is monitored during the dynamic analysis, paying attention to the distribution of displacements and stresses occurring in the tunnel and in the anchoring system, as these response parameters are relevant to assess the performance of the structure. The dynamic structural response and the influence of values assumed for the hydrodynamic force coefficient is discussed in this section.

Differences arise among the response of SFTs featuring shorter length (L=500 m) and of those featuring larger lengths (L=3000 m and 4600 m), thus they will be discussed separately. Reference is made to the results obtained considering the multi-chromatic sea state generated with the larger value of the significant wave height (see section 6.3.1.2).

The dynamic response of shorter tunnels is largely dominated by the first bending vibration mode in both horizontal and vertical direction, as it can be easily noticed observing the distributions of bending moments and displacements of the tunnel. Figures 6.23 to 6.24 show the envelope of maximum and minimum bending moments (sagging moments are negative) occurring in the tunnel during the dynamic analysis, where a comparison between the results obtained by changing the value of the hydrodynamic force coefficients is also illustrated. The graphs are referred to the SFT whose anchoring system is of type CH, made up of cables and with only one cable group per tunnel module; the value of the permanent residual buoyancy is the lower one ($RB=RB_1$). This structural configuration is thus the most deformable one among all in the horizontal bending plane.

The distribution of horizontal and vertical bending moments evidence that the dynamic excitation of the structure is extremely larger when the larger values of the inertia coefficient ($C_I=C_{I,2}=2.0$) is used to calculate the hydrodynamic force, whereas the influence of the drag coefficient C_D is minor, being actually relevant only when associated with the inertia coefficient $C_{I,2}$.

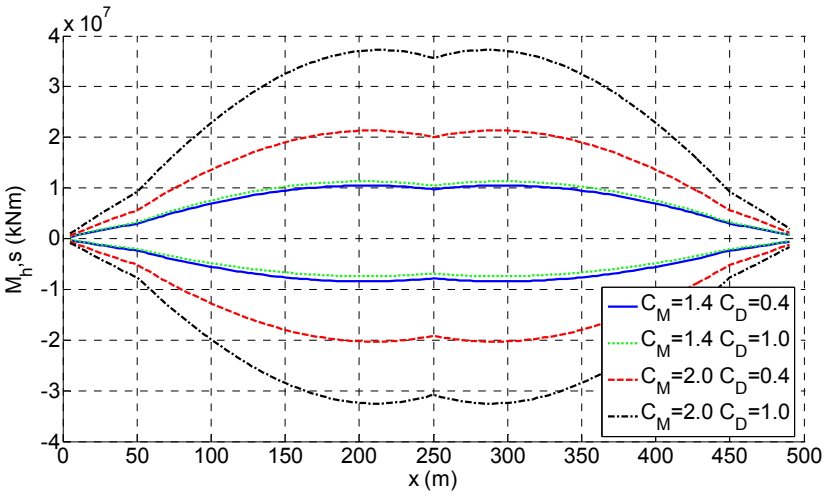

Figure 6.23. Envelope of maximum and minimum values of tunnel horizontal bending moments (cable system type CH, i=100 m, L=500, RB_1).

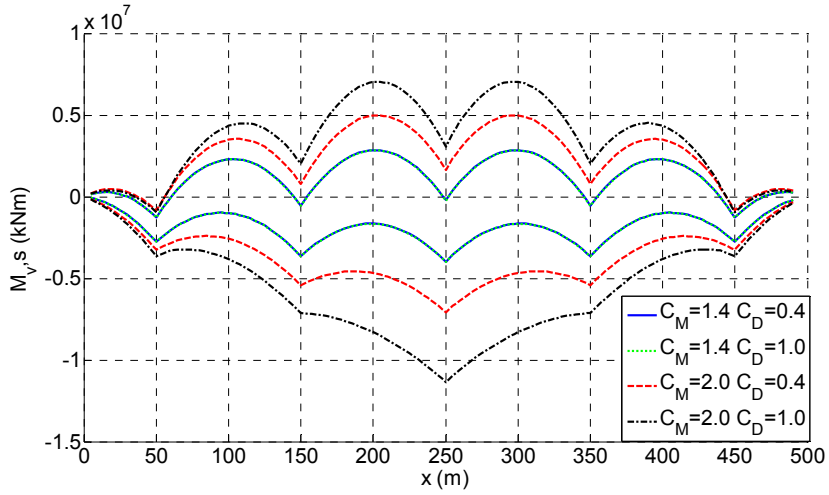

Figure 6.24. Envelope of maximum and minimum values of tunnel vertical bending moments (cable system type CH, i=100 m, L=500, RB_1).

The minimum value of vertical bending moments (i.e. the maximum value of sagging moments) is quite larger than the maximum one (i.e. the maximum hogging moment) when $C_{I,2}$ is considered as inertia coefficient. This result can

be addressed to the pendulum effect (described in section 2.1.2.2 and section 6.2.3.2): horizontal displacements are so large that 2nd order effects become relevant and the down-pulling mechanism takes place.

The previous remarks are confirmed by the distributions of maximum and minimum tunnel displacements in the horizontal and vertical plane, depicted in Figures 6.25 and 6.26, respectively.

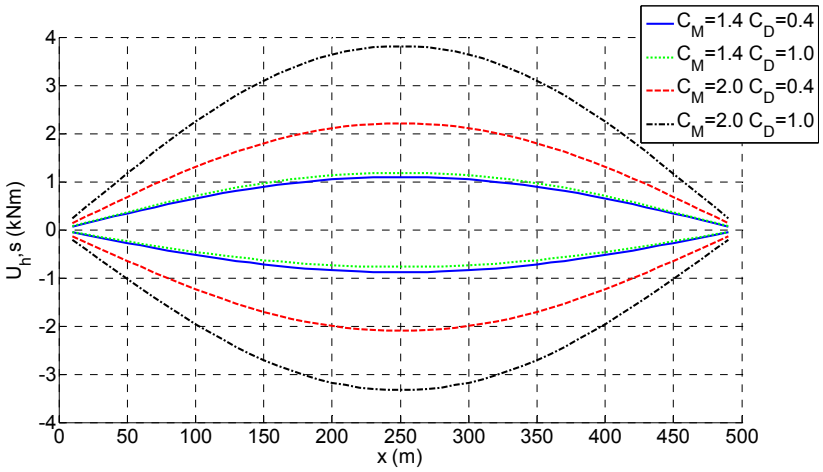

Figure 6.25. Envelope of maximum and minimum values of tunnel horizontal displacements (cable system type CH, i=100 m, L=500, RB_1).

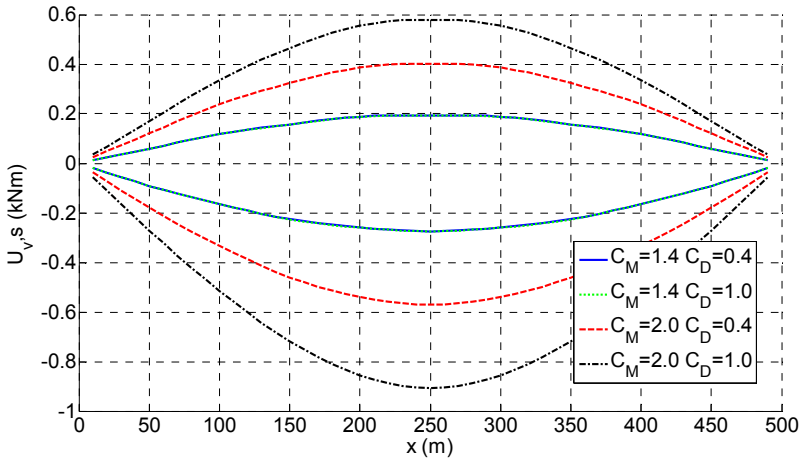

Figure 6.26. Envelope of maximum and minimum values of tunnel vertical displacements (cable system type CH, i=100 m, L=500, RB_1).

Maximum value of the axial force occurring in the anchorages is given in Figure 6.27, leading to the same considerations pointed out above: when inertia coefficient $C_{I,2}$ is assumed, the maximum value of the axial force is extremely larger, exceeding the design axial strength for sloped cables (named CbW in the Figure).

Loosening of sloped cables occurs during the dynamic analysis when $C_{I,2}$ is considered. This is probably the reason why the value assumed for the drag coefficient C_D becomes relevant in these cases: as the sloped cables loosen, the tunnel is not effectively restrained in the horizontal direction and the stresses induced by the drag force (also due to water current contribution) become more relevant.

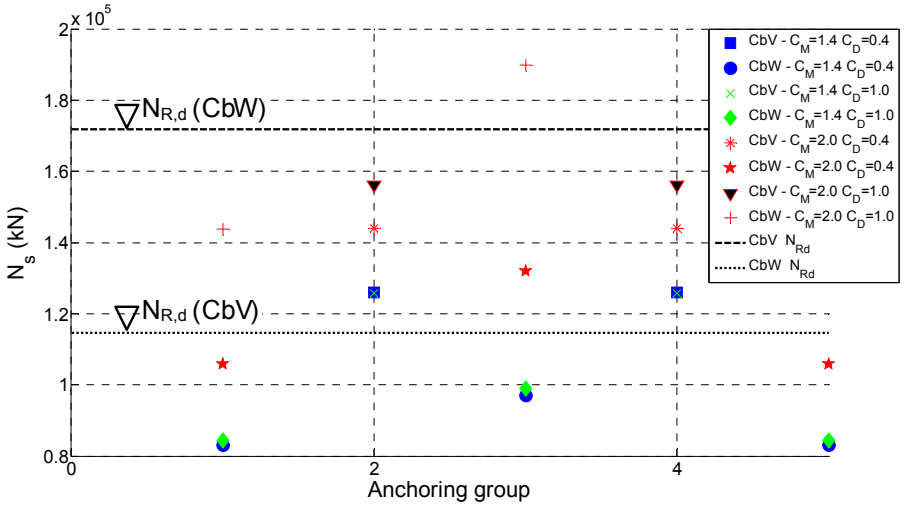

Figure 6.27. Maximum value of axial force in the SFT anchorages (cable system type CH, i=100 m, L=500, RB_1).

When stiffer structural configurations are assumed, obtained by increasing the residual buoyancy (thus increasing the cables dimensions and stiffness) and/or increasing the number of anchoring groups retaining each tunnel module and/or adopting type CW arrangement of the anchoring system, the shapes of stresses and displacements distributions do not change and the importance of the value assumed for the inertia coefficient C_I is confirmed. However, the maximum value of these structural response parameters is

lower, it being always compatible with the strength of the structural elements. Moreover, no slackening of the cables occurs and the influence of the value assumed for the drag coefficient C_D is always modest, thus confirming that the drag force contribution to the structural response becomes relevant only when sloped anchorages loosen.

No variations in the structural response can be noticed also when tubular tethers are used for anchorages in place of cables. In these cases, though, the maximum values of tunnel stresses and displacements are lower, thanks to the larger stiffness provided by the tethering system, especially in the horizontal plane, leading to suitable performances of the structure. Despite the larger axial stiffness of the tethers, the maximum values of the anchorages axial force are similar to those occurring in the cables, due to the lower dynamic amplification.

The behaviour of longer SFTs is quite different from the previous described one, due to the different dynamic properties of the system, here meaning the shape, participant mass and frequencies of natural vibration periods. In fact, as discussed in section 6.3.3.1, the shapes and the corresponding stress distributions of the tunnel vibration modes are influenced by the presence of the stiffer anchoring groups located close to the shore connections. These variations in the modal shapes lead also to a reduction of the participant mass of the first vibration mode, especially in the vertical plane, so that the contribution of superior modes becomes more important. Furthermore, first periods of vibration in the horizontal plane are larger than the ones of shorter SFTs, falling closely to the peak wave period T_p, in some cases being almost coincident with it.

Figures 6.28 and 6.29 illustrate the envelope of maximum horizontal and vertical bending moments occurring in the tunnel for the case study with the following features: cable anchoring system type CH, one anchoring group per tunnel module, $RB=RB_1$. In this case the first period of vibration of the tunnel in the horizontal plane is 8.9 seconds (added mass coefficient $C_M=C_{M,1}$) or 10.1 seconds (added mass coefficient $C_M=C_{M,2}$), thus being very close to the peak wave period T_p (9.4 sec.).

Figures 6.30 to 6.31 show the envelope of maximum horizontal and vertical displacements occurring in the tunnel.

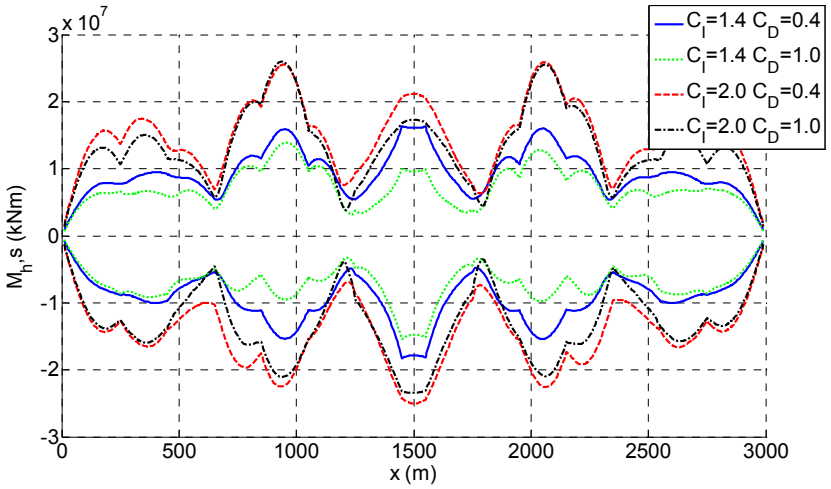

Figure 6.28. Envelope of maximum and minimum values of horizontal tunnel bending moments (cable system type CH, i=100 m, L=3000 m, RB_1).

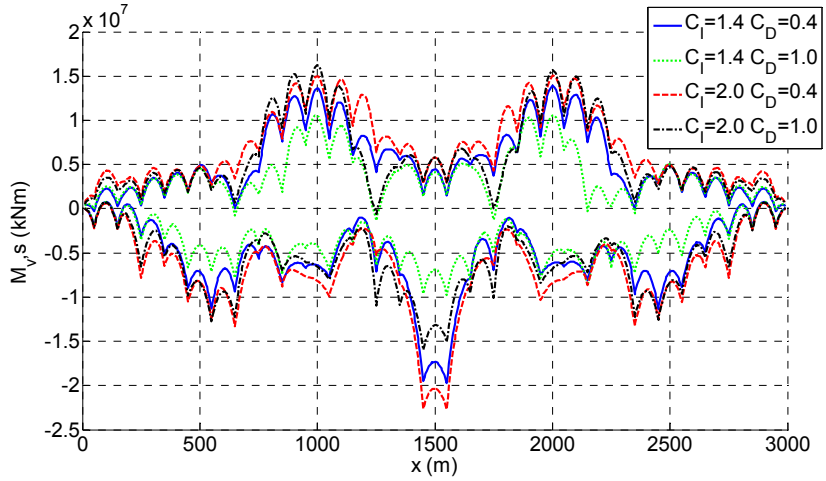

Figure 6.29. Envelope of maximum and minimum values of vertical tunnel bending moments (cable system type CH, i=100 m, L=3000 m, RB_1).

The tunnel vibrations are still governed by the first vibration mode, but the contribution of the third mode is also noticeable, although less relevant. Moreover, the influence of the assumed value of the inertia coefficient is not as relevant as for shorter crossing cases, although the larger one (C_I=$C_{I,2}$) still

leads to a slight increment of the maximum stresses and displacements occurring in the tunnel.

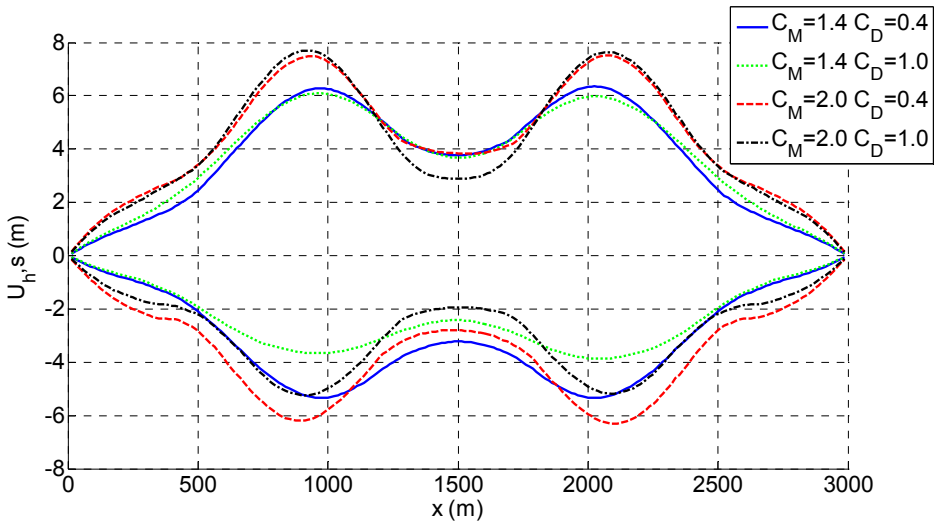

Figure 6.30 Envelope of maximum and minimum values of horizontal tunnel displacements (cable system type CH, i=100 m, L=3000 m, RB_1).

In spite of the close matching between the first tunnel period and the wave peak period, the value of maximum tunnel stresses occurring in the tunnel is lower than the one obtained for the shorter SFT with the same structural configuration (Figures 6.23 and 6.24), at least for C_I=$C_{I,2}$. This is due to the fact that in this case the largest part of the external load is absorbed by the anchoring system: in fact, the simply supported tunnel and the anchoring system can be thought as springs in parallel, so that the external load is distributed between the two components proportionally to the their stiffness. Increasing the tunnel length from 500 m to 3000 m or 4600 m, the flexural stiffness of the tunnel reduces noticeably, whereas the anchoring system stiffness is poorly affected (in case of flat seabed, it would not be affected at all; due to the presence of the sloped end segments, anchoring groups close to the shores are considerably stiffer). Therefore, in case of longer crossings, a larger part of the load (including its dynamic amplification) is carried by the anchoring system.

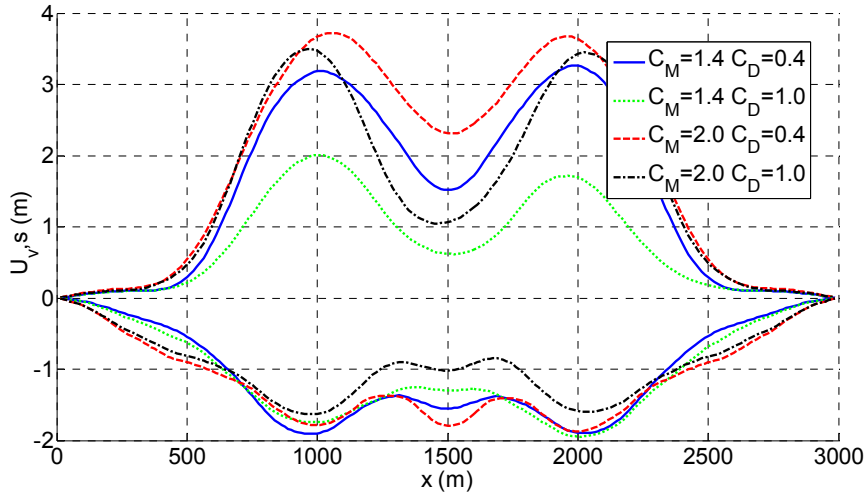

Figure 6.31 Envelope of maximum and minimum values of vertical tunnel displacements (cable system type CH, i=100 m, L=3000 m, RB_1).

Figure 6.32, showing the maximum values of axial force occurring in cable groups, confirms the previous statement. The level of axial forces in the anchorages is extremely larger than the one observed for L=500 m, always exceeding the anchorage resistance. Moreover, slackening of the cables is observed in most of the anchoring groups.

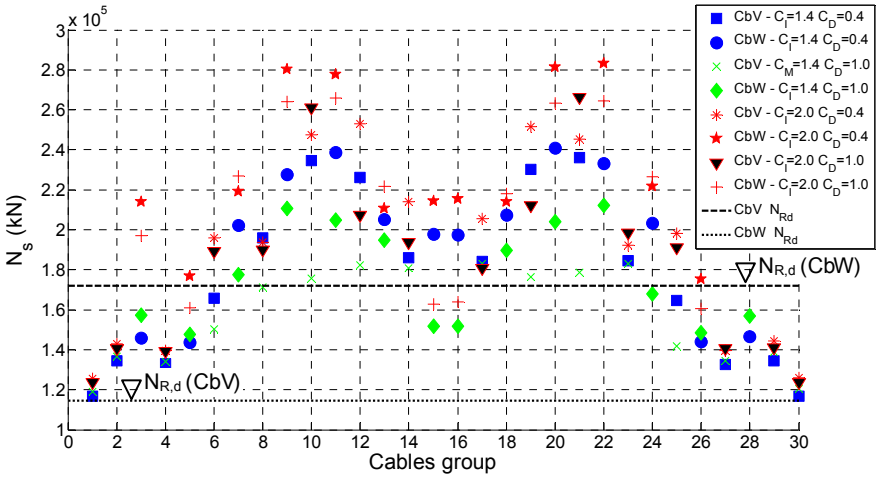

Figure 6.32. Maximum values of axial force in the SFT anchorages (cable system type CH, i=100 m, L=3000, RB_1).

Most of the aforementioned considerations on the structural dynamic behaviour can be extended to all case studies with larger crossing lengths, also for L=4600 m, where the only noticeable difference is that the contribution of higher modes is more noticeable in the bending vibrations of the tunnel. However, large values of tunnel bending moments and displacements, slackening of the cables and very large values of their axial force occur only in those cases where the first vibration period of the tunnel in the horizontal plane is quite close to the peak wave period and, generally, when the larger value of the inertia coefficient is used.

In the other considered cases (stiffer structural configurations, lower value of the inertia force coefficient), dynamic excitation of the structure is lower, so that stresses and displacements in the tunnel are very low, the anchorages do not loosen and are able to safely withstand the storm event. As an example, Figures 6.33 to 6.35 show the maximum bending stresses in the tunnel and axial force in the cables for the SFT featuring CW type cable system, two anchoring groups per tunnel module and RB=RB_2. Maximum bending moments are very low, they being one order of magnitude lower than the ones observed in the previously described case study. Most of the external load is carried by the anchorage system, it being very stiff in this case; however the maximum axial force is always safely lower than the anchorage strength, since in this case large dynamic amplification due to resonance does not occur.

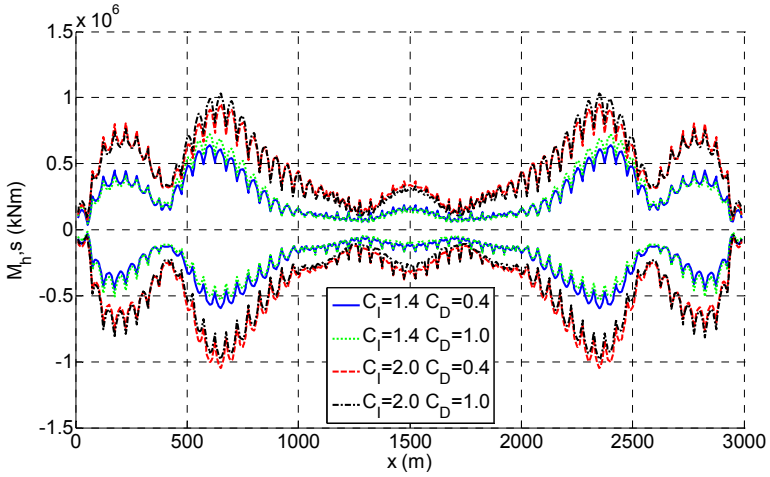

Figure 6.33. Envelope of maximum and minimum values of horizontal tunnel bending moments (cable system type CW, i=50 m, L=3000 m, RB_2).

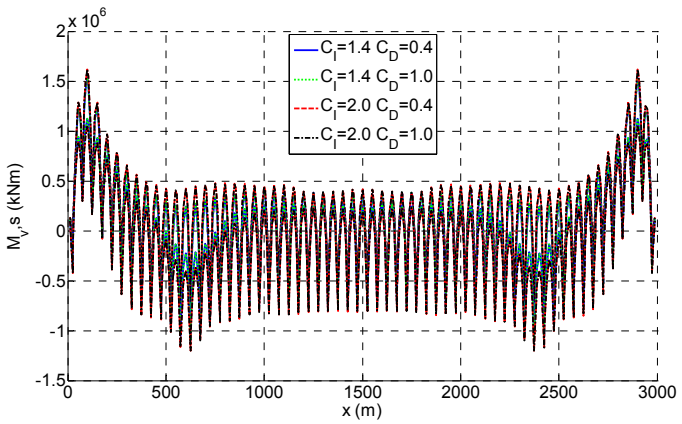

Figure 6.34. Envelope of maximum and minimum values of vertical tunnel bending moments (cable system type CW, i=50 m, L=3000 m, RB_2).

It is also worth to underline that often slackening of the anchorages occurs without being associated with unaccpetable values of stresses in the tunnel or in the anchorages themeselves; in these cases usually the loosening of the cables has an extremely short duration, it lasting few instants before the anchorage starts recovering its tension. For instance, this condition occurs in some anchoring groups of SFTs with CW type cable system and $RB=RB_1$, when the lower values of the inertia coefficient, namely $C_{I,1}$, is considered.

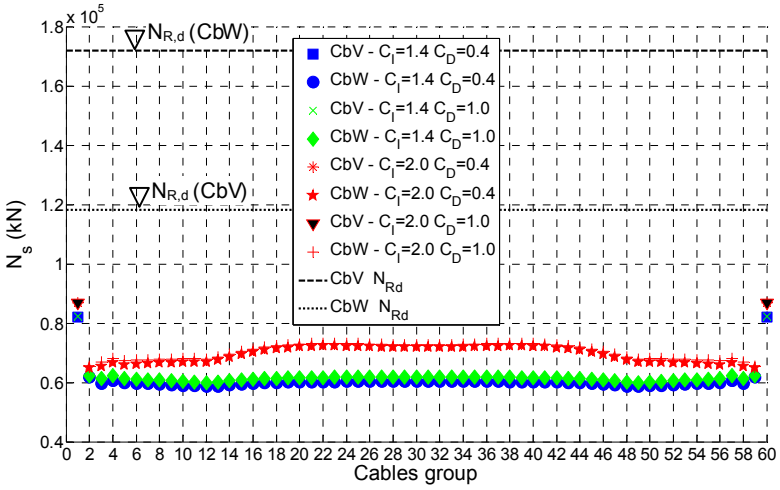

Figure 6.35. Maximum values of axial force in the SFT anchorages (cable system type CW, i=50 m, L=3000 m, RB_2).

The behaviour of SFTs featuring tubular tethers is not different in general from the one of SFTs anchored by means of cables. Since the main difference is related to the considerably larger stiffness of the anchorages, the structural response in these cases is similar to the one described for SFTs whose cable anchoring system is stiffer.

When the wave water flow is modelled through a single sinusoidal wave, the response of the structure is similar in terms of distribution of stresses and displacements and repartition of the external loads between the tunnel and the anchorage system. However, large differences arise in terms of maximum values of displacements and stresses observed in longer tunnels (L=3000 and 4600 m) with respect to the ones obtained through the wave energy spectrum method, as it is showed and discussed better in next section.

In longer SFT crossings, slackening of the anchorages occurs in many of the performed analyses and in a large number of the anchorages groups restraining the tunnel. Loosening of the anchorages often lasts for one to two seconds during each wave run. Moreover, in some cases (generally featuring $RB=RB_1$ and cable anchoring system) the non-linear behaviour of the anchorages is so pronounced that it is necessary to considerably increase the half-step residual tolerance (see section 5.2.2.3) in order to have convergence of the analysis.

6.3.3.3. *SFT Structural performances*

The performance of the different structural solutions, in terms of maximum displacements and bending stresses occurring in the tunnel and axial forces attained in the anchorages is evaluated. The influence of the values assumed for the inertia, added mass and drag coefficient is also assessed.

Moreover, the results obtained by evaluating the hydrodynamic performance of SFTs through the maximum design wave method and the wave energy spectrum method are compared.

Figure 6.36 to 6.38 illustrate the comparison between the maximum values of tunnel bending moments, displacements and anchorage axial force attained in shorter SFTs featuring cable anchoring systems, also showing the influence of the values assumed for the inertia C_I and added mass coefficient C_M (associated with CI) and for the drag coefficient C_D. The results are relative to

the analyses performed considering the multi-chromatic sea state (energy spectrum) corresponding to a return period of 2475 years (T_{R2}).

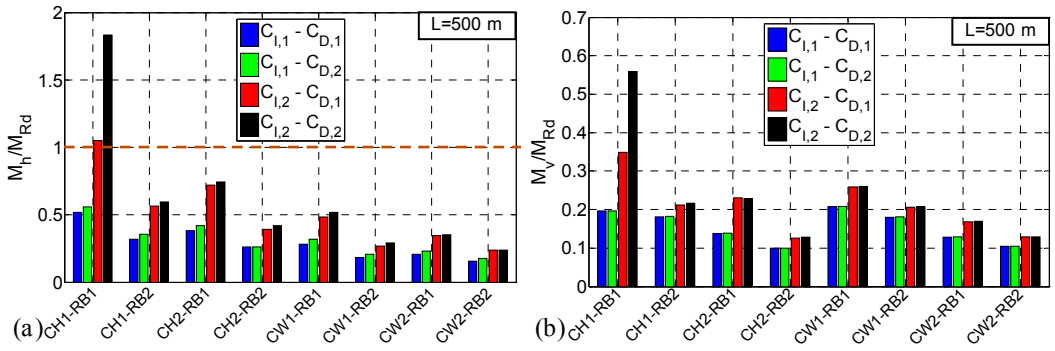

Figure 6.36. Demand/strength ratio for horizontal (a) and vertical (b) tunnel bending moment ((L=500 m, energy wave spectrum - T_R=2475 years).

All the plots are non-dimensional: the bending moments are divided by the moment strength of the tunnel $M_{R,d}$, the displacements by the crossing length L and the axial forces by the anchorage strength.

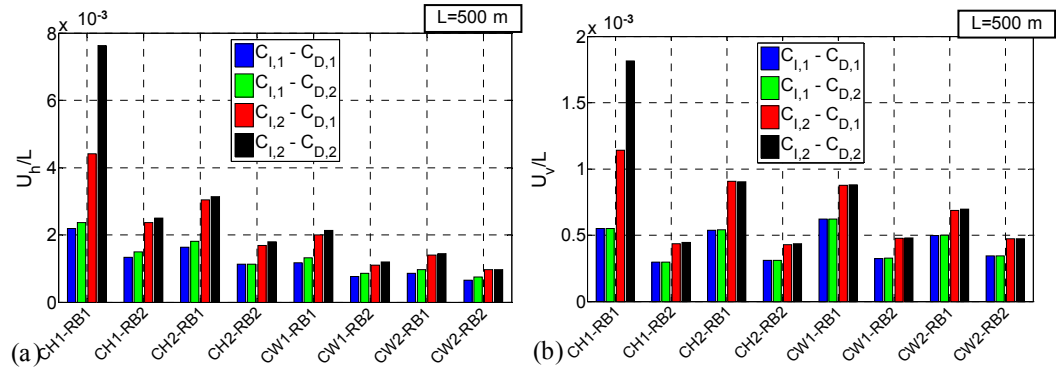

Figure 6.36. Horizontal (a) and vertical (b) tunnel displacement/length ratio (L=500 m, energy wave spectrum - T_R=2475 years).

Maximum bending moments occurring in the tunnel are always safely lower than the tunnel bending strength, exception made for the SFT featuring "hybrid" arrangement of the cable system, one cable group per tunnel module

and the lower level of residual buoyancy/stiffness of the anchorages (named CH1-RB1), when the larger value of the inertia coefficient is assumed ($C_{I,2}$).

Structural solutions featuring stiffer cable system in the horizontal transversal direction, such as CW type or those featuring larger dimensions of the anchorages (corresponding to the higher value of residual buoyancy considered, i.e. RB_2) offer a better response, but differences are not very large.

When such a severe storm event is considered, structural displacements are generally of minor concern. However the maximum values occurring during the analyses are not very large, as they are always lower than 1/100 of the tunnel length.

It is important to underline that maximum values of tunnel bending moments and displacements are not reached simultaneously. In fact the vertical and horizontal velocities and accelerations are out of phase, according to Airy wave theory. Clearly, since more harmonic waves are considered and the structural response may feature some phase shift with respect to the hydrodynamic loads, the structural responses in the two transversal directions are not perfectly out of phase.

Axial force in the cables is lower than their strength, with the same exception pointed out before for tunnel bending moments.

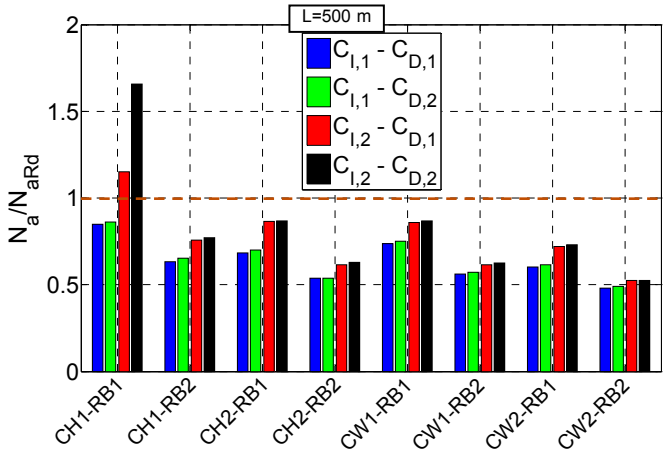

Figure 6.38. Demand/strength ratio for anchorages axial force (L=500 m, energy wave spectrum - T_R=2475 years).

The value assumed for the inertia coefficient C_I considerably affects the performance of short SFTs: larger values of displacements and stresses are

attained when the larger value ($C_{I,2}$) is considered. Not very important differences can be noticed instead when different values of the drag coefficient are considered. The increase in drag force leads to relevant increases of the level of structural stress only in conjunction with slackening of the cables (case study CH1-RB1), as discussed in the previous section.

Figures 6.39 to 6.41 show the same plots for crossings with L=3000 m .

Very large values of bending stresses occur in those cases where the anchoring system is not very stiff (CH1-RB1, CH1-RB2 and CW1-RB1 in Figure 6.36), as the first period of vibration of the structure in the horizontal plane is close to the peak period of the energy spectrum. However, the ratio between the bending moment demand $M_{S,d}$ and the tunnel bending strength $M_{R,d}$ is larger than one only when $C_I = C_{I,2}$ is considered.

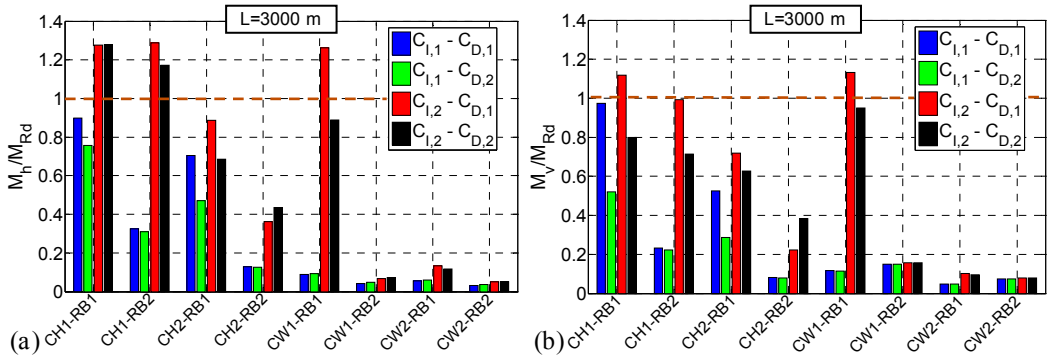

Figure 6.39. Demand/strength ratio for horizontal (a) and vertical (b) tunnel bending moment (L=3000 m, energy wave spectrum - T_R=2475 years).

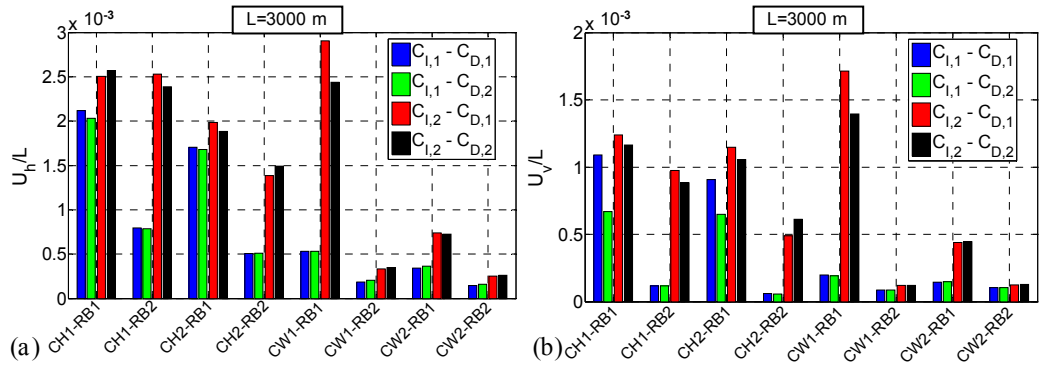

Figure 6.40. Horizontal (a) and vertical (b) tunnel displacements/length ratio (L=3000 m, energy wave spectrum - T_R=2475 years).

In few cases increasing the inertia coefficient gives rise to stresses and displacements of the tunnel being one order of magnitude larger (CH1-RB1, CW1-RB1 in Figures 6.36 and 6.37). A contribution, less important, to this effect is also given by the added mass coefficient C_M: its larger value $C_{M,2}$, associated with $C_{I,2}$, leads to natural vibration periods of the structure being closer with the wave peak period T_P (Figure 6.19). In the same case studies, the value assumed for the drag coefficient proves to be important too, the lower value ($C_{D,1}$) corresponding to larger dynamic excitation. This result can be explained remembering that damping plays a decisive role in forced vibrations of structures when the frequency of the exciting force is close to the natural frequency of the system: reducing the drag coefficient from 1.0 to 0.4 implies a reduction of the hydrodynamic damping, which, in turn, leads to larger dynamic excitation of the structure, even if the drag force induced by the water velocity is lower.

Despite the resonance effects occurring in the cases previously mentioned, maximum tunnel displacements are not large, the ratio U_{max}/L being lower than 1/400 (Figure 6.37).

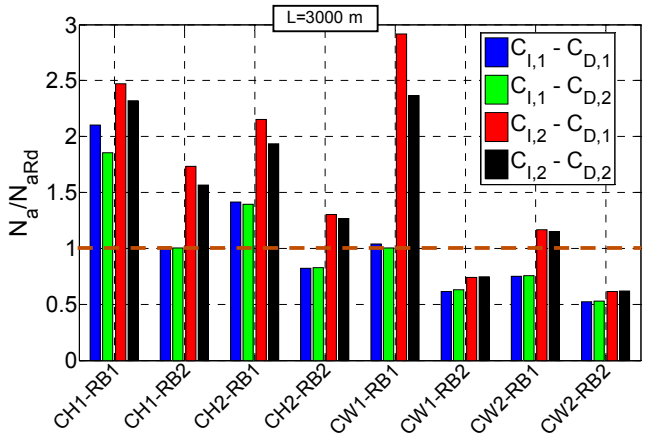

Figure 6.41 Anchorages axial force demand/strength ratio (L=3000 m, energy wave spectrum - T_R=2475 years).

The level of axial stress occurring in the anchorages is very large when compared to their strength (Figure 6.41). As a matter of fact the ratio $N_{a,Sd}/N_{a,Rd}$ is often larger than one. Only the structural configurations featuring type CW arrangement of the cable system and larger diameter (thus of

stiffness and strength too) of the cables assure satisfying performances of the cables.

Similar considerations can be made concerning the performance of longer SFTs (L=4600 m; Figures 6.42 to 6.44), whose vibration periods are close to the ones of SFTs with L=3000 m (Figure 6.18). However, it can be noticed that the level of maximum stresses occurring in the tunnel decreases, the maximum bending moments being always lower than the tunnel strength, whereas the level of axial stress induced in the anchoring cables is almost the same. These results seem to be addressable to the ratio between the transversal stiffness of the tunnel and the one of the anchorage system: as the crossing length increases, the tunnel becomes more and more deformable, so that the amount of external load carried by the anchoring system becomes larger.

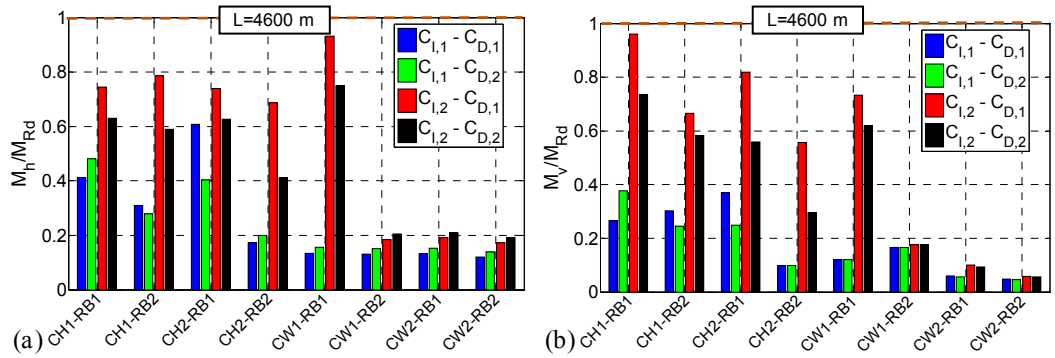

Figure 6.42. Horizontal (a) and vertical (b) tunnel bending moment demand/strength ratio (L=4600 m, energy wave spectrum - T_R=2475 years).

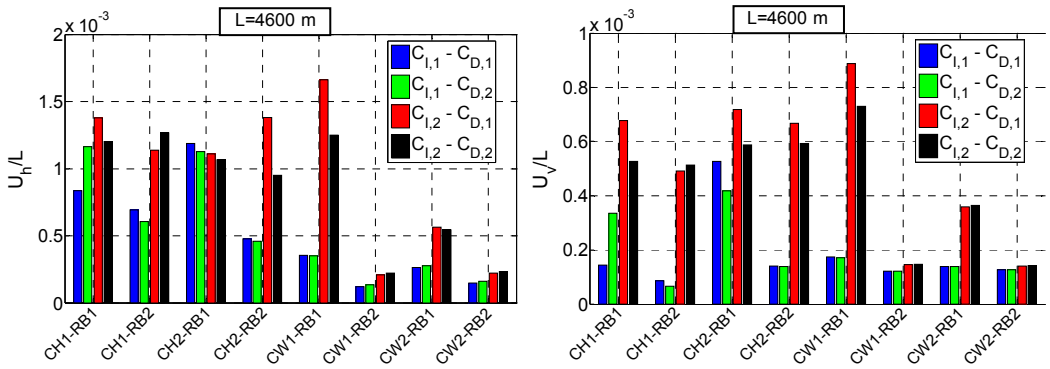

Figure 6.43. Horizontal (a) and vertical (b) tunnel displacements/length ratio (L=4600 m, energy wave spectrum - T_R=2475 years).

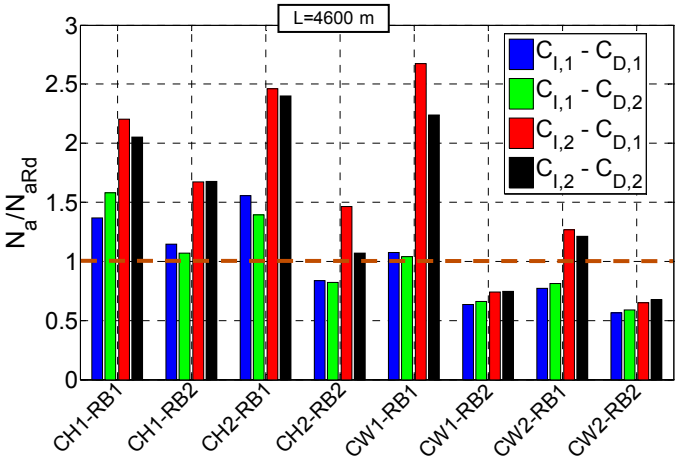

Figure 6.44. Anchorages axial force demand/strength ratio (L=4600 m, energy wave spectrum - T_R=2475 years).

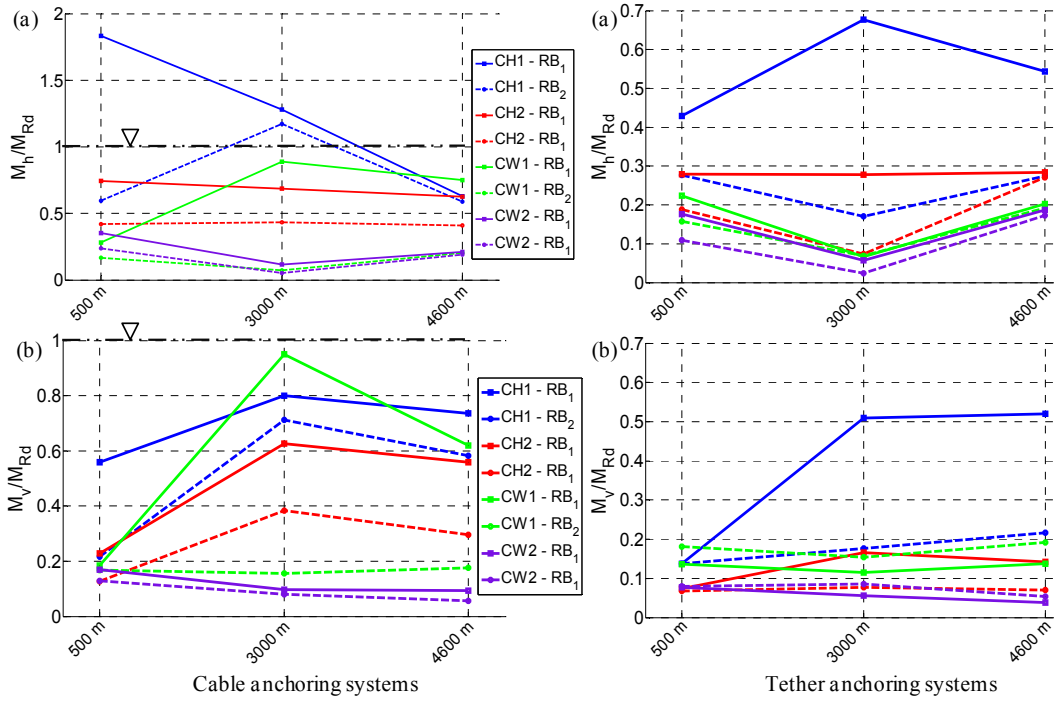

Figure 6.45. Trend of the horizontal (a) and vertical (b) moment demand/strength ratio vs length, for cable and tether anchoring systems (energy spectrum - T_R=2475 years; $C_{I,2}$-$C_{D,2}$).

Concerning the performances of the anchorages, analogous considerations can be drawn (Figure 6.46): the ratio between maximum axial force stressing the anchorages and their strength is always safely lower than one when the anchorages dimensions and the residual buoyancy are larger ($RB=RB_2$), slightly larger than one when $RB=RB_1$ and all the anchorage groups are made up of four sloped cables (type CW arrangement of the anchorage system) and considerably larger than their strength when hybrid anchoring system with smaller cross-section are used ($CH\text{-}RB_1$).

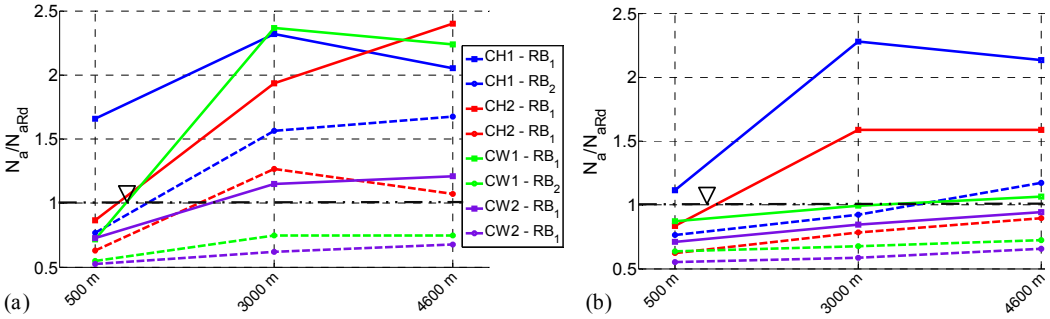

Figure 6.46. Trend of the anchorage axial force demand/strength ratio vs length:(a) Cables (b) Tethers (energy spectrum - T_R=2475 years; $C_{I,2}$-$C_{D,2}$).

Moreover, the plots given in Figures 6.45 and 6.46 seem to confirm that, in general, as the tunnel length increases, the anchorage system tends to absorb a larger percentage of the imposed loads, whereas the opposite occurs be for the tunnel structure. Clearly, since the loads induced by water waves is dynamic, the variation in the periods of vibration due to the change of length might lead to larger (most probably) or lower dynamic excitation of the whole structural system, and thus also to an increment of the stresses induced in the tunnel structure. The former condition occurs, for instance, in most of the considered structural configurations, when the length of the crossing increases from 500 to 3000 m.

When the severity of the storm event is reduced (T_R=100 years), maximum values of structural stresses and displacements clearly reduce; moreover, also the scatter between the results obtained by considering different values of the hydrodynamic force coefficients considerably reduces.

Figure 6.47 to 6.49 illustrates the comparison between the SFT

performances in terms of structural stresses and displacements in shorter tunnels anchored by cables, obtained through the energy wave spectrum method. It can be noticed that, exception made for case CH1-RB_1, the maximum values of tunnel stresses (Figure 6.44) and displacements (Figure 6.45) are quite low; in particular the latter ones are always lower than 1/200 of the tunnel length. Strength checks are always satisfied for the tunnel structure.

The axial stress level is quite larger than the one attained in the tunnel, but still safely lower than the design strength limit, exception made, again, for the case CH1-RB_1 (Figure 6.49), which shows a maximum value of the ratio $N_{a,Sd}/N_{a,Rd}$ being slightly larger than one, if the larger values of the hydrodynamic coefficient are assumed.

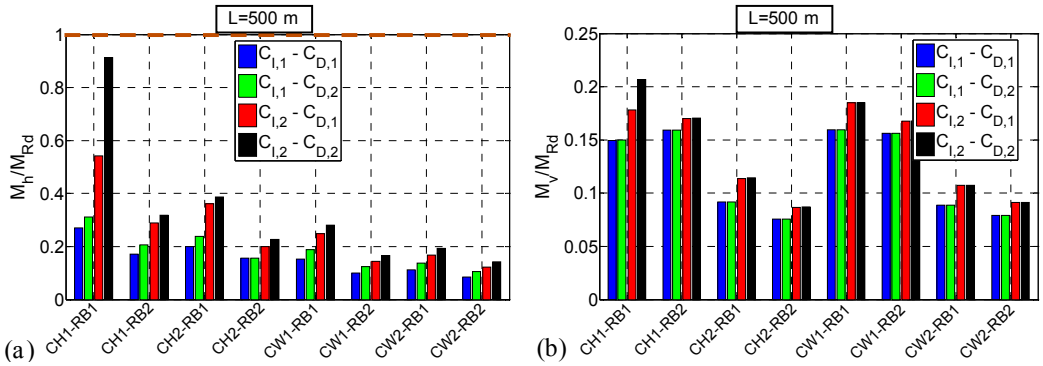

Figure 6.47. Demand/strength ratio for horizontal (a) and vertical (b) tunnel bending moment (L=500 m, energy wave spectrum - T_R=100 years).

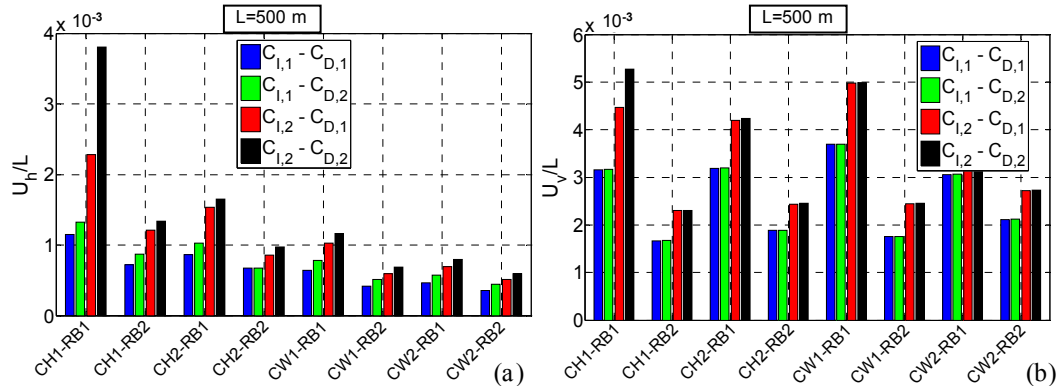

Figure 6.48. Horizontal (a) and vertical (b) tunnel displacement/length ratio (L=500 m, energy wave spectrum - T_R=100 years).

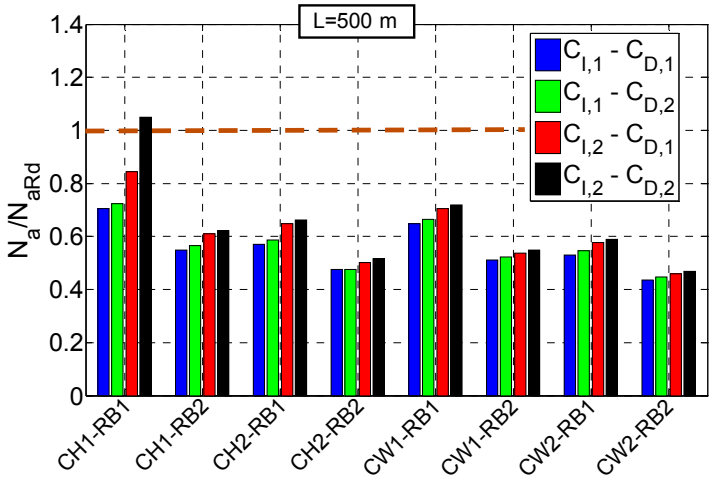

Figure 6.49 Anchorages axial force demand/strength ratio (L=500 m, energy wave spectrum - T_R=100 years).

The previous plots highlight that in most of the cases the influence of the values assumed for C_I, C_M and of C_D is not very large, the scatter between the maximum values of the structural response parameters being practically not relevant.

The same plots, relative to SFTs having a length of 3000 m and 4600 m, are given in Figures 6.50 to 6.52 and 6.53 to 6.55.

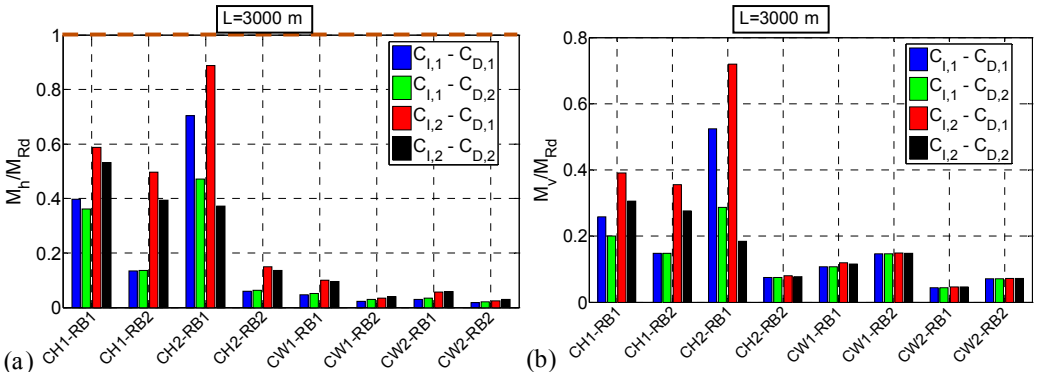

Figure 6.50. Demand/strength ratio for horizontal (a) and vertical (b) tunnel bending moment (L=3000 m, energy wave spectrum - T_R=100 years).

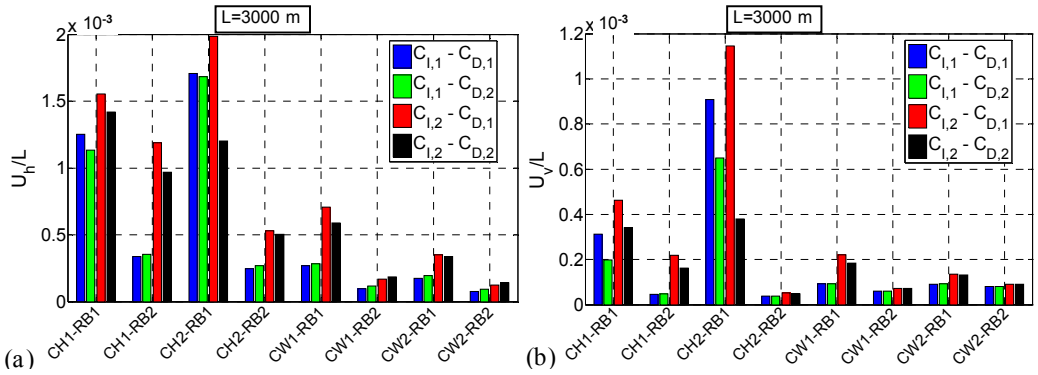

Figure 6.51. Horizontal (a) and vertical (b) tunnel displacement/length ratio (L=3000 m, energy wave spectrum - T_R=100 years).

In these cases the maximum stresses occurring in the tunnel are still quite low and safely lower than the tunnel bending strength (Figures 6.50 and 6.53). Larger dynamic amplification is still noticeable for structural configurations having hybrid cable system, in particular with respect to the maximum axial forces stressing the anchorages (Figure 6.52). In fact also in this case the wave peak period is quite close to the first vibration period of the structure in the horizontal plane.

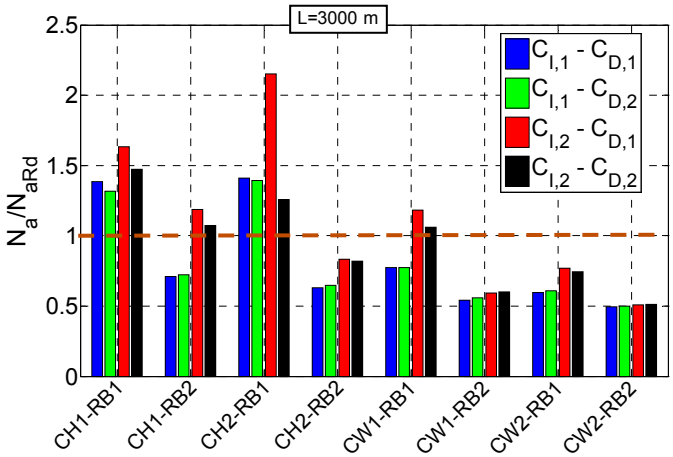

Figure 6.52. Anchorages axial force demand/strength ratio (L=3000 m, energy wave spectrum - T_R=100 years).

Nevertheless, the values of the ratio between the maximum displacements and the crossing length are even lower than those obtained for shorter crossings, being in the order of 1/1000. Thus it seems that, at least for longer SFTs, the deformability issue do not represent a problem, as strength checks are more relevant also when a storm event with a larger probability of occurrence is considered (even though the assumed value of the significant and maximum wave height for a return period T_R of 100 years in the Messina Strait could represent a less frequent scenario for locations less exposed to wave and currents).

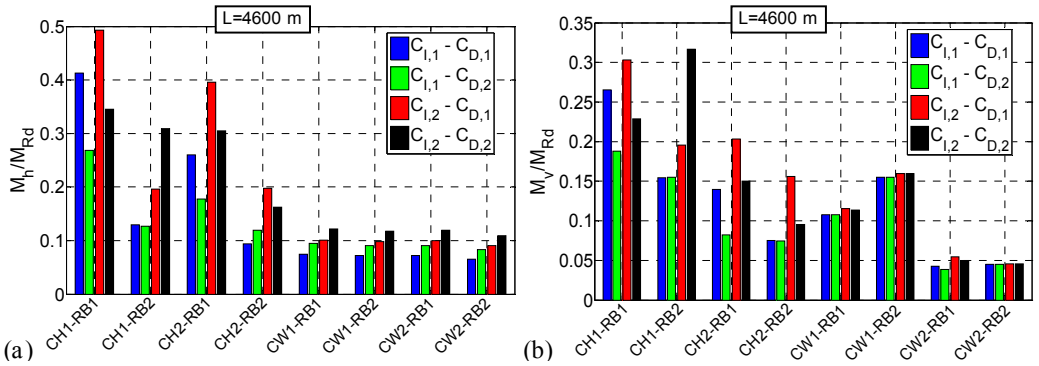

Figure 6.53. Demand/strength ratio for horizontal (a) and vertical (b) tunnel bending moment (L=4600 m, energy wave spectrum - T_R=100 years).

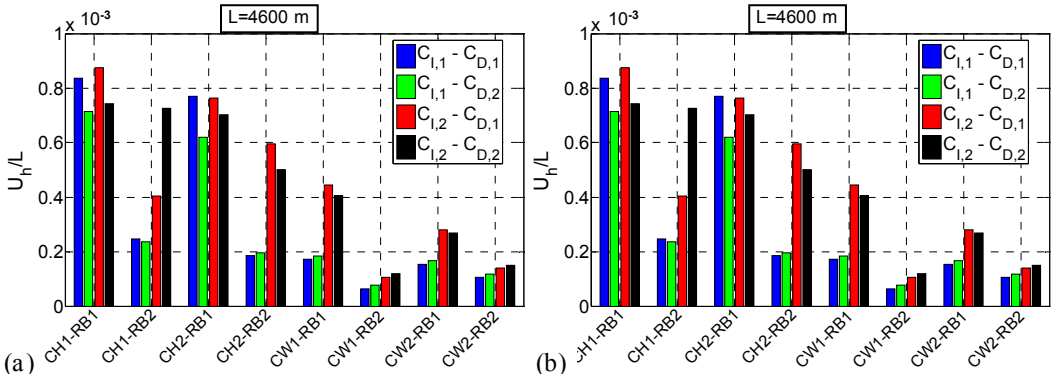

Figure 6.54. Horizontal (a) and vertical (b) tunnel displacement/length ratio (L=4600 m, energy wave spectrum - T_R=100 years).

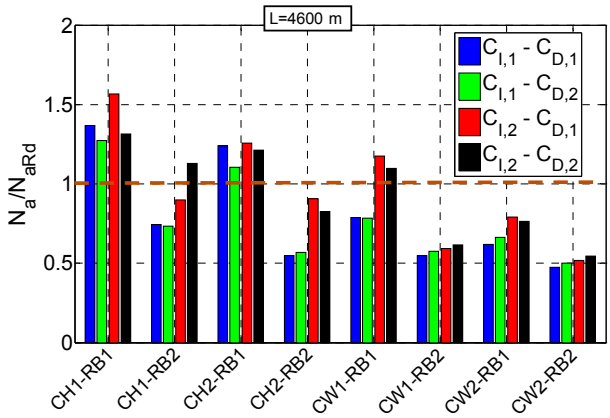

Figure 6.55. Anchorages axial force demand/strength ratio (L=4600 m, energy wave spectrum - T_R=100 years).

The results discussed up to now are all obtained by means of the energy wave spectrum method. The results obtained through the maximum design wave method are described in the following figures, relative to cable anchored SFTs and to a maximum wave height of 6.9 m, corresponding to a return period T_R of 100 years.

Figures 6.56 to 6.58, in particular, illustrate the maximum values of tunnel bending moments, displacements and cable axial force, respectively.

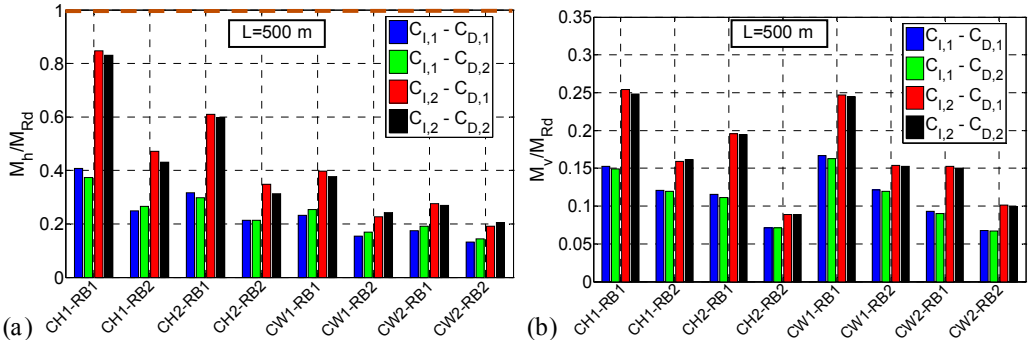

Figure 6.56. Demand/strength ratio for horizontal (a) and vertical (b) tunnel bending moment (L=500 m, maximum design wave - T_R=100 years).

Comparing these results with the ones calculated through the energy wave spectrum method (Figures 6.47 to 6.49), it can be stated that, for shorter SFTs, no relevant differences arises in the evaluation of the SFTs hydrodynamic

performance with the two methods: in fact the maximum values of structural stresses and displacements are similar.

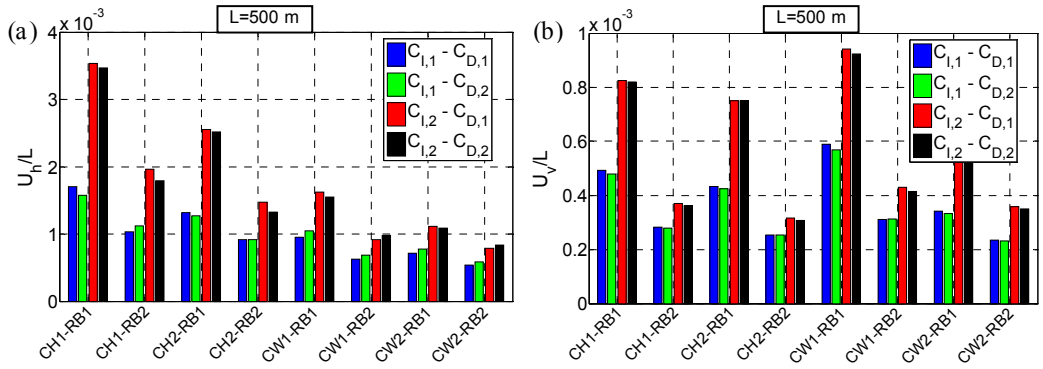

Figure 6.57. Horizontal (a) and vertical (b) tunnel displacement/length ratio (L=500 m, maximum design wave - T_R=100 years).

However, maximum values of tunnel vertical displacements estimated through the energy wave spectrum method are quite larger and also the maximum axial force attained in the anchorages is slightly overestimated in these cases with respect to the ones calculated with the maximum design wave method.

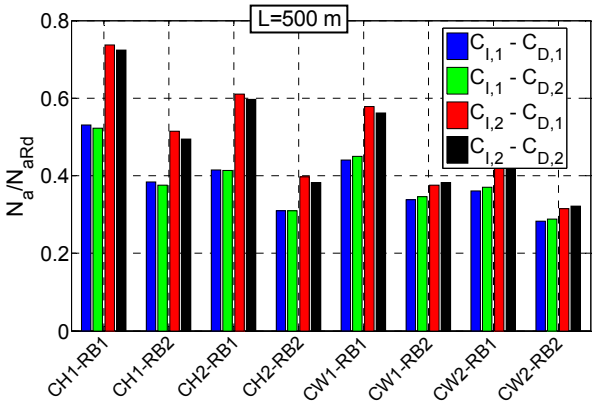

Figure 6.58. Anchorages axial force demand/strength ratio (L=4600 m, energy wave spectrum - T_R=100 years).

The comparison between the two methods lead to different conclusions when the performances of SFTs in longer crossings is considered (Figures 6.59 to 6.61 and 6.62 to 6.64 illustrate the structural performances of SFTs having a length of 3000 m and 4600 m). In fact, it can be noticed that maximum stresses in the tunnel are extremely larger in some cases, generally for those structural configurations featuring the first period of vibration in the horizontal direction being close to the peak wave period. Also the maximum axial stresses occurring in the cables are quite larger when calculated through the maximum design wave method.

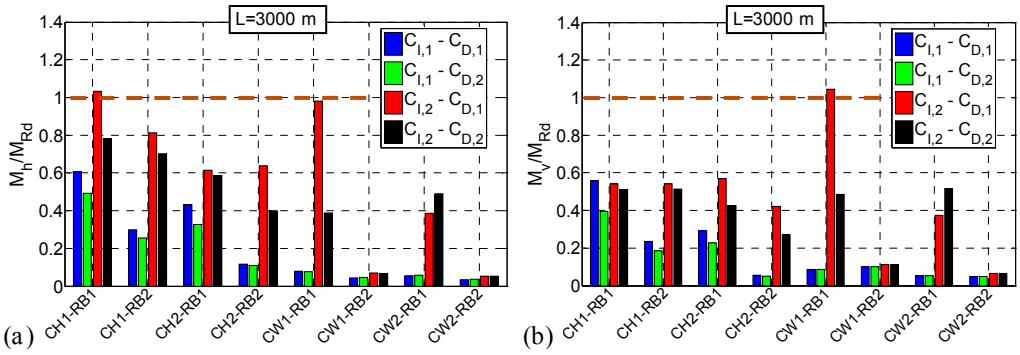

Figure 6.59. Demand/strength ratio for horizontal (a) and vertical (b) tunnel bending moment (L=3000 m, maximum design wave - T_R=100 years).

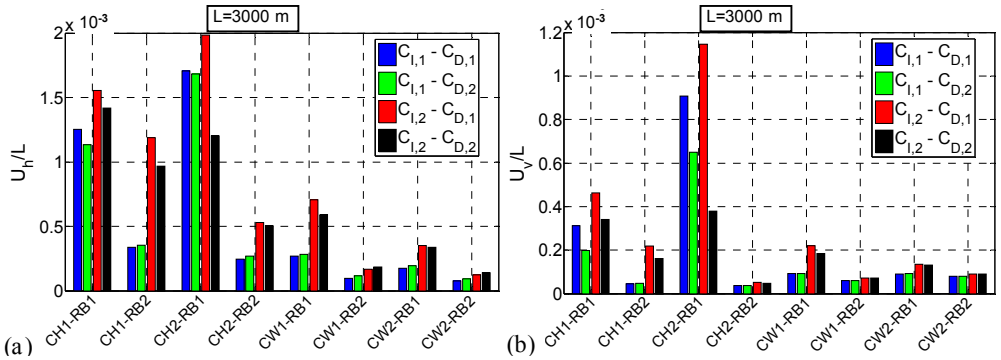

Figure 6.60 Horizontal (a) and vertical (b) tunnel displacement/length ratio (L=3000 m, maximum design wave - T_R=100 years).

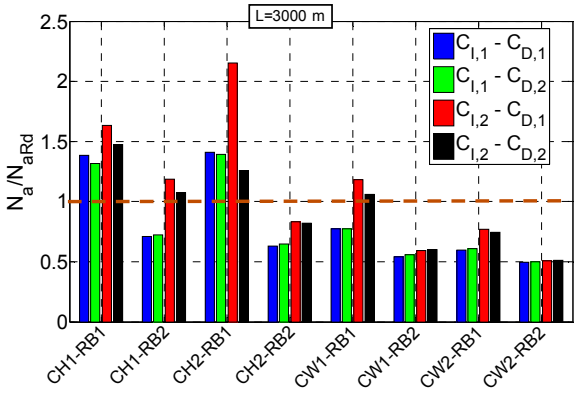

Figure 6.61 Anchorages axial force demand/strength ratio (L=3000 m, maximum design wave - T_R=100 years).

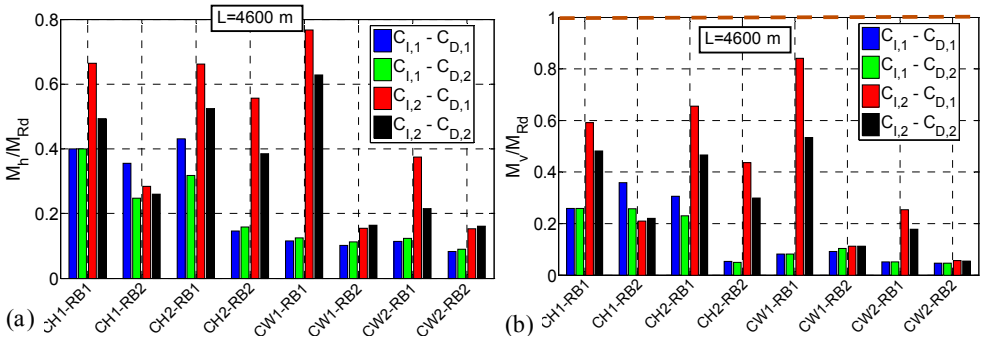

Figure 6.62. Demand/strength ratio for horizontal (a) and vertical (b) tunnel bending moment (L=3000 m, maximum design wave - T_R=100 years).

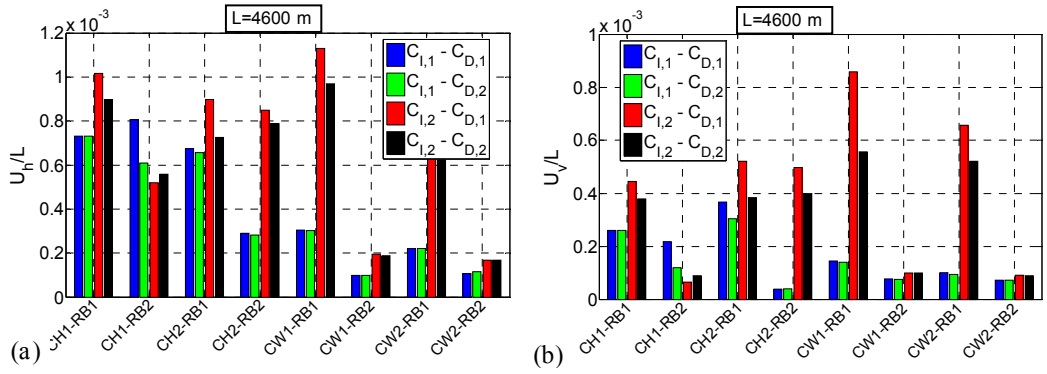

Figure 6.63. Horizontal (a) and vertical (b) tunnel displacement/length ratio (L=4600 m, maximum design wave - T_R=100 years).

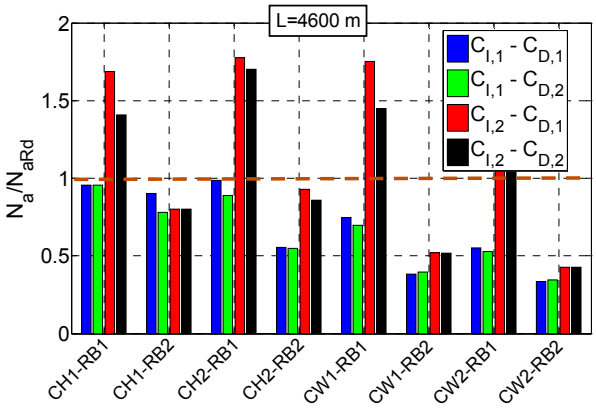

Figure 6.64. Anchorages axial force demand/strength ratio (L=4600 m, maximum design wave - T_R=100 years).

Larger differences in the obtained results arise from the comparison between the two analysis methods when the design wave height is 14.3 m (T_R=2475 years). In those cases where the first period of vibration of the structure in the horizontal plane is close to the peak wave period, it is sometimes difficult to obtain the convergence of the analyses when the design wave height is 14.3 m (T_R=2475 years).

Nevertheless, some of the considered SFT structural configurations still exhibit acceptable performances, the maximum stresses induced in the tunnel and in the anchorages being lower than the corresponding design strength. In particular, among the cable anchoring systems, those who safely withstand the passage of the maximum design wave (for all the considered values of C_I and C_D and values of the crossing length) are the ones featuring CW cable system, two cable groups retaining each tunnel module and maximum values of the residual buoyancy and cables diameter (corresponding to the residual buoyancy level RB_2). Tubular tethers, thanks to their larger stiffness, are more effective in assuring suitable structural performances, provided that the CW arrangement of the anchoring system is considered, together with stiffer and stronger tethers (RB=RB_2).

The results out coming from the comparison of the two methods considered for assessing the hydrodynamic performances of SFTs can be explained by observing that:

- in the maximum wave method all the energy is concentrated at a single frequency, instead of spreading it over a range of frequencies; thus, when the peak wave period and the vibration period of the structure get close, this method overestimate the dynamic excitation of the structure with respect to the energy spectrum method.
- The height of the design maximum wave is determined through statistical analysis of hydrographic data and can be estimated to be 1.86 times the significant wave height (see section 6.3.1.2), whereas in the energy wave spectrum method, the water kinematic field is calculated considering the significant wave height and a statistical analysis of the structural response is subsequently made, in order to get the maximum values of the response parameters. Therefore, the design maximum wave method exalts the non-linear behavior of the structure, as it considers directly into the analysis larger values of water accelerations and velocities and, consequently, of the hydrodynamic loads.

However, considering 5 consecutive runs of wave with the maximum wave height seems to be a very severe scenario; considering the alternation of maximum and significant wave heights in successive runs might be a more reasonable scenario, leading to lower scatter between the results obtained with this method and the ones calculated through the energy wave spectrum one. Such a kind of assumption has been considered, for instance, in the work by Brancaleoni et al. (1989).

6.4 SUMMARY OF THE RESULTS AND CONCLUSIONS

The study of the response of SFTs to severe storm events is investigated in this chapter, with the final goal of assessing the hydrodynamic performance of this waterway crossing solution.

The work is articulated in two phases. The first one is devoted to a preliminary evaluation, by means of dynamic non-linear analysis, of the response and performances offered by a wide range of SFT structural solutions (see section 6.2.1.2), mainly differing for the arrangement of the anchoring system and the external shape of the structure. Different design

conditions, i.e. destination of use and length of the crossing, are considered too (see section 6.2.1.1).

Physical predictions regarding cable systems performance are confirmed by the results. Vertical cables (named Type A cable group), being ineffective in withstanding the effects of the horizontal actions, should be used only in presence of very favourable environmental conditions. Type B configuration (two sloped cables per group) proves to be a suitable solution in most of the cases; with regard to the tunnel behaviour, however, it represents the worst solution for the cables integrity. Type C configuration is certainly the most effective one; since it is the most expensive solution a hybrid configuration, where it is combined with vertical cables, could represent a suitable and economically competitive solution.

Increasing the number of cable systems per tunnel module produces no relevant advantages in terms of maximum displacements, whereas it can significantly reduce maximum moments if two cable systems per module are provided instead of one.

When suitable cable system configurations are provided, maximum displacements and moments as well as cable axial force do not significantly vary with length and safety and serviceability checks are satisfied.

In the second phase a restricted number of structural configurations are considered, selected on the basis of the results obtained in the first phase. Cables and tubular tethers are both considered. Two different values of the buoyancy ratio are considered too; the cross-section dimensions of the anchorages are chosen accordingly. The attention is focused also on the method adopted to model the water kinematic field and calculate the structural response: both the wave energy spectrum and design maximum wave method are used. Moreover, the influence of the value assumed for the hydrodynamic force coefficient of the Morison equation is estimated too. Finally, two intensities of the storm event are considered, corresponding to different probabilities of occurrence.

Concerning the performance of the different structural configurations considered, it can be generally stated that stiffer anchoring systems guarantees a better response and performances of the whole structure, in particular for longer crossings (L=3000 m and 4600 m), where the first structural period of vibration in the horizontal plane is close to the peak wave period, when more

deformable anchoring systems are provided, whereas most of the proposed structural solution prove to be suitable for shorter crossings (L=500 m).

The value assumed for the buoyancy ratio R_w proves to be probably the factor influencing the most the hydrodynamic response of SFTs. In fact, when a value of 1.40 is assumed instead of 1.25, maximum stresses and displacements induced in the structure by the storm event largely reduce. However, this effect does not seem to be largely due to the increased value of the residual buoyancy (slackening can still occur) but, most probably, to the fact that quite larger cross-section dimensions are associated with the larger value of R_w, thus leading to the double beneficial effect of reducing the dynamic amplification of the structural response (basically "moving" the first period of vibration of the tunnel in the horizontal plane away from the wave peak period) and, most importantly, assuring larger strength to the anchorages. In fact, the results of the performed analyses show that, as a general trend, the anchoring system gets considerably more involved in carrying the external loads as the crossing length increases, due to the reduction of the tunnel bending stiffness, so that, the critical point in longer crossings is generally ensuring enough strength to the anchorages and/or reducing their maximum axial forces induced by the hydrodynamic loads.

The longitudinal arrangement of the anchoring system is also very important in determining the SFT response to storm events, CW type ensuring often a significant enhancement of the structural performances with respect to CH type, even though the latter configuration can still be suitably used, provided that the sloped anchorages are stiff and strong enough (for instance with tubular tethers and cross-section dimensions with $RB=RB_2$). Therefore CH solutions with two anchoring groups per tunnel module still seem to be a suitable solution, as structural redundancy assured by vertical anchorages can be associated to the effectiveness of stiff sloped anchorages in the horizontal direction.

Cable anchoring systems offer considerably worse performances with respect to tubular tethers ones, even though they can still be used in association with appropriate geometrical arrangement of the system. It has to be underlined though that they could represent the optimal solution when the water depth reduces, considering that tubular tethers should be more costly, as they need to be made with special joints, releasing rotations along their length,

in order to avoid the extremely large biaxial bending stress that would be induced by hydrodynamic loads on rigid members. Moreover, in this study a quite low value of the equivalent Young's modulus (equivalent as it takes into account the additional deformability due to slip occurring between the wires composing the cable) is assumed and the dimensions of the cross-section of tubular tethers are defined in order to have the same strength of the cables. Reasonably larger values of the Young's modulus of the cable, as well as considering tethers having the same cross-section of the cables, would reduce the gap between the performances offered by the two types of anchorages.

Among the hydrodynamic force coefficient, the most decisive one is the inertia coefficient C_I, whose value can strongly influences the magnitude of structural stresses and displacements. The value assumed for the drag coefficient C_D is generally less important, even though its influence becomes largely more relevant in those cases where resonance effects occur: in fact by reducing C_D the hydrodynamic added damping reduces too and the dynamic amplification of the structural motion grows up.

In case of shorter crossings no great differences arises between the results obtained by assessing the SFT performances through the energy wave spectrum or the design maximum wave method, even though maximum axial forces in the anchorages is sometimes slightly overestimated by the former one. Instead, in case of longer crossings the comparison between the two methods leads to different conclusions: in some cases maximum stresses in the tunnel and anchorages are considerably larger when calculated through the maximum design wave method, generally when the peak wave period is close to the first vibration period of the SFT in the horizontal bending plane. This result is not surprising, as all the energy of the sea state is concentrated in a single wave, thus maximizing the resonance effects.

On the basis of the results obtained from the comparison of the two methods, it seems advisable to use for design purposes the energy wave spectrum method, probably more representative of sea states actually occurring, but considering a large value (such as the sum of its mean value and standard deviation, for instance) of the peak parameter of the Jonswap spectrum (see section 6.3.1.2) when the peak wave period is close to the vibration periods of the structure

The deformability issue does not seem to represent a critical problem, at least for longer SFTs, as strength checks are more relevant also when a storm event with a larger probability of occurrence (T_R=100 years) is considered. However, suitable criteria for deformability checks of SFTs in serviceability conditions are not yet available and have to be developed in order to ensure a sufficient level of comfort for the users, considering the particular psychological conditions they are subjected to when travelling in such a kind of structure.

Chapter7
The response of SFTs to seismic events

7.1 AIMS OF THE STUDY

The response to strong seismic events is one of the aspects to be more carefully investigated in the design of civil engineering structures, as, unfortunately, they lead quite often to catastrophic consequences in terms of economic and, most important, human life losses.

SFTs seem to be particularly suitable to cross waterways located in high seismicity zones. As a matter of fact, due to their large transversal flexibility and to the additional damping and inertia arising from the water-structure interaction, a reduced amount of the earthquake input energy can be transferred to the tunnel, provided that its connections with the shores are equipped with proper seismic joints. Nevertheless, it is necessary to investigate the seismic behaviour of SFTs, in order to confirm the potentialities of this waterway crossing solution, discover eventual critical issues and propose related solutions.

Moreover, the behaviour of SFTs during strong earthquakes features peculiar aspects that deserve to be studied. Like most of the bridges, the seismic input cannot be considered to be the same below the supports of the tunnel, as the various modification effects of the signal due to wave traveling are not negligible. Furthermore, during a seismic event negligible propagation of the horizontal ground motion would take place in the water surrounding the structure but it seems more than reasonable to assume that the vertical ground motion would propagate in the upper water layer. The characteristics of this

propagation and its effects on the dynamic response of SFTs represent a topic of investigation almost not considered at all in literature. To the Author's knowledge, this aspect has been considered only by Brancaleoni et al. (1989).

Therefore in this chapter the response of SFTs to severe seismic events actions is studied by means of finite element analyses in order to:

- Characterize the structural behaviour of SFTs during severe seismic events;
- Estimate the performance of the different structural configurations;
- Investigate the influence of the crossing length on the seismic response of SFTs;
- Comparing the structural response when synchronous or asynchronous ground motion takes place below the supports of the structure;
- Investigate the characteristics of propagation of vertical ground motion and its effects on the SFT seismic response.studies

7.2 ANALYSIS OF THE SFT RESPONSE DURING SEVERE SEISMIC EVENTS

7.2.1. Case studies

7.2.1.1. *Geometrical features of the location site*

The location site and its geometrical features are the same ones considered in Chapter 6 for the second phase of the study of the response of SFTs to hydrodynamic actions (see section 6.3.1.1).

7.2.1.2. *Seismic scenario: ground and water motion simulations*

In order to investigate the structural response of SFTs to strong ground motion produced by a large size earthquake, the1908 Messina earthquake, featuring a magnitude M_w equal to 7.1, is simulated.The acceleration time histories arerecorded at the ground points where the SFT anchoring groups and tunnel shore connections are located. The position of the SFT path (located along the West-East direction) with respect to the seismic fault line is depicted in Figure 7.1.

The simulations are carried out by Zollo and Stabile (Department of Physic Sciences of the University "Federico II" of Naples) using the method

proposed by Lancieri and Zollo (2009), consisting in the simulation of the ground motion of the earthquake,describing its rupture process with an along-strike, line source model (represented with a red line in Figure 7.1) and complete wave field Green's functions computed for a flat-layered P and S velocity and attenuation model.

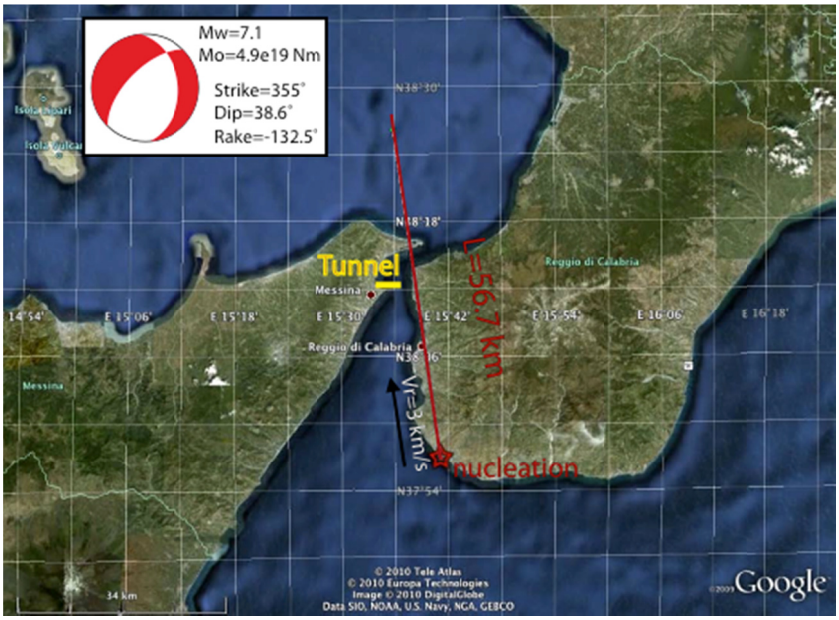

Figure 7.1. In plane position of the crossing path with respect to the 1908 Messina earthquake fault rupture.

Although engineering applications often make use of the point source model to predict earthquake ground motion parameters, in this study we prefer to use a line source model in order to reproduce the correct signal duration and to take into account the effects of rupture directivity and of fault length finiteness that can significantly affect the seismic records and the inferred damage.

The propagation model is assumed to be an anelastic one-dimensional flat-layered medium having 13 interfaces. Each layer has been characterized by different physical properties in terms of density (ρ), compressive wave (P-wave) velocity (V_P), shear wave (S-wave) velocity (V_S), P-wave quality factor (Qp), S-wave quality factor (Qs), and thickness (i.e. interface depth), as

givenin Table 7.1. Below 1 km depth the model is equivalent to that obtained by Langer et al. (2007) for the Calabro-Peloritan area, whereas,above 1km, 8 thin layers are introduced in order to simulate the complex shallow sedimentary structure of the Messina Strait. In particular the first layer is modelled as a water layer, fixing the P-velocity equal to the mean sound velocity in seawater and the density. In fact the sea is considered as a resting fluid since the changes of seawater properties are larger than the propagation velocity of seismic waves. As shown in Table 7.1, S-wave velocity V_S and quality factor Q_s (which theoretically must be equal to zero because shear waves do not propagate in fluids) are set to a very little value in order to avoid numerical over-flow problems. As the tunnel approaches the coast a new velocity model having a thinner water layer has been used, according to the considered seabed profile (Figure 6.14).

Table 7.1. Properties of the model used for simulations

Layer interfaces	Depth [m]	ρ [kg/m3]	V_P [m/s]	V_S [m/s]	Q_P	Q_s
1	0	1030	1512	0.1	9999	0.1
2	250	2500	2500	1316	150	70
3	400	2000	2000	1000	150	70
4	500	2500	2600	1368	150	70
5	600	2700	3000	1714	150	70
6	700	2500	2800	1556	150	70
7	800	2700	3100	1771	150	70
8	900	2700	3350	1914	150	70
9	1000	2700	3500	2000	150	70
10	3000	2700	5000	2857	300	150
11	10000	2700	6000	3429	300	150
12	20000	2700	7000	4000	300	150
13	35000	2700	8000	4571	300	150

Source parameters have been derived by several works carried out for 1908 Messina earthquake. In particular the epicentral coordinates of the nucleation point and the slip distribution along strike are obtained from Pino et al. (2009), while source length, focal mechanism, moment magnitude, and depth of the event are obtained from Capuano et al. (1988). Hence the

simulated event has a seismic moment M_0=4.9e19 Nm, corresponding to a moment magnitude M_w=7.1 (Hanks and Kanamori 1979). The earthquake is a normal faulting event with fault length L=56.7 km, depth *Z*=11.8 km, and fault angles strike, dip, and rake equal to 355˚, 38.6˚, and -132.5˚, respectively (see figure 1). Finally, the rupture velocity is assumed V_r=3000 m/s.

The line source model is built by positioning a series of 270 equally spaced, double couple point sources along the line, each of them having the same source duration and focal mechanism. The sum of point source seismic momentsis set to be equal to the final event seismic moment; the distribution of the point source seismic moment along the fault line is set according to the slip distribution obtained from Pino et al. (2009; Figure 7.2)

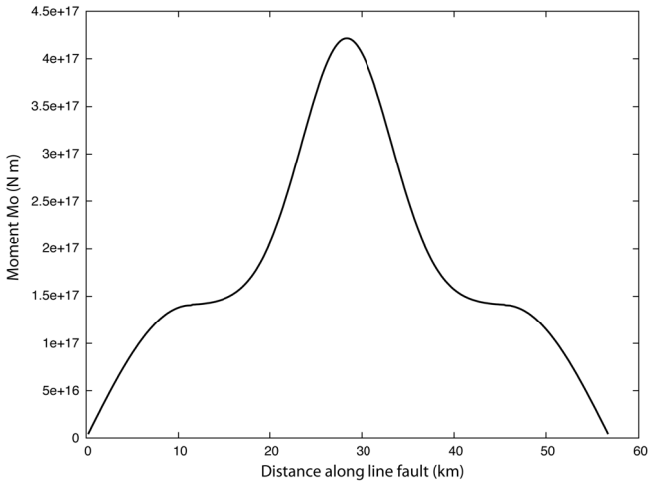

Figure 7.2. Distribution of the seismic moment along the line source from the nucleation to the last elementary source point of the fault, according to the slip distribution of the 1908 Messina earthquakes (Pino et al., 2009).

The Green's functions at the sites of interest (i.e. the position of the tunnel's cables) areusing the AXITRA code, which computes the complete wave-field solution of the wave equation by using the discretewave number method developed by Bouchon (Bouchon 1981; Cotton and Coutant 1997).

Finally, the ground motion at each selected site beneath the tunnel has been obtained by convolving the Green's functions with the moment-rate time

history of the line source. The computed synthetic accelerograms have a total duration of 30 seconds, while the maximum frequency of signals is 5 Hz.

Two scenarios are considered, differing one from the other for the considered value of the time duration (rise-time) of each point source rupture. A rise-time of 0.35 s for the first scenario in order to have a very destructive event with high amplitudes; for the second one a rise-time of 1.0 s is considered instead, this being a more realistic value for seismic events of this intensity.

The synthetic accelerograms show very large values of the PGA, ranging from 0.4 g to 0.85 g in the horizontal plane and from 0.2 to 0.45 in the vertical one in the first considered scenario (rise time=0.35 s). These large values are due to the great amount of energy released by the fault rupture concentrated in a small time period, approximately equal to 10 seconds (Figure 7.3)

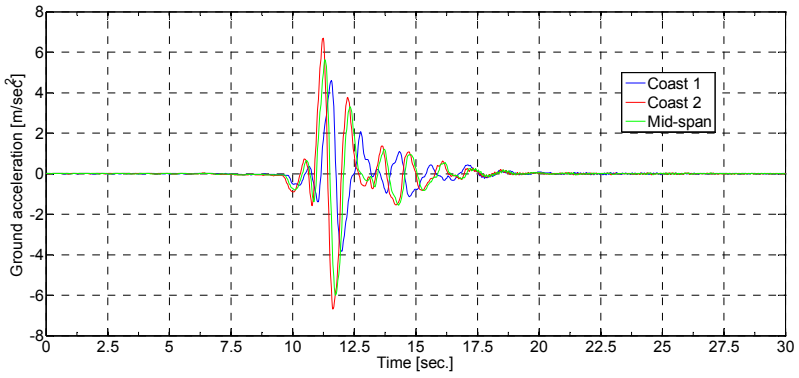

Figure 7.3. Acceleration time histories at the tunnel connections with the shores and near the tunnel mid-span (rise time=0.35 s).

Figure 7.4 shows the comparison between the elastic response spectra of the synthetic accelerograms (the average ones and at one of the coast approaches) and the design elastic spectrum provided by the Italian National Code (NTC 2008) for the Messina Strait, corresponding to: return periodT_R=2475 years, soil type D according to the soil classification provided in the code, horizontal PGA_H equal to 0.482 g and vertical PGA_V of 0.452 g. Therefore the design spectra reported in Figure are relative to the most severe design scenario considered by the Italian Code. In spite of this the average value of PGA of the simulated accelerograms in the horizontal directions are

quite larger than the one proposed by the code. In the vertical direction, instead, the PGA of the code spectrum slightly exceeds the average ones of the simulated accelerograms.

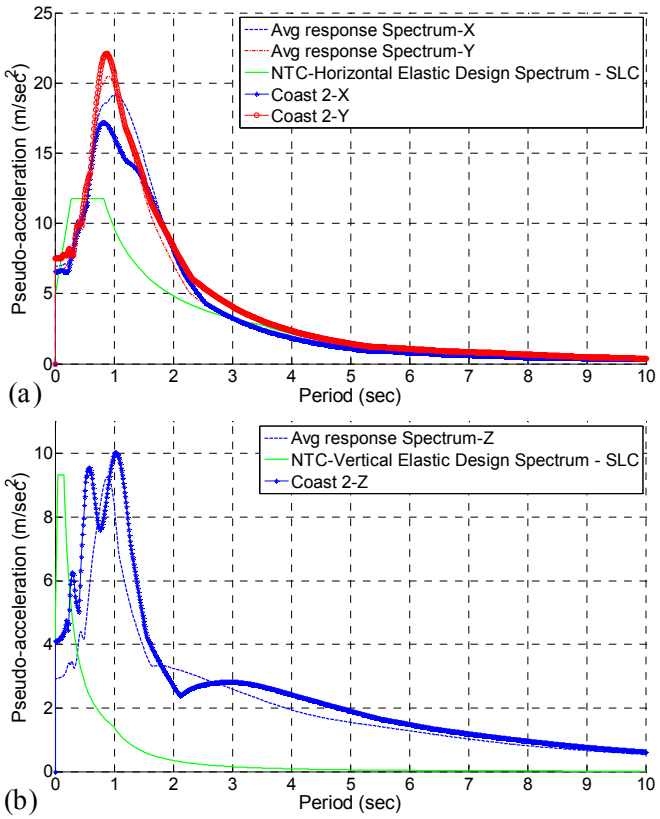

Figure 7.4. Comparison of the elastic response spectra given by the Italian National Code (NTC 2008) and by the simulated earthquake in the horizontal (a) and vertical plane (b) for the first scenario considered (rise time=0.35 s).

Figure 7.5 illustrates the same comparison for the second scenario considered, highlighting that increasing the rise-time gives rise to a reduction of the observed PGA values in both the vertical and horizontal directions, so that the average values of the PGA in the horizontal directionsare now close to the value provided by the Italian national code.

The first scenario is considered as the reference one, in order to study the SFT response to such a catastrophic seismic event.

The frequency content of the simulated accelerograms is the same for the two scenarios, beingconsiderably different from the one of the code uniform hazard spectra. As a matter of fact, the simulated elastic response spectra feature their peak at a quite low values of frequency: 0.85 Hz (horizontal directions) and 1.0 Hz (vertical direction).

This is due to a directivity effect, which is an effect similar to the Doppler effect occurring in acoustic problems. In fact, one of the advantages of using a line source model rather than a simple point source is that the former one takes into account this effect. The directivity effect can be also seen by observing the acceleration time histories, which have shorter length and bigger amplitudes respect to those expected.

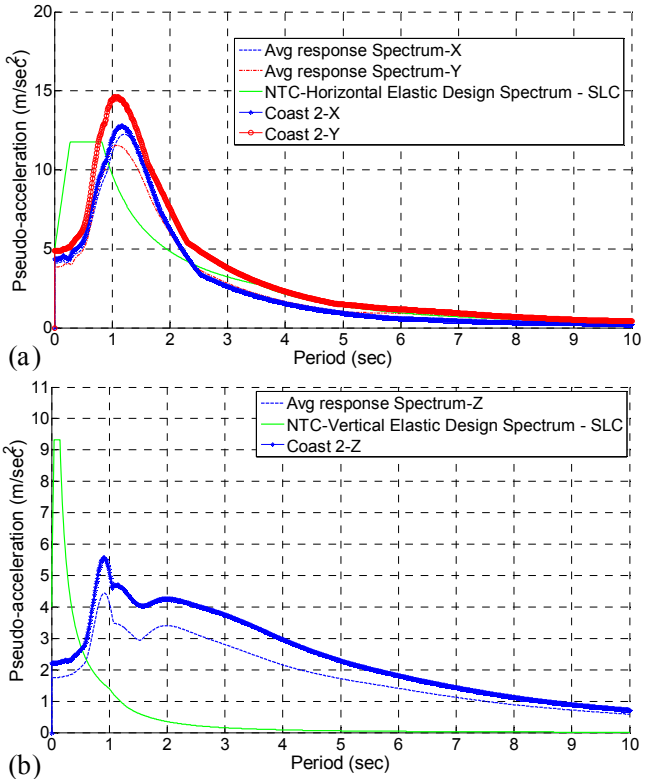

Figure 7.5. Comparison of the elastic response spectra given by the Italian National Code (NTC 2008) and by the simulated earthquake in the horizontal (b) and vertical plane (c) for the second scenario considered (rise time=1.0 s).

Directivity is caused by the particular position of the tunnel with respect to fault line and direction of propagation of the rupture. In fact the line connecting the nucleation point with the tunnel is inclined of less than10° from the line source and is just along the direction of the rupture. Considering an effective rupture length $L_e \cong 35000$ m (from Pino et al., 2009), an angle $\vartheta \cong 10°$ between the line source and the tunnel, the rupture velocity V_r=3000 m/s, and the ratio $V_r/V_S \cong 0.92$ (where V_S is the velocity of S-waves), the duration Δt of the S-wave travel to the tunnel location is:

$$\Delta t = \frac{L_e}{L_e} \cdot \left(1 - \frac{V_r}{V_s} \cdot \cos\vartheta\right) \approx 1.1\ s. \tag{7.1}$$

corresponding to a frequency of about 0.9 Hz.

Moreover, the values of the simulated response spectra feature values which are extremely larger the NTC elastic design spectra in the low frequency range. Therefore the simulated seismic event represents a very rare type of seismic event, being extremely dangerous for SFTs.

Water motion taking place during the seismic event due to propagation of the vertical ground motion in the water layer is calculated. Kinematics water data are recorded at a grid of stations located in the water layer. Peak water accelerations (PWA) range from 4.0 to 7.2 m/s^2 (seismic scenario 1) thus featuring a noticeable amplification of the vertical PGA, as proved by the comparison of the average elastic response spectrum relative to the water and ground accelerograms (Figure 7.6). Moreover, it can be seen that the energy content in low frequency range and the peak frequency of water motion is larger with respect to ground motion.

In figure 7.7 the acceleration time-histories at ground and water points located on the same vertical axis are reported. The accelerograms make reference to points located near the mid-span of the tunnel (a) and close to the east end of the tunnel, for the crossing length value of 3000 m. It can be noticed that, at least in the initial and most intense part of the earthquake, the water and the ground move in phase in the central part of the tunnel whereas some shift in the relative phase between the two signals can be noticed close to the tunnel ends.

Both PGA and PWA values increase moving from the west end to the east end of the tunnel

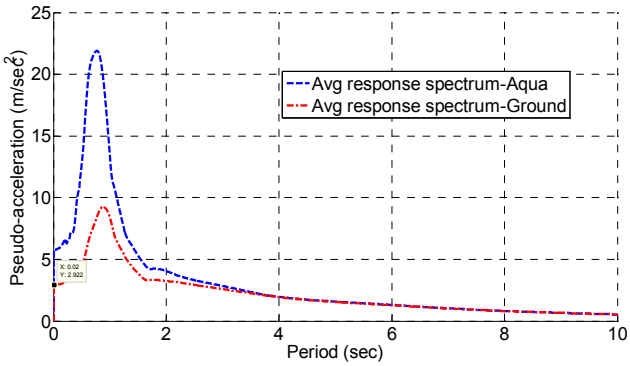

Figure 7.6. Comparison of the average elastic response spectra relative to water and ground accelerograms (rise time=0.35 s).

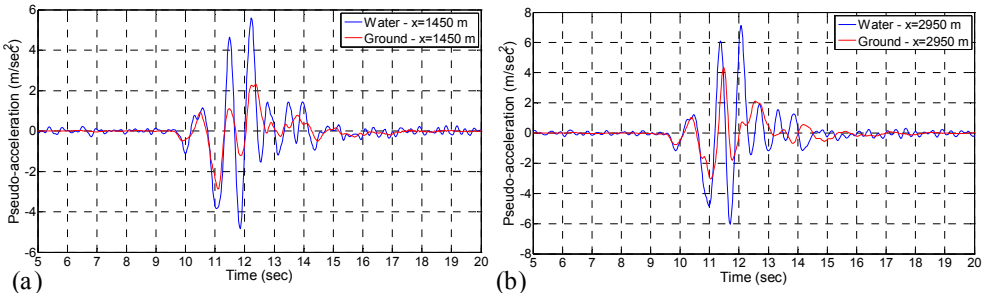

Figure 7.7. Water and ground accelerograms at: x=50 m (a) and x =2950 m (L=3000 m, rise time=0.35 s).

7.2.1.3. *Structural features*

The same SFT structural configurations described in section 6.3.1.3 are considered in this study, in order to assess also their seismic behaviour and performances.

7.2.1.4. *Environmental actions*

For each structural configuration of SFT three seismic analyses are carried out, considering:

- synchronous ground motion ("synchronous" case);
- asynchronous ground motion ("asynchronous" case);
- asynchronous ground motion and propagation of vertical ground motion in the water ("asynchronous-w" case).

The accelerograms recorded at each tunnel end are considered for synchronous ground motion analysis; these accelerograms are scaled, so that their PGA is equal to the average of the PGA values recorded at the various tunnel supports. This is made in order to have a rational comparison with the effects induced by asynchronous ground motion.

The forces F_h per unit length arising during the seismic event from the water-SFT interaction, due to their relative motion, are evaluated through the Morison's equation (see section 2.2.3.1), given here after:

$$F_h = \rho_w \cdot \frac{\pi \cdot D^2}{4} \cdot [(C_I - C_M) \cdot (a_w - a_s) + C_M \cdot a_w]$$

$$+ \frac{1}{2} \cdot \rho_w \cdot C_D \cdot D \cdot (v_w - v_s) \cdot |v_w - v_s| \tag{7.2}$$

The values assumed for the inertia coefficient C_I, added mass coefficient C_M and drag coefficient C_D are 2.0, 1.0 and 1.0, respectively.

In order to give an intuitive insight into the possible effects of the propagation of vertical ground motion in the water layer, the following simple considerations can be made.

Equation 7.2 shows that,when the water motion is considered (i.e. $a_w \neq 0$ and $v_w \neq 0$), the induced hydrodynamic loads are in phase with the acceleration and velocity of water particles:

$$\mathrm{F_{h,w}} = \left(\mathrm{C_I} \cdot \rho_\mathrm{w} \cdot \frac{\pi \cdot \mathrm{D}^2}{4}\right) \cdot \mathrm{a_w} + \frac{1}{2} \cdot \rho_\mathrm{w} \cdot \mathrm{C_D} \cdot \mathrm{D} \cdot \mathrm{v_w}^2 \tag{7.3}$$

On the contrary, the external loads induced by the ground motion (i.e. inertia forces $F_{I,s}$) are proportional to the mass of the structure (being the sum of the structural mass m_{str} and of the added mass contribution due to the surrounding water, whether this is still or moving) and to the ground acceleration a_g, as shown in the following equation (valid only for synchronous ground motion):

$$\mathrm{F_{I,s}} = -\left(\mathrm{m_{str}} + \mathrm{C_M} \cdot \rho_\mathrm{w} \cdot \frac{\pi \cdot \mathrm{D}^2}{4}\right) \cdot \mathrm{a_g} \tag{7.4}$$

Therefore it is evident that the effects induced on the SFT by the propagation of vertical ground motion in the water layer depend on the characteristic of the transfer function, defining in the frequency domain:

- the magnification of the amplitude of water particles motion with respect to the ground motion;
- the phase of water particles motion with respect to the ground motion.

Since the amplitudes of water particles motion is larger than the ones of ground motion, as shown in Figures 7.6 and 7.7, the maximum value of hydrodynamic inertial load overcomes the one of the inertial forces imposed on the structure by the ground vertical motion, also considering that, the factor $\rho_w \cdot (C_I - C_M) \cdot \pi \cdot D^2/4$ is larger than the sum of the structural and water added mass, since the buoyancy overcomes the weight of the structure and C_I and C_M are assumed equal to 2.0 and 1.0, respectively.

The phase between the harmonic components of water and ground vertical motion determines whether the effects induced on the structure by hydrodynamic inertial loads adds up to the ones due to ground inertial loads or they mitigate each other.

In case of synchronous motion (phase equal to 0), the absolute value of the total load imposed each instant on the structure will be equal to the difference of the absolute values of $F_{h,w}$ and $F_{I,s}$. In case of perfectly anti-phase motion (phase equal to π radians), the absolute value of total external load will be equal to the sum of the absolute values (thus leading to larger dynamic excitation of the structure). If the phase is larger than 0 and lower than π radians, an intermediate condition should occur.

7.2.2. Results of the SFT seismic analyses

7.2.2.1. *Analysis of the SFT seismic response*

Frequency content of tunnel vibrations

The dynamic behaviour of the structure during the simulated seismic event is investigated, with the aim of understanding its main characteristics.

The Fourier transform of horizontal and vertical acceleration time-history of some tunnel sections is calculated, in order to assess the frequency content of tunnel vibrations. In particular, the attention is focused on a tunnel section located close to the shore and to the tunnel mid-span section.

Vibration modes should, theoretically, govern the dynamic behaviour of a structure only when it behaves linearly. Despite the non-linear behaviour of SFTs during a strong earthquake, their contribution can be clearly recognized.

As for the hydrodynamic response, the seismic behaviour of shorter SFTs (L=500 m) prove to be quite different from the one of longer SFTs (L=3000 m and 4600 m). The vibrations of shorter tunnel are dominated by the third vibration mode in both, whose contribution is considerably larger than those of other modes, as it can be seen in Figures 7.8 (horizontal oscillations) and 7.9 (vertical oscillations), relative to one of the configurations of short SFTs assumed. This due to the fact that the vibration period of this mode is close to the dominant frequency of the earthquake.

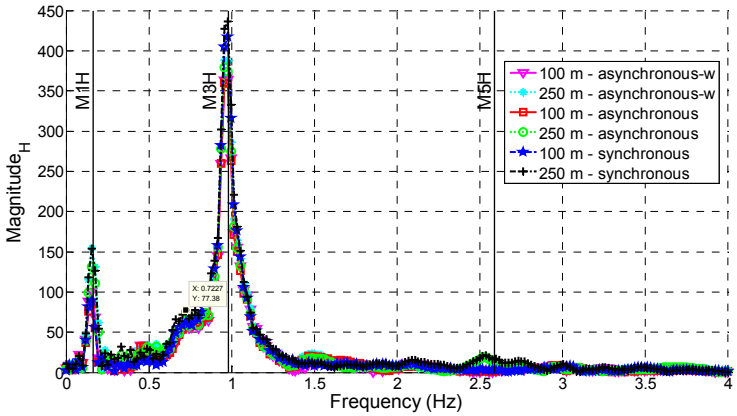

Figure 7.8. Frequency contentof horizontal vibrationsof relevant tunnel sections (L= 500 m, cable system CH, i=50 m, RB=RB$_1$).

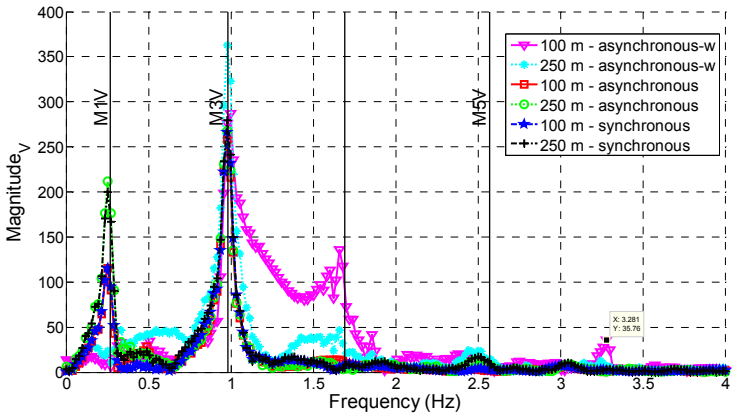

Figure 7.9. Frequency contentof vertical vibrationsof relevant tunnel sections (L= 500 m, cable system CH, i=50 m, RB=RB$_1$).

Few other modes participate considerably to the structural vibrations; generally the first mode and, in second order, the fifth mode also participate to the oscillations of the tunnel.

The influence of water motion can be noticed (Figure 7.9), as the frequency content of vertical accelerations of the tunnel sections is more relevant at higher frequencies, when this contribution is considered.

For longer crossings, more modes contribute to the tunnel vibrations, asthe distribution of natural frequencies of vibration of the structure is more concentrated in the low frequency range. (Figures7.10 and 7.11). The contribution of higher modes is of great relevance, especially for tunnel sections located close to the tunnel ends.

The multi-support excitation gives rise to a non-negligible asymmetrical excitation of the structure. In fact the contribution of some tunnel vibration modes whose participating mass is equal to zero (i.e. modes whose shape features an even number of sinusoidal waves), can be recognized; these modes are clearly not excited in case of synchronous ground motion.

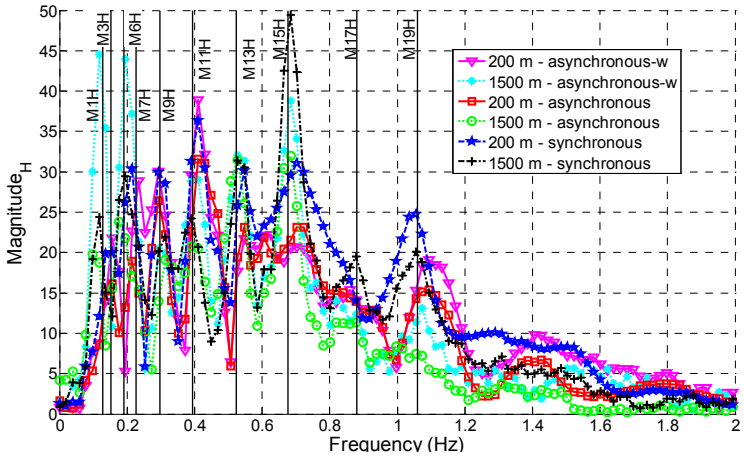

Figure 7.10. Frequency contentof horizontal vibrationsof relevant tunnel sections (L= 3000 m, cable system CW, i=100 m, RB=RB$_1$).

The contribution of high frequency components of the vertical water motion appears to be dominant. In fact, it can be noticed that the dominant frequencies of the tunnel vertical vibrations are extremely higher when the propagation of vertical ground motion is considered.

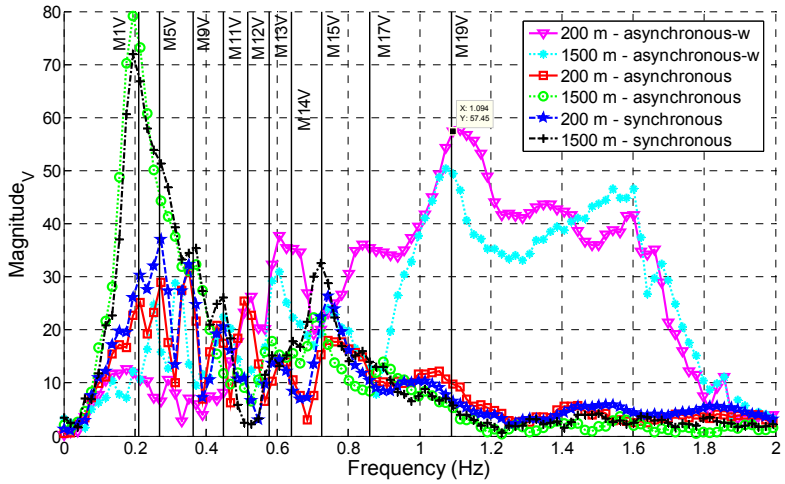

Figure 7.11. Frequency contentof vertical vibrationsof relevant tunnel sections (L= 3000 m, cable system CW, i=100 m, RB=RB$_1$).

The same remarks can be made by observing the frequency transforms of the acceleration time-histories of sections of SFTs whose length is 4600 m (Figures 7.12 and 7.13). In these cases, the contribution of higher modes becomes even more important.

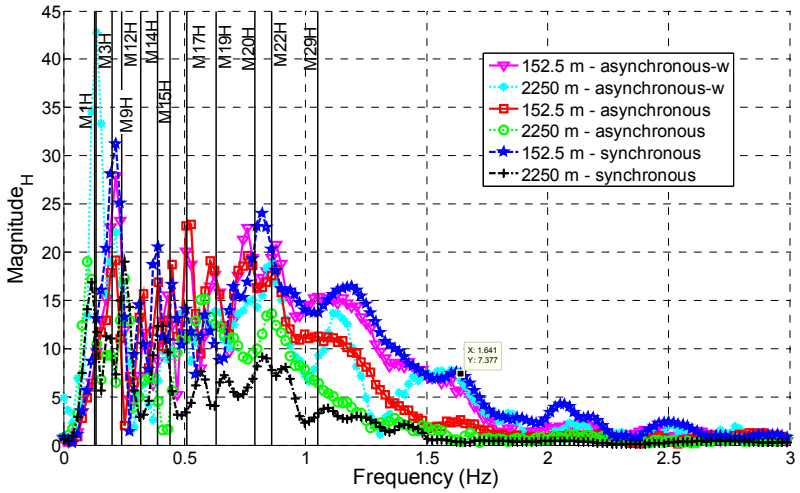

Figure 7.12. Frequency contentof horizontal vibrationsof relevant tunnel sections (L= 4600 m, cable system CW, i=100 m, RB=RB$_1$).

Structural response

In order to evaluate the ability of SFTs to withstand catastrophic earthquakes, the attention is focused on the behaviour of the structural elements in terms of stresses distribution and peaks. In fact, for a seismic event of the intensity considered in this study, the objective structural performance is to have maximum values of stresses in the tunnel and in the anchorages compatible with their own strength.

In this perspective, the attention is here focused to the distribution of maximum values of bending stresses and axial forces attained in the tunnel and anchorages, respectively.

The vibration modes excited by the ground acceleration can be also clearly individuated observing the envelopes of maximum and minimum bending moments reached in the tunnel structure, confirming the indications given by the analysis of the frequency content of tunnel.

Concerning short SFT crossings, the shape of the envelopes clearly resembles the distribution of bending moments associated with the third vibration mode of the structure, also highlighting the contribution of the first mode (Figures 7.13 and 7.14, relative to the SFT anchored by CH type cable system, RB=RB_1). The maximum values attained are large, being close to (or slightly larger than) the tunnel strength in the horizontal plane.

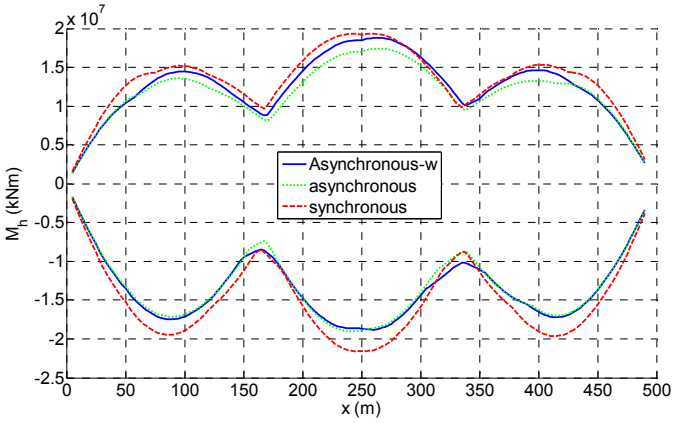

Figure 7.13. Envelope of maximum and minimum tunnel bending moment in the horizontal plane (L=500 m; Cable system CH1; RB_1)..

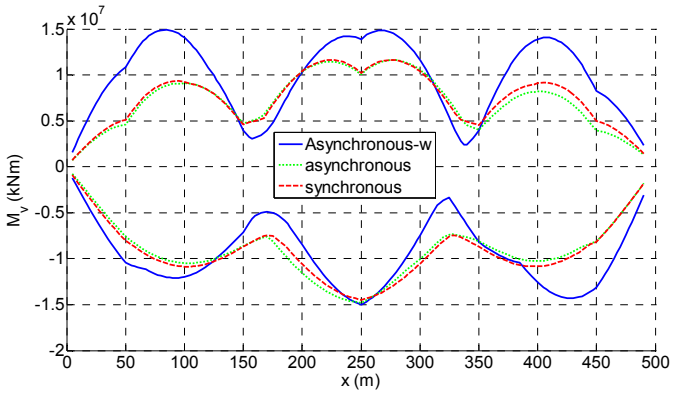

Figure 7.14. Envelope of maximum and minimum tunnel bending moment in the vertical plane (L=500 m; Cable system CH1; RB_1).

The contribution of the dynamic pressure field associated with the vertical motion of the water leads to larger values of vertical bending moment stressing the tunnel, but only in its parts located within a distance of approximately 100 m. However the maximum values attained are the same for synchronous and asynchronous ground motion.

Looking at the time variation of the vertical bending moment stressing the tunnel at its mid-span section (Figure 7.15) it can be noticed that vertical water motion largely influences the response of the structure.

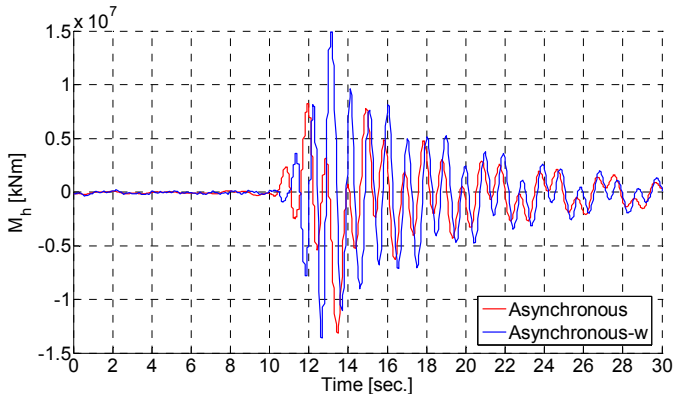

Figure 7.15. Timevariation of vertical bending moments in the mid-span section of the tunnel for asynchronous input, considering or neglecting vertical water motion (L=500 m; Cable system CH1; RB_1).

In fact the comparison between the time-histories in the two cases ("asynchronous" and "asynchronous-w") highlights that large differences arise in the structural response and a phase shift between the responses is noticed at the beginning of the seismic event.

Figure 7.16shows the distributions of the maximum axial force stressing the anchorages for the same case study. The values are always lower than the anchorage strength, even though slackening occurs in almost every cable. Moreover, the presence of contemporary vertical water motion reduces the maximum stress in the anchorages, in particular in the vertical ones.

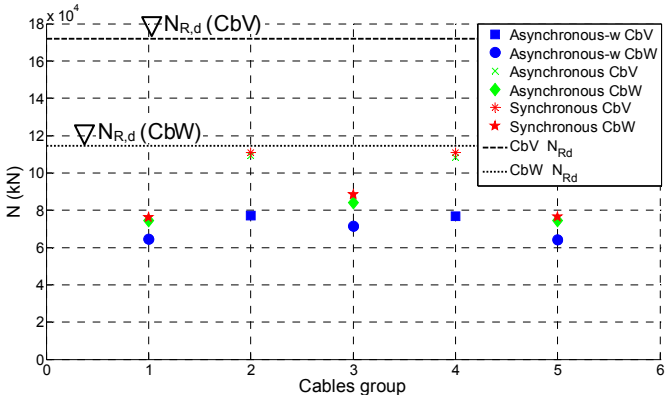

Figure 7.15. Distribution of the maximum axial force in the anchorages(L=500 m; Cable system CH1; RB_1).

The structural response of short SFTs is not very affected by the type of anchorages (tethers or cables), geometrical configuration of the anchoring system or value of the ratio of buoyancy. In fact the previous observations are still valid in general for all the considered SFT cases having a length of 500 m. Axial stress of anchorages can vary, depending on their axial stiffness and inclination but no increments so large to lead to their breaking occurs in any case. Also, loosening of the cables cannot be prevented, not even by increasing the residual buoyancy; it does not occur only in anchorage groups close to the shores, thanks to the beneficial contribution of the water vertical motion. Most important, maximum bending stress reached in the tunnel are always large, being unacceptable in most of the cases.

For longer SFTs, the distribution of maximum bending moments occurring in the tunnel evidences both the presence of the contribution of a considerably larger number of modes and the larger excitation of higher modes. Examplesare given in Figures 7.17 and 7.18, relative to a cable anchored SFT, featuring CH type longitudinal arrangement of the anchoring system, one anchorage group per tunnel module and RB=RB_1.

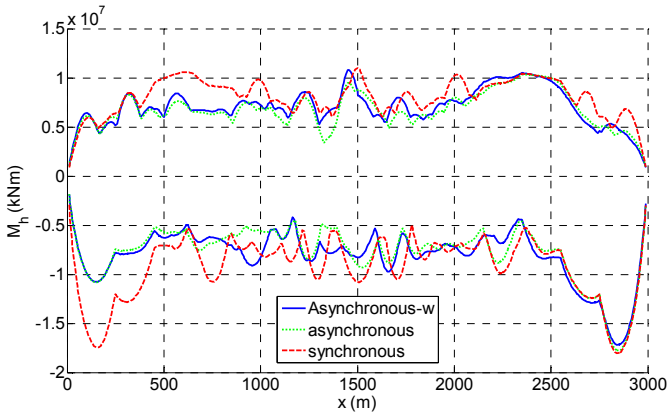

Figure 7.17. Envelope of maximum and minimum tunnel bending moment in the horizontal plane (L=3000 m; Cable system CH1; RB_1)..

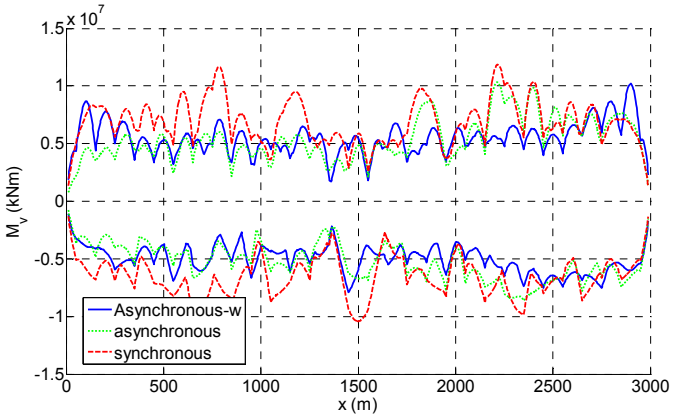

Figure 7.18. Envelope of maximum and minimum tunnel bending moment in the vertical plane (L=3000 m; Cable system CH1; RB_1).

The tunnel is less stressed with respect to shorter SFTs, as it could have been expected: the first vibration modes are in fact less excited by dynamic excitations whose energy content is concentrated in the low frequency range, such as earthquakes (even though the seismic event considered here features an unusual large value of the peak period, as discussed in section 7.2.1.2).

Nevertheless, a quite large stress concentration can be noticed in the terminal parts of the tunnel, in particular in the horizontal plane. This concentration might seem surprising at a first glance, but it is expectable and quite common for SFTs crossing large spans, as it can be observed in the results of most of the performed analyses. Moreover, similar results are shown also in the work made by Xiao and Huang (2010), where the seismic behaviour of a 4600 long SFT is studied.

This stress concentration is mainly due to:

- excitation of a large number of higher vibration modes, whose contributions sum up in the terminal part of the tunnel;
- presence of shorter and stiffer anchorage groups close to the shores, which leads to a modification of the bending moments distributions associated to first vibration modes and to larger values of participant mass associated to higher modes (see section 6.3.3.1).

In order to prove the first of the two above mentioned points, it is interesting to observe the results that are obtained by analysing the SFT behaviour through the simple model of beam on elastic foundation (BOEF), described in section 5.1. It is evident that this simple calculation model does not take into account neither the variation in the stiffness of the anchorage system due to sloped part of the seabed, nor the effect of concentrated supporting condition provided by discrete anchorage groups.

Figure 7.19a illustrates the envelope of maximum bending moments as calculated through the BOEF model analysis. In the definition of the foundation distributed stiffness of the foundation, reference is made to the lateral stiffness of the anchoring system type CW1 with $RB=RB_1$; the seismic input is the one relative to horizontal accelerations of the ground at the east coast of the tunnel (the same considered for synchronous analyses, but not scaled here). Figure 7.19b shows the envelope of maximum and minimum bending moments relative to some of the vibration modes contributing the most to the overall response. It can be noticed that the shape of the

envelopeillustrated in Figure 7.19 is not very different from the ones shown in Figure 7.17.

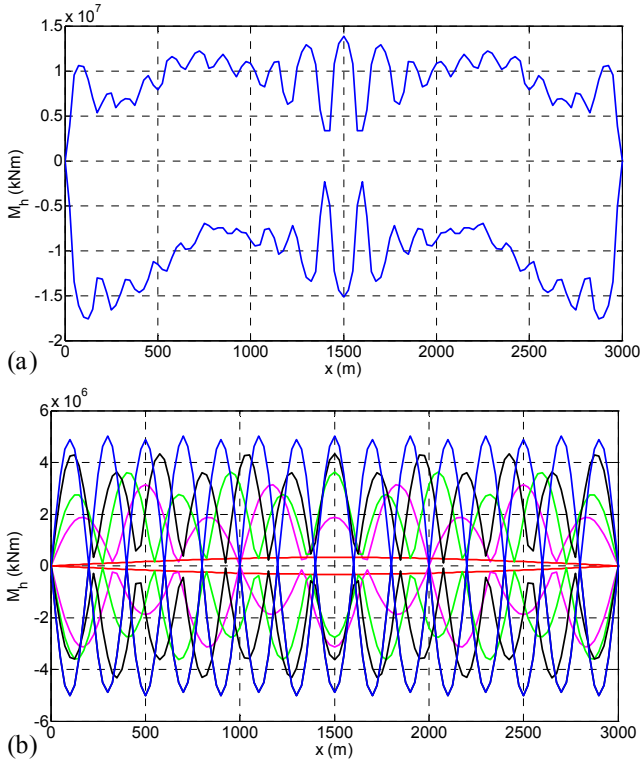

Figure 7.19. Horizontal bending moment distributions from SFT seismic analysis through the BOEF model: (a) envelope and (b) contributions arising from most relevant vibration modes.

Water vertical motion often leads to a reduction of the maximum values of the vertical bending moment attained in the tunnel structure, the most significant reductions occurring in the central part of the tunnel (Figure 7.20a); in some other cases no relevant effects can be noticed, whereas, in few cases, the contribution of the water dynamic pressure leads to larger peak of stresses in the terminal parts of the tunnel, so that a general trend is not recognized. However, often the peak value of vertical bending moment, attained close to the second (east) tunnel shore connection, is larger when the vertical water motion is taken into account in the analysis (Figure 7.20b). This

effect might be addressable to larger phase shifts noticed between water and ground acceleration-time signals in proximity of the tunnel shore connections.

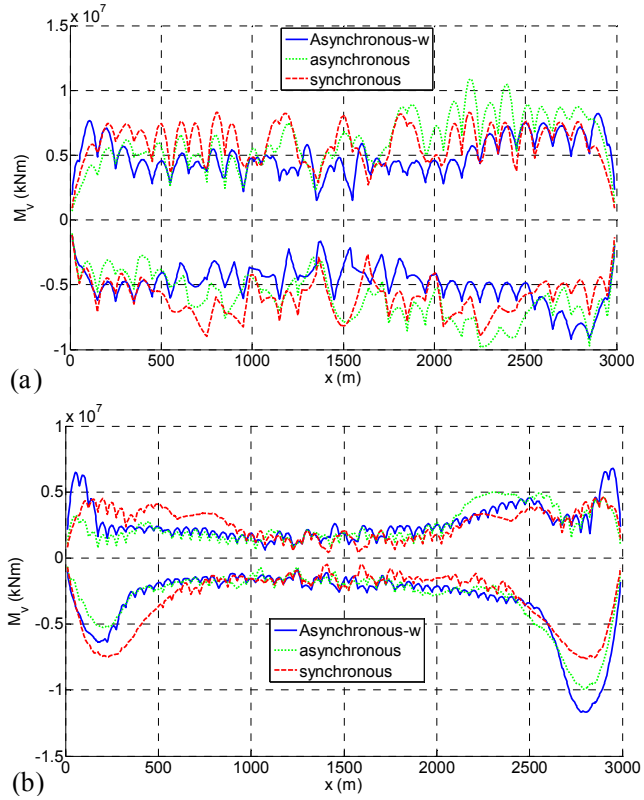

Figure 7.20. Envelope of maximum and minimum tunnel bending moment in the vertical plane (L=3000 m; (a) Cable system CH1; RB_1; (b) Tether system CW2, RB_2)

The level of axial stress induced in the anchorages during the earthquake is largely affected by the presence of sloped the progressive reduction of seabed depth, moving from the central part to the shores of the crossing, close to the shore connections. In fact, shorter anchorages located in these zones are considerably stiffer and thus subjected to axial forces being extremely larger than those attained in central anchorage groups, in most of the cases exceeding their design strength. Clearly, this amplification is greatly exalted in case of sloped anchorages, for which the dynamic increment of tension is due to both

the vertical and horizontal vibrations of the structure. This effect was recognized also in the study carried out by Di Pilato et al. (2008).

It is therefore expectable that hybrid configurations of the anchoring system would show a better response, under the point of view of ensuring the integrity of the anchorages. This is confirmed by the results obtained in the performed analyses: the value of the maximum axial force reached in the shorter anchorages is generally quite lower for CH configuration (Figure 7.21) with respect to CW type configuration (Figure 7.22) of the anchoring system. In particular, strength checks are satisfied for all the anchorage groups only when cable system of type CH with one anchoring group per tunnel module is considered; in case of tethers, probably due to their larger stiffness, the dynamic increment of axial force in the anchorages is quite larger, so that their strength is exceeded also for CH arrangement of the system.

However, it is necessary to underline that this is just a local problem, as the axial forces stressing the anchorages located away for the shore are considerably lower and compatible with the anchorage design strength, as it can be easily noticed in Figure 7.22. Moreover, a quite interesting result is that slackening of the anchorages commonly occurs, even in the anchorages located in the central part of the structure. Therefore it seems that this condition does not represent a critical condition in itself, as it does not necessarily lead to unacceptable behaviour of the anchorages.

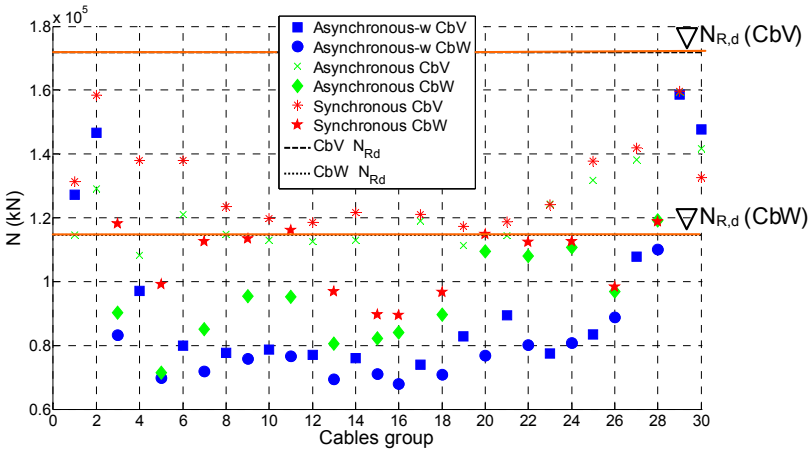

Figure 7.20. Distribution of maximum axial force in the anchorages (L=3000 m; Cable system CH1; RB_1).

The propagation of vertical water motion leads to large reduction of the maximum force attained in the anchorages in almost all the performed analyses; this reduction takes place in almost all the anchoring groups (Figures 7.21 and 7.22). However, the same effect described previously about the peak values of vertical bending moments in proximity of the tunnel shore connections can be noticed here (see cables 58 and 59 in Figure 7.22). As stated before, this occurrence could be probably explained considering that, in these zones, some phasing between vertical motion of water particles and ground points located at the same abscissa takes place (see section 7.2.1.2).

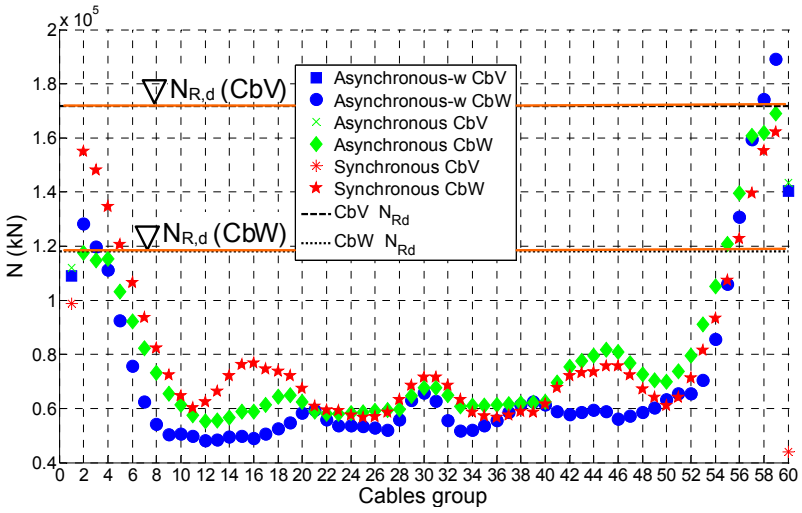

Figure 7.22. Distribution of the maximum axial force in the anchorages (L=3000 m; Cable system CW2; RB_2).

The behaviour of longer SFTs (L=4600 m) is qualitatively similar to the one of described above, but some characteristics pointed out above are generally more pronounced, such as:

- the number of modes involved in the tunnel vibrations is even larger and the bending stress concentration at the tunnel terminal parts is generally more noticeable (Figure 7.23);
- the reduction of maximum vertical bending moments occurring in the central part of the tunnel (Figure7.24) and of axial force in the anchorages (7.25) is quite larger;

- the amplification effect of the axial force stressing shorter anchorage groups located close to the shores is more noticeable (Figure 7.25), due to further reduction in the length of these anchorages.

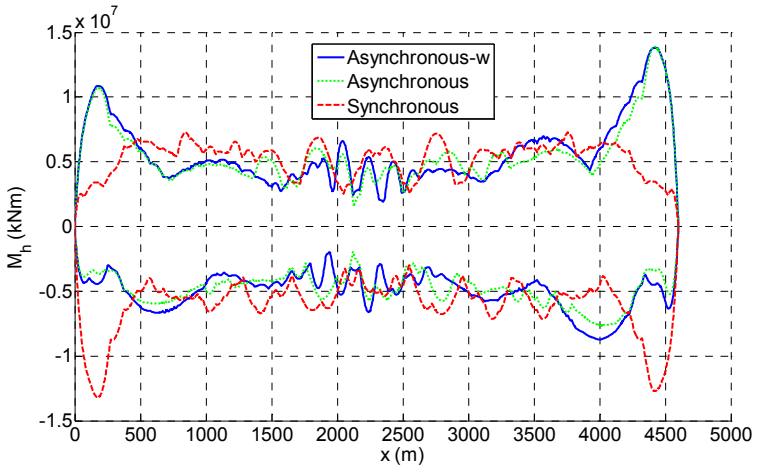

Figure 7.23. Envelope of maximum and minimum tunnel bending moment in the horizontal plane (L=4600 m; Cable system CH2; RB_1).

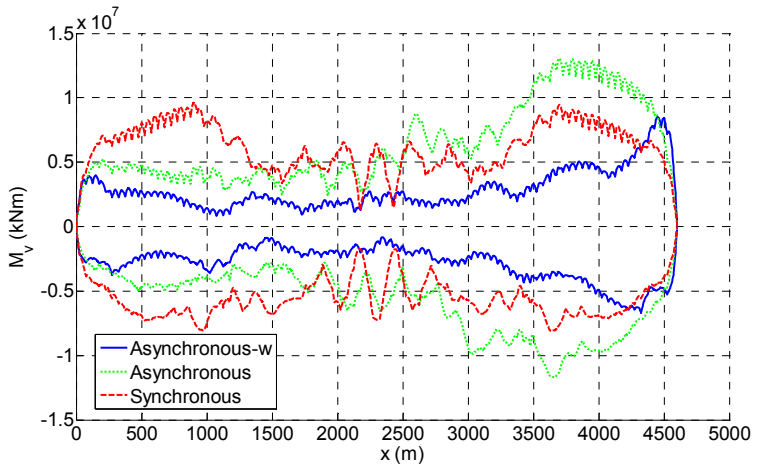

Figure 7.4Envelope of maximum and minimum tunnel bending moment in the vertical plane (L=4600 m; Cable system CH2; RB_1).

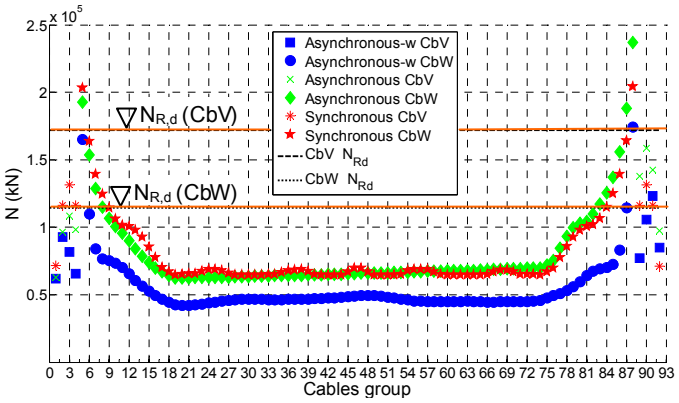

Figure 7.24. Distribution of the maximum axial force in the anchorages (L=3000 m; Cable system CW2; RB_2).

7.2.2.2. *Evaluation of the SFT seismic performance*

The seismic performance of SFT is here assessed for all the considered case studies, by calculating the values attained by the demand/capacity ratio for the main structural elements: the anchorages and the tunnel structure. Moreover, the differences obtained by considering different types of seismic input, namely synchronous, asynchronous and asynchronous with propagation of vertical motion in the water, are observed and discussed.

Figures 7.25 and 7.26 illustrate the demand/strength bending stress ratio for shorter SFTs, anchored by means of cables and tubular tethers, respectively. The ratio is relative to bi-axial bending of the structure ($M_b/M_{Rd,b}$) and is calculated by selecting among all the couples of values M_h – M_v (horizontal – vertical bending moment stressing the tunnel) occurring during the simulated seismic event, the one providing the larger value of the following combination:

$$\frac{M_b}{M_{Rd,b}} = \left(\frac{M_h}{M_{Rd,h}}\right)^{\alpha} + \left(\frac{M_v}{M_{Rd,v}}\right)^{\beta} \tag{7.5}$$

where α and β are coefficients assumed equal to 1.25. Equation 7.5 is commonly adopted to define the bi-axial bending moment strength domain of r.c and steel-r.c. composite cross-sections.

As noticed in previous section, the maximum level of bending stress reached in the tunnel often large and not compatible with the tunnel design strength. In fact the demand/capacity ratio is lower than one only when asynchronous motion with no water motion is considered as seismic input. Values attained with asynchronous ground motion and vertical water motion are enclosed between 1.15-1.30 and similar values are found when synchronous ground motion is considered.

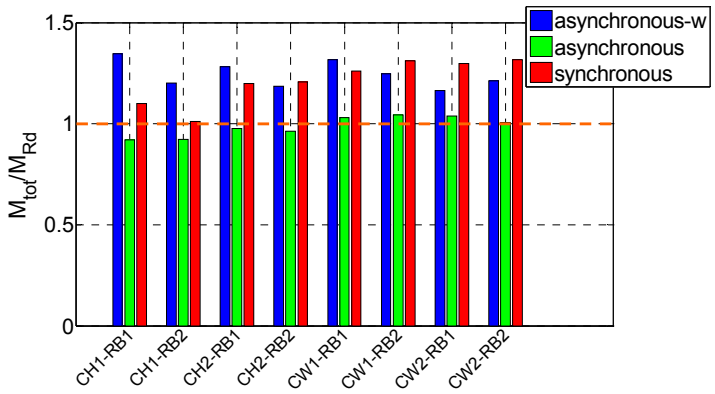

Figure 7.25. Demand/strength ratio of bi-axial tunnel bending moment (Cable anchoring systems; L=500 m).

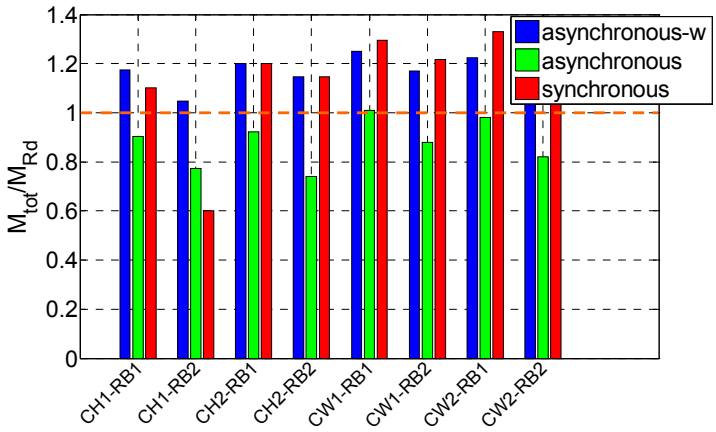

Figure 7.26. Demand/strength ratio of bi-axial tunnel bending moment (Tether anchoring systems; L=500 m).

No relevant differences in the performances offered by the different proposed structural configurations can be noticed. Some differences arises between the response provided by cable and tether anchoring systems: for the latter ones the stress level in the tunnel is slightly lower but, on the other side, the level of axial stress is slightly larger, in few cases exceeding the design strength. This difference should be due to the larger stiffness of the tethers, which therefore absorb a larger amount of stress, the intensity of dynamic excitation of the two solutions being similar (3rd vibration period is similar).

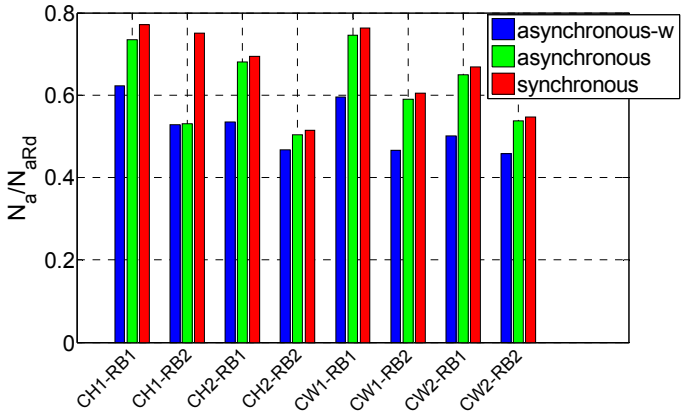

Figure 7.27. Demand/strength ratioof axial force in the anchorages(Cable anchoring systems; L=500 m).

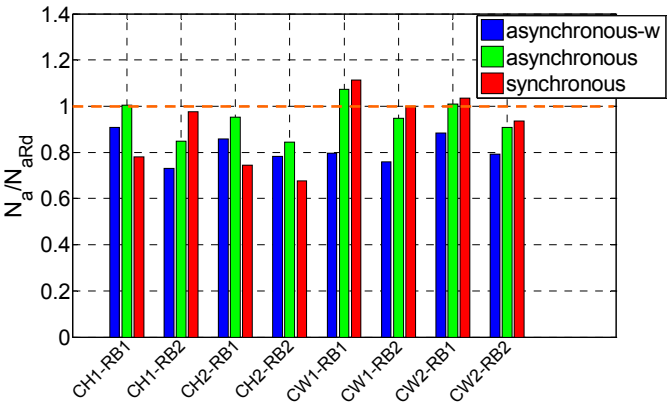

Figure 7.28. Demand/strength ratio of axial force in the anchorages(Tether

anchoring systems; L=500 m).

The same plots are showed in Figures 7.29 to 7.32 for 3000 m long SFTs. The performance charts show the effects of the peculiarities of the response of SFTs crossing large spans, pointed out in previous section: maximum bending stresses occurring in the tunnel are lower than the ones attained in shorter SFTs, so that the tunnel strength check is generally satisfied.

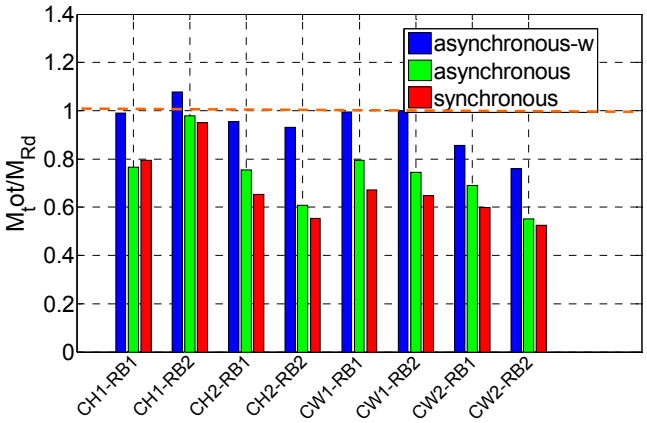

Figure 7.29. Demand/strength ratio of bi-axial tunnel bending moment (Cable anchoring systems; L=3000 m).

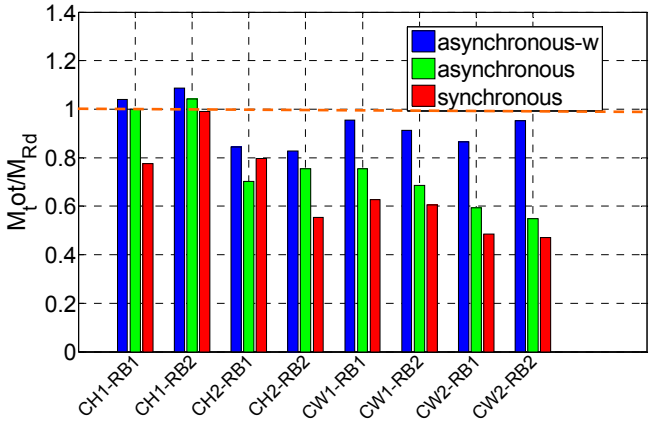

Figure 7.30. Demand/strength ratio of bi-axial tunnel bending moment (Tether anchoring systems; L=3000 m).

Peak values of bi-axial bending moment are always larger when vertical water motion is considered. However, this result is not representative of the global structural response observed (as showed and discussed in previous section): in fact, in large part of the structure the level of stress is significantly reduced thanks to the vertical motion of the water.

Similar considerations can be made with respect to the performances of the anchorages. In fact, looking at the graphs shown in Figure 7.31, it could be concluded that the anchoring system is not able to withstand such a strong earthquake, as the maximum value of the ration N_{Sd}/N_{Rd} is often largely above the allowed limit. However this unacceptable behaviour is limited to few anchorage system, located close to the tunnel shore connections, whereas the rest of the anchorage groups most often offer performances largely satisfying.

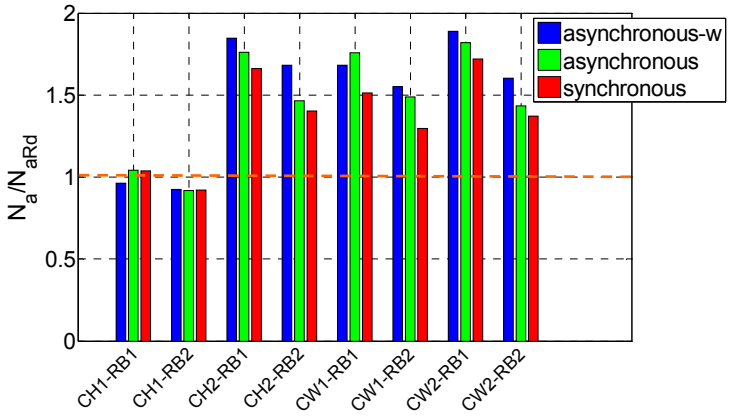

Figure 7.31. Demand/strength ratioof axial force in the anchorages (Cable anchoring systems; L=3000 m).

Also in longer crossings, using tethers rather than cables implies improvements of the tunnel performance, as the maximum value of bending stress attained reduces, but worse performances of the anchorages. This result shows again that, for seismic purposes, stiffening too much the anchorage system do not lead to acceptable performance of the anchorage system itself. Therefore a compromise solution should be found in zones characterized by high seismicity, taking into account also the hydrodynamic response of this structural system.

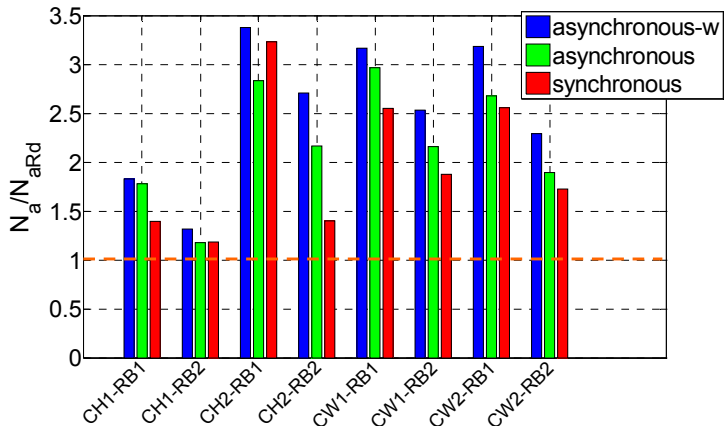

Figure 7.32. Demand/strength ratio of axial force in the anchorages (Tether anchoring systems; L=3000 m).

In this context, the performance of cable anchoring systems with hybrid longitudinal arrangement and one anchoring group per system (CH1) deserves to be underlined. This is the only structural solution showing acceptable performances of all the anchorage groups, included the stiffer ones located on the sloped segments of the seabed This result confirms that this solution features good potentialities considering both the seismic performance and the economic points of view, and it could be combined with other configurations, with the aim of optimizing the structural response and its cost together. In fact the distribution of the stiffness of the anchoring system could follow the seabed profile by using cable system with CH1 arrangement in proximity of the shore connections, where lower depths are encountered, whereas solutions featuring larger lateral stiffness (CW1 or CW2 systems, tubular tethers instead of cables, etc,) could be used in the central, deeper, part of the crossing, In this way the problem related to the large stress increment in shorter anchorages would be probably avoided, or at least mitigated, still ensuring the required later stiffness in the central part of the crossings.

However, the most rational solution to improve the SFT seismic performance when this conditions are encountered, i.e.when large spans have to be surpasses and the seabed profile is such that strong reduction of the water depth occurs approaching the shores, would be to use structural elements able to yield and dissipate the seismic input energy by means of a stable post-elastic behaviour.

Moreover, this solution would probably reduce the concentration of stress occurring in proximity of the shore connections in the tunnel, as the amount of seismic input energy transmitted by the anchorages after their yielding would be probably considerably lower lower. Such a kind of solutions is suggested also in Di Pilato et al. (2008), where similar results to the ones obtained in this work,with respect to the behaviour of terminal anchorage groups, are found.

Concerning the performances of 4600 m long SFTs, the main conclusions drawn immediately above are still valid. However some differences arise:

- the level of stress in the tunnel reduces (Figures 7.33 and 7.34) whereas the maximum axial forces reached in the anchoring system feature quite important increments, probably due to a combination of two effects: further reduction of the length of anchorages located close to the shores and increased deformability of the tunnel;
- the influence of the propagation of vertical water motion is here beneficial also in the terminal parts of the structure, leading to substantial reduction of the maximum values of the bending stress attained in the tunnel structure and of the axial force stressing the anchorages.

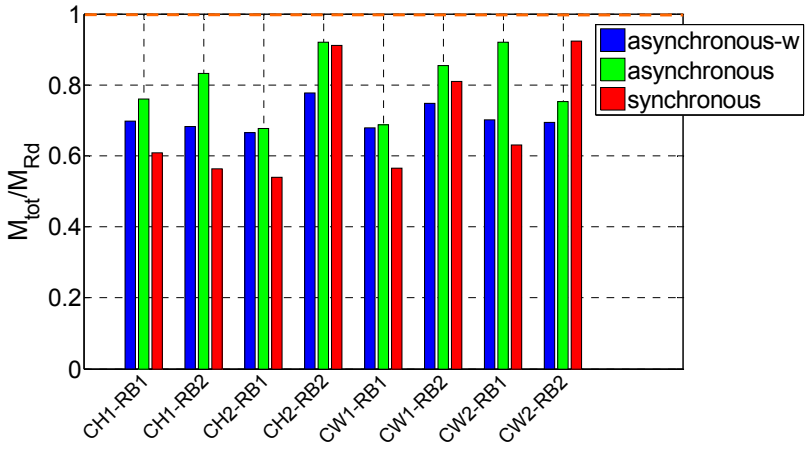

Figure 7.33. Demand/strength ratioof axial force in the anchorages (Cable anchoring systems; L=4600 m).

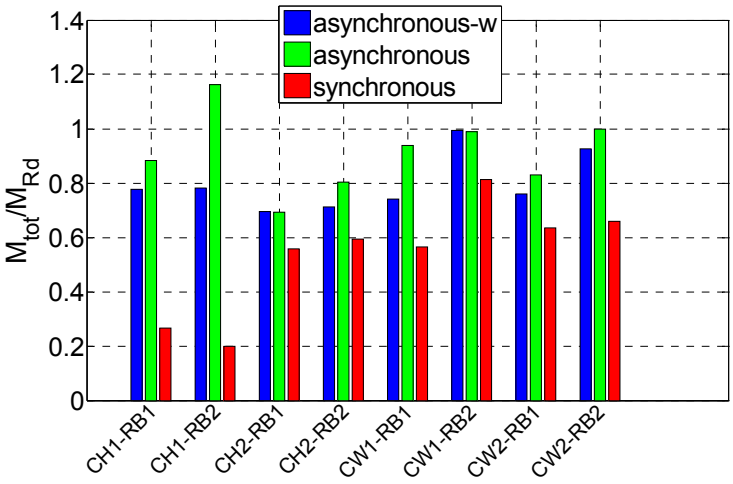

Figure 7.34. Demand/strength ratioof axial force in the anchorages (Tether anchoring systems; L=4600 m).

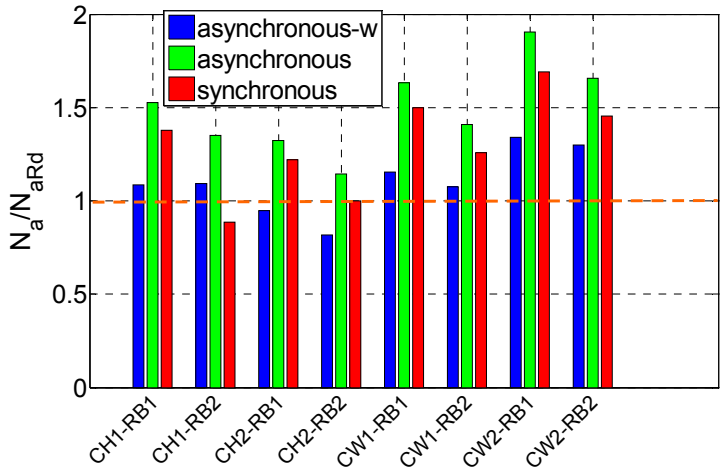

Figure 7.35. Demand/strength ratioof axial force in the anchorages (Cable anchoring systems; L=4600 m).

In conclusion it seem worth to stress again that the results obtained from the performed analyses do not prove at all that the SFT seismic performances are not as satisfactory as it was expected. In fact, the intensity of the considered seismic scenario is such that it can be easily imagined that other

waterway crossing solutions would feature many, probably more, critical issues when subjected to it.

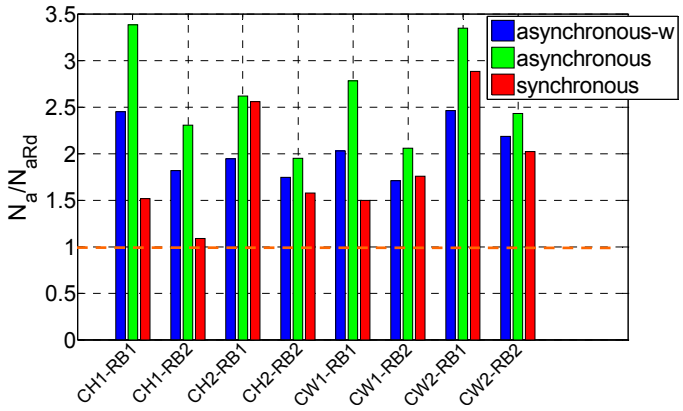

Figure 7.36. Demand/strength ratioof axial force in the anchorages (Tether anchoring systems; L=4600 m).

Moreover, the frequency content of the simulated accelerograms is quite particular, as discussed in section 7.2.1.2, and caused by the particular geometrical position of the tunnel with respect to the fault, originating directivity effects. Commonly, seismic events show a frequency content being more concentrated in the high frequency range, so that the effects induced on a deformable structure such as SFTs would be significantly lower.

In addition, if the second seismic scenario is considered (rise time=1.0 sec., whose amplitudes are lower than scenario 1, see section 7.2.1.2), the SFT performances are largely acceptable, as proved by further analyses, carried out for some of the structural configurations exhibiting the worse performance. The only issue arising from these analyses is still related to the large axial forces attained in few (fewer than for scenario 1) anchoring groups located close to the end parts of longer SFTs; however, this issue could be easily solved through rational design solutions, as observed before.

7.3 CONCLUSIVE REMARKS

The study of the response of SFTs to severe seismic events is carried out in this chapter. The 1908 Messina earthquake is simulated, by means of a fault

line source model. A set of accelerograms, featuring very large PGA (up to approximately 0.85 g), is generated at the various soil points of interest, allowing to study the response of the structure to multi-support ground motion. Moreover, the propagation of vertical ground motion in the water layer is simulated too; water kinematics data are recorded at a grid of stations surrounding the SFT and the deriving dynamic pressure field is introduced in the model through the Morison's equation. Synchronous ground motion is considered too for comparison.

It seems intuitive that the effects of vertical water motion on the seismic response of the SFT depends on its amplification with respect to the ground motion and on the phase occurring between the two motions. In the performed study, quite large amplifications (amplification factor being averagely equal to 2) of the vertical ground motion take place at the points of the water layer being close to the SFT structure; moreover, it seems that the motion of the ground and water occurs synchronously in the central part of the crossing, whereas some phase shift can be noticed at the points being closer to the shore connections.

The frequency content of the SFT oscillations is calculated, showing that shorter SFT vibrations are dominated by the third vibration mode, its period being close to the peak frequency of the accelerograms, whereas a large number of vibration modes is involved in the oscillations of longer SFTs, higher mode contribution being more relevant. Asynchronous ground motion excites also asymmetrically the structure, as the contribution of a few number of modes with no participant mass (i.e., whose shape features an even number of sinusoidal waves can be recognized. When the vertical water motion is considered, the frequency content of vertical vibrations is shifted in the high frequency range, thus showing that this contribution is very important. In fact the frequency content of the vertical water motion in the high frequency range is considerably larger than the one of ground motion.

The structural response in terms of tunnel bending moments distributions confirm the previous considerations in terms of modal contributions to the vibrations of SFTs.

In case of shorter tunnels, bending stresses reach very large values, often not compatible with the tunnel design strength. A practical design solution,

which would improve their performance, could be to provide the tunnel shore connections with special dissipative devices.

In longer SFTs the critical issue is not related to the maximum values of bending moment occurring in the tunnel, but to the axial force stressing the anchorages. In fact the anchorage groups located close to the shore connections, due to their reduced length, are considerably stiffer than anchorages located in the central part of the crossing: therefore they are subjected to extremely larger axial forces, which exceed their strength. The only configuration of the anchoring system which exhibits a significantly better performance with respect to the others is the hybrid one, with one anchoring group per tunnel module; in fact in these cases the axial forces induced by the seismic event are not as large as for other configurations, in particular when cables, more deformable than tubular tethers, are used as anchorages.

However, this is not a real critical issue for the response of SFTs to earthquakes, as it is a problem arising in a small part of the structure; in fact, a very simple and economical solution to the problem would be to build the shorter anchorages by means of structural elements able to yield and dissipate energy through a stable post-elastic behaviour, or, alternatively, by introducing specific mechanical devices, providing a special dissipative connection between the tunnel and the anchorages.

The contribution of water motion definitely proved to be a topic deserving further investigations, as its contribution to the seismic behaviour of SFTs seem to be quite relevant. The performed analyses show that stresses induced in the tunnel and in the anchorages generally reduce in presence of the vertical water motion. However, larger peaks occur at the terminal parts of the SFT, close to the shore, probably due to the phase shifts occurring in this part of the crossing between vertical motion of ground points and water particles located on the same vertical line.

Chapter 8

Cost comparison between the SFT and traditional solutions for waterway crossings

8.1 INTRODUCTION

The SFT solution presents several advantages with respect to traditional waterway crossing solutions, as discussed in section 2.3. Focusing our attention on the comparison with Cable Supported Bridges (CSB), the most important benefits of SFTs are the reduced environmental impact, both from the visual and air pollution points of view, perfect suitability for very large crossings and constant cost per unit length due to its modularity (Faggiano et al., 2005). The latter aspects are particularly interesting when comparing the effectiveness of this innovative structural typology with classical solutions such as Suspension Bridges (SB), which is the bridge typology holding the record of the longest span in the world. In fact, whereas the cost of a SFT increases linearly, the cost of a SB rises up way more rapidly as the crossing length increases, tending to become infinite as the main span length tends to a limit value, for which the suspension cable system is not even able to carry its own weight. Figure 8.1 illustrates qualitatively the trends of cost previously described.

It is worth underlining that similar considerations can be made with respect to cable-stayed bridges, which also feature a cost per unit length which increases as the main span length increases.

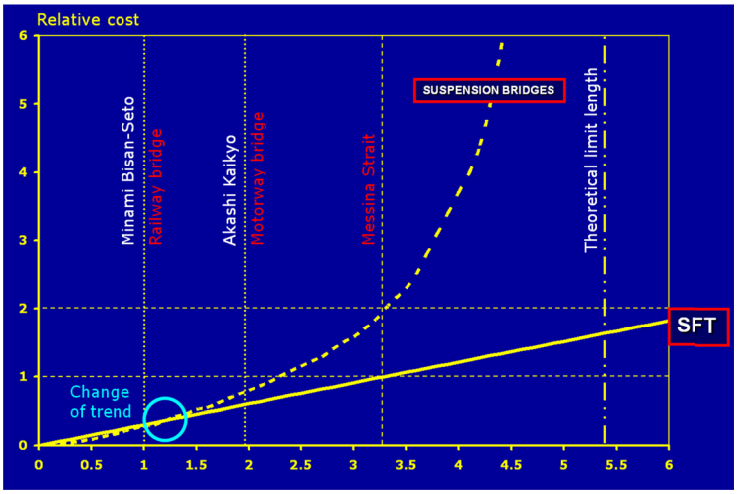

Figure 8.1. Qualitative cost trend curves for SFTs and SBs.

Concerning the comparison with underground and immersed tunnels, it is intuitive that, in moderately deep to deep waters, the reduced overall length of SFTs would lead to a substantial reduction of the structural cost, although the contribution of the anchorage system has to be added to the tunnel cost.

Economic aspects represent an issue of exceptional importance when the final structural solution to be realized in a waterway crossing has to be selected. Therefore it is fundamental to properly estimate the building cost of each available solution. Thus, simple procedures for the assessment of the cost of the crossing systems, such as the ones already developed by Gimsing (1996) for Cable Supported Bridges, have to be provided. In this chapter a similar procedure for Submerged Floating Tunnels is presented, which allows for quickly evaluating the cost of such an innovative crossing solution and for comparing its cost-effectiveness with the one of other traditional solutions, such as CSBs.

Some applications are also provided, considering different values of relevant geometrical and mechanical parameters, in order to highlight the conditions where the Submerged Floating Tunnel proves to be more economically competitive than traditional Cable Supported Bridges and to estimate the structural cost saving when the former ones are used instead of the latter ones.

8.2 SIMPLE PROCEDURES FOR THE ASSESSMENT OF CROSSING SOLUTION STRUCTURAL COST

8.2.1. General scheme of the cost evaluation procedure

In order to determine the optimal configuration of a cable supported bridge it is mainly necessary to estimate, beside of the structural performance, the structural cost, this being mainly due to the cost of the supporting system C_s and of the deck/tunnel C_d, as shown in equation 8.1:

$$C_{TOT} = C_{ss} + C_d \tag{8.1}$$

A procedure to assess the cost of the supporting system of Suspension and Cable-stayed Bridges has already been developed by Gimsing (1996). The costs relative to foundations, shore connections and anchor blocks are not considered in this simplified procedure. However, developing a simple procedure to estimate also their cost contribution and introducing it into (8.1) seems to be a fairly possible task.

8.2.2. Cable Supported Bridges (CSBs) cost assessment procedure

8.2.2.1. *Suspension bridges*

A symmetrical three-span suspension bridge, subjected to uniform dead load (g) and live load (p), is considered. The cost of the supporting system, made up of the cable system and pylons, can be evaluated through the procedure conceived by Gimsing (1996). The overall cable steel quantity is due to the quantities related to the main cable and the hangers in both the central and side spans. Reference is made to the geometric quantities illustrated in Figure 8.2.

The minimum cable steel quantity, needed to carry the assumed dead and live loads, for the main cable and the hangers in the central span (Q_{cm} and Q_{hm}, respectively) and in the side spans (Q_{ca} and Q_{ha}, respectively) are given by:

$$Q_{cm} = \frac{\gamma_{cb}}{f_{cbd}} \cdot (g + p) \cdot {l_m}^2 \cdot \frac{\sqrt{1+16\cdot\left({k_m}/{l_m}\right)^2}}{8\cdot{k_m}/{l_m} - \frac{\gamma_{cb}}{f_{cbd}}\cdot l_m \cdot \sqrt{1+16\cdot\left({k_m}/{l_m}\right)^2}} \cdot \left[1 + \frac{8}{3}\cdot\left({k_m}/{l_m}\right)^2\right] \tag{8.2}$$

$$Q_{hm} = \frac{\gamma_{cb}}{f_{cbd}} \cdot (\mathrm{g} + \mathrm{p}) \cdot (j_m + \frac{k_m}{3}) \cdot l_m \tag{8.3}$$

$$Q_{ca} = 2 \cdot \frac{\gamma_{cb}}{f_{cbd}} \cdot \frac{(\mathrm{g+p}) \cdot {l_m}^2 + Q_{cm}}{8 \cdot k_m} \cdot l_a \cdot \sqrt{1 + \left(\frac{k_m}{l_m} + 4 \cdot \frac{k_a}{l_a} + \frac{b_a}{l_a}\right)^2} \cdot$$

$$\cdot \left[1 + \frac{8}{3} \cdot \left(\frac{k_a}{l_a}\right)^2 + \frac{1}{2} \cdot \left(\frac{k_m + b_a}{l_a}\right) + \frac{l_e}{l_a}\right] \tag{8.4}$$

$$Q_{hm} = \frac{\gamma_{cb}}{f_{cbd}} \cdot (\mathrm{g} + \mathrm{p}) \cdot (j_m + \frac{k_m}{3}) \cdot l_m \tag{8.5}$$

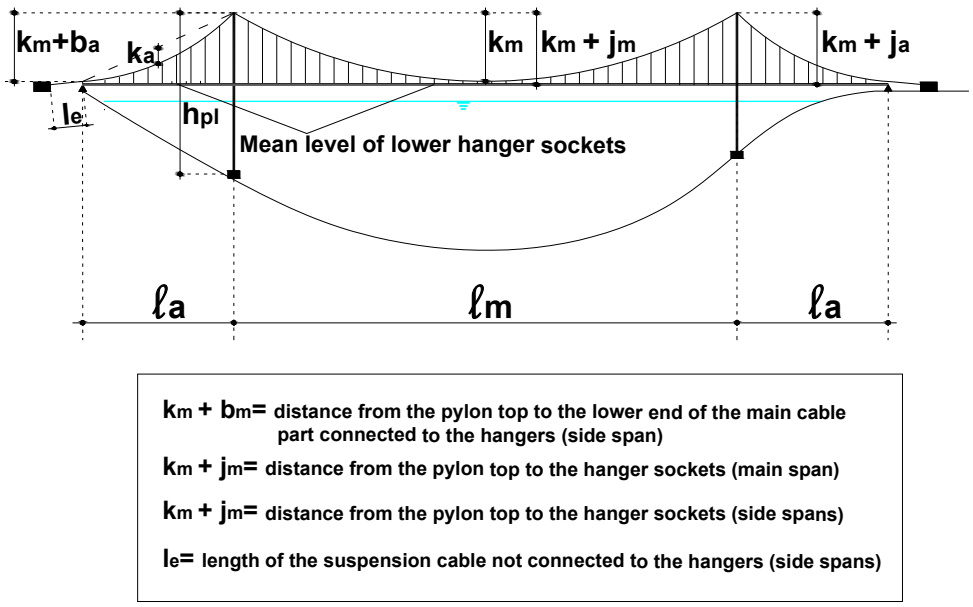

Fig. 8.2. Geometrical configuration of a symmetrical three-span Suspension Bridge.

where γ_{cb} and f_{cbd} are, respectively, the specific weight (including the weight increment due to coatings for corrosion protection) and the design strength of the cable steel, l_m and l_a are, respectively, the main span and side span lengths and k_m is the main span cable sag. The meaning of other symbols presented in equations 8.2 to 8.5 is given in Figure 8.2.

When optimizing the superstructure of a suspension bridge it is essential to take into account the variation in the quantities of the pylons. Assuming a

constant stress equal to f_{pld} throughout the pylon, the following equation for the necessary amount of steel for each pylon of a Suspension Bridge $Q_{pls,sb}$ can be derived (Gimsing, 1996):

$$Q_{pl,sb} = \frac{(g+p)\cdot l_m + Q_{cm}}{8} \cdot \left(\frac{k_m + 4\cdot k_a + b_a}{k_m} \cdot \frac{l_m}{l_a} + 4\right) \cdot \left[e^{\frac{\gamma_{pl}}{f_{pld}} \cdot h_{pl}} - 1\right] \quad (8.6)$$

where γ_{pl} and f_{pld} are, respectively, the specific weight and the design strength of the pylon steel (reduced to 60-80% of the material strength to take into account the stress induced in the pylons by the out of plane wind actions.

Therefore the total cost $C_{ss,sb}$ of the supporting system of a symmetrical three span suspension bridge is given by:

$$C_{ss,sb} = (Q_{cm} + Q_{ca} + Q_{hm} + Q_{ha}) \cdot u_{cb} + 2 \cdot Q_{pl,sb}.u_{pl} \quad (8.7)$$

where u_{cb} and u_{pl} are the unitary average prices for erected and protected suspension cable steel and pylon steel.

It is worth noticing that the maximum length of a suspension bridge, previously mentioned in section 8.1, can be calculated as the root of the denominator of equation 8.2. This theoretical limit length gives rise to the vertical asymptote depicted in Figure 8.1.

Assuming that the material quantity per unit length g related to the stiffening girder is constant, the cost of the deck C_d is equal to (u_d is the unitary average prices for erected girder steel):

$$C_d = g \cdot L \cdot u_d \quad (8.8)$$

It is evident that the material per unit length needed for the stiffening girder will vary with the crossing length; however these variations will be largely lower than those associated with the cable system and the pylons and it can be neglected in this preliminary cost assessment procedure.

8.2.2.2. *Fan Cable-Stayed Bridges*

A symmetrical three-span Fan Cable-Stayed Bridge, subjected to uniform dead load (g) and live load (p), is considered. The cable system is thus composed of the main and side fans, which are considered continuous (i.e. made up of an infinite number of elementary stays), for the sake of simplicity,

and of the anchor cables. On the basis of the previous assumptions and making reference to the geometrical dimensions illustrated in Figure 8.3, the cable steel quantities related to each fan in the main span Q_{Fm} and in the side span Q_{Fa} and to each anchor cable can be calculated through the following equations (Gimsing, 1996):

$$Q_{Fm} = \frac{\gamma_{cb}}{f_{cbd}} \cdot (\mathrm{g} + \mathrm{p}) \cdot \left[\frac{a_m}{5} \cdot \left(\frac{a_m}{h_F}\right)^4 + \frac{1}{3} \cdot \left(1 + 2 \cdot \frac{\gamma_{cb}}{f_{cbd}} \cdot h_F\right) \cdot \left(\frac{a_m}{h_F}\right)^3 + \right.$$
$$\left. + \left(1 + \frac{\gamma_{cb}}{f_{cbd}} \cdot h_F\right) \cdot \left(\frac{a_m}{h_F}\right)\right] \cdot h_F^2 \qquad (8.9)$$

$$Q_{Fa} = \frac{\gamma_{cb}}{f_{cbd}} \cdot (\mathrm{g} + \mathrm{p}) \cdot \cdot \left[\frac{1}{5} \cdot a_a \cdot \left(\frac{a_a}{h_F}\right)^4 + \frac{1}{3} \cdot \left(1 + 2 \cdot \frac{\gamma_{cb}}{f_{cbd}} \cdot h_F\right) \cdot \left(\frac{a_a}{h_F}\right)^3 + \right.$$
$$\left. + \left(1 + \frac{\gamma_{cb}}{f_{cbd}} \cdot h_F\right) \cdot \left(\frac{a_a}{h_F}\right)\right] \cdot h_F^2 \qquad (8.10)$$

$$Q_{ac} = \frac{\gamma_{cb}}{f_{cbd}} \cdot \left[\frac{1}{2} \cdot (\mathrm{g} + \mathrm{p}) \cdot a_m^2 - \frac{1}{2} \cdot g_a \cdot a_a^2 + \frac{1}{3} \cdot Q_{fm} \cdot a_m - \frac{1}{3} \cdot Q_{fa} \cdot a_a\right] \cdot$$
$$\left(\frac{a_a}{h_F} + \frac{h_F}{a_a}\right) \qquad (8.11)$$

where γ_{cb} and f_{cbd} are again, respectively, the specific weight and the design strength of the cable steel, a_m and a_a are, respectively, half of the main and side span lengths and h_f is the height of the fan cable system.

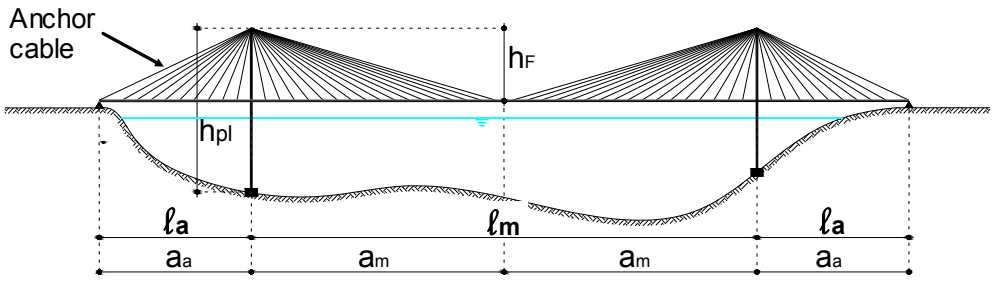

Figure 8.3. Symmetrical three-span Fan Cable-Stayed Bridge.

On the basis of the same assumptions made for the suspension bridge pylons, the necessary amount of steel for each pylon of fan cable stayed bridge Q_{plf} can be calculated (Gimsing, 1996):

$$Q_{pl,f} = \left[\frac{1}{2}\cdot(g_a + p_a)\cdot a_a + \frac{1}{2}\cdot(g_m + p_m)\cdot\left(2 + \frac{a_m}{a_a}\right)\cdot a_m + \frac{2}{3}\cdot Q_{Fa} + Q_{Fm}\cdot\left(1 + \frac{a_m}{3\cdot a_a}\right) + \frac{1}{2}\cdot Q_{ac}\right]\cdot\left[e^{\frac{\gamma_{pl}}{f_{pld}}\cdot h_{pl}} - 1\right] \quad (8.12)$$

The total cost $C_{ss,f}$ of the supporting system of a symmetrical three span fan cable-stayed bridge can be expressed as:

$$C_{ss,f} = 2\cdot(Q_{Fm} + Q_{Fa} + Q_{ac})\cdot u_{cbc} + 2\cdot Q_{pl,f}.u_{pl} \quad (8.13)$$

where u_{cbc} and u_{pl} are the unitary average prices for erected and protected cable stays steel and pylon steel.

The cost of the stiffening girder/deck can be estimated again through (8,8)

8.2.2.3. *Harp Cable-Stayed Bridges*

A symmetrical three-span Harp Cable-Stayed Bridge with supported side spans, subjected to uniform dead load (g) and live load (p), is considered. The cable system is thus composed of the main and side fans, which are considered continuous, for the sake of simplicity. Considering the geometrical dimensions illustrated in figure 8.4, the cable steel quantities related to each fan in the main span Q_{Hm} and in the side span Q_{Ha} can be determined through the following relationships (Gimsing, 1996):

$$Q_{Hm} = \frac{\gamma_{cb}}{f_{cbd}}\cdot(g_m + p_m)\cdot\frac{a_m^2 + h_H^2}{a_m\cdot h_H}\cdot\left(\frac{1}{2} + \frac{\gamma_{cb}}{f_{cbd}}\cdot\frac{a_m^2 + h_H^2}{3\cdot h_H}\right)\cdot a_m \quad (8.14)$$

$$Q_{Ha} = \frac{\gamma_{cb}}{f_{cbd}}\cdot(g_m + p_m)\cdot\frac{a_a^2 + h_H^2}{a_a\cdot h_H}\cdot\left(\frac{1}{2} + \frac{\gamma_{cb}}{f_{cbd}}\cdot\frac{a_m^2 + h_H^2}{3\cdot h_H}\right)\cdot a_m \quad (8.15)$$

where γ_{cb} and f_{cbd} are again, respectively, the specific weight and the design strength of the cable steel, a_m and a_a are, respectively, half of the main and side span lengths and h_f is the heigth of the fan cable system.

In the harp system the pylon is subjected to the forces from the cable system evenly distributed along the entire height above the girder, differently from the suspension and fan system. The pylon of the harp system should therefore be made with a pronounced variation of cross-section in order to keep the normal stress equal in the whole pylon. In a preliminary investigation it is sufficiently accurate to assume that the pylon cross-section area varies

linearly from 0 at the top of the pylon to the value strictly necessary ($\sigma=f_{pld}$) to carry the cable forces and the pylon own weight. The portion of the pylon placed below the girder behaves in the same manner of the pylons of suspension and fan systems. It is thus possible to derive the following expression for the pylon steel quantity $Q_{pl,h}$ as the sum of the contributions due to the pylon portions above (Q_{pt}) and below (Q_{pb}) the girder level (Gimsing, 1996):

$$Q_{pl,h} = Q_{pt} + Q_{pb} \tag{8.16}$$

$$Q_{pt} = \frac{\gamma_{pl}}{f_{pld}} \cdot \frac{(g_m+p_m)\cdot(a_m+a_a)\cdot a_m+\left(\frac{1}{2}a_m+a_a\right)\cdot Q_{Hm}+\frac{1}{2}a_a\cdot Q_{Ha}}{2-(\gamma_{pl}/f_{pld})\cdot h_{pt}} \cdot \frac{h_{pt}}{a_a} \tag{8.17}$$

where h_{pt} and h_{pb} are the height of the portion of the pylons above and below the girder, respectively.

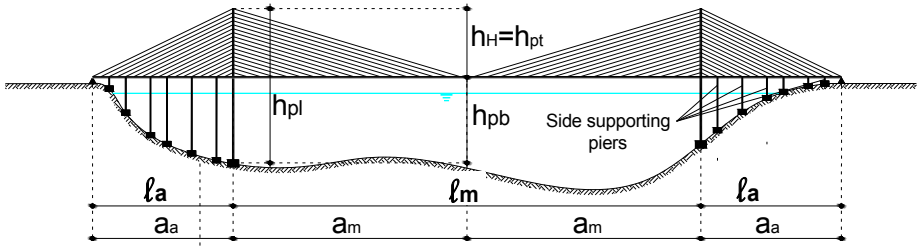

Figure 8.4. Symmetrical three-span Harp Cable-Stayed Bridge with supported side spans.

The total cost $C_{ss,h}$ of the supporting system of a symmetrical three span fan cable-stayed bridge can thus be expressed as:

$$C_h = 2 \cdot (Q_{Hm} + Q_{Ha}) \cdot u_{cbc} + 2 \cdot Q_{pl,f} \cdot u_{pl} \tag{8.18}$$

8.2.3. Submerged Floating Tunnels cost assessment procedure

The cable system of a Submerged Floating Tunnel is made up of single groups of anchorages, generally lying in the plane of the tunnel cross-section, located along the tunnel axis with a fixed inter-axis. Therefore the total cost of the supporting system $C_{ss,sft}$ is simply given by the sum of the costs of each anchorage group $C_{ag,i}$. The SFT is considered to be subjected only to the

permanent residual buoyancy rb, as the live loads reduce the cable tension forces. The geometrical configuration of the cable system is depicted in Figure 8.5: the geometrical arrangement of the cable groups is the W-shaped one, it being the most effective one (Martire et al., 2009). Clearly another configuration could be easily considered in place of the W-shaped one.

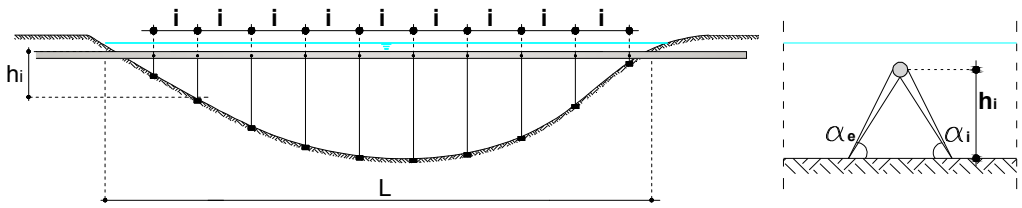

Figure 8.5. Geometrical configuration of a Submerged Floating Tunnel.

The cost of the SFT anchoring system can be thus assessed through the simple following equation:

$$C_{ss,sft} = \sum_{i=1}^{n} \frac{\gamma_a}{f_a} \cdot \frac{rb \cdot i}{2} \cdot (h_i/(\sin \alpha_e)^2 + h_i/(\sin \alpha_i)^2) \cdot u_a \qquad (8.19)$$

where α_e and α_i are the inclination of the external and internal anchorages, i is the inter-axis between subsequent anchorage groups, γ_a and f_a are, respectively, the specific weight and the design strength of the material used for the anchorages and u_a is the average unitary price of the SFT anchorages.

Equation 8.19 does not take into account hydrodynamic or seismic forces, similarly to the equations showed in previous sections for CSBs, where the contribution of wind forces is not considered. However, since the anchorages of SFTs are inclined in the tunnel cross-section plane, the stress increments due to hydrodynamic and seismic actions are larger than the ones induced in the cable system of CSBs by wind or seismic forces. Thus it is worth to modify (8.19) in order to take into account also the hydrodynamic forces:

$$C_{ss,sft} = \frac{\gamma_a}{f_a} \cdot u_a \cdot \sum_{i=1}^{n} \left(\frac{rb \cdot i}{2} + \frac{F_v \cdot i}{2} \Big/ \sin \alpha_e + \frac{F_v \cdot i}{2} \Big/ \cos \alpha_e \right) \cdot (h_i/\sin \alpha_e) +$$
$$\left(\frac{rb \cdot i}{2} + \frac{F_v \cdot i}{2} \Big/ \sin \alpha_e + \frac{F_v \cdot i}{2} \Big/ \cos \alpha_e \right) \cdot (h_i/\sin \alpha_i) \qquad (8.20)$$

where F_v and F_i are the maximum value of the vertical and horizontal components of the hydrodynamic loads induced by waves and currents, as computed by the Morison's equation in its static version (i.e. assuming that the tunnel velocities and accelerations are equal to zero).

The tunnel cost C_d can be evaluated analogously to (8.8), as the tunnel cost per unit length is actually independent of the tunnel length. Clearly the average unitary price of the tunnel will be different from the one of the CSB girder/deck system; its value will depend on the type and quantity of materials used to build the tunnel structure.

8.3 COST COMPARISON BETWEEN SUSPENSION BRIDGES AND SFTS

8.3.1. The case studies of the Messina Strait and Akashi Strait

The Akashi Strait, crossed by the suspension bridge featuring the largest main span in the world (1991 m), and the Strait of Messina, where a suspension bridge having a main span of 3300 m is planned to be built, are selected as case studies, in order to perform a cost comparison between the most advanced Suspension Bridge (SB) designs up to now and SFT preliminary proposals, assumed to be built in the same locations and to hold the same number of motorways and railways. It is worth underlining that the SB of the Akashi Strait features a heavy steel truss stiffening girder whereas the design of the SB for the Messina Strait crossing features a light streamlined stiffening girder; thus the two major design philosophies currently used for SBs (see section 1.1.2) are represented by the considered case studies.

The SFT proposed for the Strait of Messina crossing features a steel shell-concrete circular cross-section whereas the one considered for the Akashi Strait have a steel-concrete rectangular cross-section, with lateral steel keels having a hydrodynamic shape (Figures. 8.6 and 8.7). Both of the aforementioned structural solutions are considered and the cheaper ones finally selected for both case studies.

The anchorage system of SFTs is made up of W-shaped groups of cables in both cases.

The proposed SFT solutions were designed considering the stresses induced by the residual buoyancy and the hydrodynamic actions due to extreme wave and currents foreseen in the considered location and assuming a flat seabed profile, having a depth equal to the average one (250 m for the Strait of Messina, 80 m for the Akashi Strait).

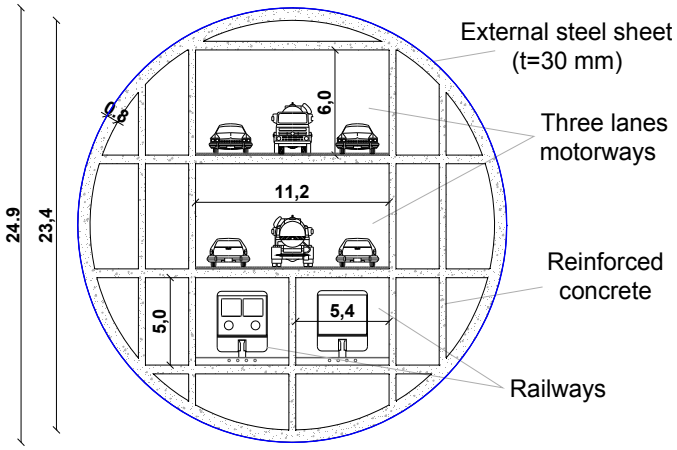

Fig. 8.6. SFT cross-section proposal for the Strait of Messina (Italy).

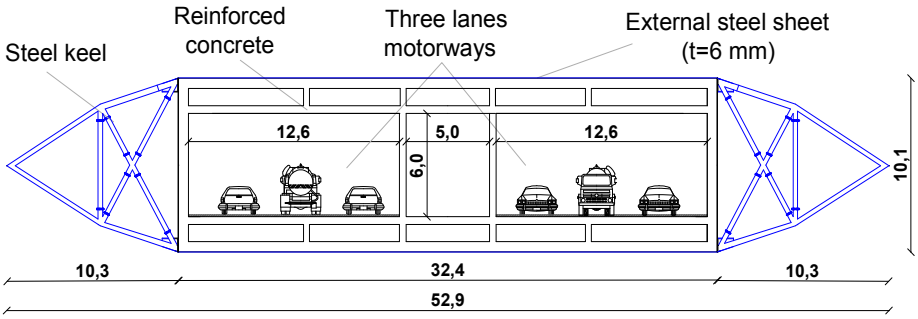

Fig. 8.7. SFT cross-section proposal for the Strait of Akashi (Japan).

The quantity of materials involved in the construction of the SBs in the Strait of Messina and Akashi Strait can be found in literature (Jansen, 2009). It is thus possible to estimate the total cost of the considered SFTs and suspension bridges, once the cost per m^3 of each material is defined, according to the indications given in Gimsing (1996) and in the Bulletin of prices for

Public Infrastructures of Campania Region (2009). The assumed unitary costs, being dimensionless as they are divided by the unitary cost of steel S460, are given in Table 8.1.

Tables 8.2 and 8.3 show the amount of materials involved in the construction of the SB and SFT for the Messina Strait and Akashi Strait, respectively.

Table 8.1. Dimensionless cost/m^3 of constructional materials used for SBs and SFTs in the Messina and Akashi Strait

Material	Cost/m3 [-]
Concrete C30/35	0.022
Steel S355	0.945
Steel S420	0.985
Steel S460	1.000
Steel S690	1.125
Cables steel (SB)	1.000
Cable steel (SFT)	2.000
Ballast	0.009

Table 8.2. Amount of materials used for SB and SFT in the Messina Strait

Material	SB [kg]	SFT [kg]
Concrete C30/35	0	964590000
Steel S355	18900000	40102920
Steel S420	8300000	0
Steel S460	143500000	0
Cables steel	154310000	31207000
Ballast	0	10296000

Table 8.3. Amount of materials used for SB and SFT in the Akashi Strait

Material	SB [kg]	SFT [kg]
Concrete C30/35	0	83214575
Steel S355	18900000	44875070
Steel S460	28800000	0
Steel S690	90000000	0
Cables steel	51300000	1068900
Ballast	0	38865400

Figures 8.8 and 8.9 shows the comparison of the total cost of the SB and SFT solutions for both case studies, also highlighting the different contributions in terms of structural elements (cable system, pylons and deck/tunnel) and materials involved (r.c., different grades of steel, steel for cables, ballast).

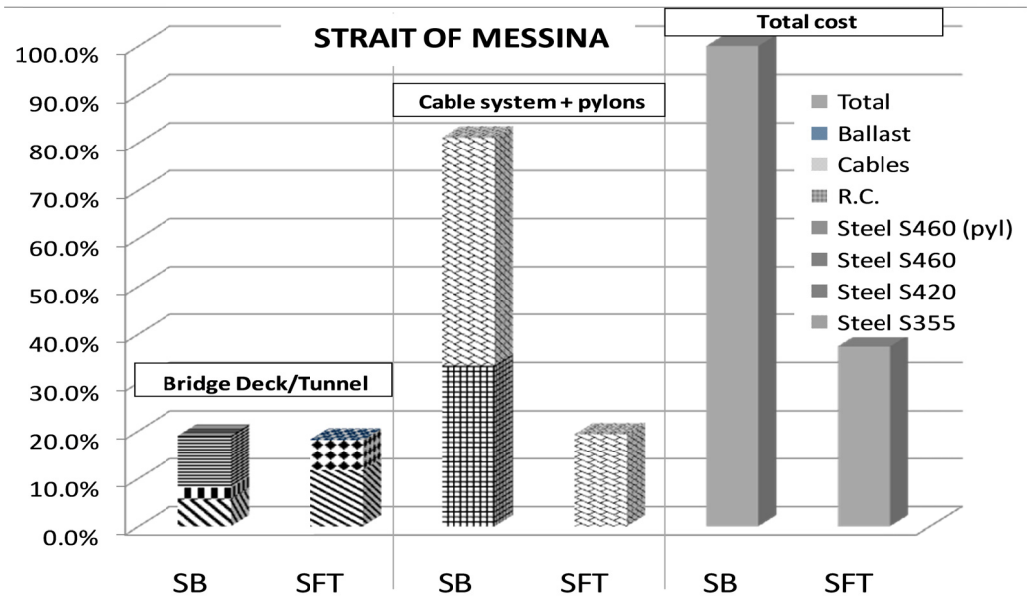

Figure 8.8. Comparison of the cost of SFT and SB solutions for the Messina Strait.

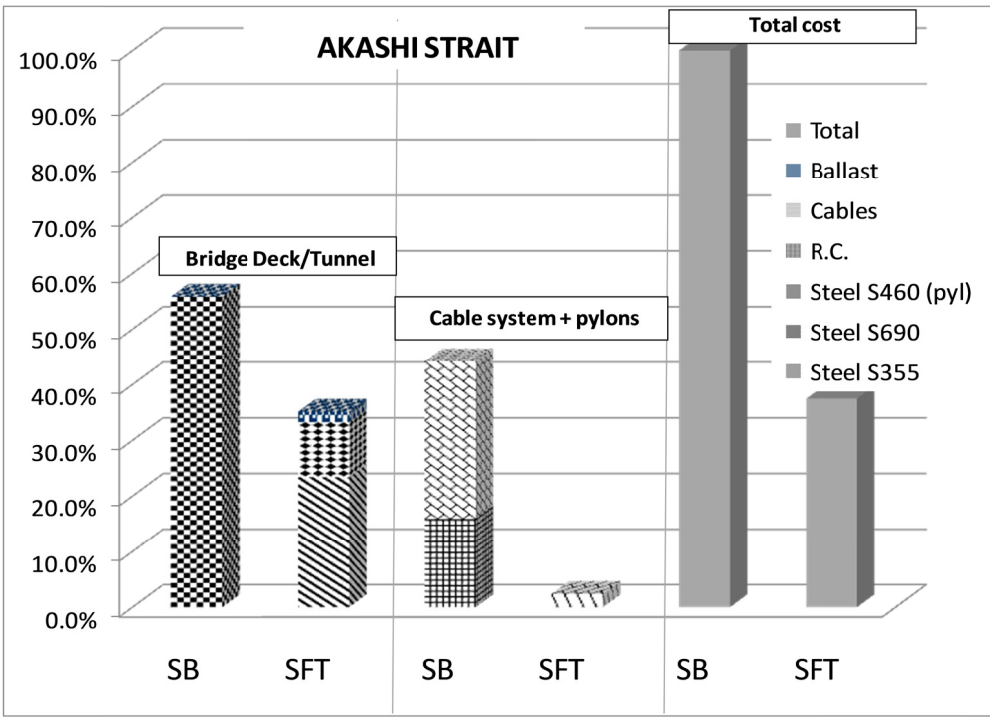

Figure 8.9. Comparison of the cost of SFT and SB solutions for the Akashi Strait.

The presented costs are divided by the total cost of the SB solution, in both case studies, thus being dimensionless. It can be immediately noted that the SFTs total cost is largely lower in both case studies, it being 37,4% (Messina) and 36,3% (Akashi) of the cost of the relative SB, basically due to the huge reduction of the cost of the supporting system. In fact SFT cable system cost is the 2,7% (Akashi Strait) and 23.3% (Messina Strait) of the cost of the SB supporting system (cable plus pylons). In the case of the Akashi Strait the difference between the cost of the SB and SFT supporting systems is so important due to the large weight of the SB truss/deck system, which leads in turn to a large amount of steel required for the pylons and cables, and to the moderate water depth, leading to a modest amount of steel required for the anchorage system of the SFT.

Furthermore, despite of the larger amount of materials necessary to build the tunnel structure of a SFT, its cost turns out to be very close to the one of

the SB deck for the Strait of Messina crossing, whereas it is the 62,9% of the cost of the SB deck for the Akashi Strait case, where the very large amount of steel required for the stiffening truss leads to a huge cost of the SB girder/deck system.

This result is due to the fact that, differently from the SBs, there is no need to minimize the weight of the SFT tunnel structure; in fact this weight is beneficial, contributing, together with the provided ballast, to reduce the residual buoyancy to the desired design value. Therefore reinforced concrete, less effective but considerably cheaper than steel, can be largely used, thus reducing the average unitary price of the SFT tunnel structure

Finally, it is worth underlining that the previous cost comparison is made between completely designed SBs and preliminary designs of SFTs. Moreover, the cost of the SB anchor blocks and of the foundations of the SFT anchorage groups is not considered. Therefore the proposed results may slightly differ from actual and definitive ones; however, due to the large scatter between the cost of SFTs and SBs, SFT would still prove to be largely cheaper.

8.3.2. Application of the cost evaluation procedure for Suspension Bridges and Submerged Floating Tunnels

A numerical application of the relationships introduced in section 8.2.2 is carried out, with the purpose of providing useful abaci for the selection of the most efficient structural solutions for strait crossings, given the crossing length and water depth.

In particular, a comparison between the structural costs of a SFT and a Suspension Bridge (SB) crossing waterways, with variable lengths L and a flat seabed profile, is considered. The SB is assumed to have a main span length l_m equal to the waterway length L, thus resembling the configuration of the Strait of Messina Bridge (Figure 8.10).

Two set of geometric and mechanical data of the SB are considered, namely C1 and C2, the first one leading to the largest structural cost whereas the second one leads to the lowest one. The values adopted for the relevant geometrical parameters are reported in Table 8.3 for both set of data. The assumed values for the mechanical parameters are shown in Table 8.4.

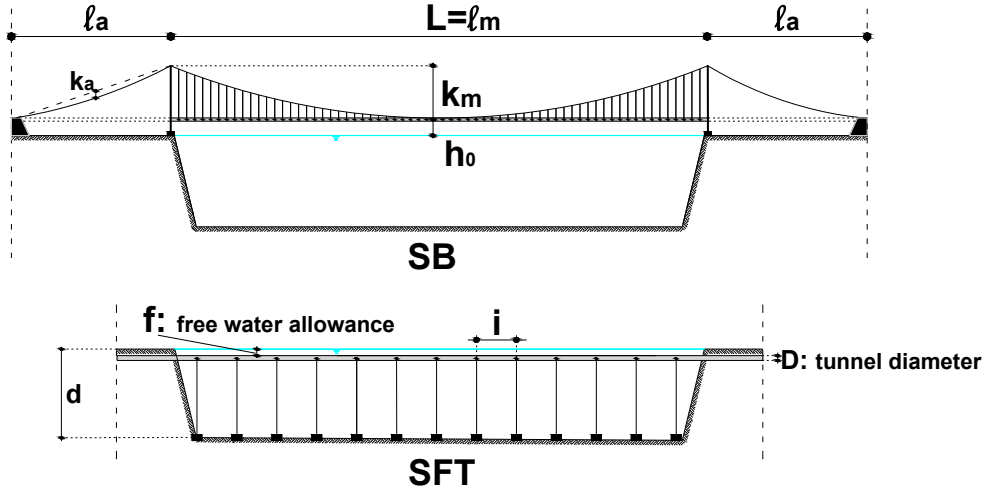

Figure 8.10. Geometrical configuration of the considered Suspension Bridge and Submerged Floating Tunnel.

Table 8.3. Set of geometrical data assumed

	D [m]	f [m]	h_0 [m]	ℓ_m	ℓ_a	k_m
C1	25	25	70	L	$0.5\cdot\ell_m$	$0.08\cdot\ell_m$
C2	25	25	30	L	$0.25\cdot\ell_m$	$0.12\cdot\ell_m$

Table 8.4. Set of mechanical data assumed

	γ_{cb} [MN/m^3]	γ_{pl} [MN/m^3]	$f_{cb,d}$ [MN/m^2]	$f_{pl,d}$ [MN/m^2]
C1	0.10	0.0785	1000	320
C2	0.08	0.0785	1860	320

The design strength of the pylon steel f_{pld} is reduced to 60-80% of the material strength to take into account the stress induced in the pylons by the out of plane wind actions.

The SB permanent loads g are assumed to be equal to 0.24 MN/m, which is a common value for a SB featuring a slender aerodynamic deck. For the live

loads p, a value of 0.16 MN/m, corresponding to a motorway plus railway crossing, is considered. The cost of the tunnel structure for SFTs is set equal to the cost of the SB deck, as it was found previously for the Messina Strait case study. The crossing length L, the seabed depth d and the residual buoyancy rb acting permanently on the SFT are considered as variables, in order to assess their influence and importance on the cost of the three crossing typologies considered.

The unitary cost u_{pl} of the steel used for the pylons is set equal to 1 and all the other unitary costs are defined proportionally to it. Table 8.5 illustrates the assumed values for the unitary costs, which are selected on the basis of the indications given in Gimsing (1996). No indications are available concerning the unitary cost of the anchorages of SFTs, thus it is assumed that their cost is equal to two times the cost of the cables of suspension bridges.

These unitary average prices are here assumed to be independent with respect to geometrical parameters such as the bridge main span length and to the sag-to-main span ratio (which determines the height of the supporting system). It is recognized that it would be more realistic to assume the average unitary prices to vary, through a function defining the values of these prices according to the value of the aforementioned geometrical parameters. However, such a kind of function should be defined on the basis of a large amount of data relative to the cost of existing bridges, featuring different values of the main span length and of the main span cable sag, and this data base is not available at the moment.

Table 8.5. Dimensionless values assumed for the materials unitary costs

	u_{pl} [-]	$u_{cb,SB}$ [-]	$u_{a,SFT}$ [-]	u_d [-]
C1	1.0	1.25	2.5	1.0
C2	1.0	2.0	4.0	1.0

Figures 8.11 and 8.12 show the comparison of the cost trend curves of SFTs and SBs as the crossing length and the seabed depth vary. The upper bound (SB1-SFT1) and the lower bound curves (SB2-SFT2) define a cost band for each of the two considered structural typologies, enclosing the cost of

any potential intermediate configurations between the ones characterized by the sets of data C1 and C2. The curves are dimensionless, as the actual costs are divided by a reference cost, assumed equal to the one of the Messina Strait suspension bridge. In particular, the curves in Figure 8.11 are referred to a variable crossing length, assuming d=200 m and rb_k=0,7 MN/m, while curves in Figure 8.12 consider a variable seabed depth and a fixed length L equal to 3000 m; clearly SFTs feature a lower limit for the seabed depth ($d_{min,SFT}$) allowing for their realization, it corresponding to the condition where the SFT cables would feature a null length.

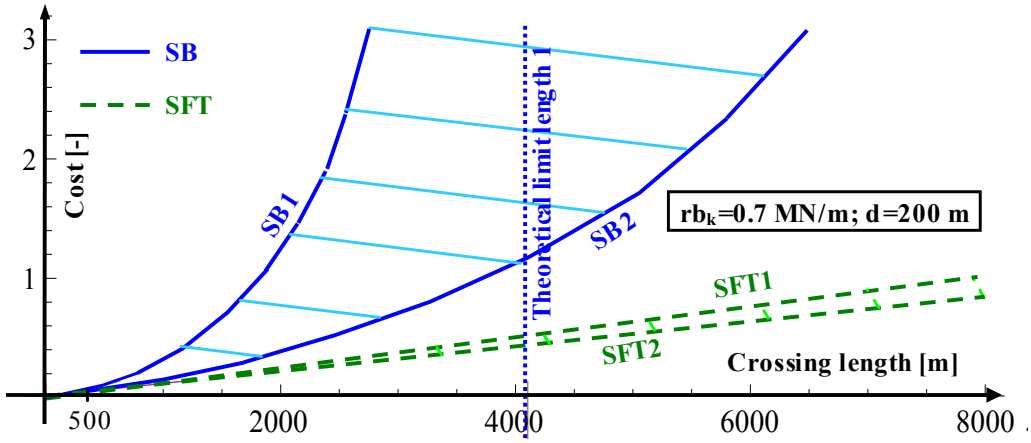

Figure 8.11. SFT and SB cost curves as a function of the crossing length (rb_k=0,7 MN/m; d=200 m).

It can be noticed that the SFT solution is noticeably cheaper than the SB one, particularly for large values of the crossing length; as a matter of fact, Suspension Bridges are economically competitive with SFTs only for crossing lengths being lower than 500 m. Furthermore, also for very large values of the seabed depth the SFT is largely less expensive than suspension bridges. It is worth noticing that the cost of SBs does not increase as the seabed depth increases, the pylon height not being influenced by it for the assumed geometrical configuration (Figure 8.10). However, it has to be recognized that the assumed value of rb_k is very low for a SFT holding both motorways and railways.

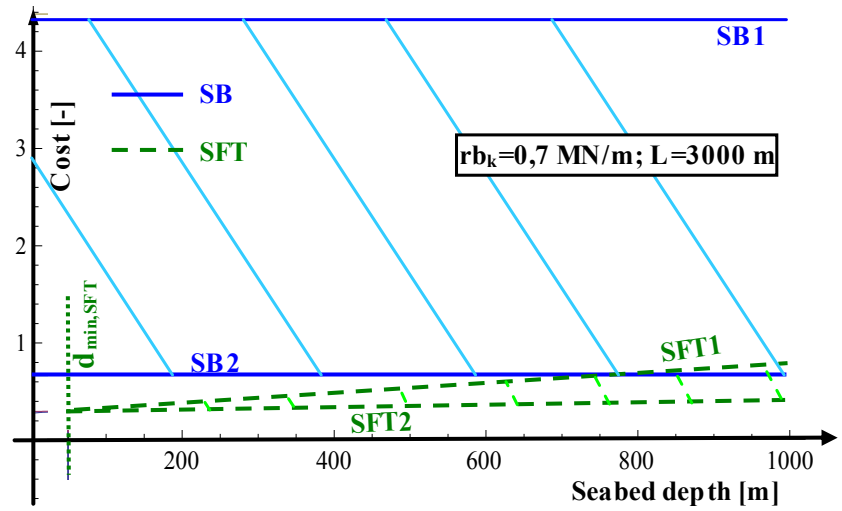

Figure 8.12. SFT and SB cost curves as a function of the seabed depth (rb_k=0,7 MN/m; L= 3000 m).

The comparison between SFTs and SBs cost curves becomes less disadvantageous for the SBs if larger values of rb_k and d, and lower values of L, are considered, as shown in figure 8.13 and 8.14, where a quite large value of rb_k, equal to 1,5 MN/m, a very large value of the seabed depth d, equal to 600 m, and a quite short value of the crossing length L, equal to 500 m, are considered.

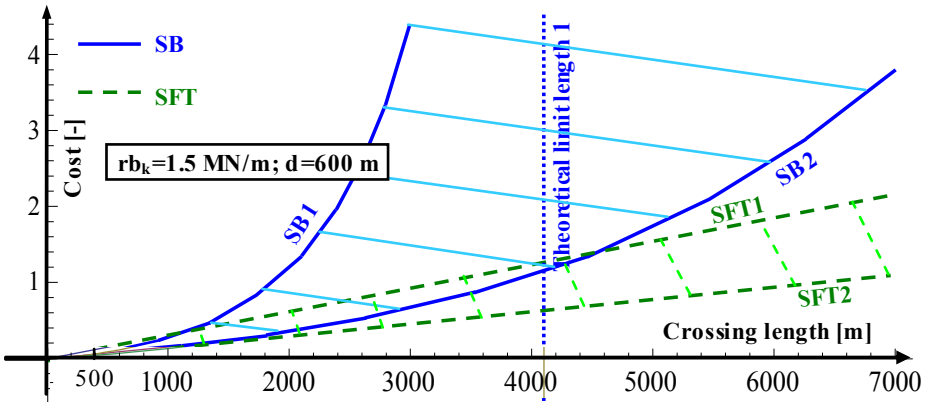

Figure 8.13. SFT and SB cost curves as a function of the crossing length (rb_k=1,5 MN/m; d=800 m).

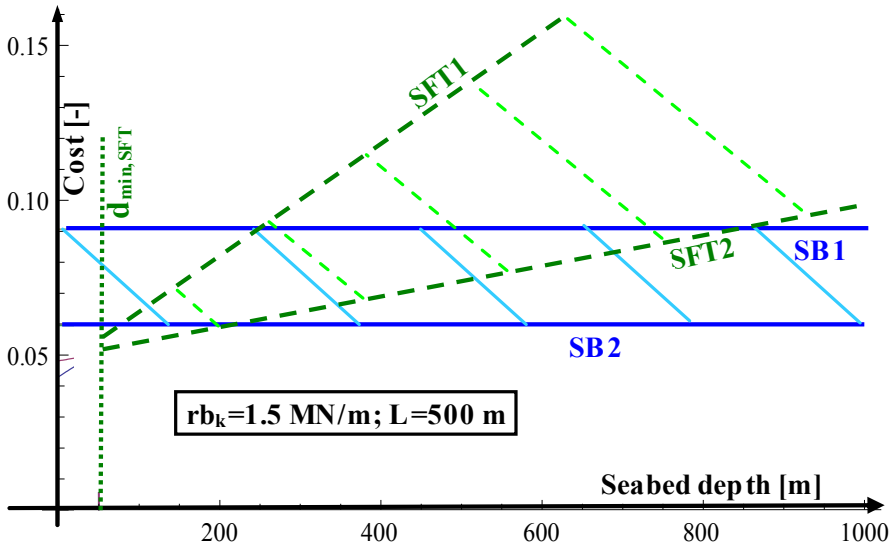

Figure 8.14. SFT and SB cost curves as a function of the crossing length (rb_k=1,5 MN/m; L=500 m).

As a matter of fact, the SB solution turns out to be economically competitive with the SFT one even for larger crossing lengths: the intersection between the mid-lines of the two cost bands occurs at a value of the crossing length approximately equal to 2700 m (Figure 8.13) in the cost-crossing length plane at a value of the seabed depth approximately equal to 300 m (Figure 8.14) in the cost-seabed depth plane. However, the SFT solution still proves to be largely more economically effective than the classic SB one.

8.4 CONCLUSIVE REMARKS

The simplified procedure presented in this chapter, for the assessment of the structural cost of a Cable Supported Bridge, similar to the one proposed by Gimsing (1996) but here including the innovative typology of Submerged Floating Tunnels, allows to quickly compare the overall cost of the superstructure, therefore constituting an important tool to help making decisions during the early stage of a waterway crossing planning.

The proposed procedure could be improved in the future, still keeping its simplicity, by estimating also the cost of the anchor blocks and pylons

foundations of the SBs and the cost of the foundations of the anchorages and the shore connections of the SFTs.

Two noticeable case studies are considered to compare the cost of potential SFT solutions and of actual SB designs: the Messina and Akashi Straits. The obtained results show that in both cases the proposed SFT solutions are considerably less expensive than the corresponding suspension bridges, as the SFTs cost approximately 1/3 of the SBs. In particular, it is the enormous difference in the supporting system cost that gives rise to such a large scatter between the SFT and SB overall costs, whereas the cost of the tunnel structure can be lower or equal than the cost of the girder/deck system of a Suspension Bridge, depending on whether the latter is made as an heavy truss or a light streamlined girder.

The cost assessment procedure developed is applied and a comparison between the cost trend curves relative to SFTs and SBs is made, considering different values of the geometrical and mechanical parameters governing the problem. The obtained curves confirm that the SFT solution is largely cheaper than traditional SB one, particularly when large distances have to be surpassed. The seabed depth and the residual buoyancy acting on the SFT are the other parameters that mainly influence the cost comparison between these structural typologies: in fact, as the value of these parameters increases, SBs become more economically competitive with SFTs. However, the SFT solution still proves to be largely more economically effective than the classic SB one.

These remarks, together with the other advantages assured by SFTs (see section 2.3), confirm the great potentialities of this revolutionary strait crossing solution.

Chapter 9
Future challenges and conclusive remarks

9.1 A NEW CHALLENGE: CABLE SUPPORTED IMMERSED INVERSED BRIDGES

9.1.1. Cable Supported Immersed Inversed Bridge solutions

Many similarities and aspects in common exist between conventional Cable Supported Bridges and Submerged Floating Tunnels, concerning the loading conditions, the anchorage system and the tunnel/deck cross-section (Mazzolani et al, 2009; Faggiano et al., 2010); some of these aspects have been discussed in Chapter 2. It is therefore worth it to investigate the possibility of transferring some of the knowledge and technologies already developed for the CSBs to the field of the SFTs.

Moreover, it is possible to develop new proposals of floating tunnels, involving cable system arrangements analogous to those commonly used in suspension and cable-stayed bridges. In fact the cable systems usually adopted for cable supported bridges can be combined with the floating tunnel concept, obtaining structural solutions which could be competitive with traditional cable supported bridges and, in some cases, also with the Submerged Floating Tunnels solutions up to now proposed.

As depicted in Figure 9.1, the idea of exploiting the bearing capacity of the water can be used to realize a suspension bridge featuring cable system having the usual configuration but being mirrored with respect to the water surface; this structural solution can be described as an “immersed inversed suspension bridge”. Similarly, structural solutions analogous to fan type and harp type

cable stayed bridges can be envisaged, thus giving rise to the "Immersed Inversed Fan Cable Stayed Bridge" (Figure 9.2) and the "Immersed Inversed Harp Cable Stayed Bridge" (Figure 9.3). In Harp Cable-Stayed bridges it is usual to stabilize the cable system providing intermediate supports in the side span, so that the stiffness of the system is considerably increased; in their immersed versions a similar solution could easily be adopted by means of vertical cable groups or piers (depending on whether the force to be transmitted is a compressive or tensile force) connecting the tunnel to the seabed in the stays anchoring points of the side span. Finally, the combination of the suspension system and the fan cable-stayed system can be considered too (Figure 9.4), this being a competitive solution in the long span range.

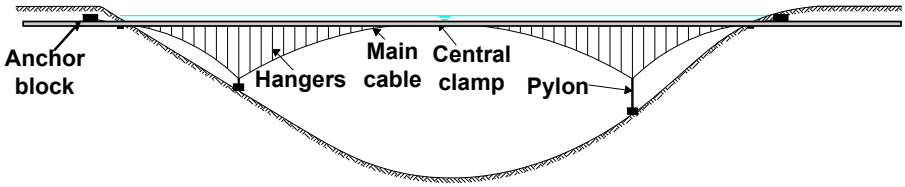

Figure 9.1. Longitudinal view of the Immersed Inversed Suspension Bridge.;

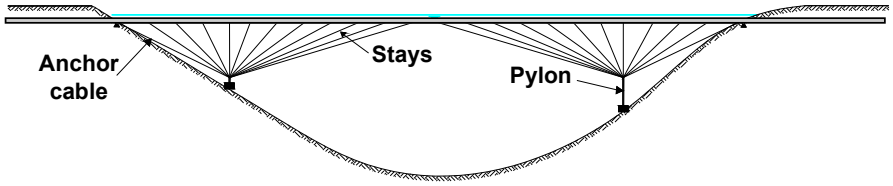

Figure 9.2. Longitudinal view of the Immersed Inversed Fan Cable-Stayed Bridge.

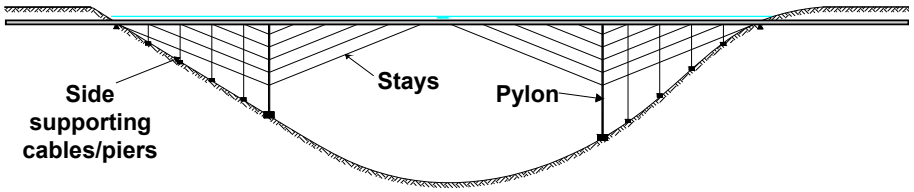

Figure 9.3. Longitudinal view of the Immersed Inversed Harp Cable-Stayed Bridge.

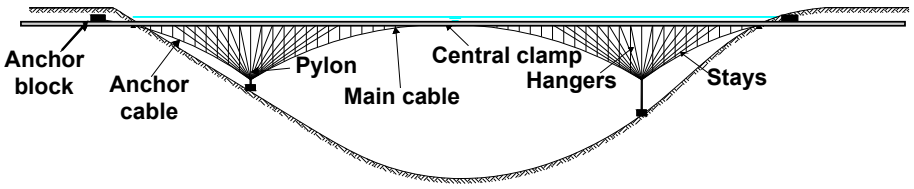

Figure 9.4. Longitudinal view of the Immersed Inversed Combined Suspension Cable-Stayed Bridge.

Clearly the idea of a Cable Supported Immersed Inversed Bridge (CSIB) makes sense only if the water depths are large enough to allow for the realization of cable systems economically competitive. In fact, given a certain span length and a uniform load to be carried, the necessary cable steel quantity significantly reduces as the cable system height increases in the lower height range(Gimsing, 1996). As a matter of fact suspension bridges usually feature h/ℓ ratio (h= height of the cable system; ℓ = span length) equal to about 1/10, due to the limitations imposed by the stiffness requirements, whereas larger values are considered for cable-stayed bridge. It is also worth noticing that slightly larger values of this ratio can be considered for immersed suspension bridges, as the deformability issues related to the presence of live loads is less relevant, due to the higher value of the permanent loads (i.e. the residual buoyancy).

Pylons of Cable Supported Bridges accomplish the double task of supporting the cable system and the stiffening girder, in particular in the lateral plane. In long span bridges the use of spatial cable systems could provide a significant improvement of the structure lateral and aerodynamic stability. Pylons having a “Y-shape” are needed when cables are disposed in laterally inclined planes (Figure 9.5). However, this is not the optimal structural solution for the lateral stability of the pylons themselves and would complicate their erection procedures.

In the case of Cable Supported Immersed Inversed Bridges, the pylon could be realized with an inverse Y or V shape (Figure 9.6), which are more rational structural schemes. Moreover, as the vehicular traffic takes place inside the tunnel, there would be no clearance requirement conditioning the cable transversal inclination, as it occur in case of a spatial Cable Supported Bridges.

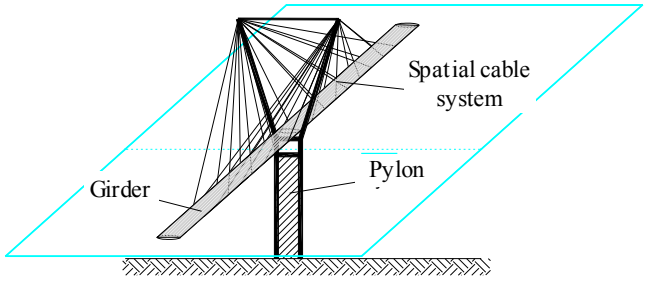

Figure 9.5. Sketch of possible pylon configuration for spatial cable system in a Cable Supported Bridge.

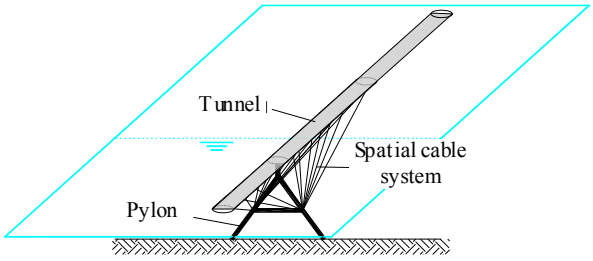

Figure 9.6. Sketch of possible pylon configuration for spatial cable system in a Cable Supported Immersed Inversed Bridge.

In CSBs, when the seabed depth at the pylons location is such that the main cables of the suspension system or the cable stays of the fan type system can be anchored directly to the seabed, the pylons would only serve as intermediate support for the tunnel. Therefore it would be convenient to substitute the pylon with one or more anchorage groups, as shown in Figure 9.7 (on the left side).

More generally, for suspension systems and fan cable-stayed system, the pylon can be interrupted at the height where the cables are anchored, providing additional vertical cables connecting the top of the pylon with the tunnel and inclined earth anchored cables restraining laterally the tunnel (Figure 9.7, on the right side). This would imply a higher tension force to be carried by the pylon foundations, as the benefic effect of the pylon weight would be lost or reduced, but the cost savings would still be convenient.

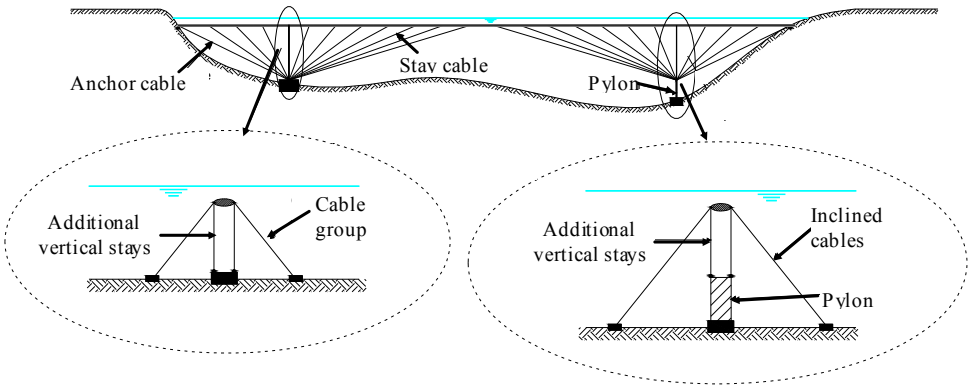

Figure 9.7. Possible variations of the configuration at the pylon location.

9.1.2. Main advantages of CSIB

The CSIB solutions present several advantages if compared to their corresponding traditional solutions.

First of all, as the tunnel would be placed 20 to 50 meters below the water surface, the water velocities taking place during a storm event would be considerably lower than the wind velocities occurring at the height where the deck of cable supported bridges are usually located. Thus the aerodynamic stability problem, representing the major issue for long span cable supported bridges, should be of minor concern for immersed bridges.

The own weight of the cables is beneficial, as it reduces the tensile force induced in the cables by the residual buoyancy, whereas in traditional CSBs the structural own weight can represent a large part of the load to be carried by the supporting system, as shown in section 8.2.2.

Furthermore, the realization of a spatial cable systems providing also a lateral support to the tunnel is more easily feasible (see section 9.1.1).

The pylons could also be realized with a significant material saving. As a matter of fact, given a certain seabed profile, in a traditional solution the overall pylon height would be equal to the sum of the seabed depth and the relative pylon height over the water surface whereas for the immersed solutions the pylon height would be lower than the seabed depth and, if the seabed depth allows it, the pylon can be substituted by a more economic cable group (see section 9.1.1). Moreover, in CSIB the own weight of the pylon has a positive

effect, as this counterbalances the vertical upward force transmitted to the pylon itself by the cable system. At the same time, also in the case of the pylons, the structural own weight reduces the tension force to be transmitted to the ground, thus reducing also the foundation costs.

CSIBs do not interfere with the vessel traffic over the water surface, so that the geometry of the system, i.e. the length of the main span and of the side spans, is only influenced by structural reasons, besides of the seabed profile.

Cable Supported Immersed Inversed Bridges are invisible structures, so that the problem of the visual environmental impact of the crossing would be totally resolved in those locations where the natural landscape has to be protected. Moreover, also the air pollution production can be faced in a more effective way considering that inside a tunnel the gas emissions due to vehicular traffic can be treated by means of modern air purification plants.

Clearly, also some specific issues must be faced, such as the attention to the hydrostatic pressure permanently stressing the tunnel and the need for various submarine operations during the construction phases and for maintenance during the service life.

Concerning the comparison with the "classic" Submerged Floating Tunnel solution, in crossings cases featuring intermediate water depths (i.e. lower than 200 m) and very large distances, SFT is still the most convenient solution, this being a modular structure which is therefore quite unaffected by the variation of the crossing length. In crossing cases with very deep waters the length of the cables composing the cable system would noticeably increase, leading to a large increment of the costs and also to a reduction of the efficiency of the cables. Moreover, the use of the cable system of traditional cable supported bridges would also imply a drastic reduction of the foundation blocks to be realized. For the aforementioned reasons, in the latter cases the Cable Supported Immersed Inversed Bridge solution seems to be more competitive than the SFT one.

9.1.3. Cost assessment of Cable Supported Immersed Inversed Bridges

The procedure for the preliminary assessment of the structural cost of Cable Supported Bridges and SFTs is here extended to the different typologies of Cable Supported Immersed Inversed Bridge introduced in section 9.1.1. The total structural cost is thus estimated by means of equation 8.1. The

contribution due to the tunnel cost C_d can be evaluated by means of equation 8.8, whereas the contribution due to the cost of the supporting system can be evaluated by means of the relationships introduced in the following sections. These relationships are developed considering vertical cable systems but could be easily adapted to the case of cable systems featuring an inclination in the

9.1.3.1. *Cost assessment procedure for the supporting system of Immersed Inversed Suspension Bridges*

A symmetrical three-span Suspension Immersed-Inversed Bridge, subjected to the permanent residual buoyancy rb (dead load) and live load (p), is considered (Figure 9.8). The overall cable steel quantity is again due to the quantities related to the main cable and the hangers in both the central and side spans. Clearly, the relationships introduced in section 8.2.2.1 for the suspension bridges must be modified in order to take into account the differences with the characteristics and the physical behaviour of Immersed Inversed Bridges.

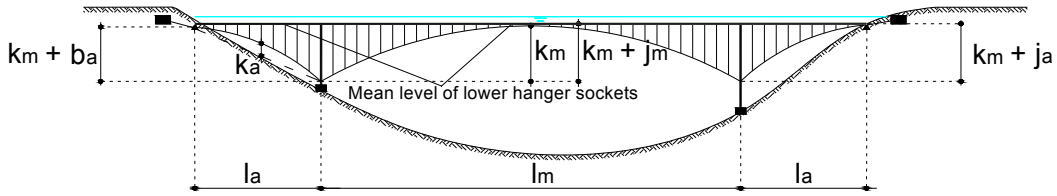

Figure 9.8. Symmetrical three-span Immersed Inversed Suspension Bridge

Considering the main cables, in the immersed case the distributed residual buoyancy is directed upward whereas the own weight of the cables is directed downward, thus reducing the tension forces induced in the cable (Figure 9.9). The following relationships to determine the steel quantity of the main cable in the main span Q_{cmi} can be derived:

$$T_{cbi} = H_{mi} \cdot \sqrt{1 + \tan \varphi_0} = \left(\frac{rb \cdot l_m^2}{8 \cdot k_m} - \frac{(\gamma_{cb} - \gamma_w) \cdot A_{cb} \cdot l_m^2}{8 \cdot k_m}\right) \cdot \sqrt{1 + \left(\frac{4 \cdot k_m}{l_m}\right)^2} \qquad (9.1)$$

$$A_{cbi} = \frac{T_{cbi}}{f_{cbd}} \quad \rightarrow \quad A_{cbi} = \frac{rb \cdot l_m \cdot \sqrt{{l_m}^2 + 16 \cdot {k_m}^2}}{8 \cdot k_m \cdot f_{cbd} + (\gamma_{cb} - \gamma_w) \cdot l_m \cdot \sqrt{{l_m}^2 + 16 \cdot {k_m}^2}} \qquad (9.2)$$

$$Q_{cmi} = \gamma_{cb} \cdot A_{cbi} \cdot l_{cb} =$$

$$= \frac{\gamma_{cb}}{f_{cbd}} \cdot (rb) \cdot {l_m}^2 \cdot \frac{\sqrt{1+16 \cdot \left({k_m}/{l_m}\right)^2}}{8 \cdot {k_m}/{l_m} + \frac{(\gamma_{cb}-\gamma_w)}{f_{cbd}} \cdot l_m \cdot \sqrt{1+16 \cdot \left({k_m}/{l_m}\right)^2}} \cdot \left[1 + \frac{8}{3} \cdot \left({k_m}/{l_m}\right)^2\right] \qquad (9.3)$$

where γ_{cb} and f_{cbd} are, respectively, the specific weight (including the weight increment due to coatings for corrosion protection) and the design strength of the cable steel, while l_m and l_a are, respectively, the main span and side span lengths, k_m is the main span cable sag, T_{cbi} is the maximum tensile force occurring the main cable, A_{cbi} is the area of the main cable and γ_w is the water specific weight.

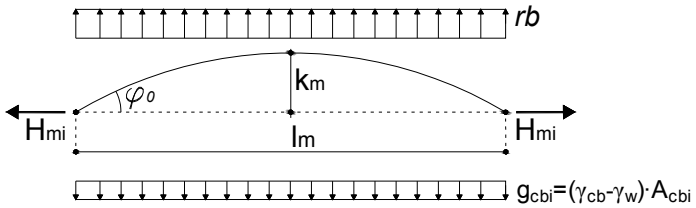

Figure 9.9. Load condition for the main cable of an Immersed Inversed Suspension Bridge

It is worth noticing that, differently from suspension bridges, there is no theoretical limit length for an Suspension Immersed Inversed Bridge, as the contribution of the cable own weight is beneficial, it reducing the maximum tensile force acting in the cable itself. In fact, the denominator in equation 9.3 do not feature any positive root, differently from equation 8.2.

The steel quantity necessary for the main cable in the side spans can be obtained through an equation analogous to (8.4), with the only difference that the contribution of the weight of the main cable weight in the main span (Q_{cmi}) to the cable tensile force is here negative:

$$Q_{cai} = 2 \cdot \frac{\gamma_{cb}}{f_{cbd}} \cdot \frac{(rb) \cdot {l_m}^2 - Q_{cm}}{8 \cdot k_m} \cdot l_a \cdot \sqrt{1 + \left(\frac{k_m}{l_m} + 4 \cdot \frac{k_a}{l_a} + \frac{b_a}{l_a}\right)^2} \cdot$$

$$\cdot \left[1 + \frac{8}{3} \cdot \left(\frac{k_a}{l_a}\right)^2 + \frac{1}{2} \cdot \left(\frac{k_m + b_a}{l_a}\right) + \frac{l_e}{l_a}\right] \qquad (9.4)$$

Concerning the cable steel quantity necessary for the hangers in the main span (Q_{hmi}) and in the side spans (Q_{hai}), equations analogous to (8.3) and (8.5) can be derived:

$$Q_{hmi} = \frac{\gamma_{cb}}{f_{cbd}} \cdot rb \cdot \left(j_m + \frac{k_m}{3}\right) \cdot l_m \tag{9.5}$$

$$Q_{ha} = \frac{\gamma_{cb}}{f_{cbd}} \cdot rb \cdot \left(k_m - \frac{4}{3} \cdot k_a + 2 \cdot j_a - b_a\right) \cdot l_a \tag{9.6}$$

As for the cable system, also in the pylon case the own structural weight reduces the stress induced by the upward residual buoyancy. Moreover the pylons height decreases when the cable system height increases (Figure 9.7), differently from traditional suspension bridges. Making reference to the quantities indicated in Figure 9.10, it is possible to derive the following equations:

$$N_{plsi}(x) = N_{pt} \cdot e^{-\frac{\gamma_{pl}}{f_{pld}} x} \tag{9.7}$$

$$N_{pt} = N_{plsi}(0) = \frac{rb \cdot l_m - Q_{cmi}}{8} \cdot \left(\frac{k_m + 4 \cdot k_a + b_a}{k_m} \cdot \frac{l_m}{l_a} + 4\right) \tag{9.8}$$

$$N_{pb} = N_{plsi}(h_{pl}) = \frac{rb \cdot l_m - Q_{cmi}}{8} \cdot \left(\frac{k_m + 4 \cdot k_a + b_a}{k_m} \cdot \frac{l_m}{l_a} + 4\right) \cdot e^{-\frac{\gamma_{pl}}{f_{pld}} h_{pl}} \tag{9.10}$$

$$Q_{plsi} = N_{pt} - N_{pb} = \frac{rb \cdot l_m - Q_{cmi}}{8} \cdot \left(\frac{k_m + 4 \cdot k_a + b_a}{k_m} \cdot \frac{l_m}{l_a} + 4\right) \cdot \left[1 - e^{-\frac{\gamma_{pl}}{f_{pld}} h_{pl}}\right] \tag{9.11}$$

where $N_{plsi}(x)$ is the axial force acting in the pylon at the abscissa x (Fig. 8), N_{pt} and N_{pb} are respectively the axial force at the top and at the base of the pylon. The seabed depth is assumed to be the same at each pylon location.

The total cost $C_{ss.sbi}$ of the supporting system of a symmetrical three span Immersed Inversed Suspension Bridge can be thus expressed as:

$$C_{si} = (Q_{cmi} + Q_{cai} + Q_{hmi} + Q_{hai}) \cdot u_{cbsi} + 2 \cdot Q_{plsi} \cdot u_{pli} \tag{9.12}$$

where u_{cbsi} and u_{pli} are the unitary average prices for erected and protected suspension cable steel and pylon steel to be erected in the water environment.

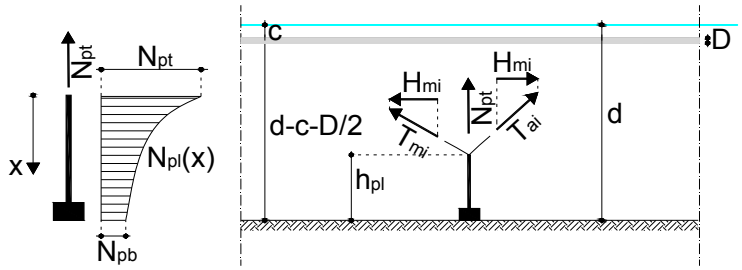

Figure 9.10. Axial force acting in the pylon of an Immersed Inversed Suspension Bridge.

9.1.3.2. *Cost assessment procedure for the supporting system of Immersed Inversed Fan Cable-stayed Bridge*

A symmetrical three-span Immersed-Inversed Fan Cable-stayed Bridge, subjected to the permanent residual buoyancy *rb* (dead load) and live load (*p*), is considered (Figure 9.11). The overall cable steel quantity is due to the quantities related to the main span and side span fans and to the anchor cables.

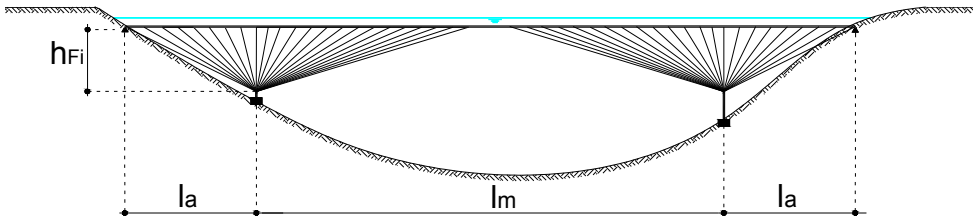

Figure 9.11. Three span symmetrical Fan Cable-stayed Immersed Inversed Bridge.

If a large number of cable stays is considered (this assumption is reliable for modern cable-stayed bridges), the fans can be assumed to be continuous. Therefore, integrating the cable steel quantity dQ_{Fi} of each elementary cable stay (segment C-D in Figure 9.12), it is possible to calculate the cable steel quantity of the main span fan Q_{Fmi} and side span fans Q_{Fai}:

$$dQ_{Fi}(x) = \gamma_{cb} \cdot dA_{cb} \cdot dl_{cb} = \frac{\gamma_{cb} \cdot rb \cdot (x^2 + h_{Fi}^2)}{f_{cbd} \cdot h_{Fi} + \gamma_{cb} \cdot (x^2 + h_{Fi}^2)} \tag{9.13}$$

$$Q_{Fmi} = 2 \cdot \int_0^{l_m/2} dQ_{Fi}(x) \cdot dx = 2 \cdot rb \cdot \gamma_{cb} \cdot \left(\frac{l_m}{2 \cdot \gamma_{cb}} - \frac{f_{cb} \cdot \sqrt{h_{Fi}} \cdot \tan^{-1}\left(\frac{l_m \cdot \sqrt{\gamma_{cb}}}{2 \cdot \sqrt{h_{Fi}} \cdot \sqrt{f_{cb} + \gamma_{cb} \cdot h_{Fi}}} \right)}{\gamma_{cb}^{3/2} \cdot \sqrt{f_{cb} + \gamma_{cb} \cdot h_{Fi}}} \right) \quad (9.14)$$

$$dQ_{Fi}(x) = \gamma_{cb} \cdot dA_{cb} \cdot dl_{cb} = \frac{\gamma_{cb} \cdot rb \cdot (x^2 + h_{Fi}^2)}{f_{cbd} \cdot h_{Fi} + \gamma_{cb} \cdot (x^2 + h_{Fi}^2)} \quad (9.15)$$

$$Q_{Fai} = \int_0^{l_a} dQ_{Fi}(x) \cdot dx = rb \cdot \gamma_{cb} \cdot \left(\frac{l_a}{\gamma_{cb}} - \frac{f_{cb} \cdot \sqrt{h_{Fi}} \cdot \tan^{-1}\left(\frac{l_a \cdot \sqrt{\gamma_{cb}}}{\sqrt{h_{Fi}} \cdot \sqrt{f_{cb} + \gamma_{cb} \cdot h_{Fi}}} \right)}{\gamma_{cb}^{3/2} \cdot \sqrt{f_{cb} + \gamma_{cb} \cdot h_{Fi}}} \right) \quad (9.16)$$

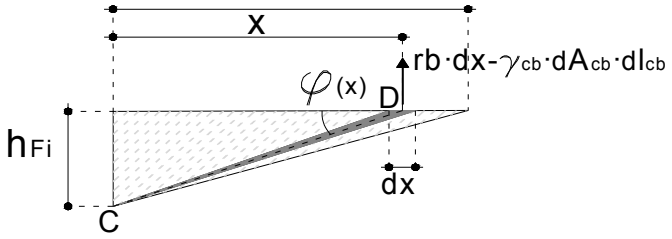

Figure 9.12. Idealized continuous fan subjected to the permanent residual buoyancy and its own weight.

Concerning the anchor cables, the maximum axial force T_{aci} can be obtained by imposing the rotational equilibrium of the fan system around the top of the pylon when the permanent residual buoyancy rb acts on the entire tunnel whereas live loads p are applied only on the side spans (Fig. 9.13), disregarding the bending stiffness of the girder and the own weight of the cable system. The equations giving T_{aci} and Q_{aci} are the following:

$$T_{aci} = \frac{\frac{1}{2} \cdot rb \cdot \frac{l_m^2}{4} - \frac{1}{2} \cdot (rb - p) \cdot l_a^2 - \frac{1}{3} \cdot \left(Q_{Fmi} \cdot \frac{l_m}{2} - Q_{Fai} \cdot l_a \right)}{h_{Fi} \cdot \cos \varphi_{aci}} \quad (9.17)$$

$$Q_{aci} = \frac{\gamma_{cb}}{f_{cbd}} \left[\frac{1}{2} \cdot rb \cdot \left(\frac{l_m^2}{4} - l_a^2 \right) + \frac{1}{2} \cdot p \cdot l_a^2 - \frac{1}{3} \cdot \left(Q_{Fmi} \cdot \frac{l_m}{2} - Q_{Fai} \cdot l_a \right) \right] \cdot$$

$$\cdot \left(\frac{l_a}{h_{Fi}} + \frac{h_{Fi}}{l_a} \right) \quad (9.18)$$

where φ_{aci} is the inclination of the anchor cables with respect to the horizontal direction (Figure 9.13).

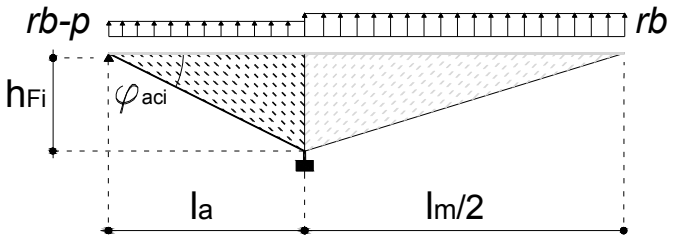

Figure 9.13. Calculation model for the anchor cable maximum force T_{aci}.

The steel quantity Q_{plFi} necessary for the pylons of the inversed fan cable system can still be determined through equations (9.7) to (9.11), considering instead of N_{pt} , given by equation (9.8), the value of the axial force acting at the top of the pylons of the fan system N_{ptFi}, determined by imposing the rotational equilibrium around the abutment (i.e. the connection of the tunnel with the shore) of half bridge subjected to the permanent residual buoyancy rb (Figure 9.14):

$$N_{ptFi} = \frac{rb \cdot l_a}{2} + \frac{rb}{2} \cdot \left(2 + \frac{l_m}{l_a}\right) \cdot l_m - Q_{Fai} \cdot \frac{2}{3} - Q_{Fmi} \cdot \left(1 + \frac{l_m}{3 \cdot l_a}\right) - \frac{Q_{aci}}{2} \tag{9.19}$$

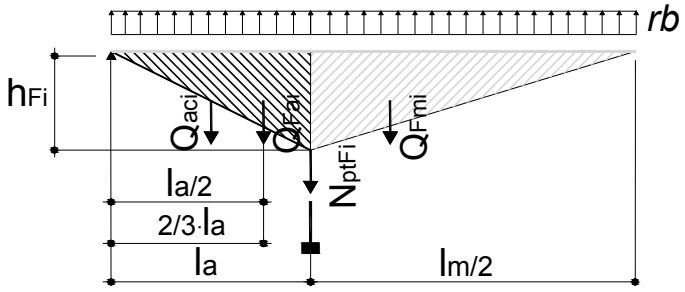

Figure 9.14. Calculation model for the normal force N_{ptFi} acting on the top of the pylons of the inversed fan system.

The total cost $C_{ss,Fi}$ of supporting system of a symmetrical three span Immersed Inversed Fan Cable-stayed Bridge can be thus expressed as:

$$C_{ss,Fi} = (2 \cdot Q_{Fai} + Q_{Fmi} + 2 \cdot Q_{aci}) \cdot u_{cbci} + 2 \cdot Q_{plFi} \cdot u_{pli} \tag{9.20}$$

where u_{cbci} and u_{pli} are the unitary average prices for erected and protected steel for cable stays and pylon steel to be erected in the water environment.

9.1.3.3. *Immersed Inversed Harp Cable-stayed Bridges*

A symmetrical three-span Immersed-Inversed Harp Cable-stayed Bridge, subjected to the permanent residual buoyancy rb (dead load) and live load (p), is here considered (Figure 9.15). Analogously to the traditional harp system described in section 8.2.2.3, it is assumed that the side spans are supported intermediately by means of cables or piers, so that the cable system becomes stable of the 1° order (see section 2.1.2.2). Depending on the values of rb, p, l_m (main span length) l_a (side span length)and h_{hi} (height of the harp cable-stayed system), the forces to be carried by the side supports can be tensile or compressive; in case of compressive forces (most probable case) or low values of tensile forces, piers have to be used as side supports.

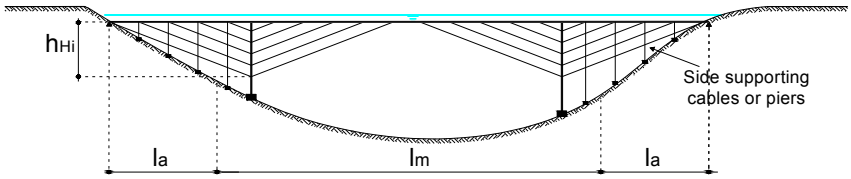

Figure 9.15. Three span symmetrical Immersed inversed Harp Cable-stayed Bridge with side spans supported by additional cables or piers.

The overall cable steel quantity is thus due to the quantities related to the main span and side span harps. The harps can be considered to be continuous, assuming that they are made up of a large number of stays. Therefore, integrating the cable steel quantity dQ_{Hmi} of each elementary cable stay of the main harps (see segment C-D in Figure 9.16), it is possible to estimate the cable steel quantity of the main span harp Q_{Hmi}:

$$dQ_{Hmi}(x) = \gamma_{cb} \cdot dA_{cb} \cdot dl_{cb} = \frac{\gamma_{cb} \cdot rb \cdot \left(\frac{l_m^2}{4} + h_{Hi}^2\right)}{f_{cbd} \cdot h_{Hi} + \gamma_{cb} \cdot \left(\frac{l_m^2}{4} + h_{Hi}^2\right) \cdot \frac{2 \cdot x}{l_m}} \cdot \frac{2 \cdot x}{l_m} \tag{9.21}$$

$$Q_{Hmi} = 2 \cdot \int_0^{l_m/2} dQ_{Hmi}(x) \cdot dx = \frac{2 \cdot f_{cbd} \cdot h_{hi} \cdot l_m \cdot rb \cdot \log(2 \cdot f_{cbd} \cdot h_{hi} \cdot l_m)}{\gamma_{cb} \cdot (l_m^2 + 4 \cdot h_{Hi}^2)} +$$

$$+\frac{\{rb\cdot{}^1/_2\cdot l_m\cdot\gamma_{cb}\cdot(l_m{}^2+4\cdot h_{Hi}^2)-2\cdot f_{cbd}\cdot h_{hi}\cdot l_m\cdot\log[2\cdot f_{cbd}\cdot h_{hi}\cdot l_m+{}^1/_2\cdot l_m\cdot\gamma_{cb}\cdot(l_m{}^2+4\cdot h_{Hi}^2)]\}}{\gamma_{cb}\cdot(l_m{}^2+4\cdot h_{Hi}^2)} \tag{9.22}$$

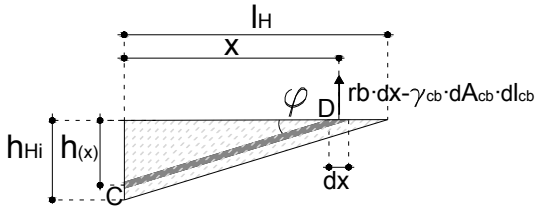

Figure 9.16. Idealized continuous harp subjected to the permanent residual buoyancy and its own weight.

Concerning the side harps, the simplified calculation model which allows to determine the cable steel quantity Q_{Hai} is described in Figure 9.17. Each elementary side span stay (segment B-C) has to carry an horizontal force equal to the one transmitted by the corresponding main span stay (segment C-D), as no horizontal forces are assumed to be absorbed by the pylons. The following equations can be derived:

$$dT_{Hai}{}^1(x') = dT_{Hmi}(x')\cdot\frac{\cos\varphi_{mi}}{\cos\varphi_{ai}} =$$

$$=\left[\frac{rb}{h_{Hi}/\sqrt{\frac{l_m{}^2}{4}+h_{Hi}^2}}-\frac{\gamma_{cb}\cdot rb\cdot\sqrt{\frac{l_m{}^2}{4}+h_{Hi}^2}\cdot\frac{l_m}{2}}{\frac{l_m}{2}\cdot f_{cbd}\cdot h_{Hi}+\gamma_{cb}\cdot\left(\frac{l_m{}^2}{4}+h_{Hi}^2\right)\cdot\frac{l_m\cdot x'}{2\cdot l_a}}\cdot\frac{\frac{l_m{}^2}{4}+h_{Hi}^2}{\frac{l_m}{2}\cdot h_{Hi}}\cdot\frac{l_m\cdot x'}{2\cdot l_a}\right]\cdot\frac{l_m\cdot x'}{2\cdot l_a} \tag{9.23}$$

$$dT_{Hai}(x') = dT_{Hai}{}^1(x')+\frac{\gamma_{cb}}{f_{cbd}}\cdot dA_{Hai}(x')\cdot dl_{Hai}(x') \tag{9.24}$$

$$dA_{Hai}(x') = dT_{Hai}(x')\cdot\frac{2\cdot\sin\varphi_{ai}}{2\cdot f_{cbd}\cdot\sin\varphi_{ai}-\gamma_{cb}\cdot dl_{Hai}(x')} \tag{9.25}$$

$$Q_{Hai} = 2\cdot\int_0^{l_a} dQ_{Hai}(x')\cdot dx' = 2\cdot\int_0^{l_a}\gamma_{cb}\cdot dA_{Hai}(x')\cdot dl_{Hai}(x')\cdot dx' =$$

$$=\frac{4\cdot f_{cb}\cdot h_{Hi}\cdot l_m\cdot rb\cdot(l_m{}^2+4\cdot h_{Hi}{}^2)\cdot\log\left(\frac{2\cdot f_{cbd}\cdot h_{Hi}\cdot l_a}{(2\cdot f_{cbd}\cdot h_{Hi}\cdot l_a)-l_a\cdot(l_a{}^2+h_{Hi}{}^2)\cdot\gamma_{cb}}\right)}{(l_m{}^2+4\cdot h_{Hi}{}^2)\cdot(4\cdot h_{Hi}{}^2+2\cdot l_a{}^2+l_m{}^2)\cdot\gamma_{cb}}+$$

$$+\frac{2\cdot(l_a{}^2+h_{Hi}{}^2)\cdot\log\left(\frac{4\cdot f_{cbd}\cdot h_{Hi}\cdot l_a}{(4\cdot f_{cbd}\cdot h_{Hi}\cdot l_a)+l_a\cdot(l_m{}^2+4\cdot h_{Hi}{}^2)\cdot\gamma_{cb}}\right)}{(l_m{}^2+4\cdot h_{Hi}{}^2)\cdot(4\cdot h_{Hi}{}^2+2\cdot l_a{}^2+l_m{}^2)\cdot\gamma_{cb}} \tag{9.26}$$

where dT_{Hai}^{1} is the contribution to the tensile force in the elementary cable stay of the side spans due to the horizontal force acting in the corresponding main span elementary stay, dT_{Hai} is the total force in the elementary side span stay, dA_{Hai} and dl_{Hai} are the area and length of the side span stay, respectively.

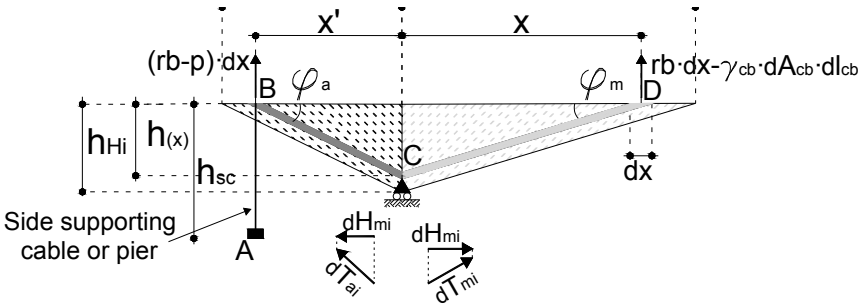

Figure 9.17. Calculation model for the cable steel quantity of the side harps of an inverse harp system.

In order to evaluate if the side supports can be made of cables or piers, the sign of the minimum tensile force $dT_{scb,min}$ is positive or negative:

$$dT_{scb,min}(x') = (rb - p) - dT_{Hai}(x') \cdot \sin\varphi_{ai} - \gamma_{cb} \cdot dA_{scb}(x') \cdot h_{scb} \tag{9.27}$$

where h_{sc} is the height of the side supports.

Since at this stage the area of the elementary supporting cables dT_{scb} is not yet known, this contribution can be neglected initially.

If $dT_{scb,min}$ is positive, assuming that the side supporting cable system is continuous (see the elementary supporting cable A-B in Figure 9.17), the cable steel quantity Q_{sci} can be calculated as follows:

$$Q_{sci} = 2 \cdot \int_0^{l_a} dQ_{scb}(x') \cdot dx' = 2 \cdot \int_0^{l_a} \gamma_{cb} \cdot \frac{\left(rb - dT_{Hai}(x') \cdot \sin\varphi_{ai}\right)}{f_{cb} + \gamma_{cb} \cdot h_{scb}} \cdot h_{sc} \cdot dx' =$$

$$= \frac{h_{sc} \cdot [-2 \cdot f_{cb} \cdot h_{Hi} \cdot l_m \cdot rb \cdot \log(2 \cdot f_{cbd} \cdot h_{Hi} \cdot l_m) + 2 \cdot f_{cb} \cdot h_{Hi} \cdot l_m \cdot rb \cdot \log(4 \cdot f_{cbd} \cdot h_{Hi} \cdot l_a)]}{(f_{cb} + \gamma_{cb} \cdot h_{sc}) \cdot (6 \cdot h_{Hi}^2 + 2 \cdot l_a^2 + l_m^2)} +$$

$$- \frac{h_{sc} \cdot [-2 \cdot f_{cb} \cdot h_{Hi} \cdot l_m \cdot rb \cdot \log(2 \cdot f_{cbd} \cdot h_{Hi} \cdot l_m) + 2 \cdot f_{cb} \cdot h_{Hi} \cdot l_m \cdot rb \cdot \log(4 \cdot f_{cbd} \cdot h_{Hi} \cdot l_a)]}{(f_{cb} + \gamma_{cb} \cdot h_{sc}) \cdot (6 \cdot h_{Hi}^2 + 2 \cdot l_a^2 + l_m^2)} +$$

$$- \frac{h_{sc} \cdot \{2 \cdot f_{cbd} \cdot h_{Hi} \cdot l_m \cdot rb \cdot \log(4 \cdot f_{cbd} \cdot h_{Hi} \cdot l_a + l_a \cdot (l_a^2 + 4 \cdot h_{Hi}^2) \cdot \gamma_{cb})\}}{(f_{cb} + \gamma_{cb} \cdot h_{sc}) \cdot (6 \cdot h_{Hi}^2 + 2 \cdot l_a^2 + l_m^2)} \tag{9.28}$$

If $dT_{scb,min}$ is negative, assuming again that the supporting pier system is continuous and that the normal stress is equal to f_{pld} throughout the whole pier, as made in previous sections for the pylons, the cable steel quantity Q_{spi} can be calculated through the following equations:

$$dN_{sp,t}(x') = dT_{Hai}(x') \cdot \sin\varphi_{ai} + p - rb \tag{9.29}$$

$$Q_{spi} = 2 \cdot \int_0^{l_a} dQ_{sp}(x') \cdot dx' == 2 \cdot \int_0^{l_a} dN_{sp,t}(x') \cdot \left[e^{\frac{\gamma_{pl}}{f_{pld}} \cdot h_{pl}} - 1 \right] \cdot dx' =$$

$$= \left[e^{\frac{\gamma_{pl}}{f_{pld}} \cdot h_{pl}} - 1 \right] \cdot \left(\frac{2 \cdot f_{cbd} \cdot h_{Hi} \cdot l_m \cdot rb \cdot \log(2)}{\gamma_{cb} \cdot (6 \cdot h_{Hi}^2 + 2 \cdot l_a^2 + l_m^2)} + \right.$$

$$\left. - \frac{l_a \cdot (6 \cdot h_{Hi}^2 + 2 \cdot l_a^2 + l_m^2) \cdot \gamma_{cb} \cdot (p - rb) + 2 \cdot f_{cbd} \cdot h_{Hi} \cdot l_m \cdot rb \cdot log\left(\frac{4 \cdot f_{cbd} \cdot h_{Hi} \cdot l_a + l_a \cdot (l_a^2 + 4 \cdot h_{Hi}^2) \cdot \gamma_{cb}}{2 \cdot f_{cbd} \cdot h_{Hi} \cdot l_a - l_a \cdot (l_a^2 + h_{Hi}^2) \cdot \gamma_{cb}} \right)}{\gamma_{cb} \cdot (6 \cdot h_{Hi}^2 + 2 \cdot l_a^2 + l_m^2)} \right] \tag{9.30}$$

where $dN_{sp,t}$ is the axial force in the elementary pier located at abscissa x' (Figure 9.17).

Concerning the pylon steel quantity, it is evident that different relationships are needed for the harp cable system, as in this case the upward loads transmitted by the cable system is distributed over the cable system height (Fig. 9.18), differently from suspension and fan cable systems, where it is concentrated on the pylon top.

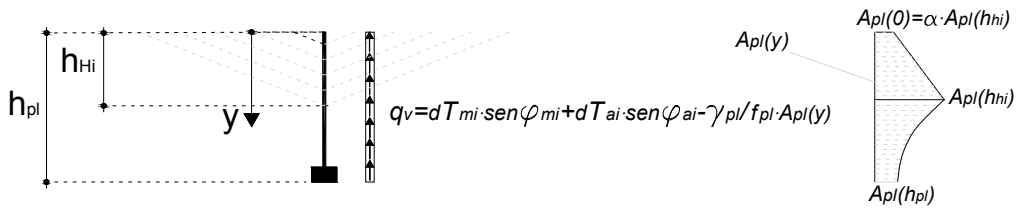

Figure 9.18. Calculation model for the pylon steel quantity of an inverse harp system.

Therefore the differential equation providing the "iso-stress" cross section area of the pylon A_{pl} is in this case the following:

$$dN_{pl}(y) = q_v(y) - \frac{\gamma_{pl}}{f_{pld}} \cdot N_{pl}(y) \tag{9.31}$$

where q(y) is the distributed load transmitted by the stays to the pylon at the height y(Figure 9.18), given by:

$$q_v(y) = dT_{Hmi}(y) \cdot \sin\varphi_{mi} + dT_{Hai}(y) \cdot \sin\varphi_{ai} \tag{9.32}$$

Since equation 9.31 is difficult to be solved analytically, it is acceptable to assume that the cross section of the pylon varies linearly from the top of the pylon to the final point of the cable system. Concerning the pylon part located below the cable system, the steel quantity necessary can be calculated through a relation similar to (9.11), by substituting N_{pt} with $N_{pl}(h_{hi})$.

In order to take into account the actions transmitted to the pylon top by the tunnel due to horizontal hydrodynamic loads, it can be assumed that the cross section area $A_{pl}(0)$ (Figure 9.18) is equal to α times the cross section area at the end of the cable systems $A_{pl}(h_{hi})$, thus obtaining:

$$A_{pl}(y) = A_{pl}(0) + \frac{A_{pl}(h_{Hi}) - A_{pl}(0)}{h_{Hi}} \cdot y \tag{9.33}$$

$$N_{pl}(h_{Hi}) = \int_0^{h_{Hi}} q_v(y) \cdot dy - \gamma_{cb} \cdot \frac{A_{pl}(h_{Hi}) \cdot (1+\alpha)}{2} \cdot h_{Hi} =$$

$$= \frac{2 \cdot f_{cbd} \cdot h_{Hi} \cdot l_m \cdot rb \cdot \log\left(\frac{2 \cdot f_{cbd} \cdot h_{Hi} \cdot l_m + l_m \cdot \left(l_m^2 + 4 \cdot h_{Hi}^2\right) \cdot \gamma_{cb}}{2 \cdot f_{cbd} \cdot h_{Hi} \cdot l_m - l_m \cdot \left(l_m^2 + h_{Hi}^2\right) \cdot \gamma_{cb}}\right)}{\gamma_{cb} \cdot \left(4 \cdot h_{Hi}^2 + l_m^2\right)} +$$

$$+ \frac{2 \cdot f_{cbd} \cdot h_{Hi} \cdot l_m \cdot rb \cdot \left[\log\left(\frac{4 \cdot f_{cbd} \cdot h_{Hi} \cdot l_a + l_a \cdot \left(l_a^2 + 4 \cdot h_{Hi}^2\right) \cdot \gamma_{cb}}{2 \cdot f_{cbd} \cdot h_{Hi} \cdot l_a - l_a \cdot \left(l_a^2 + h_{Hi}^2\right) \cdot \gamma_{cb}}\right) - \log(2)\right]}{\gamma_{cb} \cdot \left(6 \cdot h_{Hi}^2 + 2 \cdot l_a^2 + l_m^2\right)} - \frac{A_{pl}(h_{Hi}) \cdot (1+\alpha)}{2} \cdot h_{Hi} \tag{9.34}$$

$$A_{pl}(h_{Hi}) = \frac{N_{pl}(h_{Hi})}{f_{pld}} \quad \rightarrow \quad A_{pl}(h_{Hi}) = \frac{\int_0^{h_{Hi}} q_v(y) \cdot dy}{f_{pld} + \gamma_{cb} \cdot (1+\alpha)} \cdot \frac{h_{Hi}}{2} \tag{9.35}$$

The total cost $C_{ss,Hi}$ of supporting system of a symmetrical three span Immersed Inversed Harp Cable-stayed Bridge can be finally calculated as:

$$C_{ss,Hi} = 2 \cdot (Q_{Hai} + Q_{Hmi} + Q_{sci}) \cdot u_{cbci} + 2 \cdot Q_{plHi} \cdot u_{pli} \tag{9.36}$$

in case the side supports are made up of cables. If piers are used instead, the following equation can be used:

$$C_{ss,Hi} = 2 \cdot (Q_{Hai} + Q_{Hmi}) \cdot u_{cbci} + 2 \cdot (Q_{plHi} + Q_{aci}) \cdot u_{pli} \quad (9.37)$$

9.1.3.4. *Applications of the CSIB cost assessment procedure*

A numerical application of some of the relationships previously introduced is developed. In particular, a comparison between the structural cost of a SFT, a Suspension Bridge (SB) and an Immersed Inversed Suspension Bridge (ISB) crossing waterways with a variable length L and a constant seabed depth d is considered in order to draw some cost curves, as made in section 8.3.2.

The geometrical arrangement of the three solution is described in Fig. 9.19: The SB is assumed to have a main span length l_m equal to the waterway length L, whereas the ISB covers the same distance with the main span and the side spans. The seabed profile is assumed to be flat for the sake of simplicity. It is worth to underline that this condition is not favourable for CSIBs, as their convenience is exalted in crossing cases where the water depth is larger in the central part of the crossing.

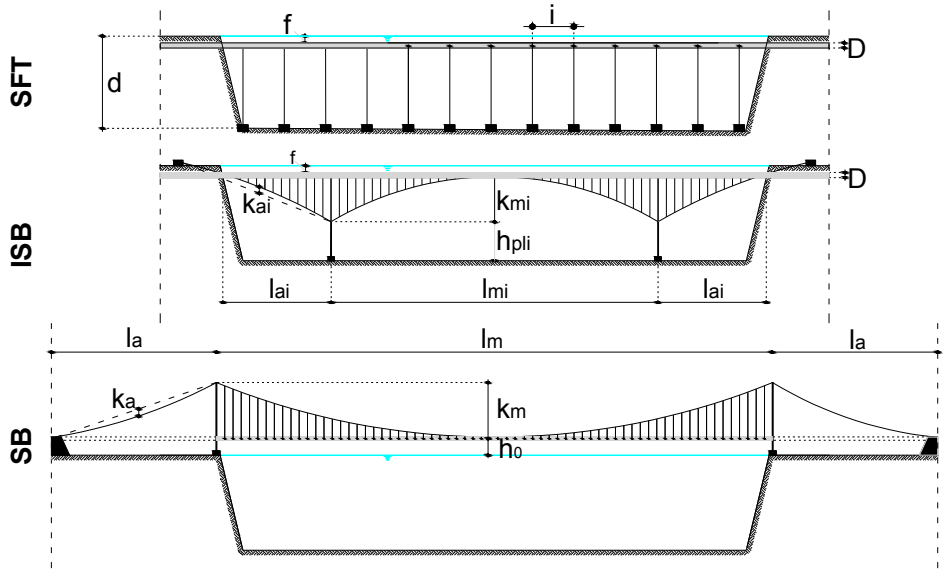

Figure 9.19. Geometrical configuration of the considered Submerged Floating Tunnel, Immersed Suspension Bridge and Suspension Bridge

Two set of geometric and mechanical data for SBs and ISBs are considered, namely C1 and C2: the first one leads to the highest structural cost whereas the second one leads to the lowest one; together they define a cost band for each structural typology. The values assumed for the relevant geometrical parameters are given in Table 9.1; the assumed values for the mechanical parameters are shown in Table 9.2. It is worth noticing that the values considered for the sag-to-main span ratio for ISBs (k_{mi}/l_{mi}) are slightly higher than the ones considered for SBs (k_m/l_m), as the deformability issue related to the presence of concentrated live loads is less relevant for the former ones, due to the higher value of the permanent loads (i.e. the residual buoyancy).

Table 9.1. Set of geometrical data assumed

	D [m]	f [m]	h_0 [m]	ℓ_m	ℓ_a	k_m	ℓ_{mi}	ℓ_{ai}	k_{mi}
C1	25	25	70	L	$0.5\cdot\ell_m$	$0.08\cdot\ell_m$	$0.5\cdot L$	$0.5\cdot\ell_{mi}$	$0.10\cdot\ell_{mi}$
C2	25	25	30	L	$0.25\cdot\ell_m$	$0.12\cdot\ell_m$	$0.66\cdot L$	$0.25\cdot l_{mi}$	$0.15\cdot\ell_{mi}$

Table 9.2. Set of mechanical data assumed

	γ_{cb} [MN/m^3]	γ_{pl} [MN/m^3]	$f_{cb,d}$ [MN/m^2]	$f_{pl,d}$ [MN/m^2]
C1	0.10	0.0785	1000	320
C2	0.08	0.0785	1860	320

The values assumed for permanent and live loads of SBs are equal to the ones considered in section 8.3.2. The cost of the tunnel structure for SFTs and ISBs is set equal to the cost of the SB deck, as it was made in section 8.3.2.

The unitary cost u_{pl} of the steel used for the pylons is set equal to 1 and all the other unitary costs are defined proportionally to it. Table 9.3 illustrates the assumed values for the unitary costs, on the basis of indications given in Gimsing (1996). It is again recognized that the average unitary prices assumed for SFTs and ISBs are questionable, as no data from actual construction are obviously available. However, the assumed values should not fall largely outside the actual price ranges.

Table 9.3. Dimensionless values assumed for the materials unitary costs

	u_{pl} [-]	$u_{cb,SB}$ [-]	$u_{cb,ISB}$ [-]	$u_{a,SFT}$ [-]	u_d [-]
C1	1.0	1.25	1.75	2.5	1.0
C2	1.0	2.0	3.0	4.0	1.0

In Figures 9.20 and 9.21 the cost trend bands of SFTs, ISBs and SBs, defined by the upper (SB1-ISB1-SFT1) and lower bound (SB2-ISB2-SFT2) cost curves are depicted. The independent variables are the crossing length and the seabed depth, respectively; SB cost curves are not shown in Figure 9.21, in order to allow for a better comparison between the cost bands of SFTs and ISBs.

The curves are dimensionless, as the actual costs are divided by a reference cost, assumed equal to the one of the Messina Strait suspension bridge (see section 8.3.1). The characteristic value of the residual buoyancy rb_k is set equal to 1.0 MN/m; curves in Figure 9.20 makes reference to a seabed depth of 200 m whereas the curves in Figure 9.21 are determined considering a crossing length of 3000 m.

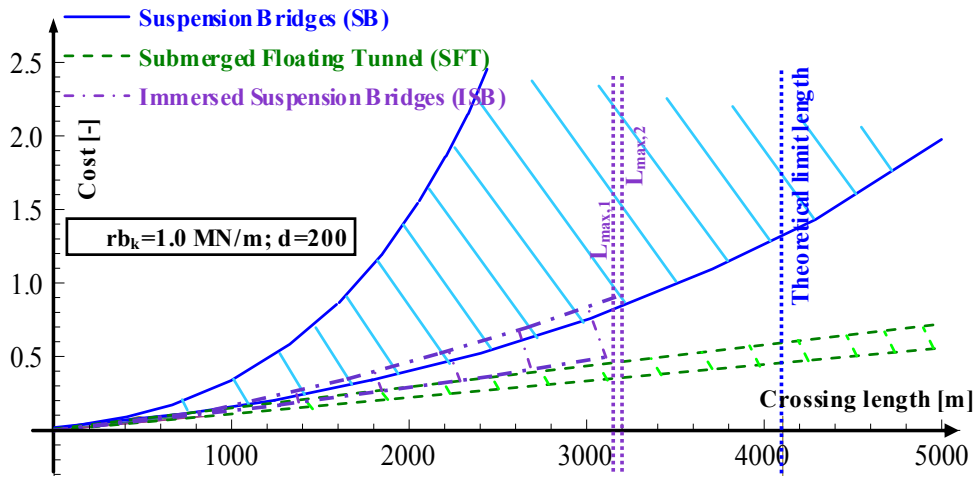

Figure 9.20. Comparison between SFT, ISB and SB cost curves as a function of the crossing length (rb_k=1.0 MN/m; d=200 m).

Looking at the curves shown in Figure 9.20, it can be noticed that the curves relative to the ISBs do not feature any vertical asymptote, as it occurs in the case of traditional SBs, because in this case the own weight of the cable has a favourable effect, as already stated in section 9.1.1. Therefore no theoretical limit length can be defined for ISBs. Nevertheless, given the seabed depth and the sag-to-main span ratio, a maximum length for ISBs can be defined, which corresponds to the condition where the cable system height is equal to the water depth (Figure 9.20). If the crossing length and the sag-to-main span ratio are given instead, a minimum seabed depth necessary to build an ISB can be defined, as shown in Figure 9.21.

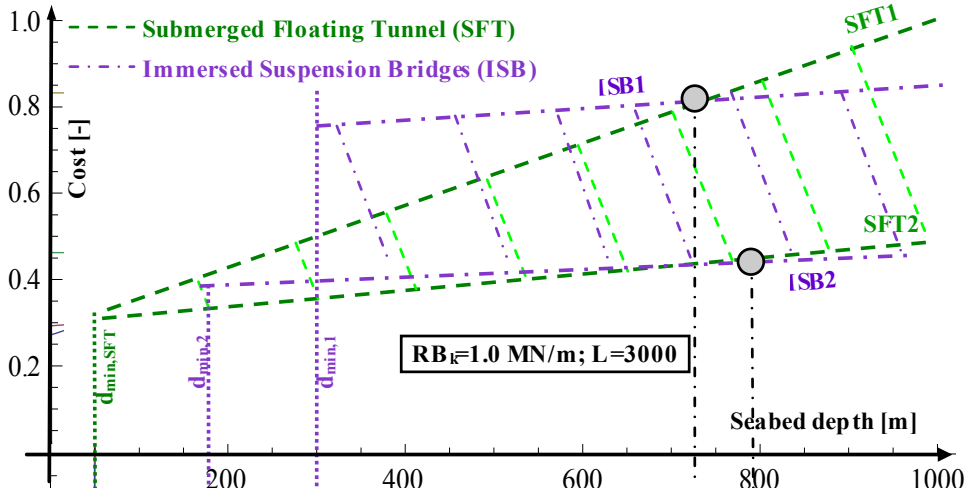

Figure 9.21. Comparison between SFT, ISB and SB cost curves as a function of the seabed depth (rb_k=1.0 MN/m; L=3000 m).

The obtained cost curves show that that in intermediate depth water (d=200 m) and large crossing lengths (L>1÷1.5 km) the SFT represents certainly the most economic solution; as the seabed depth increases the SFT cost grows more than the ISB cost due to the increased length of the anchorages linked to the seabed, whereas the ISB cost grows moderately, as only the pylons increase their height, and the SB cost does not grow at all (the SB pylons are located on the shores). For short and intermediate crossing lengths the SB and ISB solutions feature lower costs than the SFT; SB seems to represent the most economic solution only when short and deep water crossings have to be built.

Clearly larger values of the residual buoyancy would lead to larger costs of SFTs and ISBs, thus reducing their gap with the cost of SBs. The cost of both submerged crossing solutions is directly proportional to the rb_k, therefore the comparison between the cost curves of SFTs and ISBs is not influenced by this parameter.

Figures 9.22 and 9.23 show the cost trend curves of SFTs, ISBs and SBs, considering now a value of rb_k equal to 0,5 MN/m, a value of the seabed depth d, equal to 600 m and a value of the crossing length L of 500 m. It can be noticed that increasing the water depth of the crossing make the ISB economically competitive with SFTs in a wider range of crossing length, up to 3 km (Figure 9.22). Moreover, when the crossing length is reduced to 500 m, the minimum value of the seabed depth leading to lower cost of ISBs with respect to SFTs cost considerably reduces, it becoming slightly lower than 200.

In conclusion it is important to observe that the comparisons between cost curves provided in this section should be considered just as an indication of the influence of geometrical and mechanical parameters on the structural cost of the considered structural solution for waterway crossings. However, the cost assessment procedure proposed here and in Chapter 8 constitutes a simple and very useful tool to assess the structural cost of a SB, SFT or ISB in an actual crossing case, allowing to choose the most economic solution in the preliminary design phase.

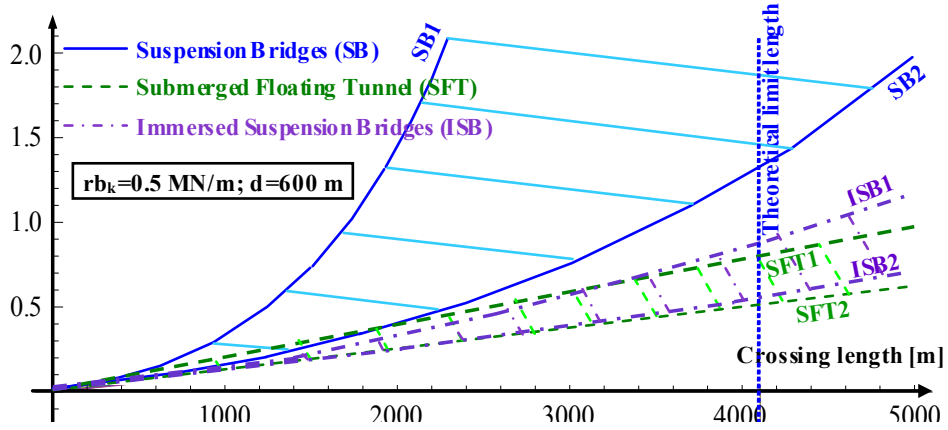

Figure 9.22. Comparison between SFT, ISB and SB cost curves as a function of the crossing length (rb_k=0.5 MN/m; d=600 m).

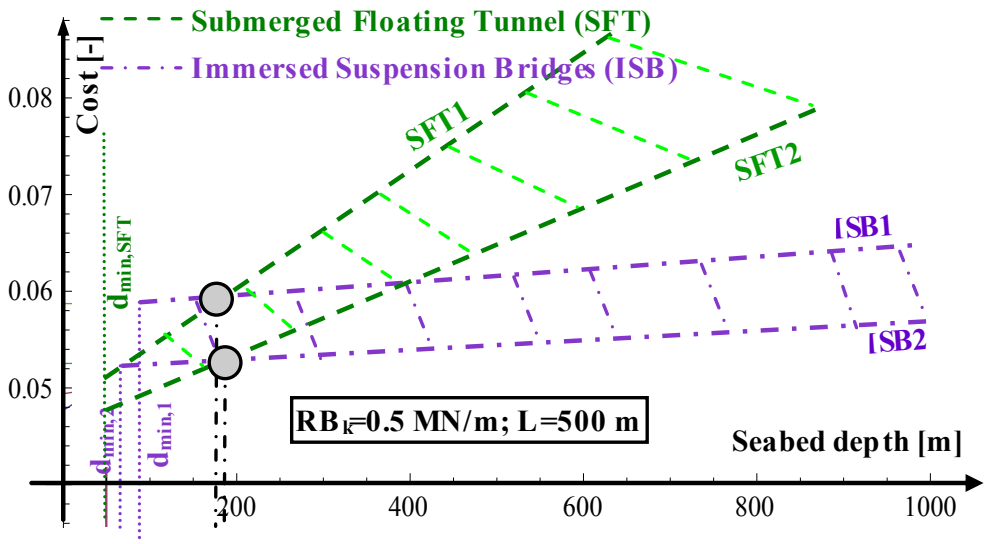

Figure 9.23. Comparison between SFT, ISB and SB cost curves as a function of the seabed depth (rb_k=0.5 MN/m; L=500 m).

9.1.4. Conclusive remarks on CSIBs

Cable Supported Bridges constitute one of the most widely adopted structural solutions for waterway crossings. Therefore the level of knowledge and technology applied in their field is based on years of developments and experiences. In this context the combination of some of the structural solutions commonly adopted in the field of Cable Supported Bridges with the concept of an immersed floating bridge seems to be absolutely feasible. For instance, due to the similarities between the wind loading and current and wave loading, the advancement in the aerodynamic shaping of the stiffening girder of CSBs can be exploited in the field of SFTs with similar solutions.

In particular a new version of immersed tunnel is envisaged: the Cable Supported Immersed Inversed Bridge, featuring the same arrangements of the cable systems traditionally used in Cable Supported Bridges, mirrored with respect to the water surface. This solution seems to be convenient in intermediate to deep waters, featuring several advantages with respect to traditional Cable Supported Bridges under the economic and the environmental impact point of view. In case of deep waters and crossing length belonging to

the range of feasibility of Cable Supported Bridge, this new solution features some important advantages also with respect to the “classic” SFT.

Therefore more studies are needed to investigate peculiar aspects of CSIBs, such as their hydroelastic behaviour, so that they could represent a competitive and available solution for waterway crossings in the next future.

9.2 EXPERIMENTAL TESTS AND DEVELOPMENT OF DESIGN GUIDELINES

The final scope of this Thesis and all the studies carried out on the Submerged Floating Tunnel is to provide design recommendations on this innovative structural typology. Suck a kind of document would strongly support the practical application of SFTs in the world, driving away most of the skepticism which often currently accompanies this waterway crossing solution.

Several theoretical and numerical studies, such as the ones presented in this work, have been carried out and have reached an important level of development. Nevertheless all these methods and studies have one fundamental missing feature. They do not have a significant experimental counterpart, allowing for their calibration and validation.

In this perspective the construction of the first Archimedes Bridge Prototype would represent a fundamental step towards the beginning of the new phase of development of SFTs: the phase of their actual application.

References

Abaqus Inc. (2007). “ABAQUS/Standard User’s Manual, v. 6.7”.

ABS (1999). “Guidance notes on the application of syntethic ropes for offshore mooring”. Published by the American Bureau of Shipping, New York, U.S.A.

Achenback E. (1971). “Influence of Surface Roughness on the Cross-Flow around a Circular Cylinder”, in Journal of Fluid Mechanics, Vol. 46.

Adachi T., Yoshida Y., Kojima A., Kajitani T., Nagai Y., Fukami H., Inoue H., Nakashima T. (2003). “Production of high strength and high toughness steel for offshore structures ”, Proceedings of the 22nd International Conference on Offshore Mechanics and Artic Engineering, Cancun, Mexico.

Ahrens D. (1997). “Submerged Floating Tunnels – a concept whose time has arrived”, Tunneling and Underground Space Technology, Volume 12, pp. 317-336..

Amoruso F., Bettoni F. (2009). “Modellazione delle vibrazioni indotte da distacco di vortici mediante oscillatore equivalente diffuso” (in Italian), Thesis presented in partial fulfilment for the Bachelor’s degree in Civil Engineering, Politecnico di Milano, Milan, Italy.

American Petroleum Institute (2002). “API RP2A-WSD-Recommended Practice for Planning, Designing and Constructing Fixed Offshore Platforms—Working Stress Design”.

Arimochi K., Konda N., Watanabe E., Fukui T., Yajima H, Tada M., Yamamoto M., Hirota K., Kidata H., Kho Y. (2003). “Development of structural steel with superior resistance against fatigue crack growth”.

Proceedings of the 22nd International Conference on Offshore Mechanics and Artic Engineering, Cancun, Mexico.

Aversa S., Maiorano R.M., Mandolini A. (2005). "La progettazione delle fondazioni su pali alla luce degli Eurocodici" (in Italian). Available at the web address: www.reluis.it/doc/pdf/Aversa_Maiorano_Mandolini-correttos.pdf.

Banfield S.P., Flory J.F. , Petruska D.J. (2004). "Defining, Measuring and Calculating the Properties of Fiber Rope Deepwater Mooring Lines", Proceedings of the Offshore Technology Conference, Houston, U.S.A.

Brancaleoni F., Castellani A., D'Asdia P. (1989). "The response of submerged tunnels to their environment", Engineering Structures, Vol. 11, Pp. 47-56, January.

Bugg D.L., Vickers D. T., Dorchak C.J. (2004). "Mad Dog Project: Regulatory Approval Process for the New Technology of Synthetic (Polyester) Moorings in the Gulf of Mexico", Proceedings of the Offshore Technology Conference, Houston, U.S.A.

Campanile A. (2002). "Strutture Offshore" (in Italian), notes of the

CEN (2002a). "EN 1990 - Eurocode – Basis of structural design".

CEN (2002b). "EN 1991-1-1 - Eurocode 1, part 1-1. Actions on structures: General actions - Densities, self-weight, imposed loads for buildings".

CEN (2004a). "EN 1994-1-1- Eurocode 4, part 1-1. Design of composite steel and concrete structures – General rules and rules for buildings".

CEN (2004b). "EN 1992-1-1 - Eurocode 2, part 1-1. Design of concrete structures – General rules and rules for buildings".

CEN (2004c). "EN 1998-1-1 - Eurocode 8, part 1, Design of structures for earthquake resistance. General rules, seismic actions and rules for buildings".

CEN (2005a). “EN 1993-1-8 - Eurocode 3, part 1-8. Design of steel structures – Design of joints”.

CEN (2005b). “EN 1993-1-1 - Eurocode 3, part 1-1. Design of steel structures – General rules and rules for buildings”.

CEN (2007). “EN 1999-1-1 - Eurocode 9, part 1-1. Design of aluminium structures – General structural rules”.

Centre for Marine and Petroleum Technology CMPT. (1998). “Floating structures: a guide for design and analysis”, Oilfield Publications Inc. Publication 101/98.

Chellini G., Salvatore W. (2008). “RELUIS Linea 5: Sviluppo di approcci innovative per il progetto di strutture in acciaio e composte acciaio-calcestruzzo” (in Italian), RELUIS research report.

Campanile A. (2005). “Offshore structures”, notes of the class of Offshore structures held at the Unversity of Naples “Federico II”.

Chopra A.K. (2006). “Dynamics of Structures (3rd Edition)”. Wiley & Sons, London, UK.

Ciria Underwater Engineering Group (1978). “Dynamics of marine structures: Methods of calculating the dynamic response of fixed structures subject to wave and current action”.

Corsini S., Inghilesi R. (2004). “Italian Wave Atlas”,

COWI Company (1995). “Gibraltar Strait Bridge, Spain – Morocco”, Technical Sheet available eat the website www.cowi.com.

COWI Company (2009). “Busan - Geoje Immersed Tunnel, Korea”, Technical Sheet available at the website www.cowi.com.

Dezi F., Leoni G., Dall’Asta A., Scarpelli G. (2007). “Dynamic spatial response of structures considering soil-foundation-structure interaction:

application to a railway bridge", Proceedings of the XII National Congress "L'ingegneria sismica in Italia", ANIDIS, Pisa, Italy.

Di Pilato M., Feriani A., Perotti F. (2008). "Numerical models for the dynamic response of submerged floating tunnels under seismic loading", in Earthquake Engineering and Structural Dynamics, Vol. 37, pp. 1203-1222.

Dobry R., Gazetas G. (1988). "Simple method for dynamic stiffness and damping of floating pile groups", Geotechnique 38 No. 4, 557-574.

Ehlers C.J., Young A.G., Chen J. (2004). "Technology assessment of deepwater anchors", Proceedings of the Offshore Technology Conference OTC, Houston, U.S.A.

Felch J., Grantz W.C., Saveur J. (2001). "The Elevated Immersed Tunnel", Proceedings of 4th International Symposium on Strait Crossings, Bergen, Norway.

Faggiano B., Mazzolani F.M. (2001). "Il Tunnel Galleggiante Sommerso:nuova frontiera per l'attraversamento di bracci d'acqua" (in Italian), Proceedings of the XVIII National Conference C.T.A. "Giornate Italiane della Costruzione in Acciaio", 26-28 September, Venice, Italy.

Faggiano B., Landolfo R., Mazzolani F.M. (2001a). "Analysis Project concerning a "Ponte di Archimede" in the Jintang Strait", Final Report of the Italian-Chinese cooperation project.

Faggiano B., Landolfo R. and Mazzolani F.M. (2001b). "Design and modelling aspects concerning the Submerged Floating Tunnels: an application to the Messina Strait Crossing". Proceedings of the 4th Symposium on Strait Crossings, Bergen, Norway.

Faggiano B., Landolfo R., Mazzolani F.M. (2005). "The SFT: an innovative solution for waterway strait crossings". Proceedings of the IABSE Symposium "Structures and Extreme Events", Lisbon, Portugal, September 14-17.

Faggiano B., Martire G., Mazzolani F.M. (2010). “Cable supported immersed inversed bridge: A challenging proposal”, ”, Procedia Engineering, Volume 4, 2010, Pp. 283-291, ISAB-2010, First International Symposium on Archimedes Bridge (ISAB-2010).

Franco L., Piscopia R., Corsini S., Inghilesi R. (2004), “L’Atlante delle onde nei mari italiani - Italian Wave Atlas”, Full Final Report by APAT-University of Roma Tre, sponsored by AIPCN Italian Section and Italia Navigando, Rome.

Fiorentino A. (2009). “Fire Protection and Fire Fighting in Tunnels”, Proceedings of the 5th Symposium on Strait Crossings, Trondheim, Norway.

Fogazzi P., Perotti F. (2000). “The dynamic response of seabed anchored floating tunnels under seismic excitation”, in Earthquake Engineering and Structural Dynamics, Vol. 29, pp. 273-295.

Forum of European National Highway Research Laboratories FEHRL (1996). “Analysis of the submerged floating tunnel concept”. FEHRL report no. 1996/2a.

Hong Y., Ge F. (2010). “Dynamic response and structural integrity of submerged floating tunnel due to hydrodynamic load and accidental load”, Procedia Engineering, Volume 4, 2010, Pp. 35-50, ISAB-2010, First International Symposium on Archimedes Bridge (ISAB-2010).

Garrison C.J. (1978). “Hydrosynamic Loading of Large Offshore Structures. Three-Dimensional Source Distribution Methods”, in Numerical Methods in Offshore Engineering, pp. 97-140,Wiley, Chichester, England.

Gimsing N.J. (1996). “Cable Supported Bridges: Concept and Design (2nd edition)”. John Wiley & Sons.

Grantz W. (1997). “Steel-Shell Immersed Tunnels-Forty Years of Experience”, Tunneling and Underground Space Technology. Vol.12, No.1, pp.23-31.

Grantz W., Tan L., Sørensen E., Burger H. (1997). “Waterproofing and maintenance”, Tunneling and Underground Space Technology. Vol.12, No.2, pp.93-109.

Grantz W. (2003). “A new concept for a steel shell submerged floating tunnel”, "(Re)Claiming the Underground Space", Vol. 1, pp. 297 – 302.

Grantz W., Iversen C. (2009). “Construction of the Bosphorus Immersed Rail tunnel”, Proceedings of the 5th Symposium on Strait Crossings, Trondheim, Norway.

Haugerud S.A., Muttoni A., Olsen T.O. (2001). “A Crossing Proposal for the Lake Lugano for the new Alp Transit railway across the Alps”, Proceedings of 4th International Symposium on Strait Crossings, Bergen, Norway.

Horiguchi H., Miyauchi N., Kanie S., Mikami T., Mizutani Y. (2001). “Effect of non-linearity in restoring force on dynamic response of SFT”, Proceedings of 4th International Symposium on Strait Crossings, Bergen, Norway.

Jakobsen B., Haaland P., Haugerud S.A. (2009). “Crossing the wide and highly exposed Sulafjord with an SFT”, Proceedings of the 5th Symposium on Strait Crossings, Trondheim, Norway.

Jensen L. (2009). “Long span suspension bridges for strait crossings”, Proceedings of the 5th Symposium on Strait Crossings, Trondheim, Norway.

Kanie S. (2010). “Feasibility studies on various SFT in Japan and their technological evaluation”, Procedia Engineering, Volume 4, 2010, Pp. 13-20, ISAB-2010, First International Symposium on Archimedes Bridge (ISAB-2010).

Kim Y, Kim J., Lee J. (2009). “Busan-Geoeje Fixed Link Immersed Tunnel”, Proceedings of the 5th Symposium on Strait Crossings, Trondheim, Norway.

Kiyomiya O., Nakamichi N., Yokota H., Shiraishi S. (2004). "New Type Flexible Joint for the Osaka Port Yumeshima Tunnel", Proceedings of the Conference Oceans'04 MTS/IEEE/Techno-Ocean'04, Kobe, Japan.

Kiyomiya O. (2003). "Flexible joints between elements for large deformation", "(Re)Claiming the Underground Space, Vol. 1, pp. 329 – 334.

Kunisu H., Mizuno S., Mizuno Y., Yamashita T., Saeki H. (1994). "Numerical analyses of wave force and dynamic response to the submerged floating tunnels", Proceedings of the 3rd Symposium on Strait Crossings, Ålesund, Norway.

Laitone E.V. (1962). "Limiting Conditions for Cnoidal and Stokes Waves", in Journal of Geophysical Research, Vol. 67, pp. 1555-1564.

Le Mehauté B. (1976).An Introduction to Hydrodynamics and Water Waves, Springer, New York.

Longuet-Higgins M.S. (1952). "On the statistical distributions of the heights of sea waves", in Journal of Marine Research, Vol. XI, N° 3.

MacCamy R.C., Fuchs R.A., (1954). "Wave Forces on Piles: A Diffraction Theory", U.S. Army of Corps Engineers, Beach Erosion Board, Tech. Memo N.59.

Maeda N., Morikawa M., Ishikawa K., Kakuta Y. (1994). "Study on structural characteristics of support systems for submerged floating tunnels", Proceedings of the 3rd Symposium on Strait Crossings, Ålesund, Norway.

Martinelli L., Barbella G., Feriani A. (2010). "Modeling of Qiandao Lake submerged floating tunnel subject to multi-support seismic input", ", Procedia Engineering, Volume 4, 2010, Pp. 311-318, ISAB-2010, First International Symposium on Archimedes Bridge (ISAB-2010).

Martire G. (2007). "Submerged Floating Tunnel performance evaluation", Master Degree Thesis in Structural and Geotechnical Engineering, University of Naples "Federico II".

Martire G., Faggiano B., Esposto M., Mazzolani F.M., Landolfo R., Zollo A., Stabile T.A. (2009a). "The structural response of Submerged Floating Tunnel to multi-support seismic excitations", Proceedings of the International Conference STESSA09 "Seismic Behaviour of Steel Structures in Seismic Areas", Philadelphia, USA.

Martire G., Esposto M., Faggiano B. & Mazzolani F.M., Zollo A. & Stabile T.A. (2009b). "The seismic response of Submerged Floating Tunnel under multi-support excitations". Proceedings of the XIII National Congress "L'ingegneria sismica in Italia", ANIDIS, Bologna, Italy.

Martire G., Faggiano B., Esposto M., Mazzolani F.M., Landolfo R., Zollo A., Stabile T.A. (2010a). "A study on the response of Submerged Floating Tunnels to seismic excitation". Proceedings of the International Conference 14th ECEE, European Conference on Earthquake Engineering, Ohrid, Republic of Macedonia.

Martire G., Faggiano B., Esposto M., Mazzolani F.M., Landolfo R., Zollo A., Stabile T.A. (2010a). "A study on the response of Submerged Floating Tunnels to seismic excitation", Proceedings of the International Conference 14th ECEE, European Conference on Earthquake Engineering, Ohrid, Republic of Macedonia.

Martire G., Faggiano B., Mazzolani F.M., Zollo A., Stabile T.A. (2010b). "Seismic analysis of a SFT solution for the Messina Strait crossing", Procedia Engineering, Volume 4, 2010, Pp. 311-318, ISAB-2010, First International Symposium on Archimedes Bridge (ISAB-2010).

Martire G., Faggiano B., Mazzolani F.M. (2010c). "Compared cost evaluation among traditional versus innovative strait crossing solutions" Procedia Engineering, Volume 4, 2010, Pp. 293-301, ISAB-2010, First International Symposium on Archimedes Bridge (ISAB-2010).

Mazzolani F.M. (2005). "Problemi strutturali relativi al ponte di Messina" (in Italian), Bulletin of the Order of Engineers of Naples, July-August.

Mazzolani F.M., Landolfo R., Faggiano B., Esposto M., Martire G., Perotti F., Di Pilato M., Barbella G., Fiorentino A. (2007). "The Archimede's Bridge Prototype in Qiandao Lake (PR of China). Design Report". Contribution of the Italian Team. "Sino-Italian Joint Laboratory of Archimedes Bridge" (SIJLAB), Research project report.

Mazzolani F.M., Landolfo R., Faggiano B., Esposto M., Perotti F., Barbella G. (2008). "Structural analyses of the Submerged Floating Tunnel prototype in Qiandao Lake (PR of China)", International Journal Advances in Structural Engineering.

Mazzolani F. M., Faggiano B., Esposto M., Martire G. (2009). "A new challenge for strait crossings: the immersed inversed cable supported bridge". Proceedings of the Nordic Steel Construction Conference 2009, Malmo, Sweden.

Mazzolani F. M., Faggiano B., Martire G. (2010). "Design aspects of the AB prototype in the Qiandao Lake", Procedia Engineering, Volume 4, 2010, Pp. 21-33, ISAB-2010, First International Symposium on Archimedes Bridge (ISAB-2010).

Mitsuyasu H. (1975). "Observation of the directional spectrum of ocean waves using a cloverleaf buoy", in Journal of Physical Oceanographic, Vol. 5, pp. 750-760.

Nicolussi F., Casola, F. (1994). "The configuration and the characteristics of the submerged tunnels for the Messina Strait crossing", Proceedings of the 3rd Symposium on Strait Crossings, Ålesund, Norway.

Odegard E. (1994). "Ardalsfjørd crossing", Proceedings of the 3rd Symposium on Strait Crossings, Ålesund, Norway.

Peregrine D.H. (1972). "Equations for Water Waves and the Approximation Behind Them", in Waves on Beaches and Resulting Sediment Transport, R.E. Meyer, Academic Press, New York, pp. 95-121.

Peroni M. (2006). “Gibraltar Straits crossing: a new design proposal”, Proceedings of IABSE Symposium on Responding to Tomorrow’s Challenges in Structural Engineering, Budapest, Hungary.

Perotti F., Di Pilato M. (2009). “Vortex Induced Vibration in Submerged Floating Tunnels: DVL a Distributed Vortex Layer Model”, Proceedings of the 5th Symposium on Strait Crossings, Trondheim, Norway.

Perotti F., Barbella G., Di Pilato M. (2010). “The dynamic behaviour of Archimede’s Bridges: Numerical simulation and design implications”, Procedia Engineering, Volume 4, 2010, Pp. 91-98, ISAB-2010, First International Symposium on Archimedes Bridge (ISAB-2010).

Pliego J.M. (2005). “Open Session – The Gibraltar Strait tunnel. An overview of the study process”, Tunnelling and Underground Space Technology, Vol. 20, Pp. 558–569.

Ponte di Archimede S.p.A. Company (1984), “Il Ponte di Archimede nello Stretto di Messina. Progetto-Fattibilità-Traffico” (in italian), Design report.

Ramasco R., Landolfo R., Realfonzo R. (1991). “Innovative criteria for the design and management of maritime infrastructures and systems” (in Italian), C.N.R. Special Project.

Remseth S., Leira B.J., Okstad K.M., Mathisen K.M., Haukas T. (1999). “Dynamic response and fluid/structure interaction of submerged floating tunnels”, in Computers and Structures, 72, pp. 659-685.

Sarpkaya T. (1976). “Vortex Shedding and Resistance in Harmonic Flow About Smooth and Rough Circular Cylinders at High Reynolds Numbers”, Report No. NPS-59SL76021, Naval Postgraduate School, Monterey, CA.

Sarpkaya T., Isaacson M. (1981). “Mechanics of wave forces on offshore structures (1st edition)”, Van Nostrand Reinhold Company.

Saveur J., Grantz W. (1997). “Structural Design Of Immersed tunnel”, Tunneling

and Underground Space Technology. Vol.12, No.2, pp.93-109.

Schlichting H. (1968). "Boundary-Layer Theory (6th edition)", Mc-Graw Hill Book Co., New York, U.S.A.

Scolari G., Zucconi A., Pigorini B., Di Tella V. (1989). "Tunnel in alveo per attraversamenti stabili stradali e ferroviari in acque profonde" (In Italian), 2° Congress A.I.O.M. (Associazione di ingegneria offshore e marina), Environment, Energy and Infrastructures, Naples, Italy.

Sirprogetti Company (1996). "Ponte galleggiante sommerso", Design report.

Skorpa L. (1994). "The Høgsfjord submerged floating tunnel project, transport, environment and energy studies", Proceedings of the 3rd Symposium on Strait Crossings, Ålesund, Norway.

Skorpa L. (2001)."The Høgsfjord submerged floating tunnel project, transport, environment and energy studies". Proceedings of 4th International Symposium on Strait Crossings, Bergen, Norway.

Skorpa L., Østlid H (2001). "Owners experience with the pilot project Høgsfjord submerged floating tunnel", Proceedings of 4th International Symposium on Strait Crossings, Bergen, Norway.

Smith D., Williams J. (2003). "Monitoring axial strain in synthetic fiber mooring ropes using polymeric optical fibers", Proceedings of the 22nd International Conference on Offshore Mechanics and Artic Engineering, Cancun, Mexico.

Solari G. (2010). Invited lecture at the seminar "La moderna Ingegneria Strutturale tra innovazione e tradizione", Second University of Naples, Faculty of Engineering, Aversa, Italy.

Trelleborg Bakker B.V. (2008). "Commercial brochure on Gina gasket", available at http://www.trelleborg.com.au/Documents/TrelleborgGina.pdf.

TWI Ltd. Friction Stir Welding. Copyright ©2006 TWI Ltd. World Centre for Materials Joining Technology, UK. Website: http://www.twi.co.uk.

Wu G., Finn W.D. (1997). "Dynamic elastic analysis of pile foundations using finite element method in the frequency domain", Can. Geotech. J. Vol. 34.

Xiao J., Huang G. (2010). "Transverse earthquake response and design analysis of submerged floating tunnels with various shore connections", Procedia Engineering, Volume 4, 2010, Pp. 233-242, ISAB-2010, First International Symposiu